Alma Mater Studiorum – Università di Bologna

DOTTORATO DI RICERCA IN

Chimica

Ciclo XXXV

Settore Concorsuale: 03/B1

Settore Scientifico Disciplinare: CHIM/03

New Gold(I) Complexes: from Ligand Design to Homogeneous Catalysis

Presentata da: Riccardo Pedrazzani

Coordinatore Dottorato **Supervisore**

Prof. Luca Prodi **Prof.ssa Magda Monari**

Esame finale anno 2023

Abstract

This PhD thesis summarize the work carried out during three years of PhD course. Several thematic concerning gold(I) chemistry are analysed by crossing data from different chemistry areas as: organic chemistry, organometallic chemistry, inorganic chemistry and computational chemistry.

In particular, the thesis focuses its attention on the evaluation of secondary electronic interactions, subsisting between ligand and Au(I) metal centre in the catalyst, and their effects on catalytic activity. The interaction that has been taken in consideration is the Au…Ar π-interaction which is known to prevent the decomposition of catalyst, but exhaustive investigations of further effects has never been done so far.

New libraries of carbene (ImPy) and biarylphosphine ligands have been designed and synthetized for the purpose and subsequently utilized for the synthesis of corresponding Au(I) complexes. Resulting catalysts are tested in various catalytic processes involving different intermediates and in combination with solid state information from SC-XRD revealed an unprecedented activation mode which is only explained by considering both electronic nature and strength of Au…Ar π-interaction. DFT calculation carried on catalysis intermediates are in agreement with experimental ones, giving robustness to the theory.

Moreover, a new synthetic protocol for the lactonization of *N*-allenyl indole-2-carboxylic acids is presented. Reaction conditions are optimized with the newly synthetized ImPy-Au(I) catalysts and different substrates are also tested providing a quite broad reaction scope. Chiral ImPy ligands have also been developed for the asymmetric variant of the same reaction and encouraging enantiomeric excess are obtained.

Index

1. Introduction

1.1 Gold: everyday life

Gold is a chemical element of the periodic table with atomic number of 79. In its elemental state is a metal, but unlike the other transition-metals which have a silver-grey aspect, gold presents a reddish-yellow colour, or commonly named “gold colour”. This property and others are the consequence of the relativistic effects, which will be analysed in the next paragraphs.

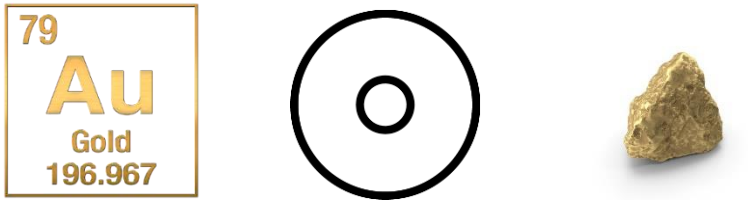

Figure 1. *Gold symbol (left) – Gold alchemical symbol (middle) – Gold nugget (right).*

In nature can be found in its metal form as nuggets, in alloys with other metals or in mineral inclusions. It is known to human-kind since the early Egyptian civilization (4.200 B.C.), which start to map the spot where gold could be found. Due to its beauty, malleability and resistance to oxidation, gold was initially used for the production of jewels and was connected also with religion and rituals. Later on in the history, other peculiar properties were discovered, such as the elevated electrical conductivity and stability to physiological ambient, which led to the use of gold in electronic products, medical application and cuisine.

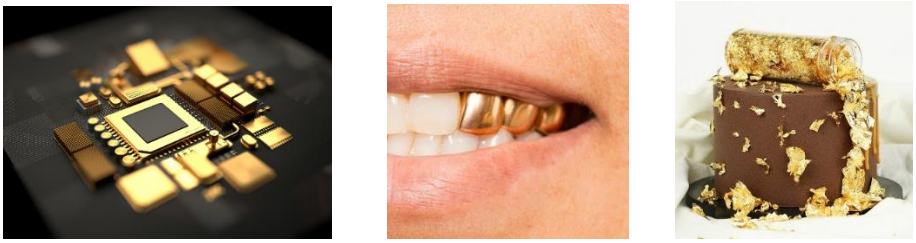

Since his resistance to corrosion/oxidation, gold is known to be a precious metal. Therefore was used as coinage metal for currency. Nowadays, gold in barley used in coinage, however still possess a great financial value since is used as economical reserve by nations and banks, because it doesn’t change its purchasing power across time and with inflation.

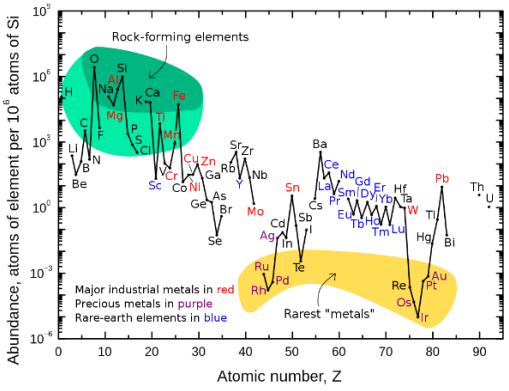

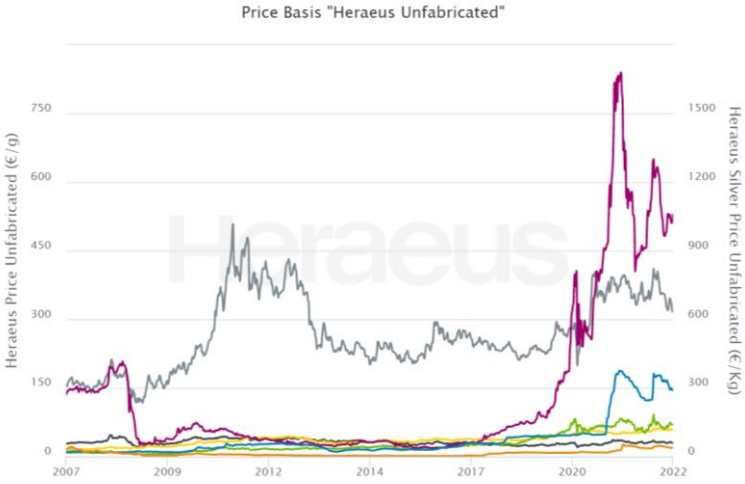

Figure 2. *Relative abundances of metals in the Earth's crust (left) – Market price of gold (yellow), platinum (black), palladium (green), ruthenium (orange), iridium (blue), rhodium (purple) and silver (grey) provided by Heraeus Group (right).*

Despite it can be found easily in everyday life, gold is one of the rarest metal on Earth and his price is the fourth in the group (Figure 2).

1.2 Birth of gold chemistry

Gold has three stable oxidation states: 0, +1 and +3, and it founds many applications across many fields of chemistry.

Gold(0) is mostly employed in the development of nanoparticles (AuNPs) and applications in sensing (colorimetric, fluorescence, electrochemical), electrocatalytic reductive processes and for biomedical applications;[1,2] this area of gold chemistry will not be part of the present thesis.

The two catalytically active species of gold employed in homogeneous catalysis are Au(I) and Au(III) cations. However, gold had for a long time the infamous appellative of "*catalytically dead metal*". In fact, gold was not undergoing the typical catalytic cycle of other more utilized transition metals (TMs) such Pd, Ni and Cu, characterized by oxidative addition (OA), transmetallation and reductive elimination (RE),[3] Figure 3.

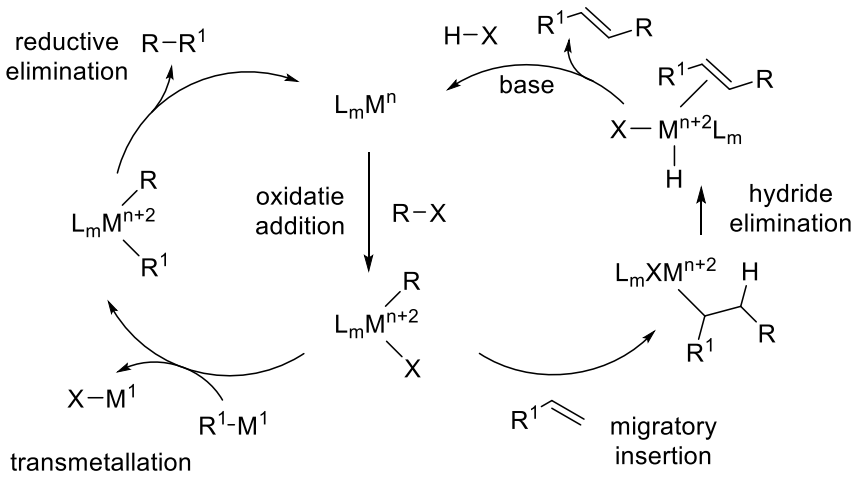

Figure 3. *Typical cross-coupling cycle (left) and Heck-type cycle (right).*

To achieve this reactivity the catalytic metal centre has to cycle between the M^n/M^{n+2} oxidation state and in the case of gold the redox potential of the Au^+/Au^{3+} couple is E^0=1.41V (vs. SHE).[4] This potential is high compared to the other TMs, and in particular if compared to the isoelectric pair Pd^0/Pd^{2+} (E^0=0.92V vs. SHE).[5] This particular reluctance showed by gold(I) led to a delayed development of his chemistry, while the other TMs were widely employed since the beginning of 20th century.

The very first application of gold in homogeneous catalysis was developed by Ito and Hayashi in the 1986 for the enantioselective synthesis of oxazolines (Figure 4).[6]

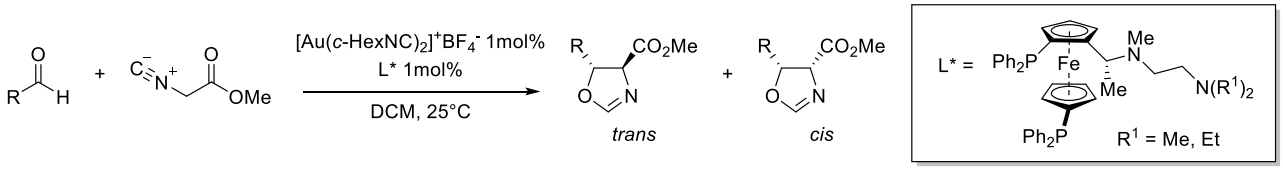

Figure 4. *Asymmetric gold(I)-catalysed aldol reaction between aldehydes and isocyanates.*

Even if the results reported in this paper were excellent in terms of yields, diasteroselectivity and enantioselectivity (up to 100% yield, 100% *d.r.* and 97% *e.e.*), the catalytic use of gold in organic synthesis was still not considered by the scientific community. A drastic route change occurred during the 90's and the beginning of the new millennium, where the use of Au(I) and Au(III) catalysts had successes in the hydration and acetal synthesis from alkynes (Figure 5).[7,8,9] Thanks to these discoveries, gold showed a interesting catalytic activity with a peculiar selectivity through C-C triple bond activation, avoiding the use of toxic mercury(II) salts.

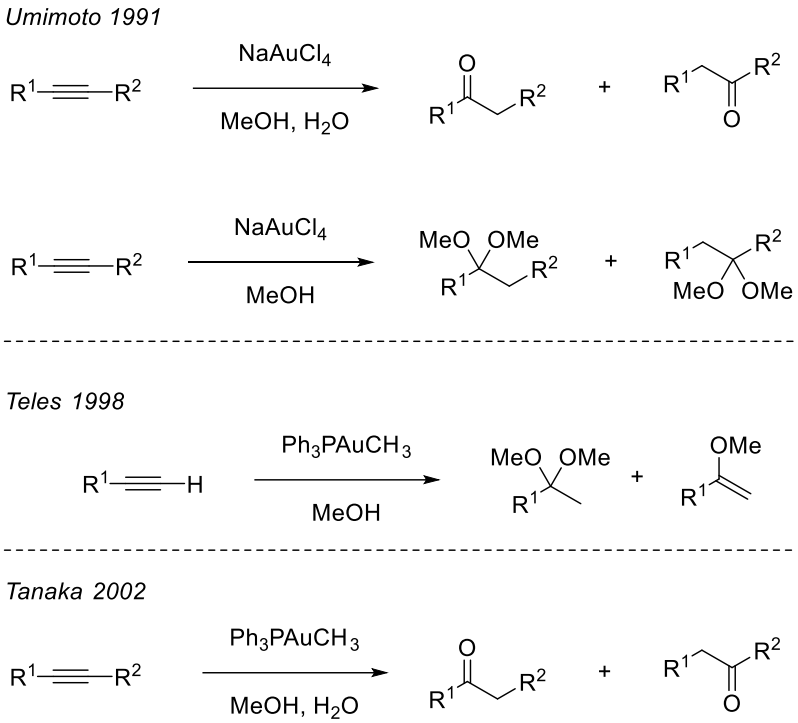

Figure 5. *Hydration and acetal synthesis by gold catalysis.*

After these pioneering results, gold was taken in serious consideration by the scientific community, and rapidly become a hot topic in catalysis. During the first decade of 2000s there was an exponential growth of publication related to homogeneous gold catalysis, this period of time was named "*gold fever*".

1.3 Relativistic effect of gold

Before going in the detail of the organic transformations accessible with gold-chemistry, the atomic nature of the gold metal centre and his unique properties need to be analysed. In fact, some of the properties already mentioned (e.g. colour, high oxidation potentials, activation of alkynes) are the direct consequences of the relativistic effect (RE) of gold. Concomitant to the rising number of publications involving gold in catalysis, different groups put their attention to underly these effects, in particular professor Pyykkö,[10,11,12] and years of results are elegantly summarized by Toste.[13] The term "relativistic effects" refers to any phenomenon resulting from the need to consider velocity as significant relative to the speed of light. In particular, the relativistic mass of an electron depends on its velocity, and the relation is reported by the equation $m_r = m_0/\sqrt{1-(v/c)^2}$. Since mass and velocity can be mutually interconverted, v/c ratio can be written as $Z/137\text{uma}$. For an electron in the 1s orbital the radial velocity is $V_r = Z(\text{uma})$, and light speed is $c = 137\text{uma}$. For example, Au

has Z=79, thus its electron in 1s orbital has a velocity of 58% of speed light. Therefore, the relativistic effect has a cascade effect:

- the electron has a greater mass and a decrease of orbital radii;
- the contraction of the orbital cause a better shielding effect;
- the more penetrating orbitals *s* and *p* are contracted too;
- the less penetrating orbitals *d* and *f* are better shielded and are expanded.

The Figure 6 shows the contraction of 6*s* orbital of elements from Z=55 to Z=100.[10] The contraction is represented as ratio of the relativistic radii over the non-relativistic radii. As show in this plot, gold is the element where the relativistic effect has the greatest impact, followed by mercury and platinum ($_{78}$Hg and $_{80}$Pt).

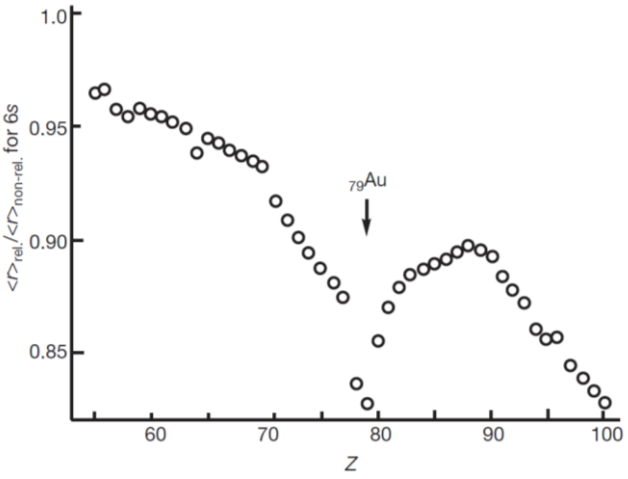

Figure 6. *$R_{rel.}/R_{non-rel.}$ vs Z.*

The firsts consequences of relativistic effects on gold properties are the elevated energy of ionization and the characteristic yellow colour due to the less energetic gap to excite electron in 5*d* orbitals. The absorption for gold excitation occurs in blue-light, while for the other metals is not in the visible band and therefore have a silver-grey colour.

Other consequences are more intrinsic and are deducted by comparison of reactivity with related metals copper (Cu) and silver (Ag) and through computational methods. Au(I) is considered a stronger Lewis acid than Cu and Ag and this was attributed to the great orbital contraction and higher electronegativity (2.54 Au vs 1.93 Ag vs 1.90 Cu); this consideration anyway results too simplistic.

Au(I) tend to do stronger σ bond with ligands than Ag(I), this was firstly analysed for AuH and AgH compounds and then extended to proper ligands as phosphine (Figure 7).

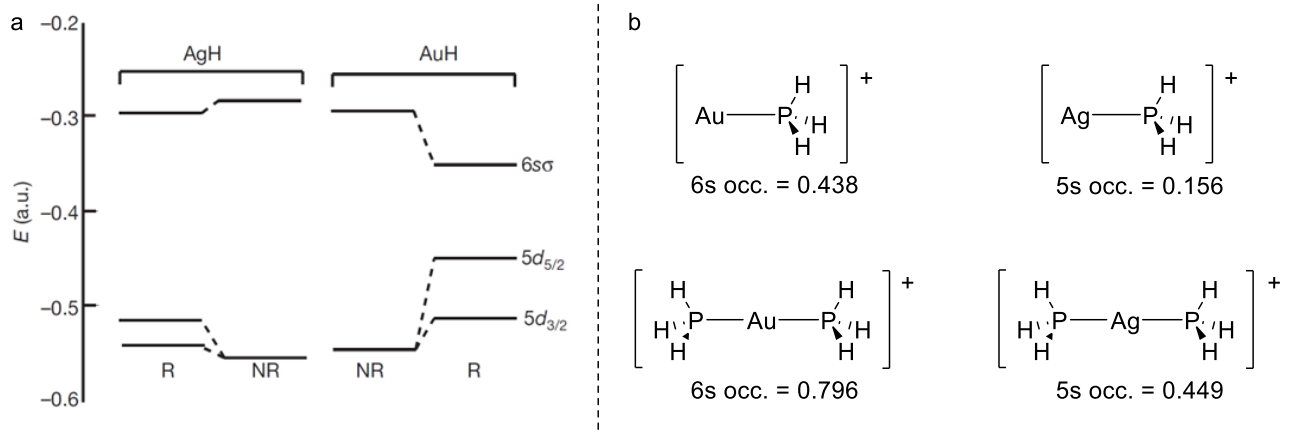

Figure 7. *a) AgH vs. AuH, calculated non-relativistic(NR) and relativistic(R) orbital energy; b) NBO population analysis for Au^+ and Ag^+ in different phosphine complexes.*

In Figure 7a the calculated molecular orbital energies of AgH and AuH are very similar if not considering the relativistic effect, but when they are taken in account, AuH has a far more stronger bond. This is a consequence of the Au atomic orbital 6s that is deeper in energy with respect of the 5s of Ag for the RE. This result was further confirmed by positive charge density which shows a 0.66 for Au and 0.86 for Ag, meaning the Au-H bond is way more covalent than Ag-H. Similar results were obtained comparing mono- and di-phosphine complexes (Figure 7b) by analysis of Natural Bond Orbital (NBO) population of the relative 6s and 5s atomic orbital. The results obtained for Au(I) are crucial in understanding his activation mode of electrophiles. Since the $[AuPH_3]^+$ has a large diffused charge shared by the metal centre and the phosphorus, the second ligand must be bounded by orbital interaction rather than charge attractions; this is highlighted by the NBO of $[Au(PH_3)_2]^+$ that shows a population of 0.796 in the 6s with a 3 centre 4 electron bond by rehybridization of the mono-phosphine Au(I) complex. This makes phosphine-Au complexes soft Lewis acids able to activate soft electrophile as π-systems (alkenes, alkynes and allenes).

Since the development of catalytic protocols, gold was defined as "alkynophilic" because it seemed to preferentially activate alkyne rather than alkenes. This is confirmed by catalysis results, but is not due to the preferential coordination of alkynes over alkenes; on the contrary, alkenes tend to make stronger coordination bond with Au(I) than alkynes (Table 1).[14]

	Au^+	
	C_2H_4	C_2H_2
$E_{int.}$	-79.1	-70.8
E_{Pauli}	157.2	161.0
$E_{el.stat.}$	-134.7	-134.1
$E_{orb.}$	-101.6	-97.8

Table 1. *Comparison between interaction energies ($E_{int.}$) of ethylene- and acetylene-Au(I) complexes; energies in kcal/mol.*

The special selectiveness of gold to alkynes is attributed to lowest unoccupied molecular orbital (LUMO) of the alkyne adduct, which is lower than alkene adduct by ~11.5 kcal/mol, and is more electrophilic for the addition of a nucleophile. This difference is clear in the cycloisomerization of 1,n-enynes, Figure 8.

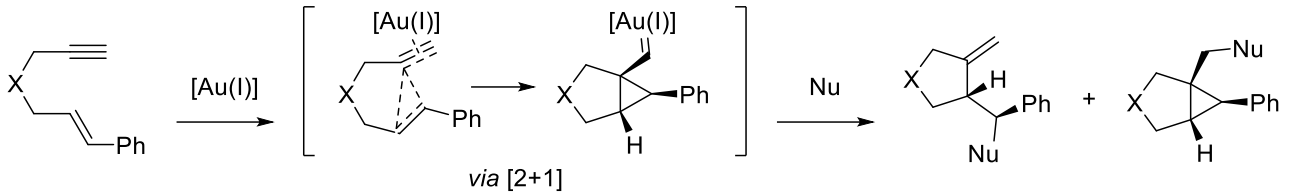

Figure 8. *1,6-enyne cycloisomerization catalysed by Au(I).*

In this example the gold catalyst can coordinate both alkyl and alkenyl moiety; however, for the previous discussion, when coordinated to the alkyne, the non-coordinated alkene acts as nucleophile to provide the [2+1] cycloadduct as intermediate, which in the presence of a further nucleophile gives the products. Further examples of this transformations will be shown in the next section.

To fully understand the coordination/activation mode of gold, the π-backbonding interaction has been evaluated, since this interaction plays an important role in TM catalysis. Calculation on the $[Au(I)CH_2]^+$ and $[Au(I)C]^+$ shows a multiple bond type interaction between gold and carbon, however, vibrational frequency of carbon monoxide (ν_{CO}) in $[Au(I)CO]^+$ is greater than free CO (2.194 cm^{-1} *vs* 2.143 cm^{-1}), suggesting only σ-bonding with no π-backbonding. These contradictory results agreed in the absence of π-backbonding from 5*d* orbitals to π* (too high in energy) but the existence of an interaction between 5d to a vacant p orbital (more accessible in energy). The stabilizing interactions led to two resonance intermediates (Figure 9).[15]

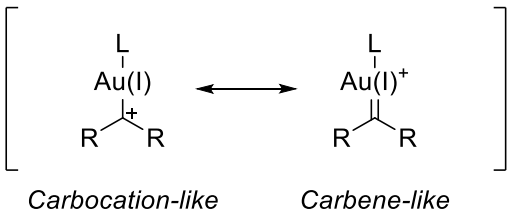

Figure 9. *Resonance limit structures of carbocation-like and carbene-like intermediates.*

The existence of the carbene-like intermediate finds evidences, besides computationally, in catalytic transformation. The cyclopropanation reaction in Figure 10 is a clear example.

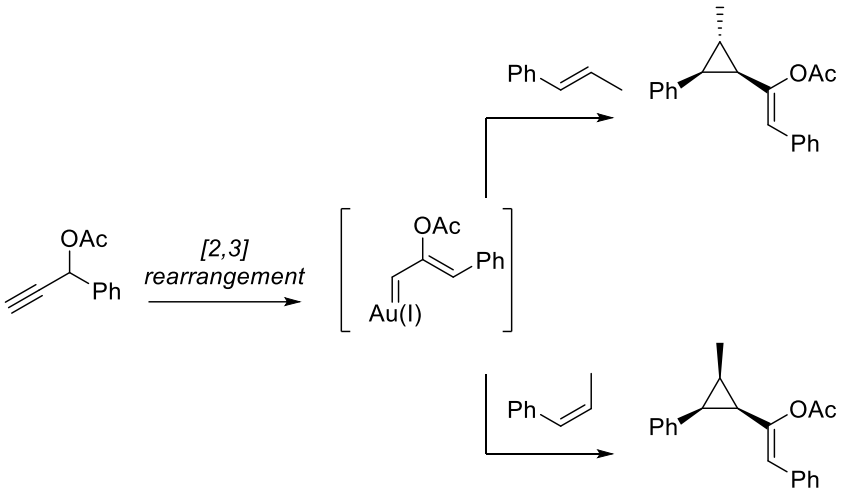

Figure 10. *Cyclopropanation reaction via carbene-like intermediate.*

The high diastereoselectivity observed in this transformation with the retention of the configuration of the β-methyl styrene are consistent with a [2+1] cycloaddition, which is a typical reactivity of

carbene intermediates. Although no X-ray structure has ever been analysed for such intermediates, theorical, mechanistic and reactivity observed are in accordance with the stabilization of gold by backbonding from 5*d* to empty *p* orbital.

1.4 Gold-catalysed reactions

After the very pioneering work on gold chemistry and a careful analysis on his peculiar properties, a more exhaustive discussion concerning catalytic transformations involving this precious metal is mandatory. Many reactions have been developed, across twenty years of research, employing the special reactivity of gold, these include: nucleophilic additions (including rearrangements and cycloisomerizations), oxidations and, more recently, cross-couplings.[16]

Gold-catalysed nucleophilic addition to C-C multiple bonds is one of the main applications firstly discovered and largely employed. Since Teles work in 1998,[8] mechanistic studies for the nucleophilic addition were proposed (Figure 11).

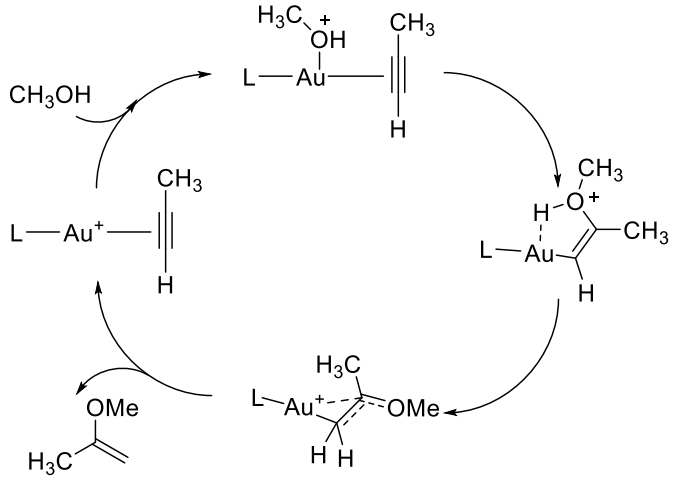

Figure 11. *First proposed catalytic cycle for the alkoxylation of alkynes.*

The proposed *cis*-alkoxylation however, was disproved by labelling experiment by Toste[17] and Hashmi.[18] These experiments (Figure 12) evidenced, by NMR $^{3}J_{CH}$, a clear *anti*-addition to gold, where the nucleophile approach the electrophile from the outer coordination sphere.

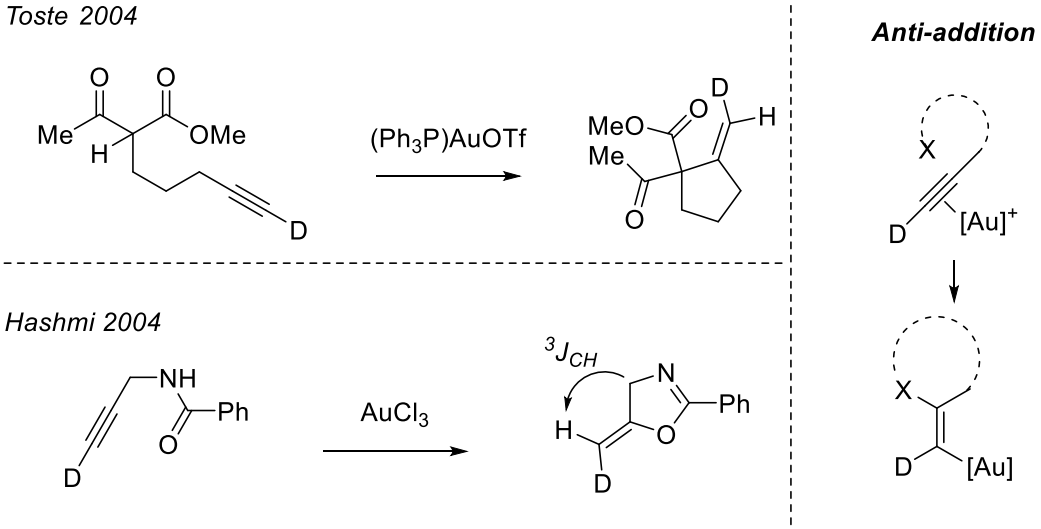

Figure 12. *Labelling experiments and proposed anti-addition mechanism.*

Therefore, the general activation of C-C multiple bonds, through nucleophilic addition is represented in Figure 13. The functional groups that undergo this activation are: alkenes, alkynes and allenes.

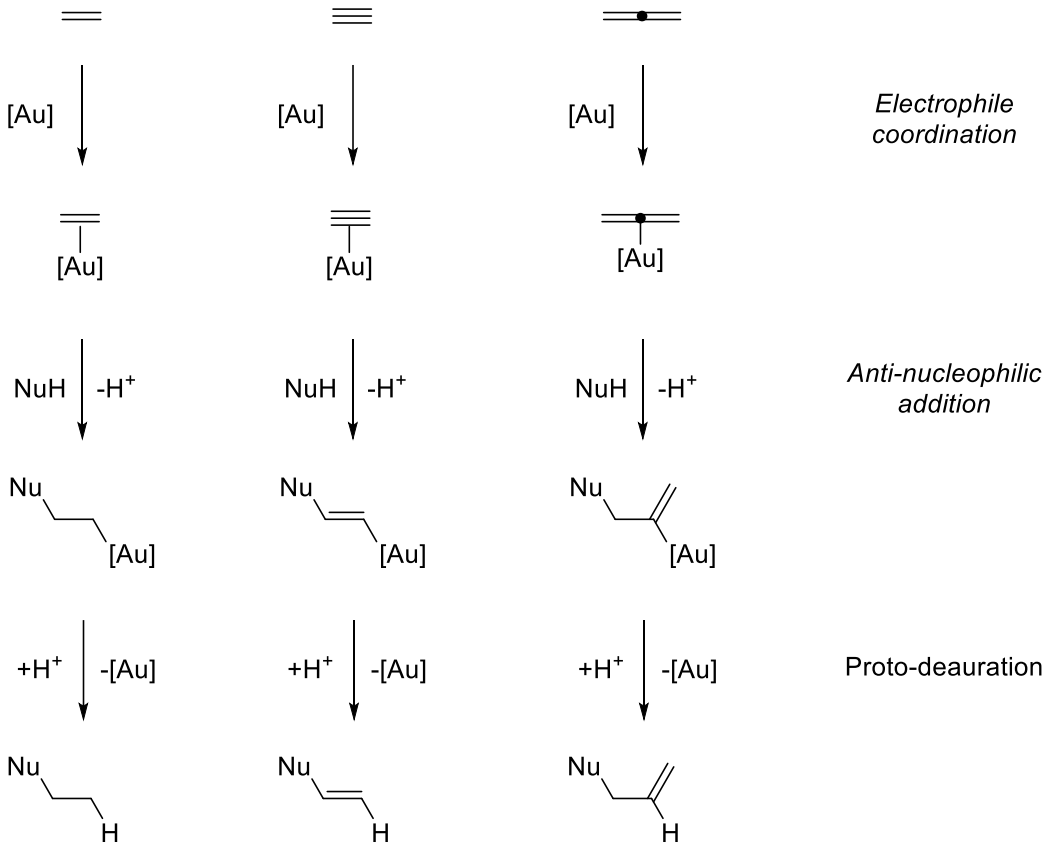

Figure 13. *Representative activation of alkenes, alkynes and allenes. [Au]=Au(I) or Au(III). Nu=N, O, C or S based nucleophiles.*

Nucleophilic addition to alkenes

Despite the less electrophilic behaviour, as described in Paragraph 1.3, alkenes can undergo nucleophilic attack.
This reactivity can be divided in two main types of alkene: non-activated and activated alkenes.

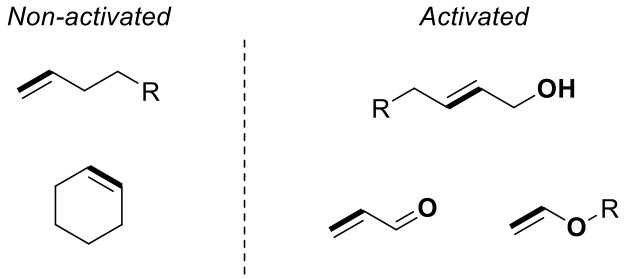

Figure 14. *Examples of non-activated and activated alkenes.*

The very first evidence of nucleophilic addition to an alkene was observed by Hashmi at the beginning the 2000's,[19] where the intermediate generated by a cascade reaction is further attacked by the remote hydroxyl group, leading to the spirocyclic compound (Figure 15).

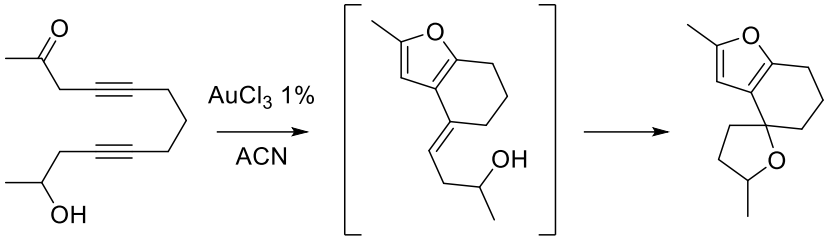

Figure 15. *First evidence of gold-catalysed nucleophilic addition to an activated alkene.*

Reactivity of activated alkenes was further extended and also α,β-unsaturated ketones are suitable to undergo nucleophilic addition at room temperature.

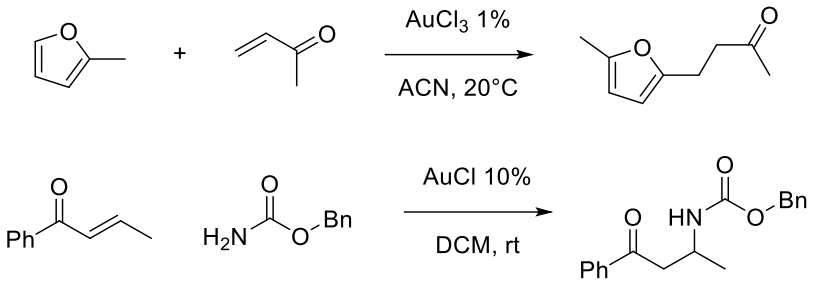

Figure 16. *Gold-catalysed Friedel-Craft[19] and aza-Michael reactions with enones.[20]*

Other kind of activated alkenes are the terminal allyl alcohol. This moiety in presence of dinuclear gold catalysts is able to eliminate water upon nucleophilic addition of indole (Figure 17).[21]

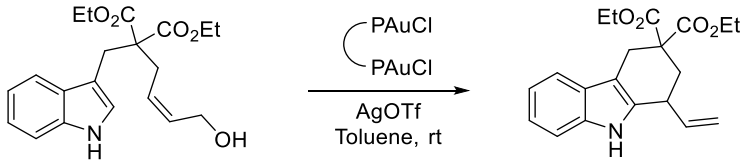

Figure 17. *Intramolecular gold-catalysed allylic alkylation.*

Less electrophile alkenes undergo to nucleophilic addition by N-, O-, C-nucleophile as well but usually requires higher temperature to observe satisfying results (Figure 18).

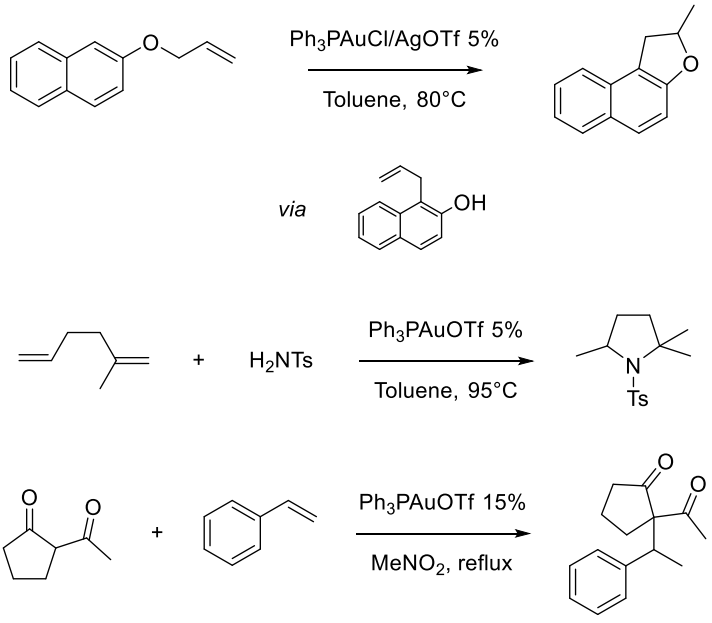

Figure 18. *Gold-catalysed O-,[22] N-[23] and C-[24] nucleophile addition to alkenes.*

Nucleophilic addition to alkynes

Alkynes are the most employed functional group in gold catalysis, in fact it can react as simple electrophile for nucleophilic addition, participate in rearrangement and cycloisomerization reactions. Complexity of substrates and products can variate significantly. Common test-reactions of new catalysts are the hydroamination and hydroalkoxylation reactions of terminal alkynes.

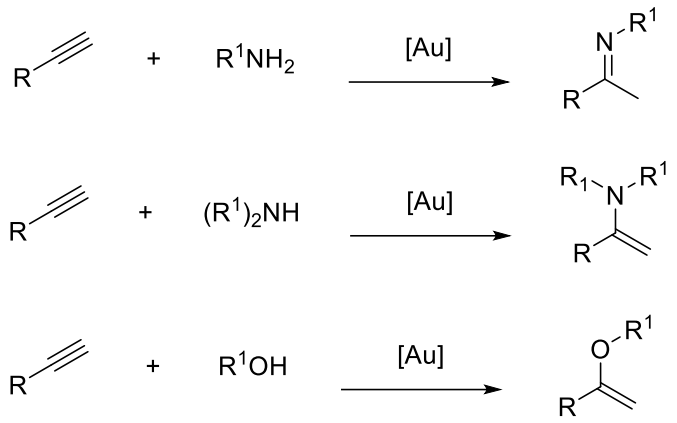

Figure 19. *Hydroamination and hydroalkoxylation of terminal alkynes.*

Reactivity works wonderfully in both intra- and inter-molecular fashion, leading to product with high synthetic value.[25] At the initial stage, simple alkynes were employed, as terminal alkynes or internal alkynes, but with development of organic chemistry specially activated alkynes emerged and their reactivity with gold catalysts is exhaustively summarized by Gagosz.[26]

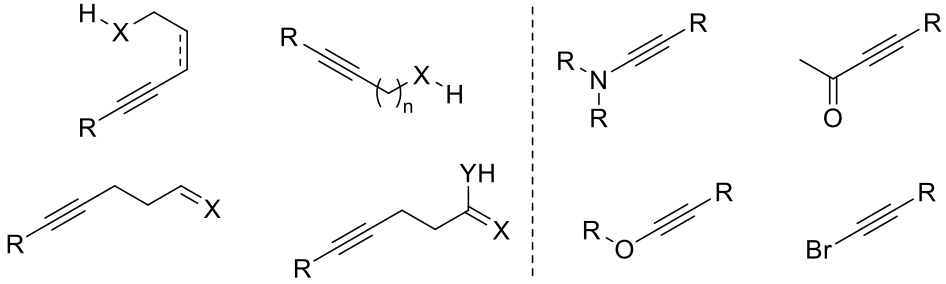

Figure 20. *Common alkynyl substartes (left) and specially activated alkynes (right).*

Gold-catalysed rearrangement

Gold can also catalyse a great number of rearrangement reactions starting from a nucleophilic addition to alkynes, including rearrangement of propargylic esters (Figure 21).

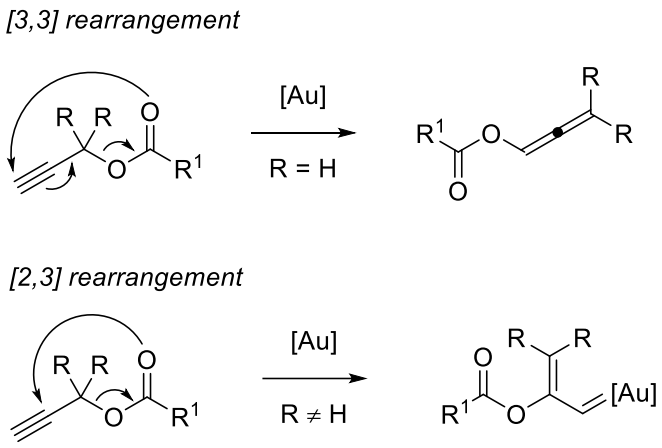

Figure 21. *[3,3] vs. [2,3] rearrangement.*

In case of [3,3] rearrangement, that is observed in absence of R substituent (R=H), allenoate product are obtained and can be isolated, if stable, or in presence of nucleophile react further (Figure 22 top).[49b] On other hand, when at least one R is different from hydrogen, [2,3] rearrangement is observed. The second process is catalysed as well by gold, but the metal is trapped in the product of rearrangement. These products are described as carbene-like and have a great synthetic value in the cyclopropanation reaction of alkenes (Figure 22 bottom).[59]

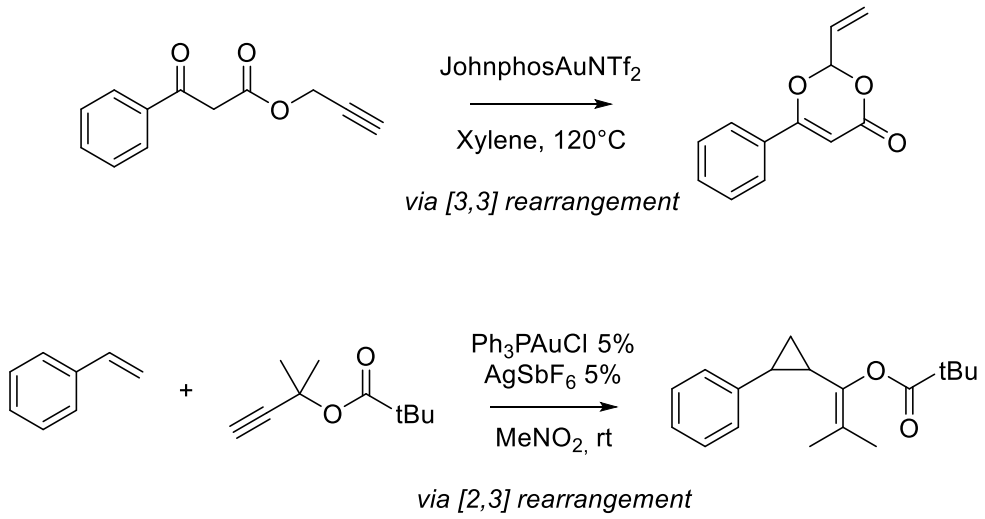

Figure 22. *Examples of rearrangement involving gold-catalysed reactions.*

Cycloisomerization reactions

Another class of reactions that can be achieved by gold catalysis are the cycloisomerizations and in particular the cycloisomerization of 1,n-enynes,[27] which can lead to highly complex molecule occurring in natural products. Several metals are able to activate these substrates, however gold provided excellent results under milder conditions.

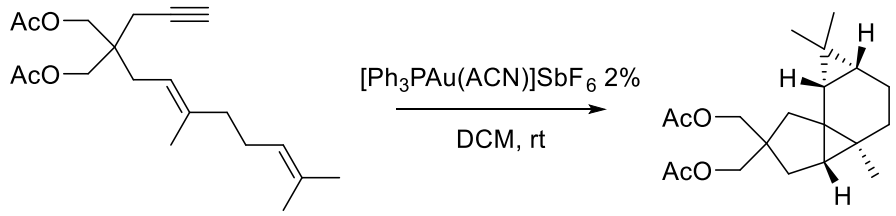

Figure 23. *Example of high complexity product obtained from enyne cycloisomerization.*

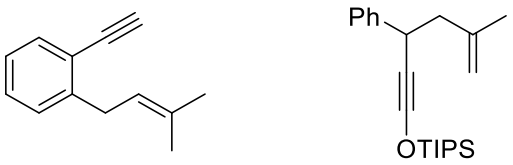

Figure 24. *Example of 1,6-enyne (left) and 1,5-enyne (right).*

Reactivity and most importantly the selectivity of products obtained by this catalytic transformation is strongly influenced by the metal employed, the substituents on alkene moiety and presence or not of an external nucleophile. Experimental results and calculations have provided across time a roadmap to of possible products.[28,29]

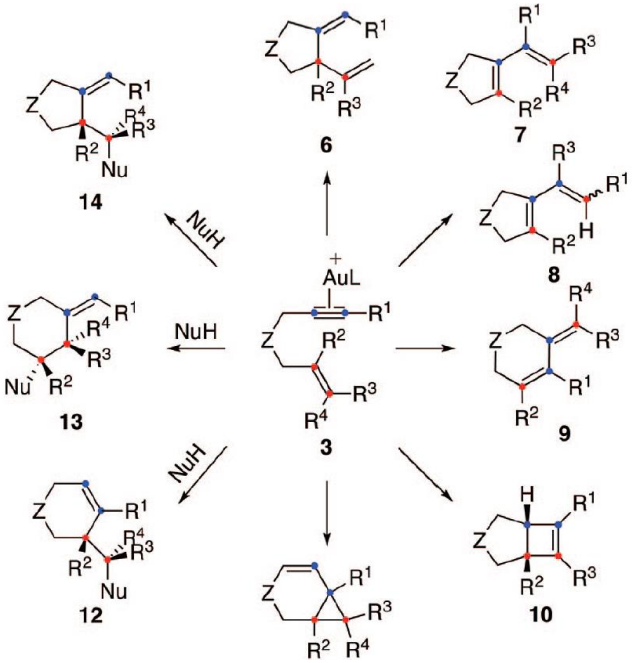

Figure 25. *Possible wheel of products by enyne cycloisomerization.*

1.5 Carbene ligands

Ligands employed in gold(I) chemistry are in most cases carbenes or phosphorus ligands. Some notes regarding P-ligands will be discussed in comparison with carbene ligands and other dedicated notes in Paragraph 3.1 and 4.1.

A carbene is a divalent carbon atom with two electrons that are not shared. Carbenes may exist in both triplet and singlet state which are influenced by steric and electronic properties.

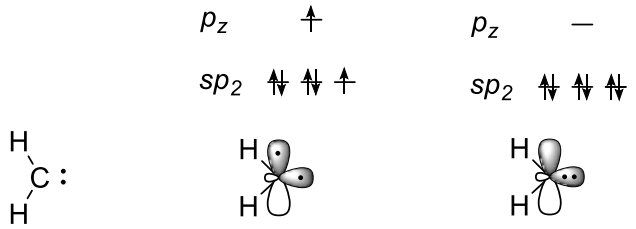

Figure 26. *general representation of carbene (left), carbene triplet (middle) and carbene singlet (right).*

These species are highly reactive as free radical and undergo dimerization and decomposition. The first to isolate a free-carbene compound was Arduengo in the 1991 by deprotonation of IAd precursor.[30] Despite their high reactivity as free-radical, when coordinated to transition metals, carbenes are highly useful tools and can be used in organic transformation. An example of synthetically useful TM-carbene compound is the Tebbe's reagent (Figure 27) that is used for the synthesis of vinyl ethers form the corresponding esters or as replacemet of Wittig procedure for hindered ketones.

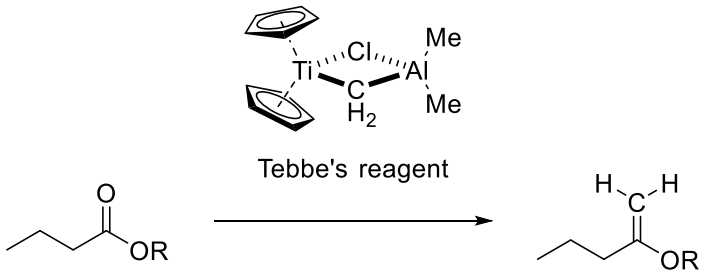

Figure 27. *Tebbe's reagent and general example of its application.*

More than as reagent, carbenes found huge utility as ligands for TM catalysis and two examples are below.

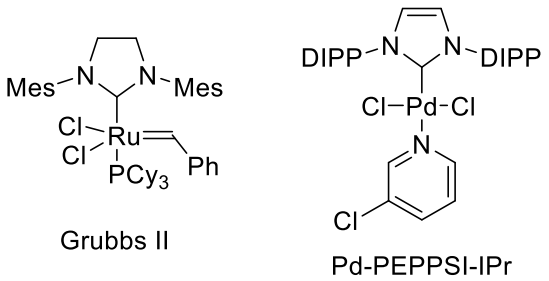

Figure 28. *Relevant TM-carbene catalysts.*

The great success of carbenes as ligands and in particular N-heterocyclic carbenes (NHC) relies in the properties of the ligands. NHC are cyclic carbenes where the two atom adjacent to the carbonic carbon are nitrogen. The two lone pair of nitrogen stabilize, by orbital interaction, the empty *p* orbital

of carbon, which results more electron rich and therefore is able to make strong σ coordination bonds with transition metals. [31,32]

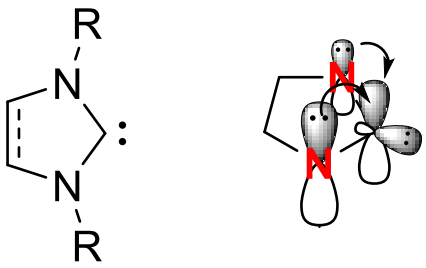

Figure 29. *General structure of NHC (left) and stabilizing orbital interaction (right).*

This strong σ bond make NHC-Au(I) complexes, and relative cationic catalytic active species, more stable to dissociation and degradation with respect to phosphorus ligands. On the contrary, this stabilization by π donation from nitrogen to empty orbital decrease significantly the M→L π-backbonding and results in less acidic and then less active Au(I) cation through scarcely activated C-C multiple bonds.

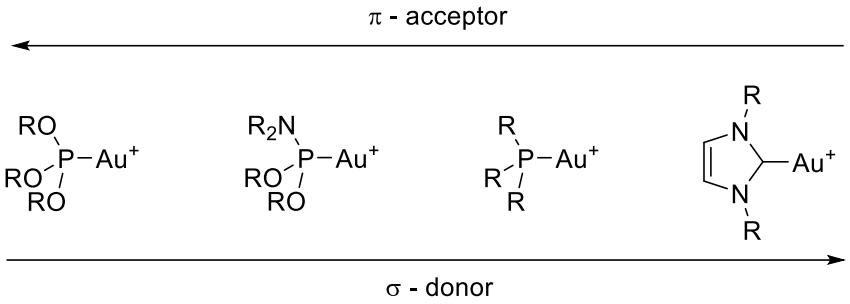

Figure 30. *Comparison of σ-donor and π-acceptor properties of phosphorus-based ligands and NHCs.*

When activated substrates are used the NHC donating properties play an important role to the stabilization of reaction intermediates or activation mode of electrophile. A clear example of divergence achieved by different ligands is reported below.[33]

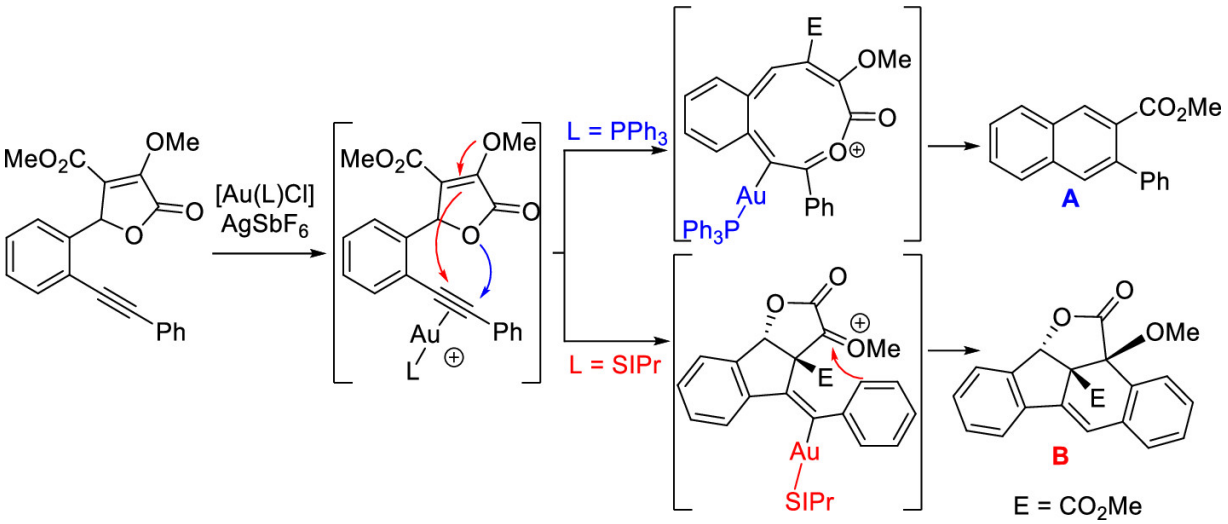

Figure 31. *Divergent selectivity obtained with phosphine ligand (top) and NHC ligand (bottom).*

The unique properties of NHC ligands do not relies only in the stability of complexes and different selectivity in catalytic transformations, but also in their great tunability of electronic and steric

parameters *via* facile synthetic procedure. Both electronic effect and steric hinderance can be quantified by Tolman electronic parameter (TEP, described as the frequency of CO stretching)[34] and the buried volume (%V_{bur} the volume occupied by ligand in the sphere around the metal)[35].

The most commons NHC ligands are the ones the derivate from the imidazole, its saturated form and benzimidazole.

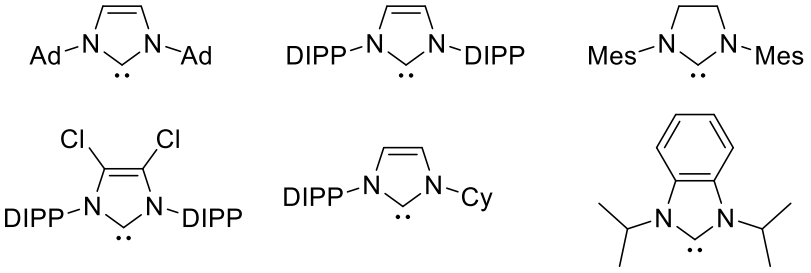

Figure 32. *Some exemplificative representation of common NHC ligands.*

With the explosion of interest in NHC ligands for Au(I) chemistry, researchers also explored NHC with larger ring.[36,37] These ligands resulted more electro-donating respect to 5-memebered and with an higher steric hinderance, which correlated well with the full conversion time in Figure 33.

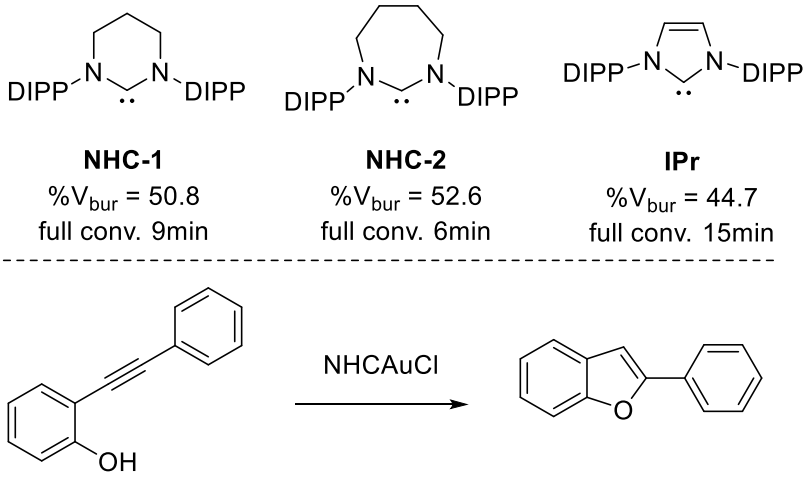

Figure 33. *Comparison of 6- and 7-membered ring NHC.*

Other NHC of relevance in Au(I) catalysis are the cyclic(alkyl)(amino)carbene (CAAC) and principal architectures of these ligands are reported below (Figure 34). One nitrogen atom is replaced by a quaternary carbon, and this substitution has significant effect on the electronic of the ligand, resulting better σ-donor and better π-acceptor by decreasing of both HOMO and LUMO energies of the carbenic carbon.[26]

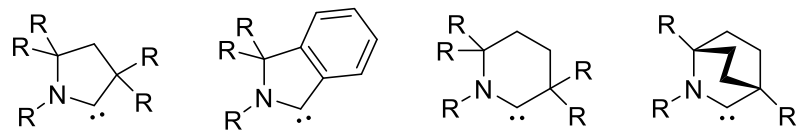

Figure 34. *General architectures of CAAC ligands.*

Last family of carbene ligands is the acyclic diamino carbenes (ADC). These ligands have higher NCN angle compared to common NHC due to the absence of ring constraints.

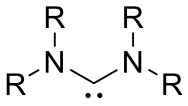

Figure 35. *General structure of ADC.*

Hashmi and co-worker, developed an extremely facile way to synthesize new ADCs where on each nitrogen an hydrogen substituent is present.[38] This procedure was robust and allowed the synthesis of a large library of both symmetric and asymmetric substituted ADC-Au(I), reaching an elevated number of catalysts in a very short time.

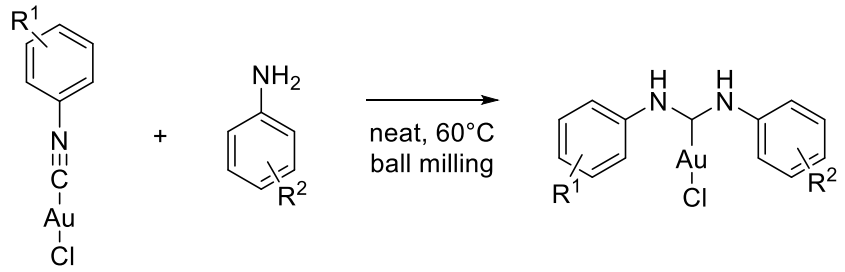

Figure 36. *Efficient synthesis of ADC-Au(I) complexes.*

2. New imidazo[1,5a]pyridine-based NHC-Au complexes

2.1 Introduction: the ImPy scaffold

As already shown in Paragraph 1.5 carbene ligands raised a great interest in the TM chemistry including gold as well. In the family of the NHCs, the most employed are the derivatives from imidazolium and benzimidazolium salts. In 2005, two independent groups led by Glorius[39] and Lassaletta[40], respectively, developed a new highly modulable NHC scaffold, the imidazo[1-5a]pyridine (ImPy, Figure 37).

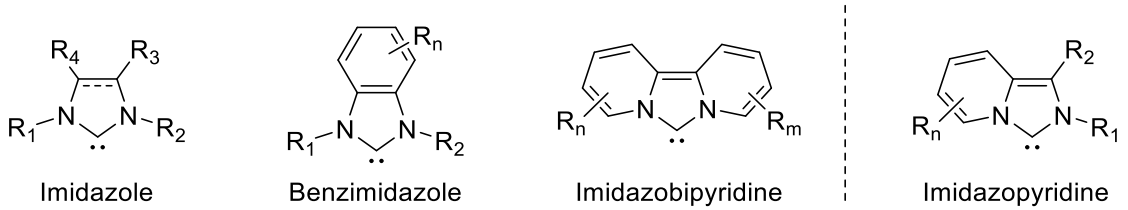

Figure 37. *General representation of various NHC scaffold; ImPy scaffold on the right.*

The early synthetic routes are illustrated in Figure 38. The precursor salts could be obtained by the alkylation on the nitrogen with primary halides, but this methodology is restricted to a limited number of substrates (top left). Thus, a more versatile strategy, passing through pyridine-2-methyl formamides, allows the synthesis of bulkier *N*-functionalised ImPy (bottom left). Glorius, on the contrary, proposed a deeper retrosynthetic analysis, and with that strategy was able to achieve a variety of ligand precursors (right).

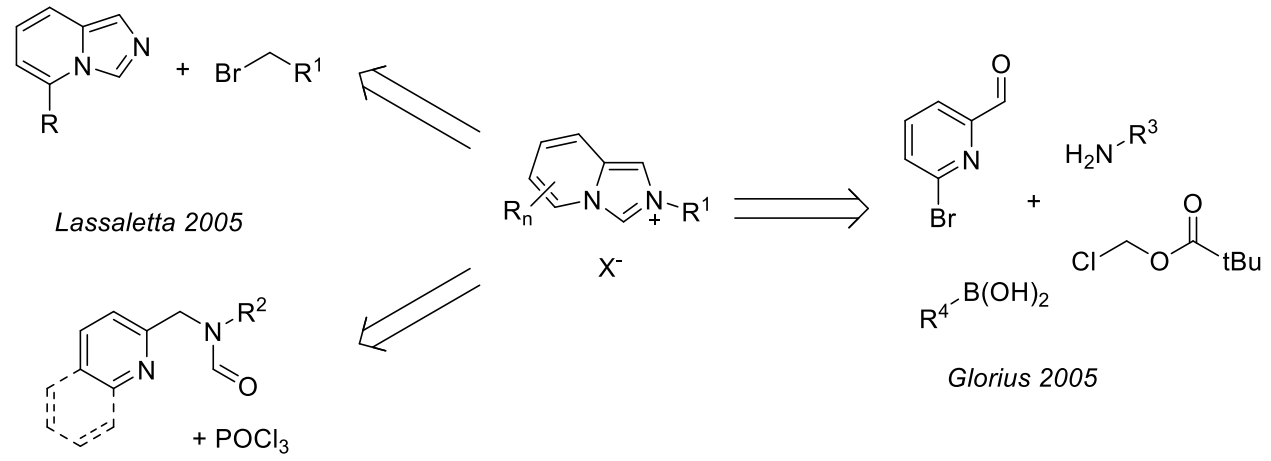

Figure 38. *General retrosynthetic strategy adopted by Lassaletta and Glorius. R = H, Me; R^1 = H, Ph; R^2 = tBu; R^3 = Mes, R^4 = vinyl, aryl.*

With these ligands in hands, they were able to prepare the very first ImPy-TM complexes with Rh and Pd. In particular, the Pd(II) complexes obtained by Glorius, were also tested in cross-coupling reactions (Figure 39) with moderate to good yields (Table 2).

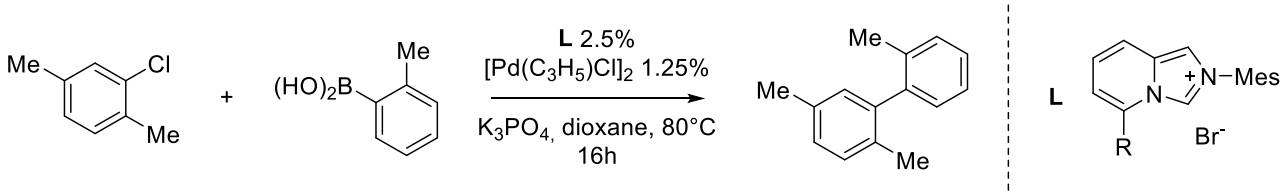

Figure 39. *Cross-coupling reaction involving ImPy-Pd(II) complexes.*

Entry	L	Yield
1	R = H	(<10)
2	R = Me	(38)
3	R = Ph	(39)
4	R = OMe	(34)
5	R = styryl	(22)
6	R = 9-phenantrhyl	86
7	R = 2,6-dimethoxy phenyl	(67)

Table 2. *In brackets yields by GC-MS.*

From their discovery to date, more than 200 ImPy-TM crystal structures have been deposited in the Cambridge Crystallographic Data Centre (CCDC), suggesting that the number of complexes synthetized is even higher.

2.2 ImPy-Au(I) complexes: the background

As already elucidated in Paragraph 1.5, carbenes are suitable for synthesis of gold complexes due to their resulting high robustness. After the development of the new family of ImPy ligands, gold chemists started to use it to achieve new catalysts with very interesting properties. In the CCDC database around 50 structures of gold-ImPy complexes have been deposited, including both Au(I) and Au(III).

The first report of ImPy-Au complexes was in 2010, from Fürstner.[41] He carried out an interesting research not only to test the new catalysts but also to investigate the electronic properties of the ligands and their impact on the catalytic results (Figure 40).

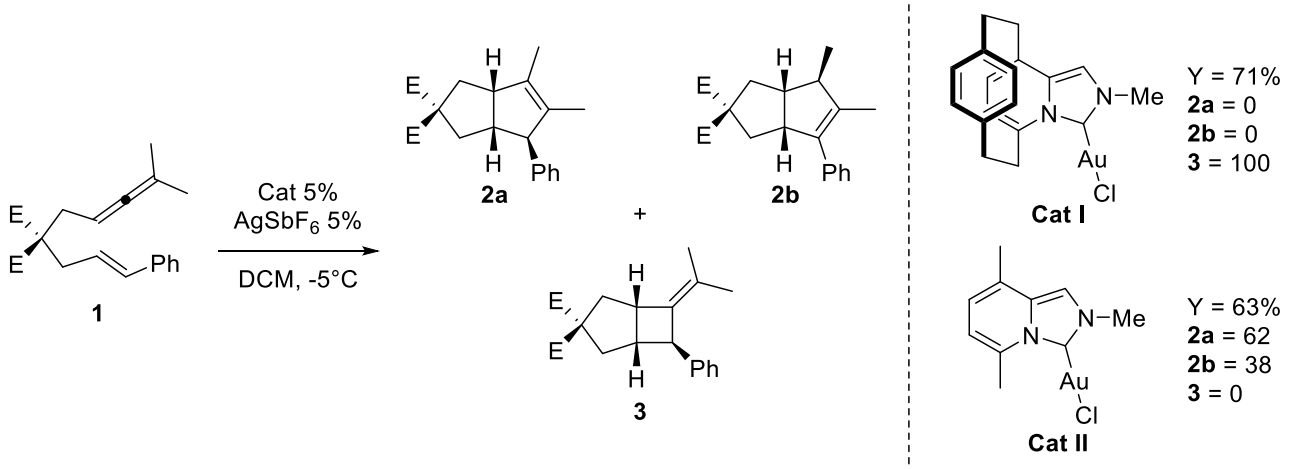

Figure 40. *1,6-eneallene cycloisomerization catalysed by Au(I) complexes.*

The two catalysts are both active through the activation of the substrate but they are selectively divergent in the product distribution. **Cat I** with the paracyclophane structure is selective for the 4-exo-dig cyclization, while **Cat II** is selective for the 5-endo-dig products. The differences of selectivity are attributed to the electronic properties of the two ligands. The more electron rich **Cat II** stabilizes better the intermediate **Int. IIIa** and then by a 1,2-methyl shift lead to **2a** and **2b** products (Figure 41). On the contrary, **Cat I** is more electron deficient, due to the π-π interaction of cyclophane,

so does not provide **Int. IIIa** but **Int. II** instead, with consequent production of **3**. The electronic nature of the ligand is evaluated by the computational calculation of the energy of the electronic doublet on the carbenic carbon (E_σ) and the empty *p* orbital (E_π). While E_σ is almost identical for both ligands, difference of E_π is more significant, -0.63eV for the ligand of **Cat II** and -1.14eV for the ligand of **Cat I**, and this explains the selectivity for the generated intermediate.

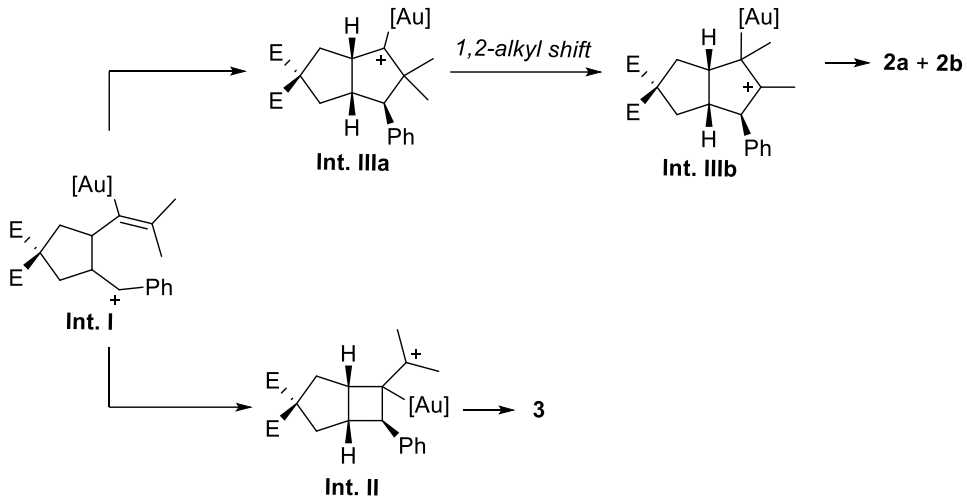

Figure 41. *Comparison of the two possible mechanistic pathways depending on ligands nature.*

Subsequently to these interesting findings, different researchers started to produce library of ImPy-Au(I) complexes to better understand the efficacy of these ligands. In particular, researches were focused on a particular sub-family of ImPy ligands (Figure 42).

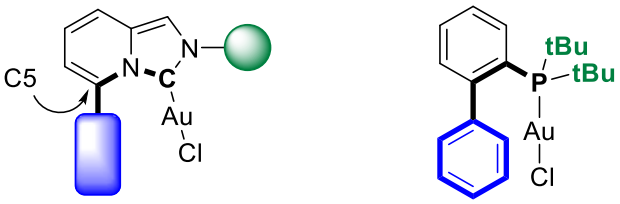

Figure 42. *Analogies between C5-substituted ImPy and Buchwald phosphines (Johnphos).*

This general scaffold has two main positions where modifications are of great interest and importance. In fact, the architecture of this ligand resembles the structure of the Buchwald-type phosphines. The spacing between the carbenic C atom and the substituent in C5-position is the same found between P and the phenyl ring in *ortho* position (black and bold). Additionally, the functionalization on the imidazolic nitrogen acts as steric hindrance and provides rigidity as the alkyl group on phosphorus (green). Finally, the possibility to install functional groups at C5 position of the pyridine ring allows ligand to establish interaction with the near gold metal centre, whereas, in the case of *ortho*-biaryl phosphines, to this interaction are attributed both stabilizing and activity effects (blue).

A clear view of these similarities is represented in Figure 43, where a crystal structure of ImPy-Au(I) complex, by Lee,[42] is compared to the structure of JohnphosAuCl.[43] As it emerges by comparison of the two complexes, the similarities are evident for the spatial arrangement of the whole fragments of the molecules. ImPy complexes generally possess a higher angle between the C5 pendant and the carbenic C with respect to the Johnphos, this is intrinsic to the fused imidazolium ring. However, the angle is not that high to avoid the π-interaction between the aryl ring and the Au(I) centre and therefore is observed also in this specific group of ImPy complexes.

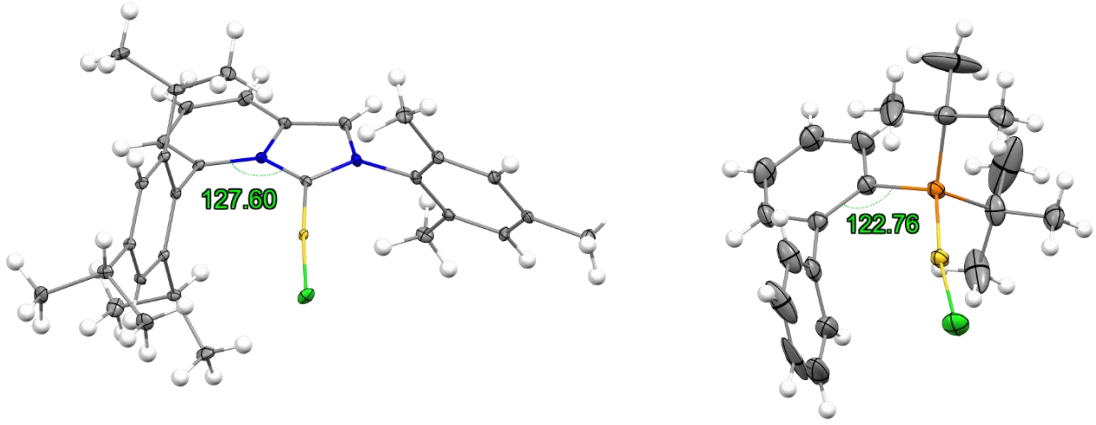

Figure 43. *Structures obtained by SC-XRD of an ImPy-Au(I)Cl and JohnphosAuCl complexes. Angles measured by Mercury.*

Lassaletta & co-workers, after the development of the earliest ImPy ligands, focused their attention on the synthesis of chiral derivatives.[44] The synthetic strategy is straightforward and start from **4**, or **6**, by Pd-catalysed cross-coupling, or aldehyde reduction, to provide alcohol **5** which is converted in the corresponding bromide **7.** The chiral moiety is introduced by the SN_2 of the *N*-(pyrrolidinyl)formamide **8** promoted by base. Imidazopyridinum salt is obtained by cyclization of **9** in presence of $POCl_3$ or triflic anhydride. Gold complexes **Cat III** are obtained by common two step synthesis by transmetallation from silver complexes.

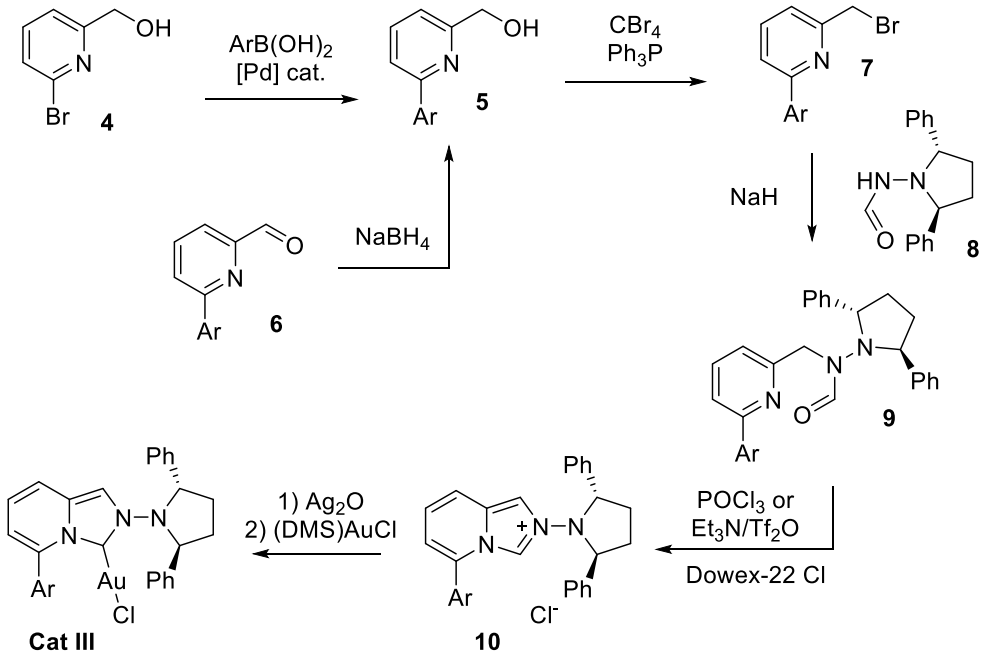

Figure 44. *Synthetic strategy adopted for the synthesis of chiral complexes* ***Cat III****.*

With this strategy the authors were able to obtain all the corresponding complexes of the coinage metals (Cu, Ag, Au) with different substitution at the C5 position (Ar = Ph, 4-F-C_6H_4, 4-OMe-C_6H_4, 4-tBu-C_6H_4, 3,5-$(CF_3)_2$-C_6H_3, 2,6-$(OMe)_2$-C_6H_3, Mes, 2,4,6-$(Me)_3$-C_6H_2). The crystallographic studies of Au(I) complexes show in all structures a high percentage of buried volume (%V_{bur}), the highest recorded for NHC ligands at that time.

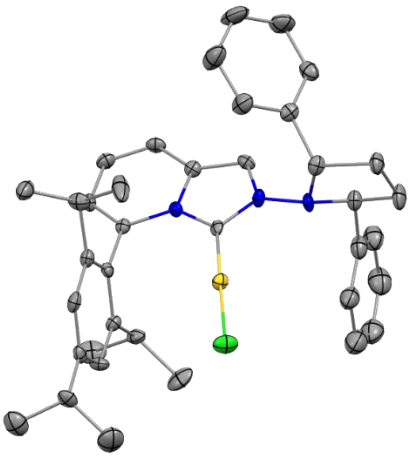

Figure 45. Cat III *with Ar = 2,4,6-(Me)$_3$-C$_6$H$_2$. %V$_{bur}$ = 51.1 .*

Despite the efficient synthesis of these complexes, no application has been made with them.

Similar results in terms of %V$_{bur}$ were obtained by Michelet and her collaborators few years later. Instead of placing an aryl unit at the C5 position, they selected a more polar barbituric derivate (Figure 46).[45]

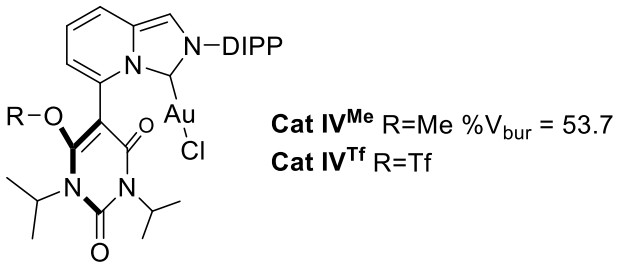

Figure 46. *The two Au(I) complexes with different R substituent. DIPP = 2,6-diisopropyl phenyl.*

With these new complexes in hand they looked for application in catalysis to evaluate their activity. Different benchmark reactions were selected: hydroamination of terminal alkynes, addition of carboxylic acids to terminal alkynes and cycloisomerization reaction with a variety of nucleophiles. During this catalytic activity screening, catalysts **Cat IV** were also compared with common commercially available imidaziolium derived Au(I) complexes (IMesAuCl, IPrAuCl) and the results are summarized in the following Figure 47. While **Cat IV^{Tf}** doesn't provide enthusiastic results, **Cat IV^{Me}** led to the desired products with high yields even at very low catalyst load (from 0.01% to 1%). Comparing **Cat IV^{Me}** with benchmark NHC-Au(I) showed a remarkable superior activity in the cycloisomerization reactions, proving that ligands containing an ImPy scaffold can be successfully utilized in gold catalysis.

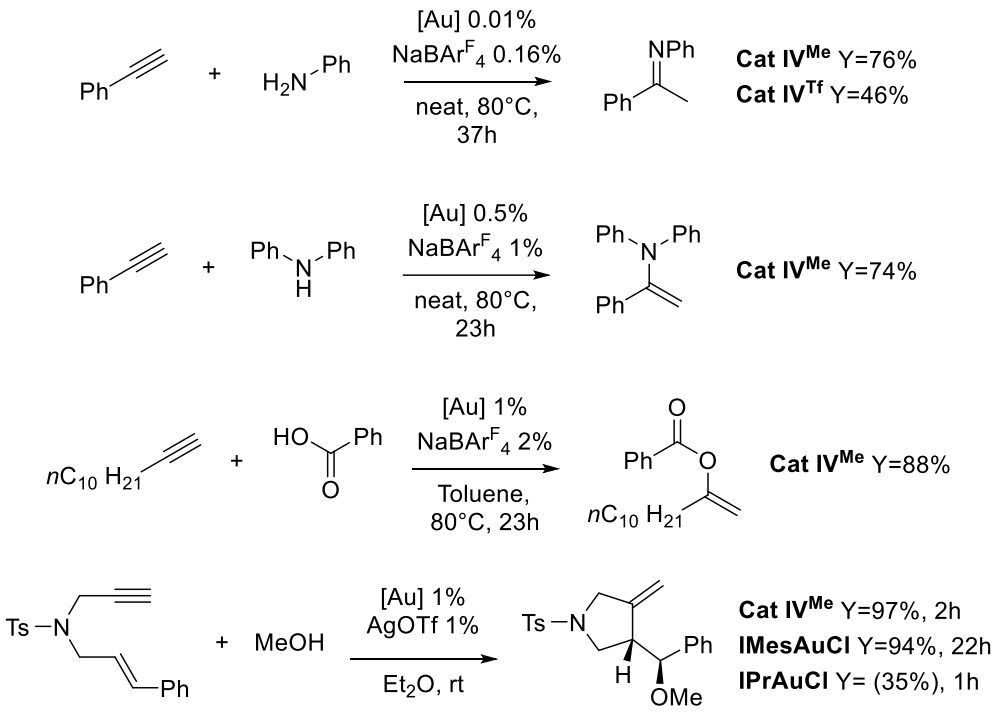

Figure 47. *Catalytic application and condition for* ***Cat IV^{Me}*** *and* ***Cat IV^{Tf}****.*

The research group of Liming Zhang for many years has worked on the synthesis of bifunctional ligands to be used in gold catalysis. In particular they focused the attention on bifunctional phosphines, chiral and not, bearing a remote basic moiety (e.g. amines, amides) to enable H-bonding interaction with the substrate in order to facilitate the catalytic process (Figure 48).[46,47]

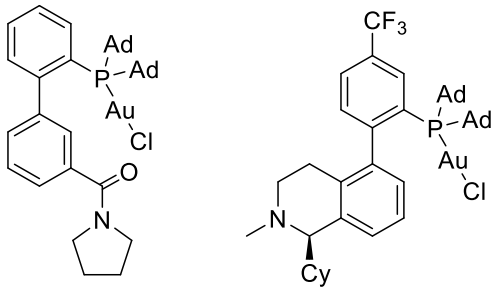

Figure 48. *Two ortho-biarylphosphine Au(I) catalysts synthetised by Zhang.*

Concomitantly with the development of the chiral phosphines, they also investigated the emerging ImPy scaffold as ligand for the synthesis of chiral ImPy-Au(I) complexes (Figure 49).[48]

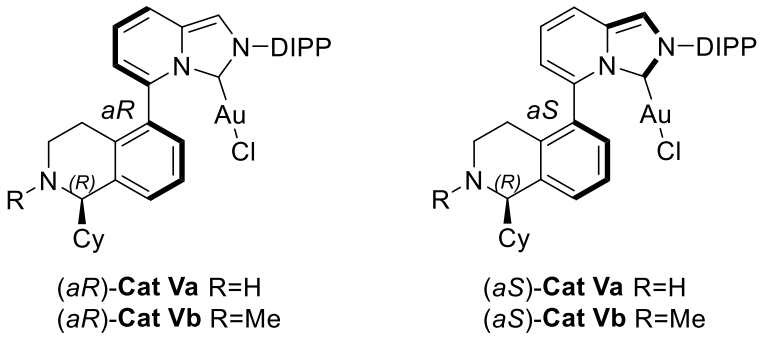

Figure 49. *Four bifunctional catalysts with two stereogenic elements.*

The two axial diasteroisomers are obtained during the synthetic step of complexation with gold (Figure 50) but they can be easily separated by normal flash chromatography purification.

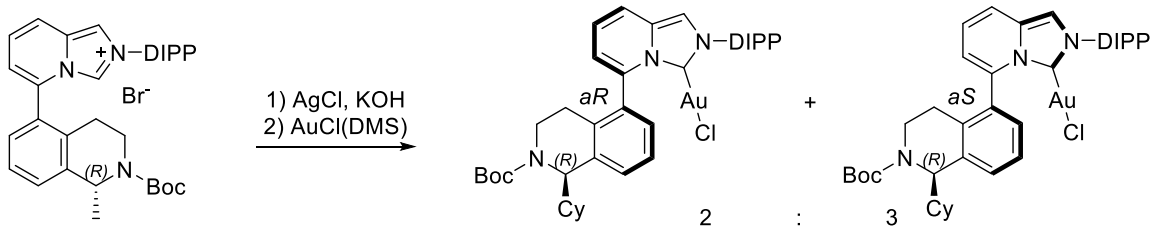

Figure 50. *Complexation with gold and generation of the two axial diastereoisomers.*

The authors were curious about the rotational flexibility of the chiral axis and therefore they carried out ^{1}H NMR experiments to verify it. The experiment was done for both diasteroisomers of **Cat Va** and they found that rotation of the axes is possible and the (*aR*)-**Cat Va** is the most stable. Under catalytic condition (*aS*)-**Cat Va** isomerize almost quantitatively to the *aR* in 24 hours, while (*aR*)-**Cat Va** does not. On the contrary, solutions of only catalysts without any reactant, reach a ratio of 2:1 in favour of (*aR*)-**Cat Va** independently of which is the starting diasterisomer. The rationalization behind this observation is that in *aR* epimer the spatial arrangement of the complex allows the cationic gold stabilization by interaction with amine. Further details of these experiments can be found at reference paper.[47]

Catalytic application of these catalysts finds high reactivity but the enantioselectivity is strongly dependent on the type of reaction (Figure 51). Moreover, in some cases (*aS*)-**Cat Va** proved to be better in enantioselective terms, because this configuration of the axis displays the cyclohexyl near the catalytic site providing an efficient chiral pocket.

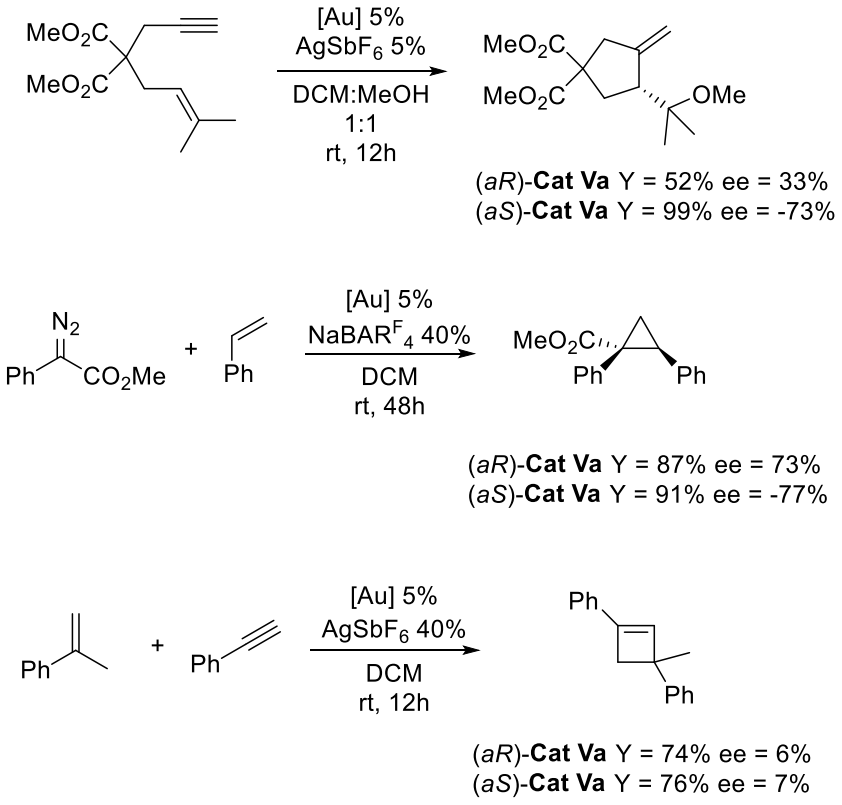

Figure 51. *Some examples of asymmetric transformations using chiral ImPy-Au(I) catalysts.*

2.3 Abstract

In line with our interest in gold(I)-catalysed organic transformations[49] and the rising of interest in the synthesis of new ligands by gold chemists, we wanted to further explore the applicability and properties of ImPy-Au(I) complexes. In particular we were interested on the effect of secondary L-M interactions on the catalysis. For the purpose, a new family of ImPy gold(I) complexes have been synthetized and the full characterization in both solid state and solution is presented. Furthermore the combination of catalytic results and DFT calculations provide a proof of the activating role of these interactions.[50,51]

2.4 Ligands design and synthesis

In order to carefully investigate the role of secondary interactions in gold catalysis, the ligand design process is crucial. In our case, as shown in Figure 52, we selected the ImPy scaffold as NHC ligand bearing the 2,6-diisopropyl phenyl on the imidazole ring. These two moieties are unchanged in all the new catalysts to provide the same steric hindrance and binding mode. The portion that will be changed is the substituent at the C5 carbon of the pyridine ring, where a series of different aryl and oligo-aryl groups are placed in order to investigate their interactions with the metal centre.

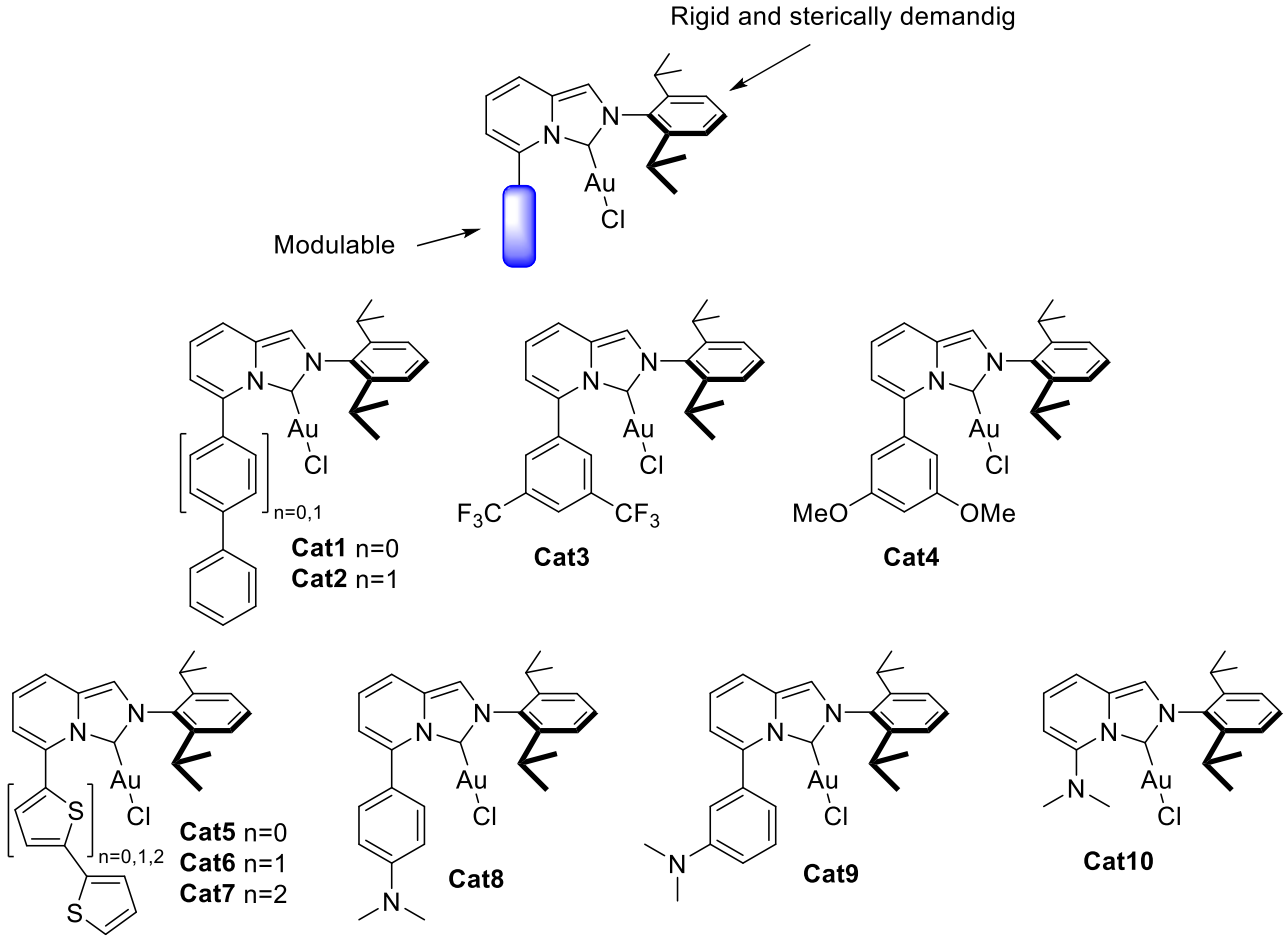

Figure 52. *Ligand design approach for development of new catalysts (above); complexes developed (down).*

For the synthesis of these complexes different methodologies are applied and discussed case by case. In literature are known various synthetic strategies and the main two that are feasible for our aim are represented in Figure 53. Path A and path B provide both the desired ImPy scaffold, the chemical

transformations are the same but in different order which let the operator flexibility to adopt one or the other, in case of incompatibility of the functional groups. Path A was followed for the synthesis of **Cat1-6** and **Cat10**, path B was followed for **Cat7-9**.

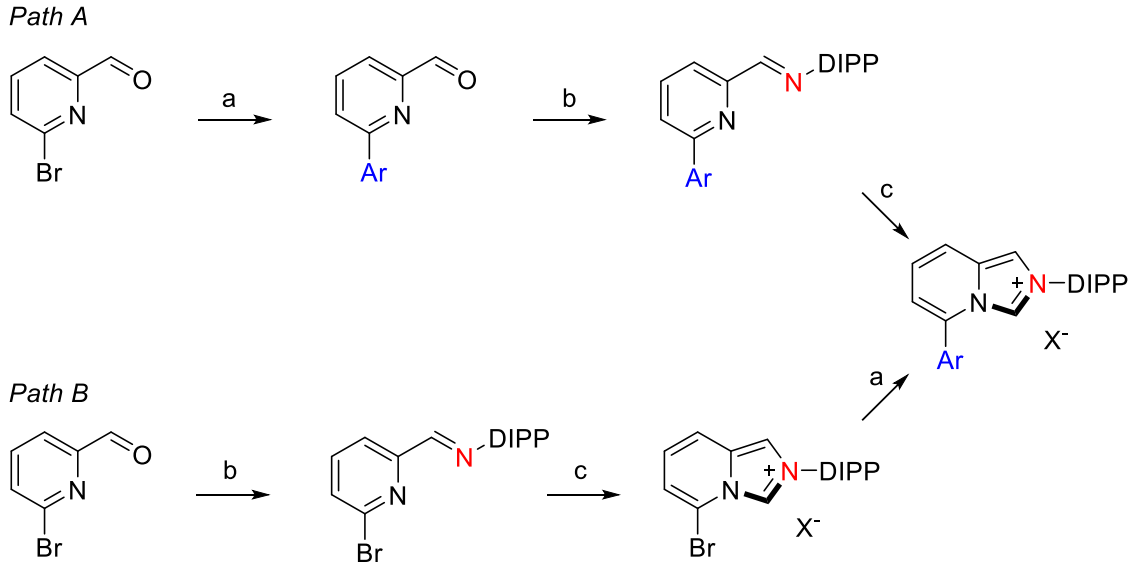

Figure 53. *Two possible synthetic routes. a) cross-coupling; b) imine condensation; c) imidazolium ring closure.*

The first synthetic step of Path A is the Suzuki-Miyaura cross coupling for the insertion of the aryl pendant at the C5 position of the pyridine. Two different conditions were applied: conditions A[52] were useful for most of the substrates, conditions B were adapted to achieve **6c** and **6d**, which were difficult to obtain under conditions A.

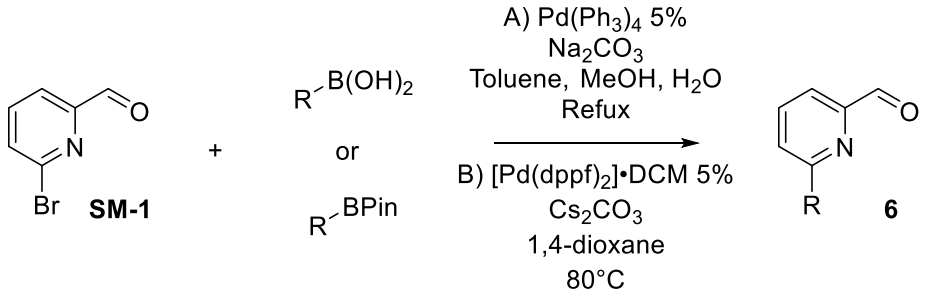

Compound	R	Conditions	Yield, %
6a	Ph	A	95
6b	4-biphenyl	A	80
6c	3,5-$(CF_3)_2$-phenyl	B	62
6d	3,5-$(OMe)_2$-phenyl[a]	B	32
6e	2-thienyl	A	93
6f	2,2'-bithiophen-5-yl[a]	A	68

Table 3. *Cross coupling results. a) pinacol ester instead of boronic acid.*

All the desired 6-aryl-pyridine-2-carboxaldehydes were obtained in synthetic useful yields, except for **6d**. However, operating a 1-2mmol scale provides enough product to proceed with the synthesis. Different approach is required for the synthesis of aldehyde **6g**. In fact, while working on different

substrates we observed that direct Buchwald-Hartwig coupling was unsuccessful, and only provides the reduction of aldehyde when operating with morpholine (Figure 54).

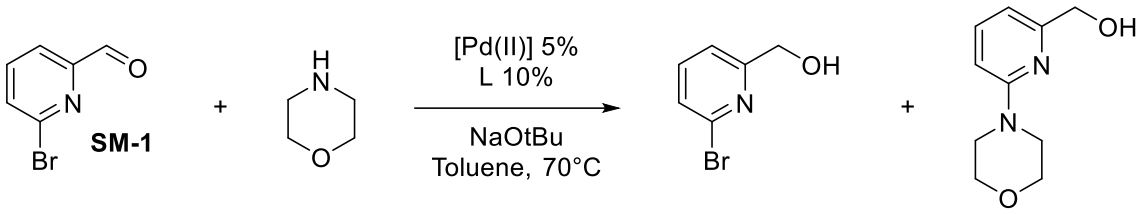

Figure 54. *Side products obtained under B-H conditions using morpholine as coupling partner.*

To achieve the desired aldehyde, **SM-1** has to be turned into the corresponding acetal with ethylene glycol (**SM-1'**),[53] in this way reduction is avoided. An optimization process was carried on **SM-1'** with morpholine before using dimethylamine and the results are reported in Table 4.

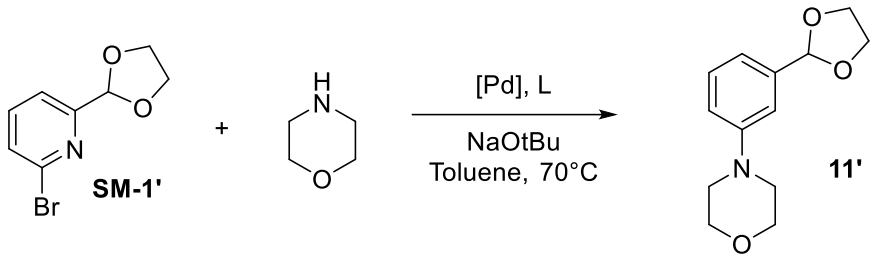

Entry	[Pd]	L	Y
1	$PdCl_2$ 5%	dppf 10%	70%
2	$PdCl_2$ 7,5%	dppf 15%	82%
3	$PdCl_2$ 5%	Xantphos 10%	60%
4	$Pd_2(dba)_3$•$CHCl_3$ 2,5%	dppf 10%	99%

Table 4. *Optimization experiments for the B-H coupling; morpholine 1.1eq, NaOtBu 1.2eq.*

The conditions shown in entry 4 provided product **11'** in quantitative yield that was used for the synthesis of **6g**. The cross coupling with dimethylamine proceeds well and the intermediate **11** can be readily hydrolysed to the desired aldehyde **6g** in 80% yield over 2 steps.

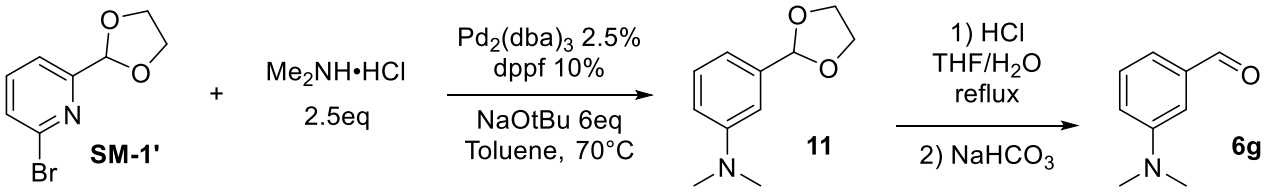

Figure 55. *Synthesis of aldehyde **6g**.*

The condensation to afford the imine is a common synthetic step in organic chemistry and a wide range of procedure can be applied including distillation of water/solvent azeotropes, highly hygroscopic solvent and salts or reagents that subtract water from the equilibrium. For our purpose, the procedure adopted is that reported by Michelet,[45] using diethyl ether as solvent and anhydrous $MgSO_4$ as anhydrifying agent.

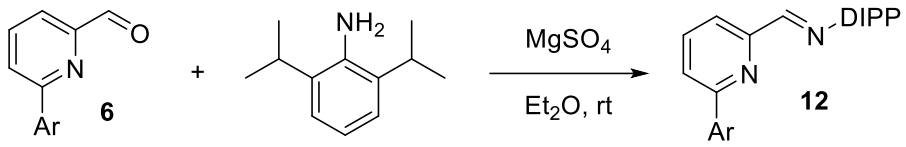

Figure 56. *Imine condensation.*

Due to the high rate of hydrolysis of silica gel, the conversion of the reaction has to be monitored by GC-MS and not TLC. In this reaction a slight excess of the 2,6-diidopropyl aniline is used and has to be removed from the product because can interfere in the next steps. The excess can be easily removed by vacuum evaporation at 145°C and at 0.2 mbar. This process can be applied for all the primary amines that have a low or relatively low boiling point whereas for those having an higher boiling point, different synthetic strategies can be used as illustrated in Figure 44. Yields of this step are almost quantitative and used in the next step without further purification. Absence of aniline can be checked by both GC-MS and NMR.

Final ligands precursors were obtained by imidazolium ring closure of the corresponding imines. Originally for this transformation were employed hazardous triphenyl arsine derivatives, that were slowly replaced by more convenient formaldehyde surrogates (Figure 57).

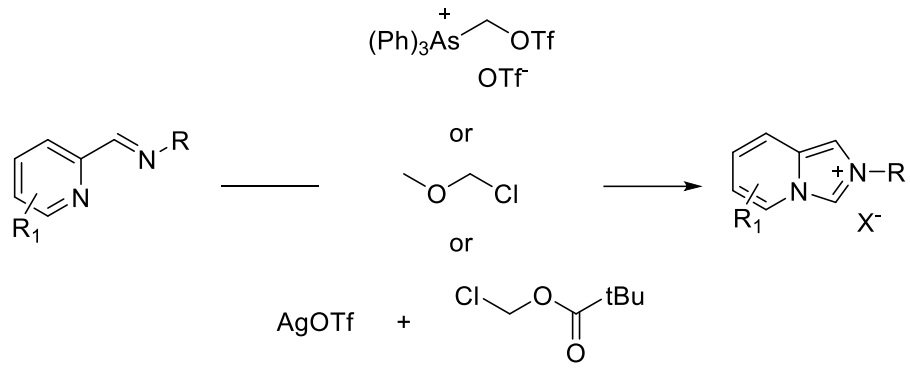

Figure 57. *Previous methodology for imidazolium ring closure.*

Finally, the direct use of paraformaldehyde was investigated[42] with great success. Therefore we adopted the procedure and applied to the imines **12**.

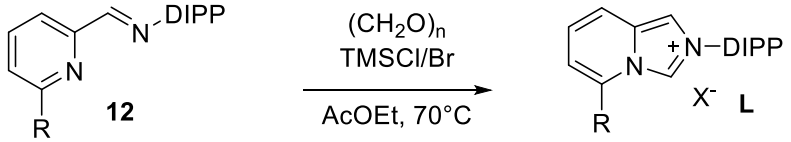

Compound	R	X	Yield, %
L1	Ph	Br	88
L2	4-biphenyl	Br	78
L3	3,5-$(CF_3)_2$-phenyl	Cl	90
L4	3,5-$(OMe)_2$-phenyl	Cl	60
L5	2-thienyl	Br	90
L6	2,2'-bithiophen-5-yl	Br	74
L10	NMe_2	Cl	80

Table 5. *Results of imidazolium ring closure.*

The resulting salts are insoluble in the ethyl acetate and thus can be filtered and washed with ether. Some problems in terms of purification were observed with **L3**, the only ImPy salt that is soluble in ethyl acetate and needs to be precipitated, after evaporation of solvent, by *n*-hexane.

This strategy can not be applied for the synthesis of **L8** and **L9** because decomposition of the corresponding imines was observed under these conditions. Path B (Figure 53) is therefore applied for these two ligands and also for **L7**. The choice to adopt this strategy for **L7** came from the expensiveness of tert-thiophenyl boronic acid pinacol ester, so it was decided to use it in the final step of a synthesis instead of in the first one with the risk of low yielding reactions with consequent waste of product.

The synthesis proceeded with the preparation of common $\mathbf{L_{Br}}$ intermediate with the previously described condensation and ring closure reactions, carried on **SM-1**. $\mathbf{L_{Br}}$ was then utilized in cross coupling reaction using the conditions reported by Zhang[47] yielding desired ligands in discrete yields. On the contrary of path A, this process did not provide pure products by precipitation in the reaction media, and therefore these salts needed to by purified by flash chromatography. Using DCM/MeOH 20 to 1 as eluent the purification proceeded smoothly affording the desired compounds in high purity level.

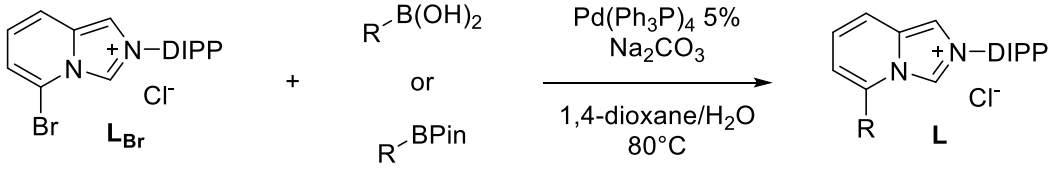

Compound	R	X	Yield, %
L7	2,2':5',2''-terthiophen-5-yl	Cl	69
L8	4-(NMe_2)-phenyl	Cl	72
L9	3-(NMe_2)-phenyl	Br	67

Table 6. *Cross coupling results on* $\boldsymbol{L_{Br}}$.

As final step, the synthesis of gold(I) complexes was done. Different techniques have been developed by time for the synthesis of NHC-Au(I) catalysts and are mainly divided in three classes: free carbene route, transmetallation route and weak base route (Figure 58).

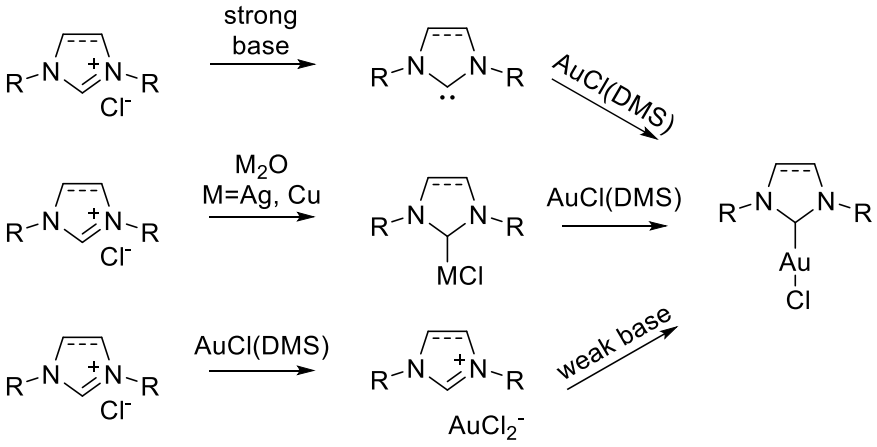

Figure 58. *Possible routes for the synthesis of Au(I) complexes.*

The transmetallation route was the first developed,[54] and for long time the most common strategy. However, the intermediate, mostly Ag(I) complexes, are light and moisture sensitive and moreover can lead to undesired metal trace in the final product. The use of strong bases such as KHMDS, KOtBu, NaH are useful but need strictly inert conditions to prevent the decomposition of the free carbene. The last developed is the weak base route,[55,56] which requires under very mild conditions, no need of inert atmosphere, no dry solvents and bases as potassium carbonate or triethyl amine. This useful condition permitted also the development of flow synthesis of NHC-Au complexes with almost quantitative yields.[57]

Both transmetallation and weak base routes were used for the synthesis of **Cat1-10**.

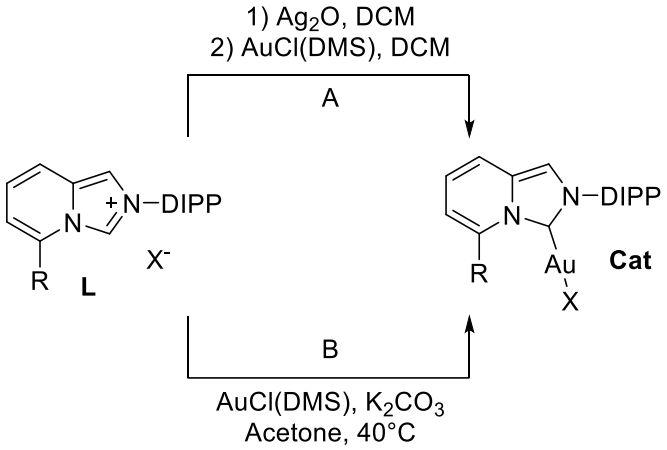

Compound	R	X	Procedure	Yield, %
Cat1	Ph	Cl	A	83
Cat2	4-biphenyl	Cl	A	80
Cat3	3,5-$(CF_3)_2$-phenyl	Cl	A	77
Cat4	3,5-$(OMe)_2$-phenyl	Cl	A	75
Cat5	2-thienyl	Cl	A	92
Cat6	2,2'-bithiophen-5-yl	Cl	A	87
Cat7	2,2':5',2''-terthiophen-5-yl	Cl	A	80
Cat8	4-(NMe_2)-phenyl	Cl	B	97
Cat9	3-(NMe_2)-phenyl	Br	B	99
Cat10	NMe_2	Cl	B	96

Table 7. *Gold(I) complexation reaction. a) yield over 2 steps.*

Desired complexes were obtained pure by evaporation of the reaction solvent after filtration over Celite® to remove AgCl and Na_2CO_3 salts. In all the cases [ImPy-Au(I)] compounds resulted in high and reproducible yields following both procedures.

2.5 SC-XRD analysis

All the complexes were subjected to crystallization by vapour diffusion of *n*-hexane to a solution of complex in DCM/toluene or by slow evaporation of DCM from solution of complex in DCM and layered with *n*-hexane. A comprehensive analysis of the SC-XRD data will now be illustrated. Methods and supplementary information are given in the characterization Section 2.8.

***Figure 59**. ORTEP drawing of **Cat1** (top) and **Cat2** (bottom)**.** Thermal ellipsoid are drawn at 30% of the probability level.*

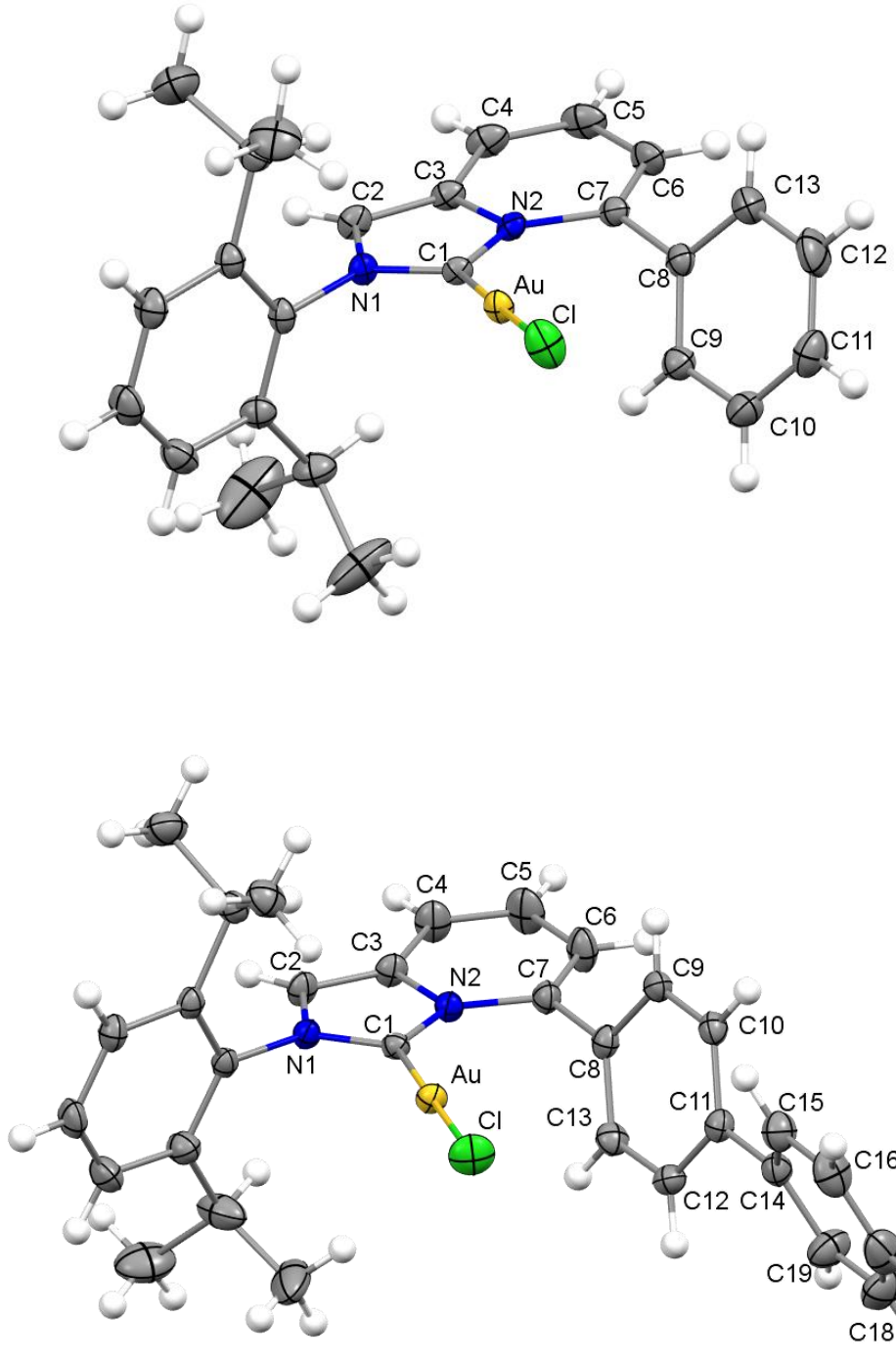

Figure 60. *ORTEP drawing of one of the two independent molecules of* ***Cat3*** *(top) and* ***Cat4*** *(bottom). Thermal ellipsoid are drawn at 30% of the probability level.*

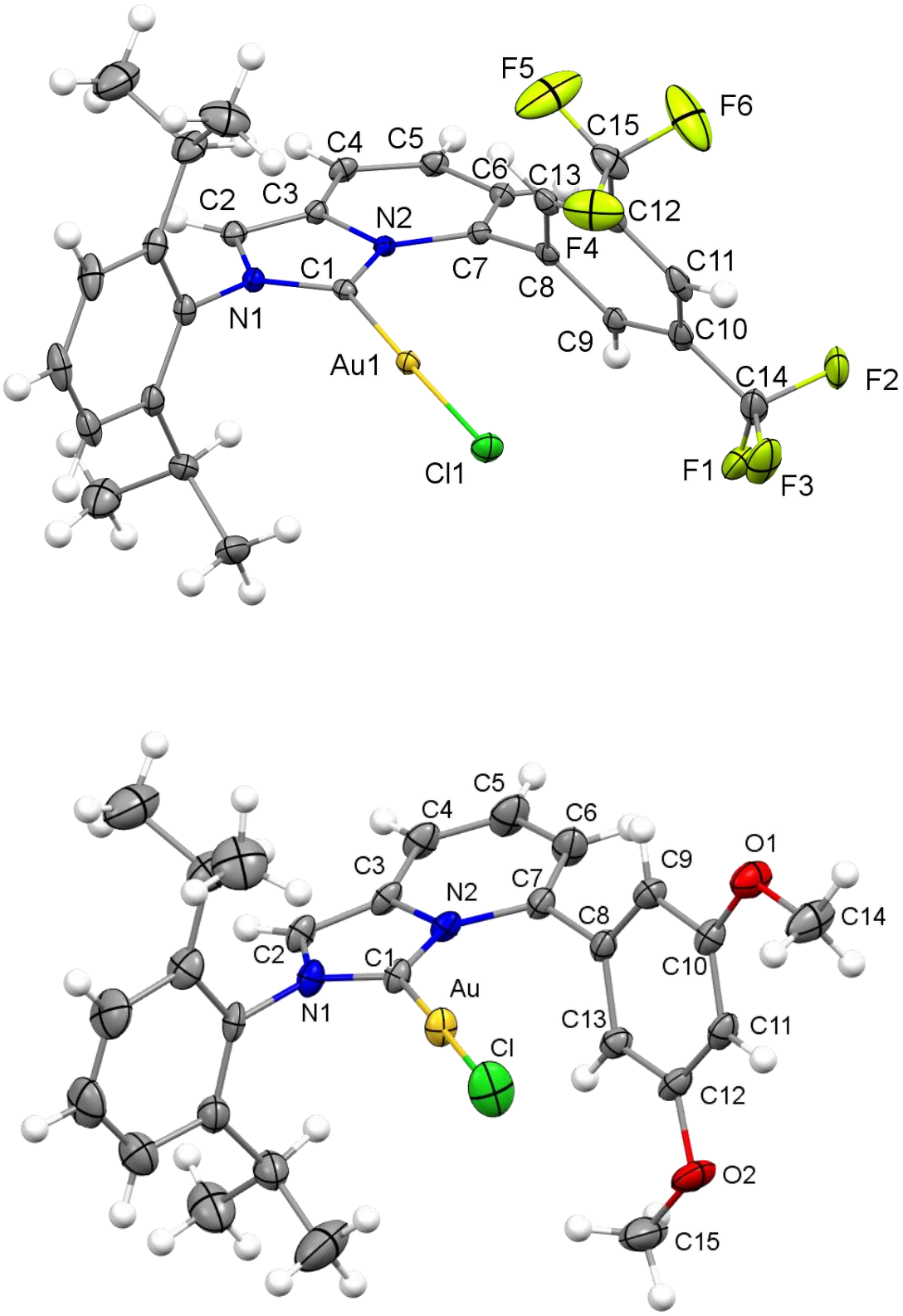

Figure 61. *ORTEP drawing of* ***Cat5*** *(top) and* ***Cat6*** *(bottom)****.*** *Thermal ellipsoid are drawn at 30% of the probability level.*

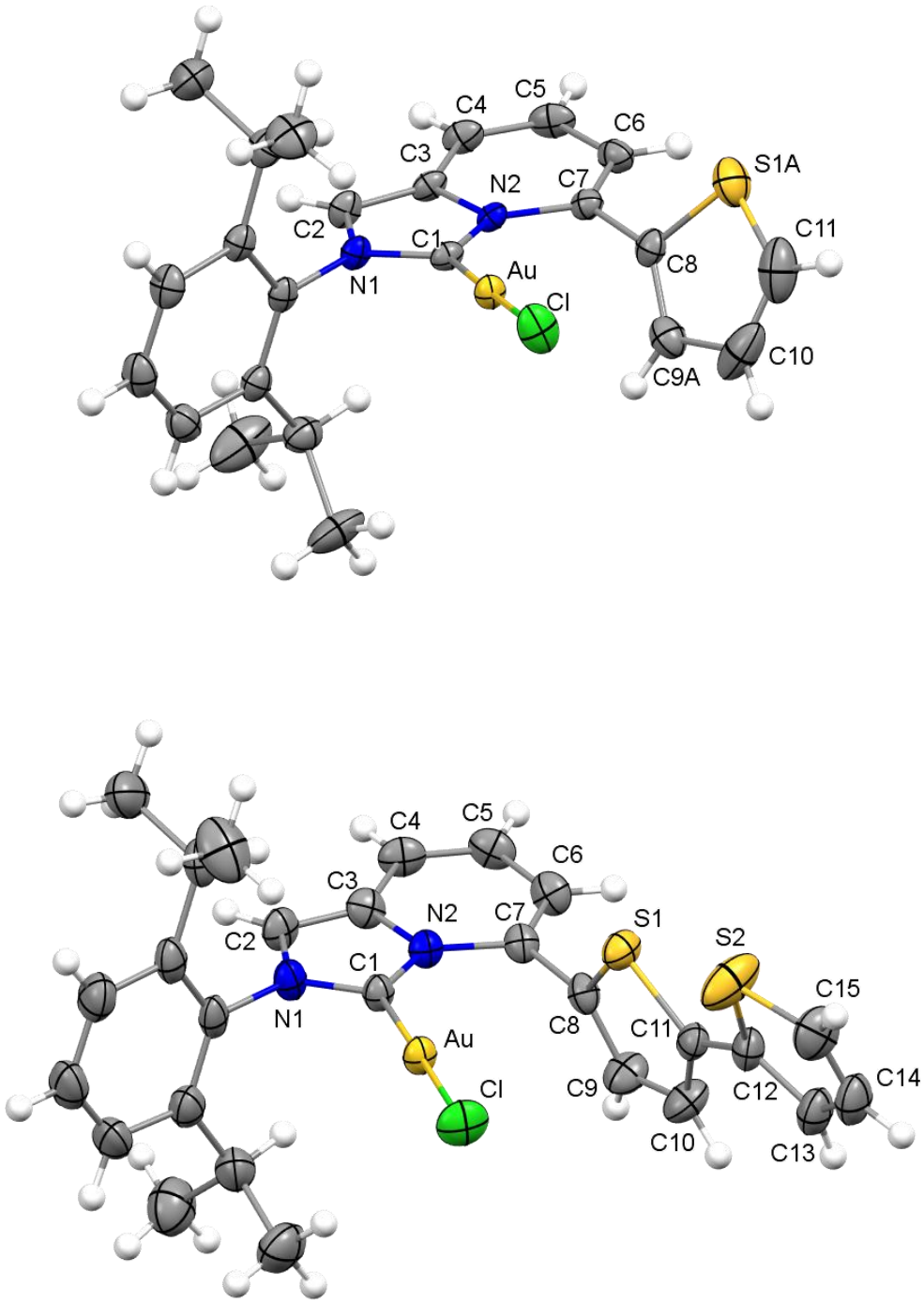

Figure 62. *ORTEP drawing of* ***Cat7*** *(top) and* ***Cat8*** *(bottom)****.*** *Thermal ellipsoids are drawn at 30% of the probability level.*

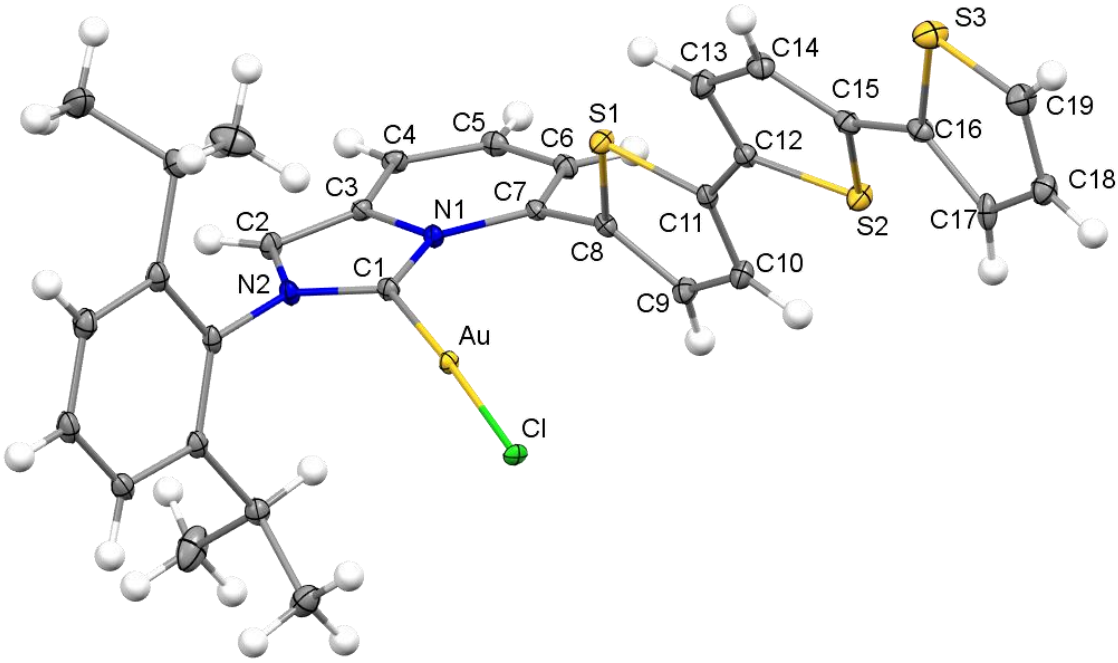

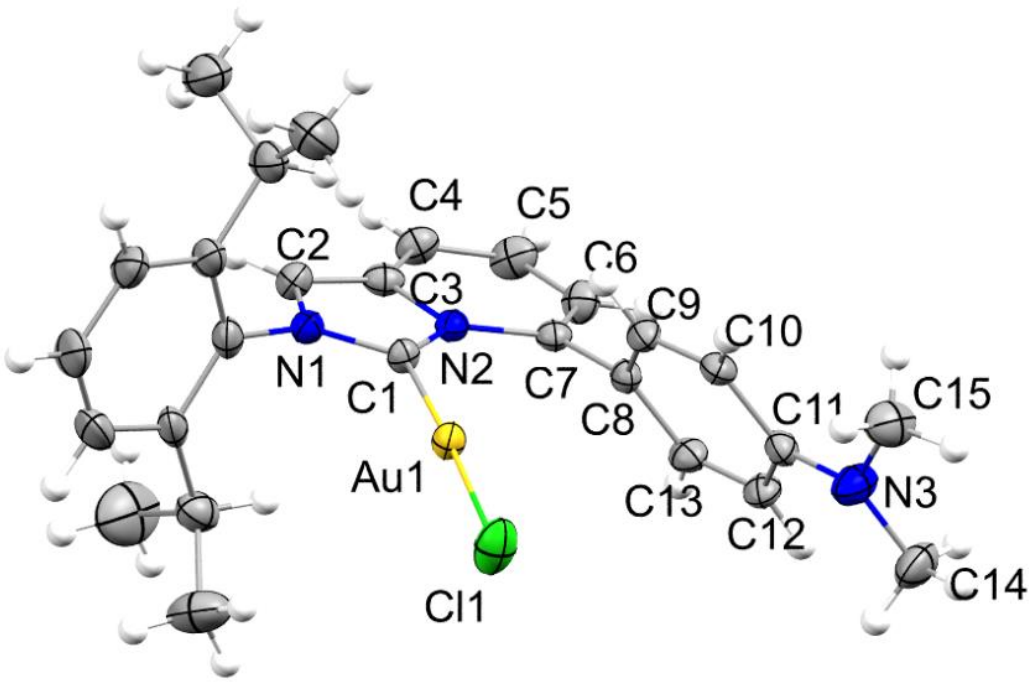

Figure 63. *ORTEP molecular drawing of* ***Cat9*** *(top) and* ***Cat10*** *(bottom). Thermal ellipsoids are drawn at 30% of the probability level.*

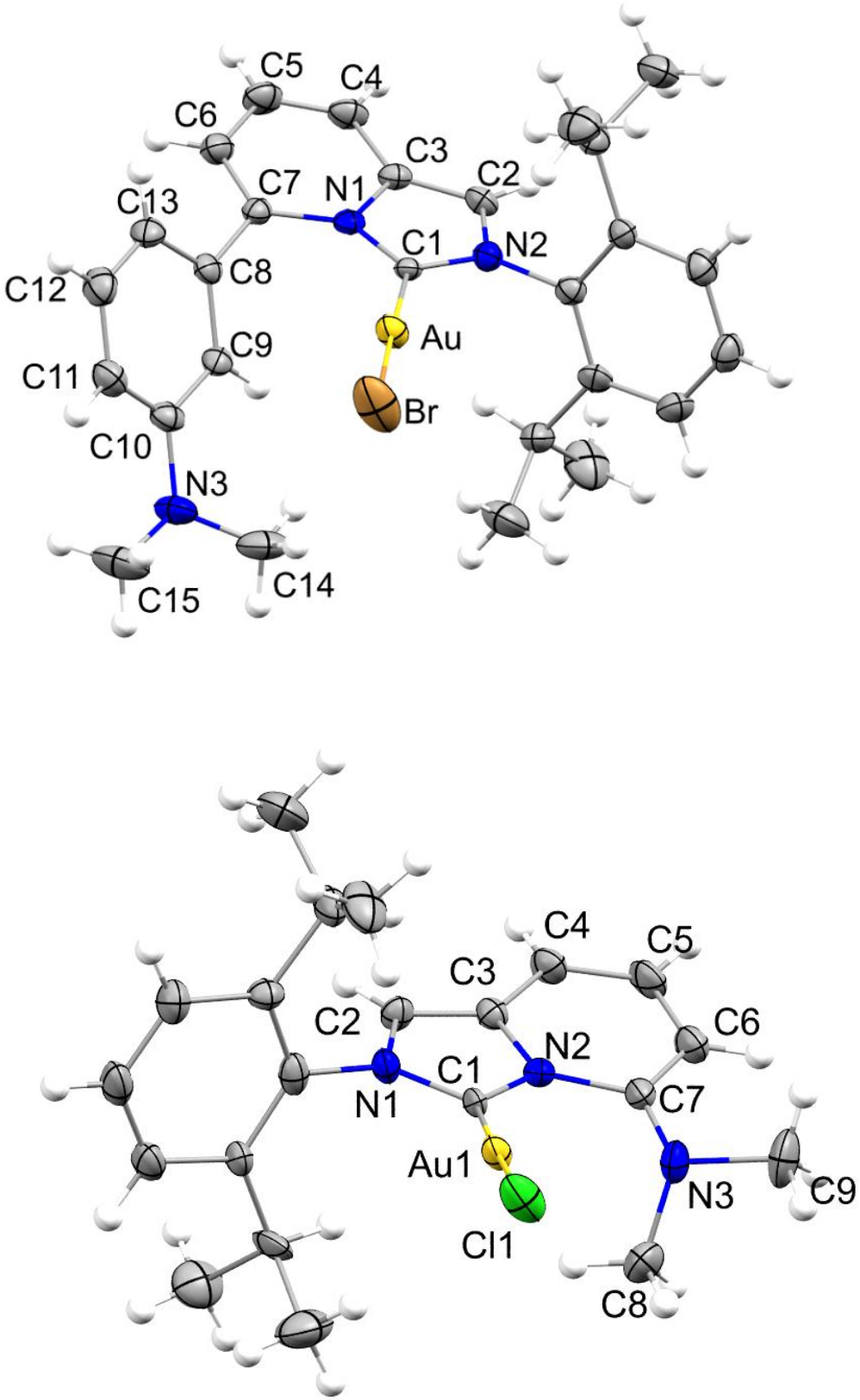

A series of interaction as hydrogen bond, S…S and π…π are observed for the Au(I) complexes and are listed below.

Table 8. *Relevant interaction for* ***Cat1-10****.*

Cat1

D-H	d (H…A) [Å]	<DHA [°]	d (D…A)	A
C6-H6	2.89	132.0	3.580(9)	Cl[a]
C2-H2	2.80	148.8	3.629(9)	Cl[b]

Symmetry operation used to generate equivalent atoms: [a] x+1/2, y+1/2, z; [b] x+1/2, -y+3/2, z-1/2.

Cat2

D-H	d (H…A) [Å]	<DHA [°]	d (D…A)	A
C4-H4	2.86	149.7	3.687(4)	Cl[a]

Symmetry operation used to generate equivalent atoms: [a] x+1, y, z.

Cat3

D-H	d (H…A) [Å]	<DHA [°]	d (D…A)	A
C6-H6	2.99	127.4	3.643(6)	Cl1B
C4-H4	2.80	136.2	3.544(6)	Cl1B[a]
C2B-H2B	2.84	129.7	3.524(6)	Cl1[b]
C1S-H1S1	2.55	136.7	3.34(2)	F3[b]
C1S-H1S2	2.90	158.1	3.83(2)	Cl1[c]

Symmetry operation used to generate equivalent atoms: [a] -x+1, -y+1, -z+1; [b] -x+1, -y, -z+1; [c] x-1, y, z-1

Cat4

D-H	d (H…A) [Å]	<DHA [°]	d (D…A)	A
C15-H15B	2.78	132.9	3.508(8)	Cl[a]

Symmetry operation used to generate equivalent atoms: [a] -x+1, -y, -z+1.

Cat5

D-H	d (H…A) [Å]	<DHA [°]	d (D…A)	A
C2-H2	2.74	148.0	3.562(7)	Cl[a]
C6-H6	2.84	134.0	3.554(8)	Cl[b]

Symmetry operation used to generate equivalent atoms: [a] x+1/2, -y+3/2, z-1/2; [b] x+1/2, y+1/2, z.

Cat6

D-H	d (H…A) [Å]	<DHA [°]	d (D…A)	A
C4-H4	2.71	169.1	3.628(7)	Cl[a]
C13-H13	2.87	159.0	3.75(1)	Cl[b]

Symmetry operation used to generate equivalent atoms: [a] x, -y+1, z+1/2; [b] -x+3/2, -y+3/2, -z+1.

Sulphur-Sulphur	d [Å]
S1…S2	3.301

Cat7

D-H	d (H…A) [Å]	<DHA [°]	d (D…A)	A
C4-H4	2.88	137.2	3.621(3)	Cl[a]
C9-H9	2.80	153.0	3.656(3)	Cl[b]
C2-H2	2.74	137.6	3.490(3)	Cl[a]
C13-H13	3.03	144.8	3.825(4)	S1[c]

Symmetry operation used to generate equivalent atoms: [a] x+1, y, z; [b] -x+1, -y+1, -z+2; [c] -x+1, -y+1, -z+1.

Cat8

D-H	d (H…A) [Å]	<DHA [°]	d (D…A)	A
C2-H2	2.98	138.8	3.730(8)	Cl1[a]

Symmetry operation used to generate equivalent atoms: [a] x-1/2, -y+3/2, z+1/2.

Cat9

D-H	d (H…A) [Å]	<DHA [°]	d (D…A)	A
C2-H2	3.06	144.0	3.850(1)	Br[a]

Symmetry operation used to generate equivalent atoms: [a] x, -y+1/2, z+1/2.

Cat10

D-H	d (H…A) [Å]	<DHA [°]	d (D…A)	A
C2-H2	2.71	145.2	3.51(1)	Cl1[a]

Symmetry operation used to generate equivalent atoms: [a] -x+1, y-1/2, -z+1/2.

Moreover, **Cat1**, **Cat5** and **Cat7** showed also π-π interactions in the solid state. **Cat1** and **Cat5** were very similar, in fact, the view down the *b* axis of the crystal packing of both complexes shows intermolecular π-π interactions (black dashed lines) between terminal phenyls (or thiophene) and

pyridine rings belonging to adjacent molecules (centroid-centroid distance 3.745 Å for **Cat1**, 3.737 Å for **Cat5**) generating zig-zag chains.

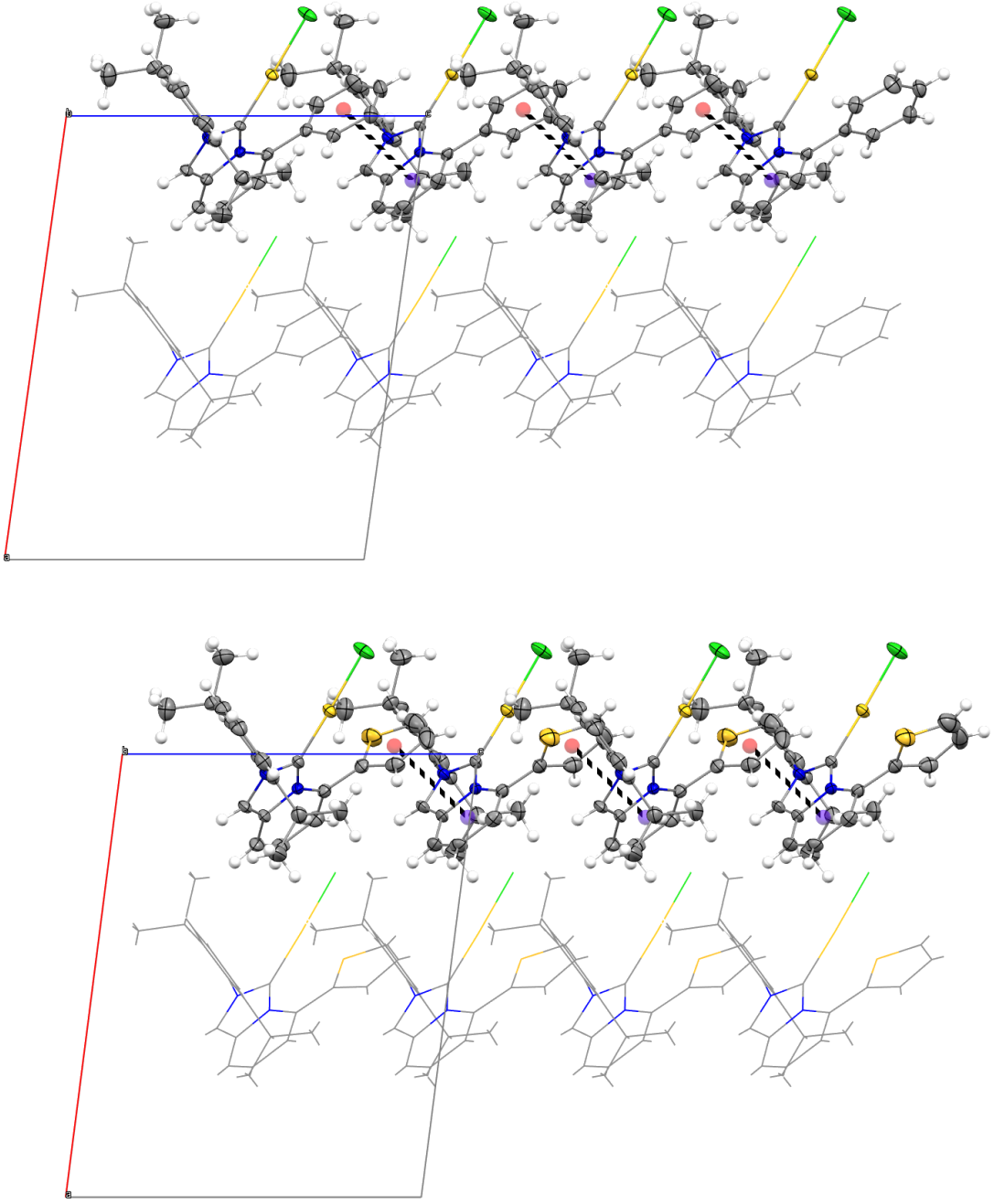

Figure 64. *view along b axis for* ***Cat1*** *(top) and* ***Cat5*** *(bottom).*

Differently, **Cat7** shows two intermolecular π-π interactions (black dashed lines) involving the second and the third thienyl ring of one molecule and the third and second thienyl ring, respectively of the adjacent molecule (centroid-centroid distances 3.922 Å) generating dimeric units.

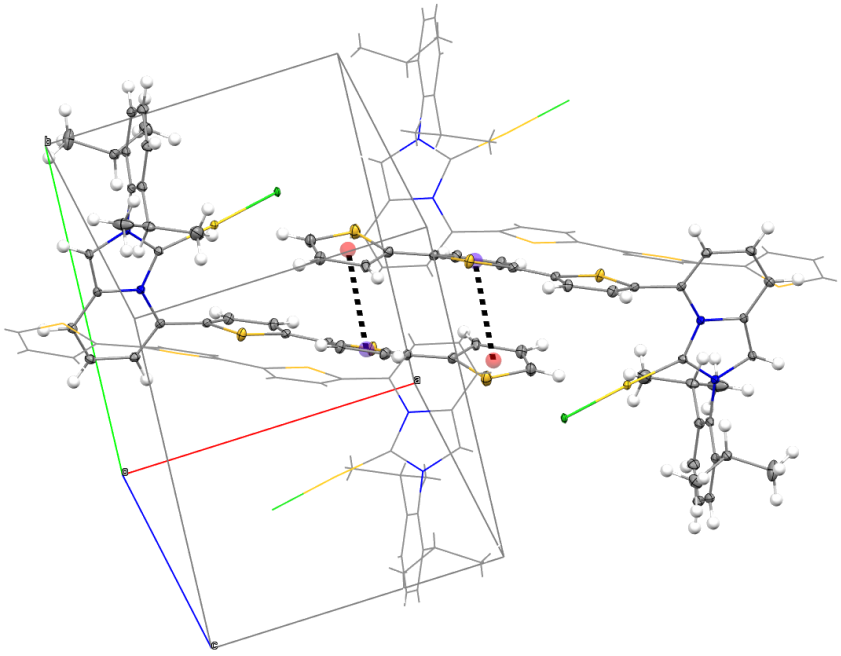

Figure 65. *Arbitrary view of the* ***Cat7*** *packing.*

Since these catalysts had to be applied in homogeneous catalysis we looked at other parameters (Table 9) that are not influenced by packing optimization, but may affect the catalytic outcome.

Cat	R	Au-C1, Å	Au-Cl, Å	ImPy-DIPP, °
Cat1	Ph	1.983(7)	2.304(3)	86.93
Cat2	4-biphenyl	1.985(3)	2.2828(9)	84.06
Cat3	3,5-$(CF_3)_2$-phenyl	1.982(5)	2.287(1)	86.75
Cat4	3,5-$(OMe)_2$-phenyl	1.980(2)	2.2765(9)	87.89
Cat5	2-thienyl	1.981(7)	2.277(2)	85.41
Cat6	2,2'-bithiophen-5-yl	1.9873(6)	2.267(2)	86.06
Cat7	2,2':5',2''-terthiophen-5-yl	1.970(3)	2.2932(6)	85.35
Cat8	4-(NMe_2)-phenyl	1.981(7)	2.275(2)	87.64
Cat9	3-(NMe_2)-phenyl	2.002(6)	2.3913(9)[a]	84.74
Cat10	NMe_2	1.98(1)	2.259(3)	84.62

Table 9. *a) Au-Br instead of Au-Cl.*

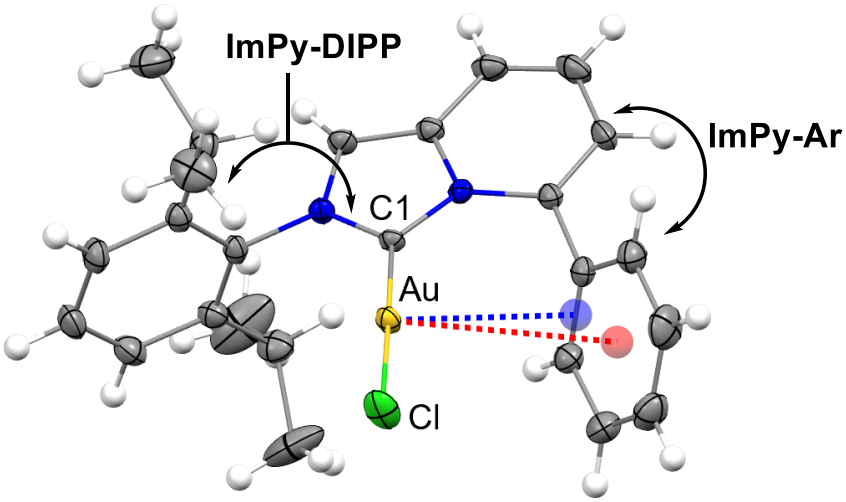

Figure 66. Cat1 *with representation of structural parameters analysed. Ar···Au interaction in red dashed line, η_2 interaction in blue dashed line.*

All the structures showed, as expected, that the orientation of the DIPP unit is almost perpendicular to the ImPy plane due to the steric hindrance of the bulky iPr groups (range 84.06-87.89°). Also the Au-C(1) and Au-Cl distances are very similar along all the complexes, without significant variations (range 1.970(3)-1.9873(6) Å and 2.267(2)-2.304(3) Å, respectively) except for **Cat9** (Au-C1 2.002(6) Å), but in this case the effect has been attributed to the presence of Br instead of Cl. The constancy of these two parameters relies in the high dihedral angles between the aryl substituent at the C5 position and the ImPy scaffold (range 49.00-82.58°), which causes a truncated conjugation with the ImPy system thus impeding the electronic influence transmission to the C1 carbon. As far as the ImPy aryl dihedral angles are concerned, there are other factors to be taken into account such as the presence of weak interactions of the aryl with the metal centre. This interaction showed in most cases an approximative distance of 3.07Å for **Cat1-2** and for **Cat8-9**, while significantly higher values were recorded for the thiophene containing complexes **Cat5-7** and shorter for **Cat3** and **Cat4**. Since no correlation is observed between ImPy-Ar dihedral angle and Ar η^2 interaction, an extra parameter was taken into account: the Ar(centroid)···Au distance, calculated from Au to the aryl center of mass. This parameter is more general and does not depend from the aryl-ImPy angle, which may rotate in homogeneous solution where packing forces are absent (Table 10).

Cat	R	ImPy-Ar, °	Ar···Au, Å[a,b]	η^2 interaction, Å[b,c]
Cat1	Ph	56.95	3.511	3.070
Cat2	4-biphenyl	67.65	3.412	3.068
Cat3	3,5-$(CF_3)_2$-phenyl	64.63	3.352	2.995
Cat4	3,5-$(OMe)_2$-phenyl	64.94	3.353	3.030
Cat5	2-thienyl	57.52	3.526	3.119
Cat6	2,2'-bithiophen-5-yl	82.58	3.477	3.174
Cat7	2,2':5',2''-terthiophen-5-yl	73.20	3.456	3.241

Cat8	4-(NMe_2)-phenyl	58.54	3.623	3.074
Cat9	3-(NMe_2)-phenyl	49.00	3.567	3.077
Cat10	NMe_2	/	3.116[d]	/

Table 10. *a) distances between Au and the aryl centroid; b) calculated by Mercury; c) nearest C=C to Au was considered; d) N···Au interaction*

Some trends were observed in the two oligo-aryl series, where increasing the number of aryl units a shortening of the Au…Ar(centroid) contact was recorded. A surprising outcome was observed by comparison of **Cat3** and **Cat4**, where functional groups with opposite electronic effects (CF_3 and OMe, respectively) placed on the phenyl ring, showed the same Au…Ar(centroid) distance. The interaction for **Cat4** was quite expected as an electron rich arene interacts with partially positive charged Au(I) metal centre by electronic attraction, but for **Cat3** an electronic repulsion was expected, which, as a matter of fact, was not revealed. Furthermore, **Cat8** and **Cat9** showed the weakest interactions with the metal centre. **Cat10** has a dimethyl amino group instead of arene at the C5 position, which adopts a high pyramidalized conformation with the nitrogen lone pair pointed at gold generating a N···Au interaction. In the other two dimethyl amino containing complexes **Cat8** and **Cat9**, the nitrogen atom assume a high planar geometry, as a consequence of the fact that their lone pair are delocalized on the arene.

Cat8		
C11-N3-C14	C11-N3-C15	C14-N3-C15
120.5(8)°	119.7(8)°	117.1(8)°

Cat9		
C10-N3-C14	C10-N3-C15	C14-N3-C15
117.8(7)°	115.8(7)°	114.9(8)°

Cat10		
C7-N3-C8	C7-N3-C9	C8-N3-C9
114.4(1)°	113.6(1)°	110.0(1)°

Table 11. *Angles relative to the amino N atoms for **Cat8-10**.*

2.6 Catalytic application

With this plenitude of catalysts in our hands, we were interested in application in homogeneous catalysis to evaluate the efficiency and the key interaction governing the reactivity. We started the investigation with our benchmark reaction of naphthol dearomatization (Figure 67).[4c]

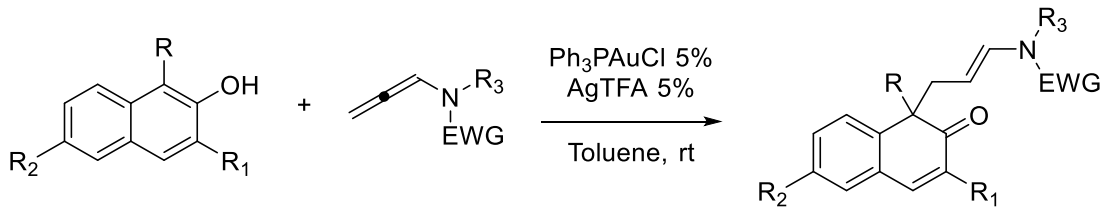

Figure 67. *Au(I)-catalysed dearomatization of naphth-2-ol with allenamides.*

During the optimization process of this reaction IPrAuCl was also tested as NHC-based catalyst, yielding a 55% of product. It was not the optimal catalysts, however the promising result obtained with an Au-NHC complex convinced us to test the new family of ImPy-Au(I) (Table 12).

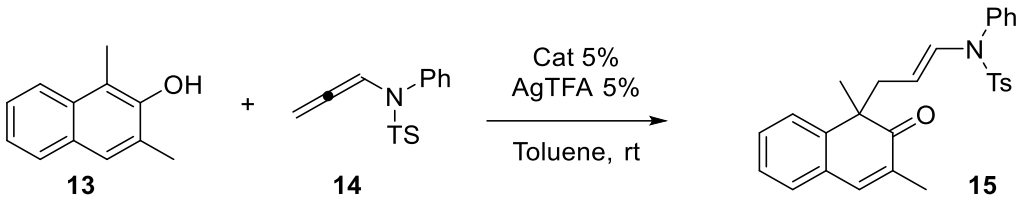

Catalyst	R	Yield, %
IPrAuCl	-	55
Cat1	Ph	35
Cat2	4-biphenyl	70
Cat3	3,5-$(CF_3)_2$-phenyl	95
Cat4	3,5-$(OMe)_2$-phenyl	26
Cat5	2-thienyl	87
Cat6	2,2'-bithiophen-5-yl	22
Cat7	2,2':5',2''-terthiophen-5-yl	74

Table 12. *Results obtained for naphthol dearomatization.*

All the tested catalysts were able to activate allenamide through the nucleophilic addition of naphthol, with yields from very low to almost quantitative. Very interesting results were observed in the phenyl series of complexes **Cat1-4**, where a correlation between the electronic nature of the pendant group and yield emerged. **Cat3**, the most electron poor phenyl, and **Cat4**, the most electronrich phenyl, showed a completely opposite catalytic outcome, since the first gave a 95% of **15** while the second just 26%, and **Cat1** and **Cat2** which are electronically neutral are in between the other two. These results are surprising because commonly electron neutral and electron rich arene are placed parallel to the Au(I) metal centre in most catalysts to stabilize cationic gold and carbocationic intermediates,[58] but in our case the electron-rich and neutrals showed less activity than the electron-poor one. To further prove these results kinetic experiments were carried out with **Cat1-4**, and also in this case **Cat3** was the best performing catalyst. The corresponding **Cat(TFA)** catalysts were prepared prior to use by counter anion exchange with AgTFA (full detail of kinetic experiments in the SI section).

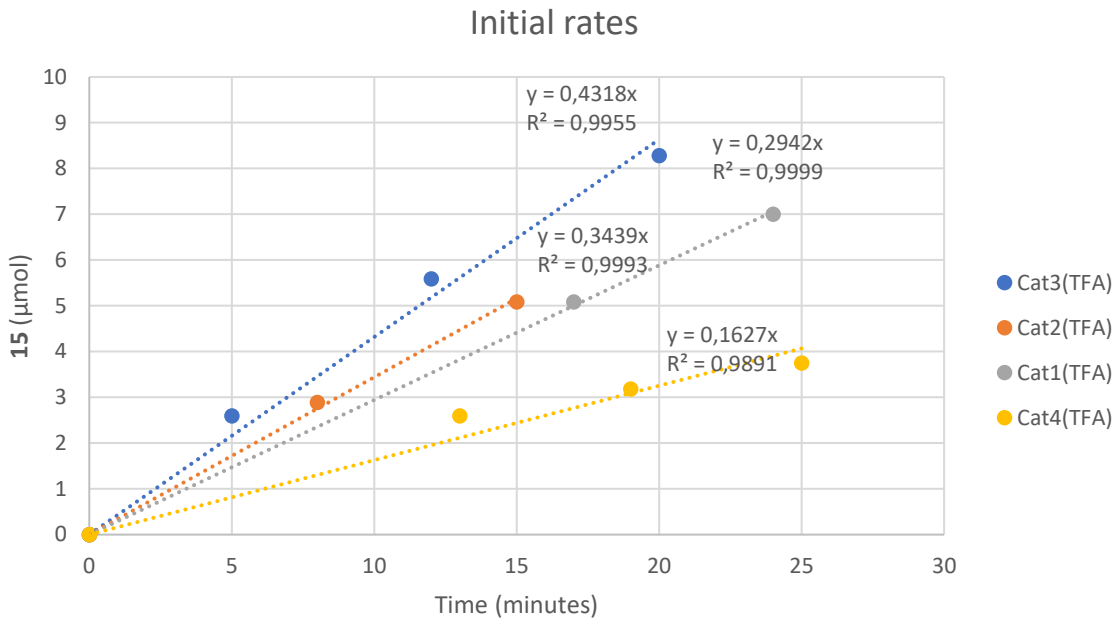

Figure 68. *Plot of yield over time obtained by NMR using internal standard.*

Since the role of electron poor arene···Au interaction was unprecedented, DFT calculations were performed in collaboration with Prof. Carlos Silva López from the University of Vigo (Spain) to have a better view.

As first step molecular geometry of complexes **Cat1**, **Cat3** and **Cat4** were optimized and reproduced faithfully the ones obtained from SC-XRD analysis. Secondly, the electron density was analysed with Atoms In Molecules (AIM) and Non-Covalent Interactions (NCIs) models at B3LYP/6-31+G8(d) level for main group atoms and SSD basis set and Electron Core Potential (ECP) for gold atom. The analysis revealed close steric interaction between gold and the aryl of **Cat3** but also a topology of electron density which is like a full covalent bond (Figure 69).

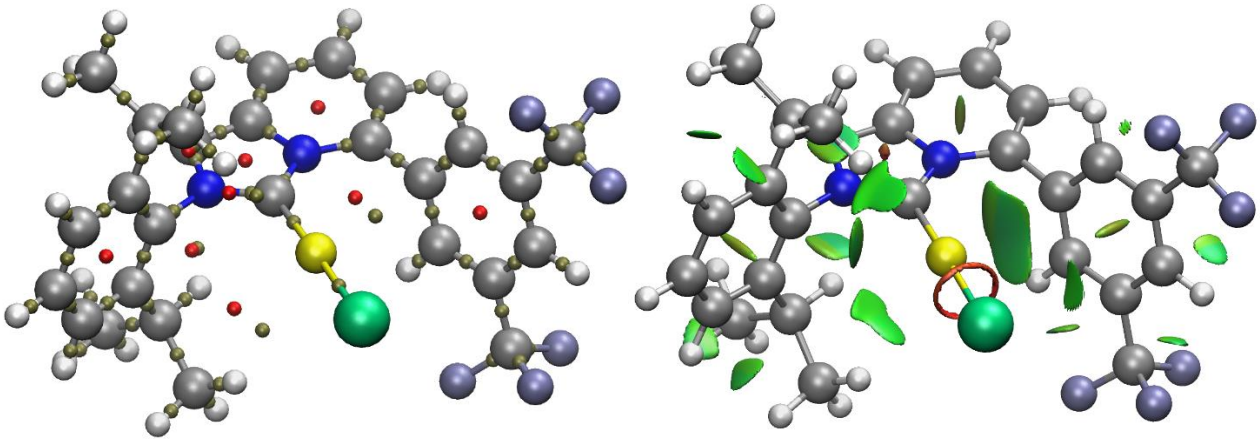

Figure 69. *Ring and bond critical point (left); non covalent close steric Ar…Au interaction (right).*

Furthermore electron density population analysis was carried out on the intermediate for the three catalysts. The positively charged activated allene showed an increased positive charge on the electrophilic carbon for the **Cat3** with respect to **Cat1** and **Cat2**, and these results correlate well with the experimental observation.

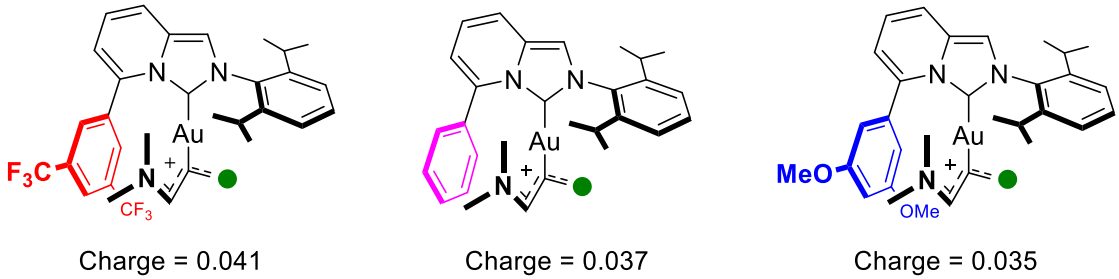

Figure 70. *Charge in arbitrary unit,* ***Cat3*** *(left),* ***Cat1*** *(middle) and* ***Cat4*** *(right).*

To prove the generality of the observed effect, **Cat1**, **Cat3** and **Cat4** were used in other catalytic transformation. The first one is the cyclopropanation reaction of olefines with propargyl esters, that was reported by Toste.[59]

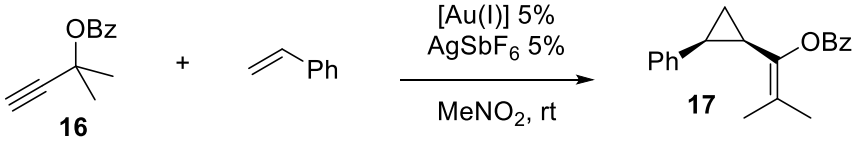

Catalyst	R	Yield (d.r. syn:anti)
Cat1	Ph	79% (10:1)
Cat3	3,5-$(CF_3)_2$-phenyl	88% (7:1)
Cat4	3,5-$(OMe)_2$-phenyl	64% (7:1)

Table 13. *Cyclopropanation reaction results.*

The second one is the alkynylbenzaldehyde cyclization reported by Slaughter.[60]

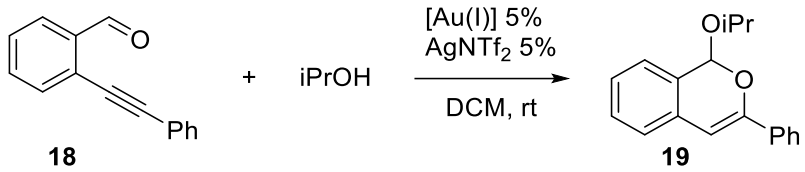

Catalyst	R	Yield
Cat1	Ph	41%
Cat3	3,5-$(CF_3)_2$-phenyl	68%
Cat4	3,5-$(OMe)_2$-phenyl	13%

Table 14. *Alkynylbenzaldehyde cyclization reaction results.*

Also in all of these control experiments, involving different kinds of intermediate, the same trend of reactivity for the catalysts was observed and the superior activity of **Cat3** emerged, confirming the unprecedent activating role of the Ar(EWG)…Au interaction.

The catalysts bearing the amino group were synthetized with the aim to participate in bifunctional catalysis, so we designed the intramolecular lactonization of *N*-allenyl indole-2-carboxylic acid where lone pairs of nitrogen atoms in the ligands might direct and activate the substrate. Intramolecular

nucleophilic addition to allenes is widely explored in Au(I) catalysis, however the addition of carboxylic acid is far less explored and only limited to the synthesis of γ-butyrolactones.

Therefore substrate **23a** was elected as model substrate and the optimization of reaction conditions was carried out (Table 15).

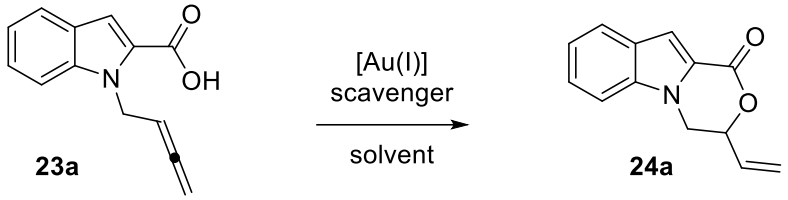

23a **24a**

Entry	Catalyst	R	Scavenger	Solvent	Yield
1	Cat8	4-(NMe_2)-phenyl	$AgSbF_6$	THF	87
2	Cat9	3-(NMe_2)-phenyl	$AgSbF_6$	THF	83
3	Cat10	NMe_2	$AgSbF_6$	THF	82
4	Cat1	Ph	$AgSbF_6$	THF	83
5	Cat3	3,5-(CF_3)$_2$-phenyl	$AgSbF_6$	THF	90
6	Cat4	3,5-(Ome)$_2$-phenyl	$AgSbF_6$	THF	72
7	IPrAuCl	-	$AgSbF_6$	THF	69
8	JohnphosAuCl	-	$AgSbF_6$	THF	42
9	Ph_3PAuCl	-	$AgSbF_6$	THF	<5
10	$PicAuCl_2$	-	$AgSbF_6$	THF	<5
11	Cat3	3,5-(CF_3)$_2$-phenyl	AgTFA	THF	traces
12	Cat3	3,5-(CF_3)$_2$-phenyl	NaBARF	THF	traces
13	Cat3	3,5-(CF_3)$_2$-phenyl	none	THF	NR
14	none	-	$AgSbF_6$	THF	NR
15	Cat3	3,5-(CF_3)$_2$-phenyl	$AgSbF_6$	Toluene	36
16	Cat3	3,5-(CF_3)$_2$-phenyl	$AgSbF_6$	ACN	NR
17	Cat3	3,5-(CF_3)$_2$-phenyl	$AgSbF_6$	DCM	63

Table 15. *Optimization screening.* ***20a*** *0.1 mmol, [Au(I)] 5%, scavenger 5%, solvent 1 mL, rt, 24h.*

From the optimization (Table 15), the best ligands for Au(I) are the NHC (entry 1-7) while phosphine and Au(III) catalysts did not provide sufficient results. Solvent screening (entry 5, 15-17) showed that THF was the optimal solvent because it was the only one to dissolve completely the substrate, while in other cases the substrate remained suspended in a heterogeneous mixture. The catalysts screening initially was encouraging because of the great results obtained by **Cat8-10**, where different positions of the dimethyl amino moiety seemed to have relevance on the catalytic result. However, when **Cat1**, **Cat3** and **Cat4** were tested, **Cat3** still was the best catalysts above all the other and the same trend, as shown before, was maintained (**Cat3**>**Cat1**>**Cat4**). Rationalization of these results was trickier, but H-bonding interactions can be ruled out for two main considerations: THF saturates all the H-

bonds with the substrate and the dimethyl amino groups of **Cat8-9** have a very low basicity due to the delocalization of lone pair, and for **Cat10** the lone pair is interacting with the Au(I) metal centre.

Therefore, the previously discussed Ar…Au interaction was investigated. The intermediate generated during the reaction is almost the same shown in Figure 70, since is activation of an allenyl group. If for **Cat1**, **Cat3** and **Cat4** the correlation of electronic properties is the same described before, for **Cat8-9** the correlation was not immediate. Both of them are electron rich, less than **Cat4**, but provided a significantly higher yields. A plausible explanation was that only the nature of the interaction is not sufficient, and the strength of the interaction itself had to be considered (Figure 71). **Cat4** has a very electron rich arene ring strongly interacting with gold metal centre, causing a consistent decrease of intermediate reactivity. **Cat8** and **Cat9** have the same impact on the electronic nature of the arene, however differences in the strength of the interaction with gold were observed, showing that **Cat8** is far less involved than **Cat9** (3.623 Å *vs* 3.567 Å). Therefore, **Cat8** quench less the electrofilicity of the intermediate than **Cat9** resulting slightly more active.

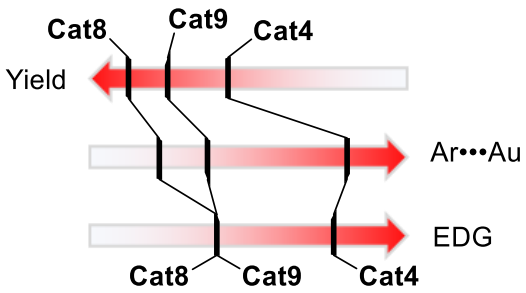

Figure 71. *Visual representation of correlation of EDG properties, Ar···Au interactions and yields for* ***Cat4***, ***Cat8*** *and* ***Cat9****.*

For **Cat10** a similar estimation was possible since the lone pair points directly to the metal centre and act as an electron rich arene, decreasing the activity of gold.

The optimized conditions (entry 5, Table 15) were applied to a library of allenyl carboxylic acids. All the modification on the indole core were well tolerated in position 3, 4, 5 and 6 (66-98%) where both EWG and EDG could be accommodated. The allenyl moiety could be modified as well, however only less hindered **23i** provided synthetically useful yield. Some limitation were observed in the synthesis of fused 7-membered ring and when pyrrole was used as tethering.

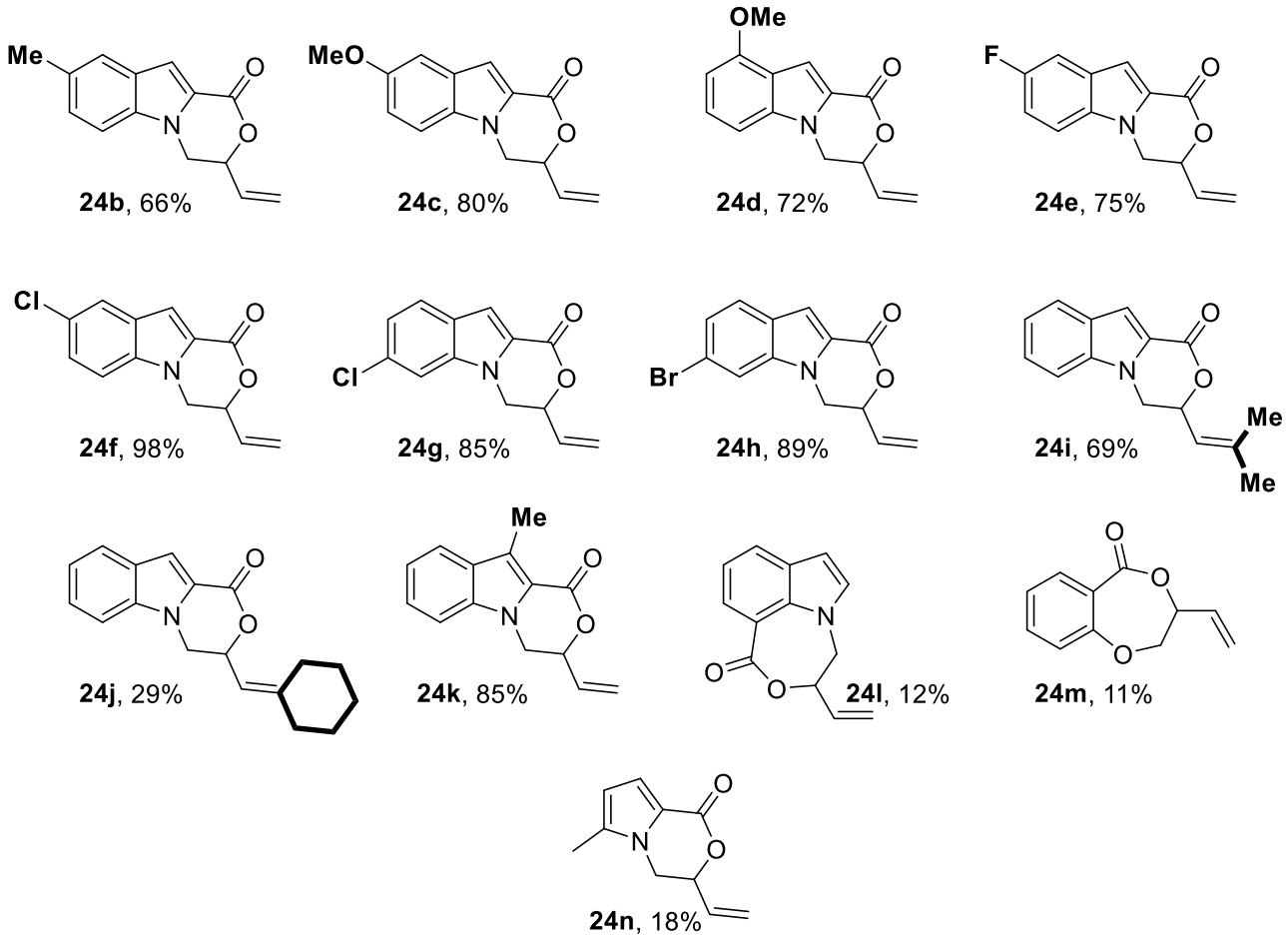

Figure 72. *Intramolecular lactonization scope.*

2.7 Conclusions

In conclusion, a new synthetically accessible family of [ImPyAu(I)] were synthetized and fully characterized in both solid and solution. The electronic effect on π-interaction with Au(I) were carefully investigated by SC-XRD structures and by DFT calculations, revealing a strong orbital interaction which, in case of electron-poor arene, resulted in a strong activating effect through electrophiles activation. Crystal structure provided qualitative information which allows prediction on the catalytic outcome by analysing the nature and the strength of the interaction. All the analysis carried in solid state and with DFT correlate very well with three benchmark reactions and a new synthetic methodology results, giving robustness to our hypothesis of key role of this interaction in gold(I)-catalysed reactions.

2.8 Experimental section

^{1}H NMR spectra were recorded on Varian 400 (400 MHz) spectrometers. Chemical shifts are reported in ppm from TMS with the solvent resonance as the internal standard (deuterochloroform: 7.27 ppm). Data are reported as follows: chemical shift, multiplicity (s = singlet, d = doublet, t = triplet, q = quartet, sext = sextet, sept = septet, p = pseudo, b = broad, m = multiplet), coupling constants (Hz).

^{13}C NMR spectra were recorded on a Varian 400 (100 MHz) spectrometers with complete proton decoupling. Chemical shifts are reported in ppm from TMS with the solvent as the internal standard (deuterochloroform: 77.0 ppm).
^{19}F NMR spectra were recorded on a Varian 400 (377 MHz). Chemical shifts are reported in ppm from $CFCl_3$.

GC-MS spectra were taken by EI ionization at 70 eV on a Hewlett-Packard 5971 with GC injection. They are reported as: m/z (rel. intense).

LC-electrospray ionization mass spectra were obtained with Agilent Technologies MSD1100 single-quadrupole mass spectrometer.

Elemental analyses were carried out by using a EACE 1110 CHNOS analyser.

Melting points were determined with Bibby Stuart Scientific Melting Point Apparatus SMP 3 and are not corrected.

Chromatographic purification was done with 240-400 mesh silica gel.

Anhydrous solvents were supplied by Sigma Aldrich in Sureseal® bottles and used without any further purification. Ethyl acetate was dried on activated 5Å molecular sieves.

Commercially available chemicals were purchased from Sigma Aldrich, Fluorochem and TCI and used without any further purification.

The X-ray intensity data were measured on a Bruker Apex II CCD diffractometer. Cell dimensions and the orientation matrix were initially determined from a least-squares refinement on reflections measured in three sets of 20 exposures, collected in three different ω regions, and eventually refined against all data. A full sphere of reciprocal space was scanned by 0.5° ω steps. The software SMART[3] was used for collecting frames of data, indexing reflections and determination of lattice parameters. The collected frames were then processed for integration by the SAINT program,[61] and an empirical absorption correction was applied using SADABS.[62] The structures were solved by direct methods (SIR 2014)[63] and subsequent Fourier syntheses and refined by full-matrix least-squares on F^2 (SHELXTL)[64] using anisotropic thermal parameters for all non-hydrogen atoms. The aromatic, methyl, methylene and methine hydrogen atoms were placed in calculated positions, refined with isotropic thermal parameters *U(H)* = 1.2 *Ueq*(C) and allowed to ride on their carrier carbons. Molecular drawings were generated using Mercury.[65]
In the asymmetric units of three crystal structures one toluene (**Cat2)** and one CH_2Cl_2 (**Cat3**) solvent molecules are present, respectively. Moreover in the asymmetric unit of **Cat3** two indipendent molecules have been found.
Crystallographic data have been deposited with the Cambridge Crystallographic Data Centre (CCDC) as supplementary publication number CCDC 2091513-2091514, 2091516-2091520, 2167546-2164548, 2164553. Copies of the data can be obtained free of charge via www.ccdc.cam.ac.uk/getstructures .

Synthesis of aldehydes

Procedure A)

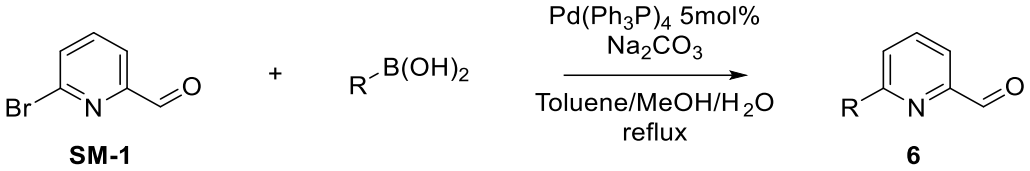

A 2 necked-round bottom flask equipped with a condenser was evacuated with vacuum and back-filled with N_2 (3 times). To a solution of 6-bromopyridine-2-carboxaldehyde (**SM-1**, 279mg, 1.5mmol, 1 eq) dissolved in the minimum amount of toluene was added a solution of aryl boronic acid (2.25mmol, 1.5 eq, 2.5 M in MeOH) and 1.5mL of aqueous solution of Na_2CO_3 (318mg, 3mmol, 2 eq, 2 M) followed by a degassing with N_2 under vigorous stirring (2 minutes). Then, 4.3mL of degassed toluene solution of [$(Ph_3P)_4Pd$] (5 mol%, 86mg, 0.075mmol, 20 mg/mL) was added and the mixture was heated to reflux. The reaction was monitored by TLC (10/1 *c*Hex/AcOEt). The reaction was cooled down to room temperature and extracted with DCM (2x15mL). The organic phase was dried over Na_2SO_4 and evaporated. The product was purified by flash chromatography with *n*Hexane/AcOEt 20/1 as eluent.

Procedure B)

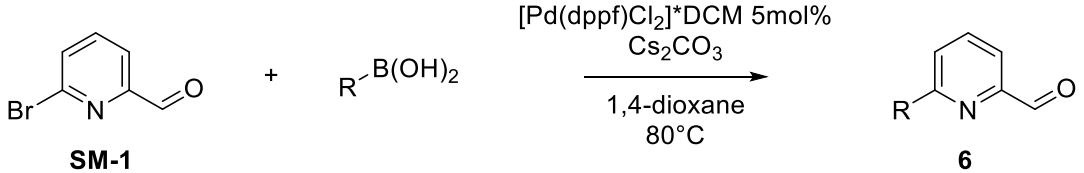

To a Schlenk tube 6-bromopyridine-2-carboxaldehyde (**SM-1**, 186mg, 1mmol, 1 eq), aryl boronic acid (**2**, 1.5mmol, 1.5 eq), Cs_2CO_3 (978mg, 3mmol, 3eq) and 5mL 1,4-dioxane were added, and the mixture was degassed with N_2 flux. Then, [$Pd(dppf)Cl_2$]•DCM adduct (65mg, 0.075mmol, 5 mol%) was added and the mixture stirred at 80 °C overnight. After complete consumption of **SM-1** by TLC, water was added and the biphasic mixture extracted with ethyl acetate (2x10mL). The product was purified by flash chromatography with *n*-Hex/AcOEt 10:1.

6a, procedure A, yield 95%, colourless solid. ^1H, ^{13}C NMR, GC-MS(EI) spectra were in agreement with reported values.[66]

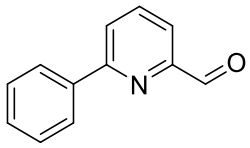

6b, procedure A, yield 80%, colourless solid.

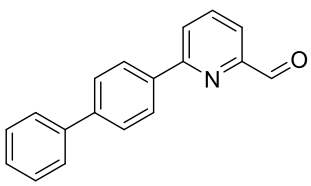

^1H NMR (400 MHz, $CDCl_3$) δ =10.19 (d, J = 0.9 Hz, 1H), 8.17 (d, J = 8.4 Hz, 2H), 8.03 – 7.88 (m, 3H), 7.75 (d, J = 8.5 Hz, 2H), 7.69 – 7.64 (m, 2H), 7.50 – 7.44 (m, 2H), 7.41 – 7.35 (m, 1H).

^{13}C NMR (100 MHz, $CDCl_3$) δ = 193.89, 157.50, 152.75 142.47, 140.35, 137.83, 136.91, 128.87, 127.71, 127.64, 127.40, 127.11, 124.32, 119.74.

GC-MS(EI): 259 (100%, M^{*+}); 230 (63%, -CHO); 202 (22%)

Melting point: 145-148 °C

Elemental analysis, calc. for $C_{18}H_{13}NO$: C, 83.37; H, 5.05; found: C, 83.44; H, 4.97.

6-(3,5-bis(trifluoromethyl)phenyl)picolinaldehyde (**6c**), procedure B, yield 62%, colourless solid. ^{1}H, ^{13}C NMR, GC-MS were in agreement with reported values. [42]

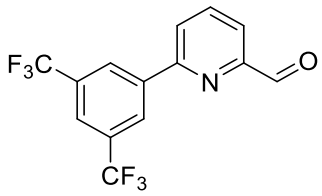

6d, procedure B, yield 32%, colourless solid.

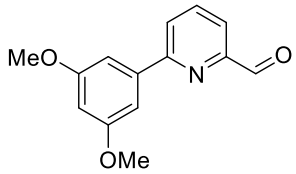

^{1}H NMR (400 MHz, $CDCl_3$) δ =10.12 (d, *J* = 1.1 Hz, 1H), 7.85 (s, 3H), 7.20 (dd, J = 2.3, 1.1 Hz, 2H), 6.53 (td, J = 2.3, 1.1 Hz, 1H), 3.84 (s, 6H).
^{13}C NMR (100 MHz, $CDCl_3$) δ = 193.81, 161.26, 157.46, 152.52, 140.07, 137.75, 124.59, 119.93, 105.10, 101.65, 55.46.
GC-MS(EI): 243 (100%, M^{*+}), 213 (38%)

Melting point: 106-108 °C.
Elemental analysis, calc. for $C_{14}H_{13}NO_3$: C, 69.12; H, 5.39; found: C, 69.10; H, 5.24.

6e, procedure A, yield 93%, pale yellow solid.

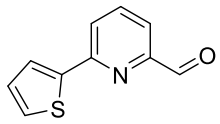

^{1}H NMR (400 MHz, $CDCl_3$) δ = 10.04 (d, J = 1.0 Hz, 1H), 7.80 – 7.71 (m, 3H), 7.62 (dt, J = 3.7, 1.2 Hz, 1H), 7.41 (dt, J = 5.0, 1.2 Hz, 1H), 7.09 (ddd, J = 4.9, 3.7, 1.0 Hz, 1H).
^{13}C NMR (100 MHz, $CDCl_3$) δ = 193.46, 153.12, 152.43, 143.45, 137.65, 128.51, 128.23, 125.67, 122.73, 119.35.
GC-MS(EI): 189 (100%, M^{*+}), 160 (88%, -CHO)
Melting point: 60-62°C
Elemental analysis, calc. for $C_{10}H_7NOS$: C, 63.47; H, 3.73; found: C, 63.53; H, 3.70.

6f, procedure A, yield 68%, yellow solid

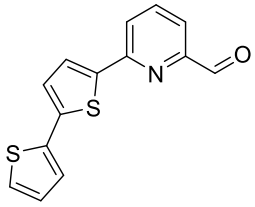

Note: boronic acid pinacol ester was used instead of boronic acid.
^{1}H NMR (400 MHz, $CDCl_3$) δ = 10.16 (s, 1H), 7.90 – 7.76 (m, 3H), 7.66 (d, J = 3.8 Hz, 1H), 7.28 (ddd, J = 6.3, 4.3, 1.1 Hz, 2H), 7.20 (dd, J = 4.2, 1.3 Hz, 1H), 7.08 – 7.02 (m, 1H).
^{13}C NMR (100 MHz, $CDCl_3$) δ = 193.36, 152.88, 152.46, 141.75, 140.44, 137.64, 137.08, 128.02, 126.34, 125.14, 124.55, 124.36, 122.44, 119.33.
GC-MS(EI): 271 (100%, M^{*+}); 242 (25%, -CHO)
Melting point: 104-107 °C
Elemental Analysis, calc. for $C_{14}H_9NOS_2$: C, 61.97; H, 3.34; found: C, 62.07; H, 3.30.

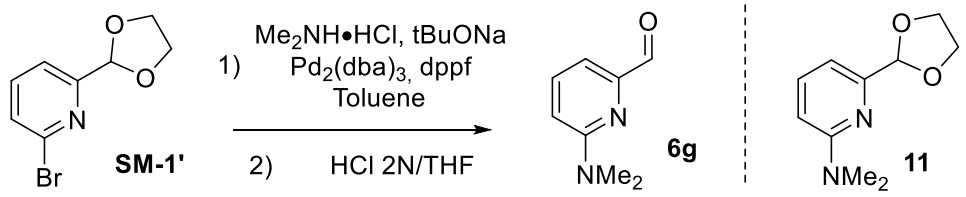

Step 1) To an oven dried Schlenk tube, under nitrogen atmosphere, Me_2NH•HCl (408 mg, 5 mmol), $Pd_2(dba)_3$ (31 mg, 30 µmol, 2.5mol%) and dppf (65 mg, 0.12 mmol, 10 mol%) were added. Then, 8

mL of dry toluene and **4** (460 mg, 2 mmol) were added and the mixture was degassed by nitrogen bubbling. Finally, *t*BuONa (1.15 g, 12 mmol) was added and the reaction mixture heated to reflux. The progress of the reaction was monitored *via* GC-MS. After complete consumption of **4** the reaction was cooled to room temperature, 10 mL of distilled water were added and the crude extracted with DCM (3 x 10 mL). The organic phase was filtered through Celite®, dried over Na_2SO_4 and solvents evaporated with rotavapor.

Step 2) Crude **4'** was dissolved in 6 mL of THF and transferred into a one neck flask. Equal volume of HCl 2 M (6 mL, 12 mmol) was added and reaction heated at 70 °C. Reaction monitoring was executed by picking up few drops of mixture and quenching it in a saturated solution of $NaHCO_3$. AcOEt was added to extract organic compound and TLC was done. After complete conversion the reaction was cooled to room temperature and transferred to an Erlenmeyer flask. Saturated solution of $NaHCO_3$ was slowly added until pH ≈ 8. The mixture was extracted with diethyl ether 3 x 15 mL and dried over Na_2SO_4. Solvents were evaporated and **5** was purified by flash chromatography using *n*Hex/AcOEt 20:1 as the eluent.

6g, yield 80% over 2 steps, light yellow oil.

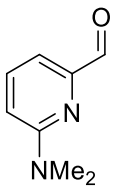

^{1}H NMR (400 MHz, $CDCl_3$) δ = 9.87 (t, *J* = 2.5 Hz, 1H), 7.59 – 7.48 (m, 1H), 7.17 (dd, *J* = 7.3, 2.1 Hz, 1H), 6.68 (dd, *J* = 8.5, 2.1 Hz, 1H), 3.12 (d, *J* = 2.1 Hz, 5H).
^{13}C NMR (100 MHz, $CDCl_3$) δ = 194.53, 159.31, 151.15, 137.63, 110.25, 109.89, 37.83.
GC-MS(EI): 135 (100%, -Me), 121 (90%), 150 (72%, $M^{\bullet+}$).
Anal. El. Calc. for $C_8H_{10}N_2O$: C, 63.98; H, 6.71; N, 18.65; O, 10.65; found: C, 63.89; H, 6.81; N, 18.60; O, 10.69.

Condensation to immie

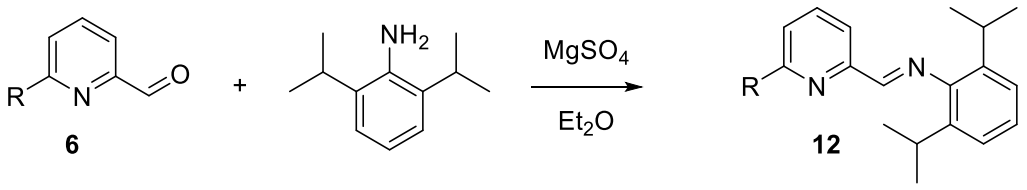

A 2 necked-round bottom flask, under inert atmosphere, was charged with **6** (1.3 mmol, 1 eq), 0.5g of anhydrous $MgSO_4$, 10 mL diethyl ether and 2,6-diisopropylaniline (293 µL 1.56 mmol, 1.2 eq). The reaction was stirred at room temperature overnight. The complete consumption of **6** was evaluated by GC-MS. Then $MgSO_4$ was filtered off and washed with diethyl ether. The organic phase was evaporated and the excess of aniline was distilled at 140 °C 0.2 mbar. Product **12** was used immidiately in the next steps without further purification.

Imidazole ring closure

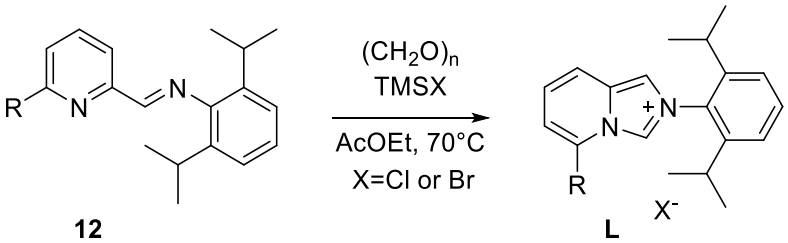

In a 2 necked-round bottom flask, under inert atmosphere, **12** (1 mmol, 1 eq) was dissolved in 5mL of dried AcOEt and then paraformaldehyde (33 mg, 1.1 mmol, 1.1 eq) was added and heated at 70 °C.

After 15 minutes at the same temperature TMSX (1.1 mmol, 1.1 eq., X = Br, 145 µL, or X = Cl, 138 µL) was added dropwise. The reaction was stirred at the same temperature until **12** was consumed. TLC *c*Hex/AcOEt 5:1. The reaction was cooled to 0 °C and filtered with a Gooch funnel. The solid was washed once with cold ethyl acetate and twice with diethyl ether. The solid was dried in vacuum and used without further purification.

L1, yield 88%, pale yellow solid.

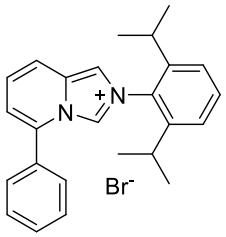

^{1}H NMR (400 MHz, $CCDl_3$) δ = 9.04 (s, 1H), 8.73 (d, J = 9.3 Hz, 1H), 8.60 (d, J = 1.8 Hz, 1H), 7.68 – 7.65 (m, 1H), 7.64 (d, J = 1.9 Hz, 1H), 7.61 (dt, J = 3.3, 2.0 Hz, 2H), 7.59 (d, J = 1.9 Hz, 1H), 7.57 – 7.48 (m, 2H), 7.31 (d, J = 7.9 Hz, 2H), 7.19 (dd, J = 7.0, 1.1 Hz, 1H), 2.20 (hept, J = 6.7 Hz, 2H), 1.23 (d, J = 6.8 Hz, 6H), 1.11 (d, J = 6.8 Hz, 6H).
^{13}C NMR (100 MHz, $CDCl_3$) δ = 144.97, 134.70, 132.40, 132.15, 131.53, 130.73, 130.50, 130.30, 128.21, 126.33, 124.64, 122.28, 120.28, 119.89, 119.18, 28.66, 24.52, 24.26.

LC-MS(ESI+): 355.4 ($-Br^-$)
Melting point: 287-290 °C
Elemental Analysis, calc. for $C_{25}H_{27}BrN_2$: C, 68.96; H, 6.25; found: C, 68.87; H, 6.28.

L2, yield 78%, colourless solid.

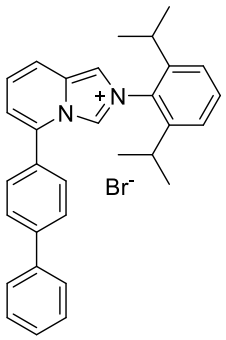

^{1}H NMR (400 MHz, $CDCl_3$) δ = 9.11 (d, J = 1.8 Hz, 1H), 8.78 (d, J = 9.3 Hz, 1H), 8.68 (d, J = 1.7 Hz, 1H), 7.82 (d, J = 8.1 Hz, 2H), 7.77 – 7.71 (m, 2H), 7.60 (d, J = 7.4 Hz, 2H), 7.58 – 7.50 (m, 2H), 7.47 (t, J = 7.4 Hz, 2H), 7.42 – 7.37 (m, 1H), 7.32 (d, J = 7.8 Hz, 2H), 7.24 – 7.21 (m, 1H), 2.23 (hept, J = 6.7 Hz, 2H), 1.25 (d, J = 6.7 Hz, 6H), 1.14 (d, J = 6.8 Hz, 6H).
^{13}C NMR (100 MHz, $CDCl_3$) δ = 145.18, 144.23, 139.31, 134.68, 132.46, 132.13, 130.55, 129.60, 129.05, 128.85, 128.74, 128.34, 127.13, 126.73, 124.65, 122.44, 119.95, 119.77, 118.53, 28.64, 24.56, 24.38.

LC-MS(ESI+): 431.4 ($-Br^-$)
Melting point: 130-132 °C
Elemental Analysis, calc. for $C_{31}H_{31}BrN_2$: C, 72.79; H, 6.11; found: C, 72.72; H, 6.09.

L3, yield 90%, yellow solid.

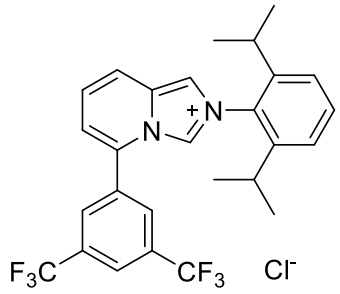

^{1}H NMR (400 MHz, $CDCl_3$) δ = 9.03 – 8.97 (m, 1H), 8.45 (s, 1H), 8.35 (d, *J* = 9.2 Hz, 1H), 8.27 (s, 2H), 8.00 (s, 1H), 7.52 (td, *J* = 8.2, 7.6, 2.3 Hz, 2H), 7.28 (d, *J* = 7.9 Hz, 2H), 7.25 (d, *J* = 4.9 Hz, 1H), 2.26 (hept, *J* = 6.6 Hz, 2H), 1.16 (d, *J* = 6.6 Hz, 6H), 1.10 (d, *J* = 6.6 Hz, 6H).
^{13}C NMR (100 MHz, $CDCl_3$) δ = 145.23, 133.61, 133.43, 133.28, 132.15, 132.11, 130.37, 129.26, 126.37, 124.82, 124.62, 123.96, 123.82, 121.24, 121.21, 120.48, 118.06, 28.54, 24.33, 24.31.
^{19}F NMR (377 MHz, $CDCl_3$) δ = -62.96 (s, 6F).

LC-MS(ESI+): 491.4 ($-Cl^-$)
Melting point: decomposition.
Elemental Analysis, calc. for $C_{27}H_{25}ClF_6N_2$: C, 61.54; H, 4.78; found: C, 61.57; H, 4.83.

L4, yield 60%, pale yellow solid

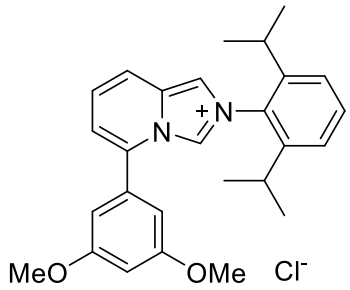

^{1}H NMR (400 MHz, $CDCl_3$) δ = 8.71 (dt, *J* = 7.2, 1.8 Hz, 1H), 8.66 (d, *J* = 1.9 Hz, 1H), 8.49 (t, *J* = 8.5 Hz, 1H), 7.51 (ddd, *J* = 19.9, 8.9, 6.9 Hz, 2H), 7.30 (dd, *J* = 7.9, 2.5 Hz, 2H), 7.20 (d, *J* = 6.9 Hz, 1H), 6.75 (dt, *J* = 3.2, 1.9 Hz, 2H), 6.58 (d, *J* = 2.6 Hz, 1H), 3.79 (d, *J* = 2.6 Hz, 6H), 2.19 (tt, *J* = 10.9, 5.2 Hz, 2H), 1.20 (dd, *J* = 6.9, 3.3 Hz, 6H), 1.10 (dd, *J* = 6.9, 2.2 Hz, 6H).

^{13}C NMR (100 MHz, $CDCl_3$) δ = 162.05, 145.11, 134.72, 132.46, 132.34, 132.18, 130.50, 126.44, 124.65, 122.53, 119.87, 119.57, 118.52, 106.26, 102.80, 55.74, 28.63, 24.58, 24.24.

LC-MS(ESI+): 415.4 (-Cl^-)

Melting point: decomposition.

Elemental Analysis, calc. for $C_{27}H_{31}ClN_2O_2$: C, 71.91; H, 6.93; found: C, 71.98; H, 6.87.

L5, yield 90%, yellow solid.

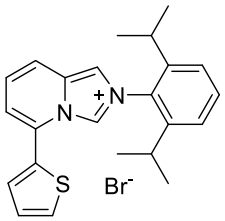

^{1}H NMR (400 MHz, $CDCl_3$) δ = 9.08 (dt, J = 1.8, 0.9 Hz, 1H), 9.01 (d, J = 1.9 Hz, 1H), 8.75 – 8.67 (m, 1H), 7.70 (dd, J = 3.7, 1.2 Hz, 1H), 7.63 (dd, J = 5.1, 1.1 Hz, 1H), 7.56 (t, J = 7.9 Hz, 1H), 7.51 – 7.43 (m, 1H), 7.33 (ddd, J = 7.9, 3.6, 1.1 Hz, 3H), 7.27 (ddd, J = 5.0, 3.7, 0.9 Hz, 1H), 2.19 (hept, J = 6.6 Hz, 2H), 1.24 – 1.20 (m, 6H), 1.15 (dd, J = 6.9, 0.8 Hz, 6H).

^{13}C NMR (100 MHz, $CDCl_3$) δ = 145.03, 132.35, 132.24, 130.75, 130.48, 130.29, 129.61, 129.02, 128.69, 126.00, 124.70, 123.03, 120.88, 120.58, 119.29, 28.73, 24.54, 24.39.

LC-MS(ESI+): 361.4 (-Br^-)

Melting point: decomposition.

Elemental Analysis, calc. for $C_{23}H_{25}BrN_2S$: C, 62.58; H, 5.71; found: C, 62.50; H, 5.73.

L6, yield 74%, yellow solid.

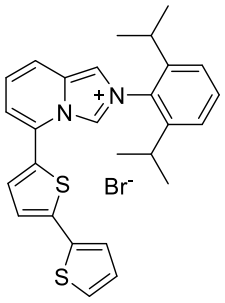

^{1}H NMR (400 MHz, CD_2Cl_2) δ = 9.61 – 9.56 (m, 1H), 8.57 (d, J = 1.8 Hz, 1H), 8.35 (dt, J = 9.3, 1.0 Hz, 1H), 7.73 (d, J = 3.9 Hz, 1H), 7.63 (t, J = 7.9 Hz, 1H), 7.54 (dd, J = 9.3, 7.1 Hz, 1H), 7.43 (d, J = 1.1 Hz, 1H), 7.41 (s, 1H), 7.39 (s, 1H), 7.37 (dd, J = 5.1, 1.2 Hz, 1H), 7.35 (d, J = 3.9 Hz, 1H), 7.32 (dd, J = 3.7, 1.2 Hz, 1H), 7.09 (dd, J = 5.1, 3.7 Hz, 1H), 2.21 (hept, J = 6.8 Hz, 2H), 1.22 (d, J = 5.2 Hz, 6H), 1.21 (d, J = 5.3 Hz, 6H).

^{13}C NMR (100 MHz, CD_2Cl_2) δ = 145.04, 141.55, 135.20, 132.23, 131.17, 129.03, 128.74, 128.26, 126.47, 126.37, 125.52, 124.92, 124.69, 124.26, 124.15, 120.20, 119.08, 118.12, 28.75, 24.20, 24.08.

LC-MS(ESI+): 443.4 (-Br^-)

Melting point: 266-270 °C

Elemental Analysis, calc. for $C_{27}H_{27}BrN_2S_2$: C, 61.94; H, 5.20; found: C, 61.93; H, 5.27.

L10, yield 80%, brown powder.

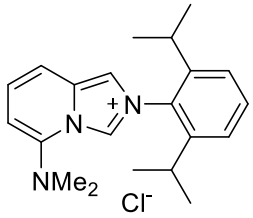

^{1}H NMR (400 MHz, $CDCl_3$) δ = 9.70 (t, *J* = 8.6 Hz, 1H), 8.31 (s, 1H), 7.94 (dd, *J* = 9.3, 2.3 Hz, 1H), 7.55 (td, *J* = 7.8, 3.8 Hz, 1H), 7.37 (ddd, *J* = 9.7, 7.5, 2.8 Hz, 1H), 7.31 (dd, *J* = 7.9, 4.3 Hz, 2H), 6.68 (d, *J* = 7.2 Hz, 1H), 2.96 (d, *J* = 4.8 Hz, 6H), 2.12 (h, *J* = 6.7 Hz, 2H), 1.17 (ddd, *J* = 11.1, 7.0, 4.6 Hz, 12H). ^{13}C NMR (100 MHz, $CDCl_3$) δ = 144.96, 144.15, 132.33, 132.04, 130.73, 127.44, 124.55, 123.84, 117.02, 113.40, 105.22, 41.95, 28.71, 24.55, 24.24.

LC-MS(ESI): 322.4 (-Cl^-).

Melting point: decomposition.

Anal. El. Calc. for $C_{21}H_{28}ClN_3$: C, 70.47; H, 7.89; N, 11.74; found: C, 70.58; H, 7.78; N, 11.84.

Synthesis of L7-8

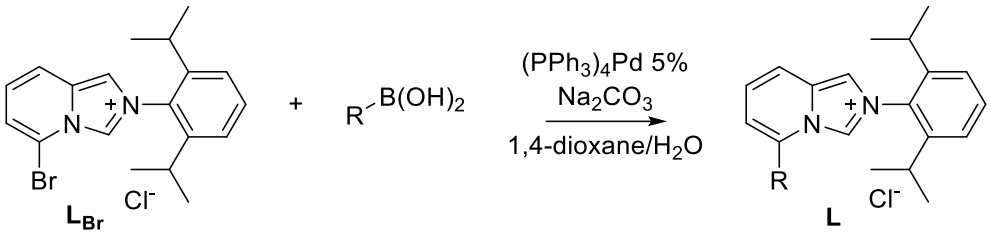

A 2 necked-round bottom flask equipped with a condenser, under inert atmosphere, was charged with **L_{Br}** (197 mg, 0.5 mmol, 1 eq), [$Pd(PPh_3)_4$] (29 mg, 0.025 mmol, 5 mol%), aryl boronic acid (224 mg, 0.6mmol, 1.2 eq) and 3.5mL of degassed 1,4-dioxane. The reaction was stirred at room temperature for 30 min, then 1.2mL of 0.5 M solution of Na_2CO_3 (1.2 eq) in degassed water was added and the reaction mixture heated at 80 °C. The reaction was monitored by TLC DCM/MeOH 10:1. After consumption of **7** the reaction mixture was extracted 3 times with CH_2Cl_2, dried on Na_2SO_4 and purified by flash chromatography with DCM/MeOH from 100/1 to 20/1 as eluent.

L7, yield 69%, brown solid.

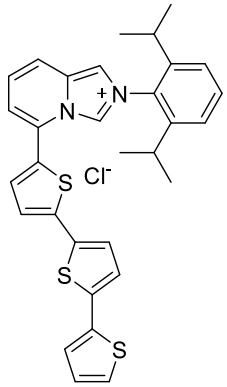

^{1}H NMR (400 MHz, $CDCl_3$) δ = 9.35 (d, J = 1.8 Hz, 1H), 8.94 (d, J = 1.8 Hz, 1H), 8.64 (d, J = 9.3 Hz, 1H), 7.72 (d, J = 3.9 Hz, 1H), 7.57 (t, J = 7.9 Hz, 1H), 7.46 (dd, J = 9.3, 7.1 Hz, 1H), 7.34 (t, J = 7.2 Hz, 3H), 7.29 (d, J = 3.9 Hz, 1H), 7.24 (d, J = 4.8 Hz, 1H), 7.16 (dd, J = 12.7, 3.7 Hz, 2H), 7.08 (d, J = 3.8 Hz, 1H), 7.03 – 6.99 (m, 1H), 2.20 (h, J = 6.7 Hz, 2H), 1.22 (d, J = 6.8 Hz, 6H), 1.19 (d, J = 6.8 Hz, 6H).

^{13}C NMR (100 MHz, $CDCl_3$) δ = 144.99, 141.02, 138.28, 136.35, 133.71, 132.28, 132.21, 131.35, 130.53, 128.54, 128.03, 126.12, 126.08, 125.21, 124.97, 124.66, 124.50, 124.32, 123.59, 120.41, 120.04, 118.96, 28.75, 24.50, 24.46.

LC-MS(ESI+): 525.0 (-Cl^-)

Melting point: decomposition

Elemental Analysis, calc. for $C_{31}H_{29}ClN_2S_3$: C, 66.35; H, 5.21; found: C, 66.41; H, 5.18.

L8, yield 72%, pale yellow powder.

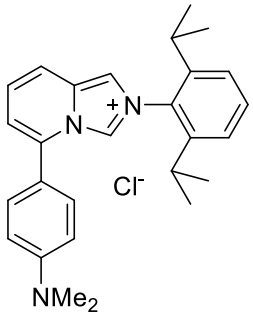

^{1}H NMR (400 MHz, $CDCl_3$) δ = 8.79 (d, *J* = 1.9 Hz, 1H), 8.60 (dd, *J* = 2.0, 0.9 Hz, 1H), 8.42 (dt, *J* = 9.4, 1.0 Hz, 1H), 7.43 (t, *J* = 7.9 Hz, 1H), 7.37 – 7.16 (m, 5H), 6.98 (dd, *J* = 7.0, 1.1 Hz, 1H), 6.73 – 6.65 (m, 2H), 2.90 (s, 6H), 2.02 (hept, *J* = 6.8 Hz, 2H), 1.09 (d, *J* = 6.8 Hz, 6H), 1.00 (d, *J* = 6.8 Hz, 6H).
^{13}C NMR (100 MHz, $CDCl_3$) δ = 151.85, 144.84, 135.73, 132.46, 132.08, 130.46, 128.86, 126.57, 124.56, 122.13, 118.51, 118.43, 118.37, 116.61, 112.44, 40.01, 28.59, 24.51, 24.17.
LC-MS (ESI): 398.6 (-Cl^-).

Melting point: decomposition.
Anal. El. Calc. for $C_{27}H_{32}ClN_3$: C 74.72; H 7.43; N, 9.68; found: C 74.94; H 7.36; N, 9.75.

L9, yield 67%, pale yellow powder.

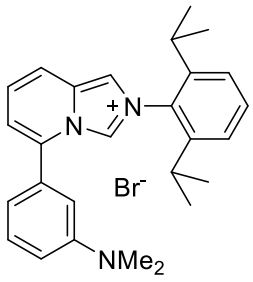

^{1}H NMR (400 MHz, $CDCl_3$) δ = 8.92 (d, *J* = 1.8 Hz, 1H), 8.59 (d, *J* = 9.4 Hz, 1H), 8.56 (d, *J* = 1.1 Hz, 1H), 7.48 (t, *J* = 7.9 Hz, 1H), 7.42 (dd, *J* = 9.3, 6.9 Hz, 1H), 7.32 (t, *J* = 8.1 Hz, 1H), 7.23 (d, *J* = 7.9 Hz, 2H), 7.14 (dd, *J* = 6.9, 1.0 Hz, 1H), 6.82 – 6.71 (m, 3H), 2.91 (s, 6H), 2.07 (hept, J = 6.6 Hz, 2H), 1.15 (d, *J* = 6.8 Hz, 6H), 1.03 (d, *J* = 6.8 Hz, 6H).
^{13}C NMR (100 MHz, $CDCl_3$) δ = 151.24, 144.89, 135.75, 132.27, 132.17, 131.39, 130.81, 130.43, 126.37, 124.62, 122.27, 119.80, 119.24, 118.87, 114.64, 114.61, 110.76, 40.18, 28.65, 24.50, 24.23.
LC-MS(ESI): 398.6 (-Br^-).

Melting point: decomposition.
Anal. El. Calc. for $C_{27}H_{32}BrN_3$: C 74.72; H 7.43; N, 9.68; found: C 74.82; H 7.51; N, 9.73.

Synthesis of Au(I) metal complexes

Procedure A)

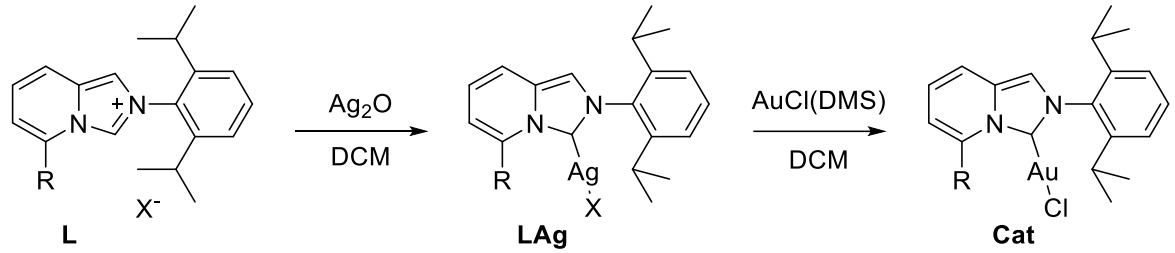

In a two-necked round bottom flask, covered with aluminium foil to provide darkness, **L** (0.2 mmol, 1 eq) was dissolved in 1 mL of dry DCM and then Ag_2O (56 mg, 0.24 mmol, 1.1 eq) was added. The reaction mixture was stirred at room temperature overnight. TLC monitoring using *c*Hex/AcOEt 2:1. The reaction was filtered through Celite® pad and washed with DCM. The organic phase was then evaporated. The crude **LAg** was redissolved in 1 mL of dry DCM and transferred in a 2 necked-bottom flask covered with foil. AuCl(DMS) (59 mg, 0.2 mmol, 1 eq) was then added and stirred at room temperature for 5 h. After all Ag complex was completely consumed the reaction was filtered through Celite® pad and washed with DCM and evaporated. The residual solid was dried under vacuum to remove DMS.

Procedure B)

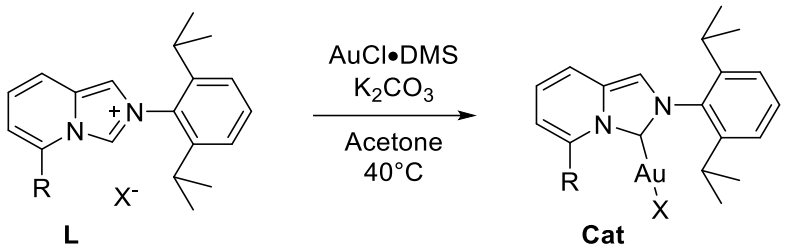

Ligand precursor **L** (0.1 mmol), K_2CO_3 (41.4 mg, 0.3 mmol) and AuCl(DMS) (29.4 mg, 0.1 mmol) are added into a vial. Then, 1 mL of acetone (reagent grade) was added, and the closed vial stirred at 40 °C for 2 h. After complete consumption of starting salts, acetone was evaporated under reduced pressure and the crude dissolved in DCM and filtered on Celite® pad. DCM was evaporated yielding [Au(I)] complexes that were triturated in *n*Hex before use.

Cat1, procedure A, yield 83%, pale orange solid.

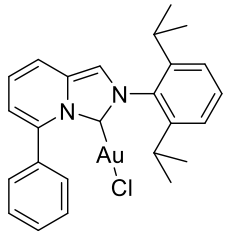

^{1}H NMR (400 MHz, $CDCl_3$) δ = 7.60 – 7.48 (m, 5H), 7.48 – 7.41 (m, 2H), 7.32 (s, 1H), 7.21 (d, J = 7.8 Hz, 2H), 7.05 (dd, J = 9.3, 6.6 Hz, 1H), 6.60 (dd, J = 6.6, 1.3 Hz, 1H), 2.18 (hept, J = 6.8 Hz, 2H), 1.22 (d, J = 6.8 Hz, 6H), 1.10 (d, J = 6.9 Hz, 6H).
^{13}C NMR (100 MHz, $CDCl_3$) δ = 145.12, 135.63, 132.34, 132.09, 131.57, 130.61, 130.33, 130.30, 128.62, 127.37, 124.78, 123.55, 119.91, 118.36, 116.98, 28.68, 24.68, 24.57.
Melting point: decomposition.
Exact mass, calc for $C_{25}H_{26}AuClN_2$: 586.1450, found: 586.1455.

Cat2, procedure A, yield 80%, colourless solid.

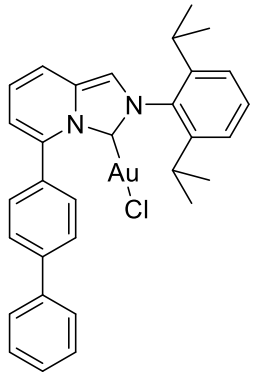

^{1}H NMR (400 MHz, $CDCl_3$) δ 7.74 – 7.65 (m, 3H), 7.66 (s, 1H), 7.61 (d, J = 8.0 Hz, 2H), 7.46 (dd, J = 8.5, 3.7 Hz, 2H), 7.40 (t, J = 7.8 Hz, 3H), 7.36 – 7.29 (m, 2H), 7.21 (d, J = 7.8 Hz, 2H), 7.07 (dd, J = 9.3, 6.7 Hz, 1H), 6.66 (dd, J = 6.7, 1.3 Hz, 1H), 2.26 – 2.14 (m, 2H), 1.24 (d, J = 6.8 Hz, 6H), 1.10 (d, J = 6.9 Hz, 6H).
^{13}C NMR (101 MHz, $CDCl_3$) δ 145.18, 144.19, 139.36, 135.44, 132.34, 132.16, 130.36, 129.35, 129.08, 129.04, 128.78, 128.29, 127.38, 127.21, 124.79, 123.46, 119.92, 118.24, 116.78, 28.66, 24.67, 24.59.
Melting Point: decomposition.
Exact mass, calc for $C_{31}H_{30}AuClN_2$: 662.1763, found: 662.1766.

Cat3, procedure A, yield 77%, pale yellow solid.

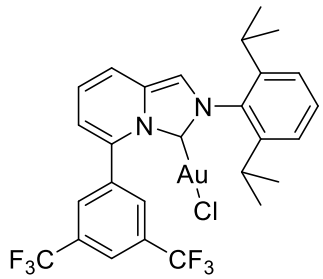

^{1}H NMR (400 MHz, $CDCl_3$) δ = 8.08 – 7.92 (m, 2H), 7.55 (d, J = 9.5 Hz, 1H), 7.44 (t, J = 7.8 Hz, 1H), 7.40 (s, 1H), 7.25 – 7.19 (m, 2H), 7.09 (dd, J = 9.3, 6.7 Hz, 1H), 6.71 (d, J = 6.8 Hz, 1H), 2.15 (hept, 6.6 Hz, 2H), 1.25 – 1.20 (d, J = 6.6 Hz, 6H), 1.11 (d, J = 6.6 Hz, 6H).
^{13}C NMR (100 MHz, $CDCl_3$) δ = 145.09, 145.03, 136.36, 135.89, 135.07, 132.41, 132.07, 131.44, 130.78, 129.99, 124.18, 123.28, 118.56, 117.90, 117.67, 114.32, 28.48, 24.35, 24.17.

^{19}F NMR (377 MHz, $CDCl_3$) δ = -62.96 (s, 6F).
Melting Point: decomposition.
Exact mass, calc for $C_{27}H_{24}AuClF_6N_2$: 722.1198, found: 722.1199.

Cat4, procedure A, yield 75%, colourless solid.

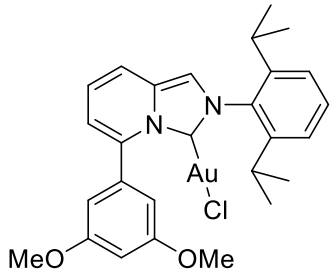

^{1}H NMR (400 MHz, $CDCl_3$) δ = 7.46 – 7.40 (m, 2H), 7.31 (s, 1H), 7.21 (d, J = 7.8 Hz, 2H), 7.03 (dd, J = 9.3, 6.7 Hz, 1H), 6.73 – 6.69 (m, 2H), 6.65 – 6.60 (m, 2H), 3.81 (s, 7H), 2.18 (hept, J = 6.7 Hz, 2H), 1.24 (d, J = 6.8 Hz, 6H), 1.10 (d, J = 6.9 Hz, 6H).
^{13}C NMR (100 MHz, $CDCl_3$) δ = 161.09, 145.06, 139.69, 135.57, 135.25, 131.57, 130.54, 124.06, 123.49, 117.03, 116.00, 113.51, 108.48, 102.18, 55.54, 28.40, 24.41, 24.23.

Melting point: decomposition.
Exact mass, calc for $C_{27}H_{30}AuClN_2O_2$: 646.1661, found: 646.1668.

Cat5, procedure A, yield 92%, pale yellow solid.

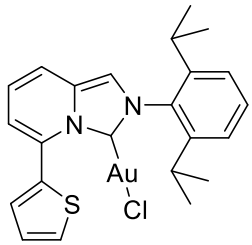

^{1}H NMR (400 MHz, $CDCl_3$) δ = 7.60 (dd, *J* = 5.0, 1.3 Hz, 1H), 7.52 – 7.38 (m, 3H), 7.33 (d, *J* = 1.3 Hz, 1H), 7.23 – 7.17 (m, 3H), 7.01 (ddd, *J* = 8.1, 6.7, 1.4 Hz, 1H), 6.76 (dd, *J* = 6.7, 1.4 Hz, 1H), 2.22 – 2.15 (m, 2H), 1.23 (d, *J* = 7.2 Hz, 6H), 1.09 (d, *J* = 7.0 Hz, 6H).
^{13}C NMR (100 MHz, $CDCl_3$) δ = 145.11, 135.52, 133.78, 132.54, 131.55, 130.76, 130.60, 128.49, 127.73, 124.07, 123.10, 119.14, 118.17, 114.02, 28.39, 24.46, 24.22.

Melting point: decomposition.
Exact mass, calc for $C_{23}H_{24}AuClN_2S$: 592.1014, found: 592.1021.

Cat6, procedure A, yield 87%, dark yellow solid.

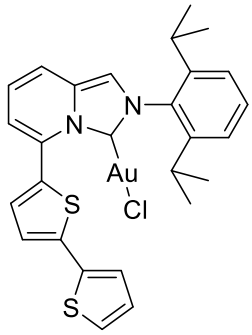

^{1}H NMR (400 MHz, $CDCl_3$) δ = 7.51 – 7.40 (m, 2H), 7.35 (d, J = 3.7 Hz, 1H), 7.32 (s, 2H), 7.27 – 7.18 (m, 4H), 7.05 – 6.98 (m, 1H), 6.97 (dd, J = 5.3, 3.7 Hz, 1H), 6.79 (dd, J = 6.8, 1.2 Hz, 1H), 2.20 (hept, J = 6.9 Hz, 2H), 1.25 (d, J = 6.8 Hz, 6H), 1.10 (d, J = 6.9 Hz, 6H).
^{13}C NMR (100 MHz, $CDCl_3$) δ = 145.11, 140.50, 136.38, 135.52, 132.19, 131.55, 130.62, 127.79, 125.35, 125.30, 124.58, 124.09, 123.11, 119.18, 118.19, 114.08, 28.41, 24.47, 24.27.
Melting point: decomposition.

Exact mass, calc for $C_{27}H_{26}AuClN_2S_2$: 674.0891, found: 674.0886.

Cat7, procedure A, yield 80%, brown solid.

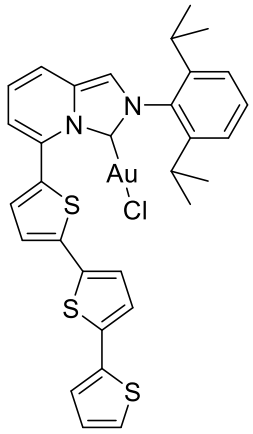

^{1}H NMR (400 MHz, CD_2Cl_2) δ = 7.59 – 7.51 (m, 2H), 7.41 (s, 1H), 7.39 (d, J = 3.8 Hz, 1H), 7.31 (d, J = 7.8 Hz, 2H), 7.28 – 7.24 (m, 2H), 7.22 (dd, J = 3.6, 1.2 Hz, 1H), 7.19 (d, J = 3.8 Hz, 1H), 7.12 (d, J = 3.8 Hz, 1H), 7.06 (d, J = 6.7 Hz, 1H), 7.05 – 7.02 (m, 2H), 6.84 (dd, J = 6.7, 1.2 Hz, 1H), 2.24 (hept, J = 6.9 Hz, 2H), 1.26 (d, J = 6.8 Hz, 6H), 1.13 (d, J = 6.9 Hz, 6H).
^{13}C NMR (100 MHz, CD_2Cl_2) δ = 145.27, 139.86, 137.10, 136.89, 135.71, 135.23, 132.71, 131.79, 131.72, 131.59, 130.56, 127.91, 125.68, 125.64, 124.70, 124.42, 124.39, 124.23, 124.07, 124.04, 123.93, 123.05, 123.01, 119.35, 118.39, 114.32, 28.38, 24.13, 23.89.
Melting point: 248-252°C.
Exact mass, calc for $C_{31}H_{28}AuClN_2S_3$: 756.0769, found: 756.0765

Cat8, procedure B, yield 97%, orange powder.

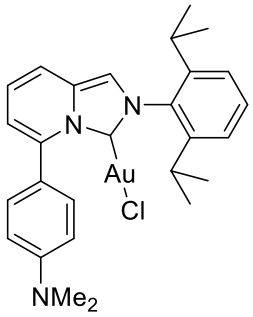

^{1}H NMR (400 MHz, $CDCl_3$) δ = 7.43 (t, *J* = 7.8 Hz, 1H), 7.41 – 7.31 (m, 2H), 7.25 (d, *J* = 9.0 Hz, 2H), 7.20 (d, *J* = 7.8 Hz, 2H), 7.01 (dd, *J* = 9.2, 6.7 Hz, 1H), 6.86 – 6.75 (m, 2H), 6.58 (dd, *J* = 6.7, 1.3 Hz, 1H), 2.99 (s, 6H), 2.19 (hept, *J* = 6.8 Hz, 2H), 1.23 (d, *J* = 6.9 Hz, 6H), 1.09 (d, *J* = 6.9 Hz, 6H).
^{13}C NMR (101 MHz, $CDCl_3$) δ 165.99, 152.21, 145.12, 140.79, 135.73, 131.70, 130.44, 130.37, 123.99, 123.69, 121.56, 116.07, 115.99, 113.38, 112.57, 40.66, 28.35, 24.50, 24.28.
Melting point: decomposition.
Exact mass: calc. for $C_{27}H_{31}AuClN_3$: 629.1872, found: 629.1879.

Cat9, Procedure B, yield 99%, orange powder.

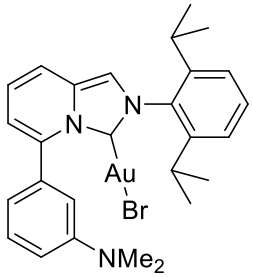

^{1}H NMR (400 MHz, $CDCl_3$) δ = 7.47 – 7.40 (m, 2H), 7.36 (dd, *J* = 8.4, 7.3 Hz, 1H), 7.29 (s, 1H), 7.21 (d, *J* = 7.8 Hz, 2H), 7.03 (dd, *J* = 9.2, 6.7 Hz, 1H), 6.90 (ddd, *J* = 8.5, 2.7, 0.9 Hz, 1H), 6.88 – 6.83 (m, 2H), 6.64 (dd, *J* = 6.7, 1.3 Hz, 1H), 2.98 (s, 6H), 2.20 (hept, *J* = 6.9 Hz, 2H), 1.26 (d, *J* = 6.8 Hz, 3H), 1.21 (dd, *J* = 6.8, 3.2 Hz, 3H), 1.15 – 1.04 (m, 6H).
^{13}C NMR (100 MHz, $CDCl_3$) δ = 150.74, 145.07, 140.89, 137.66, 135.60, 134.44, 131.54, 130.48, 129.86, 124.09, 123.93, 123.62, 117.06, 116.54, 115.68, 114.55, 113.75, 113.20, 40.52, 28.41, 28.36, 24.80, 24.50, 24.33, 24.28, 24.17.
Melting point: decomposition.
Exact mass: calc. for $C_{27}H_{31}AuClN_3$: 629.1872, found: 629.1868.

Cat10, procedure B, yield 96%, light yellow powder.

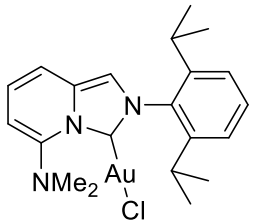

^{1}H NMR (400 MHz, $CDCl_3$) δ = 7.48 (t, *J* = 7.8 Hz, 1H), 7.30 – 7.21 (m, 3H), 7.15 (d, *J* = 9.1 Hz, 1H), 6.96 (dd, *J* = 9.1, 7.0 Hz, 1H), 6.25 (d, *J* = 7.0 Hz, 1H), 2.92 (s, 6H), 2.20 (hept, *J* = 7.0 Hz, 2H), 1.29 (d, *J* = 6.8 Hz, 6H), 1.09 (d, *J* = 6.9 Hz, 6H).
^{13}C NMR (100 MHz, $CDCl_3$) δ = 164.46, 148.58, 145.16, 135.74, 132.51, 130.53, 124.23, 124.08, 113.71, 112.47, 102.45, 44.23, 28.41, 24.46, 24.28. Melting point: decomposition.

Exact mass: calc. for $C_{21}H_{27}AuClN_3$: 553.1559; found: 553.1563.

General procedure for the synthesis of Cat(TFA) complexes

The counterion metathesis was carried in a two-necked round bottom flask under inert atmosphere and in darkness. The gold(I) chloride complex **Cat** (0.015 mmol, 1eq) was dissolved in 0.5 mL of dry DCM, then 3.3 mg of AgTFA (0.015 mmol, 1 eq) was added. The reaction was stirred for 1 h at room temperature in the dark. The reaction was filtered through a pad of Celite® and washed with 1.5 mL of dry DCM. The organic phase was evaporated affording the desired product without any further purification in almost quantitative yields.

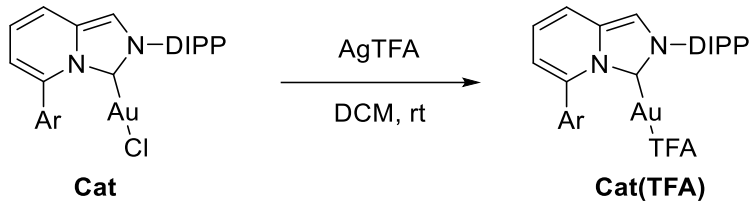

Cat **Cat(TFA)**

Cat1(TFA), yield 96%, brown powder.

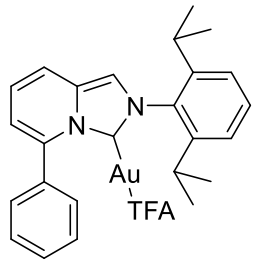

^{1}H NMR (400 MHz, $CDCl_3$) δ = 7.59 – 7.53 (m, 2H), 7.53 – 7.43 (m, 5H), 7.35 (s, 1H), 7.24 (s, 2H), 7.08 (dd, *J* = 9.3, 6.7 Hz, 1H), 6.64 (dd, *J* = 6.7, 1.2 Hz, 1H), 2.17 (hept, *J* = 6.9 Hz, 2H), 1.24 (d, *J* = 6.7 Hz, 6H), 1.11 (d, *J* = 6.9 Hz, 6H).

^{19}F NMR (377 MHz, $CDCl_3$) δ -74.29 (s, 3F).

Cat2(TFA), yield 98%, orange powder.

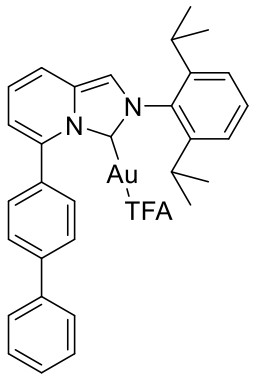

^{1}H NMR (400 MHz, $CDCl_3$) δ = 7.86 (q, *J* = 8.3 Hz, 4H), 7.62 – 7.56 (m, 2H), 7.56 – 7.47 (m, 2H), 7.45 – 7.33 (m, 4H), 7.26 (d, *J* = 7.9 Hz, 2H), 7.15 (dd, *J* = 9.3, 6.7 Hz, 1H), 6.74 (dd, *J* = 6.7, 1.2 Hz, 1H), 2.25 (hept, *J* = 7.1 Hz, 2H), 1.23 (d, *J* = 6.8 Hz, 6H), 1.10 (d, *J* = 6.8 Hz, 6H).

^{19}F NMR (377 MHz, $CDCl_3$) δ = -73.23 (s, 3F).

Cat3(TFA), yield 98%, pale yellow powder.

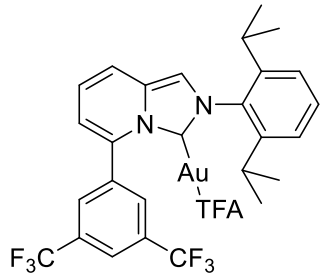

^{1}H NMR (400 MHz, $CDCl_3$) δ = 8.05 (s, 2H), 7.97 (s, 1H), 7.56 (dd, J = 9.3, 1.2 Hz, 1H), 7.46 (s, 0H), 7.43 (d, J = 1.2 Hz, 1H), 7.28 – 7.22 (m, 2H), 7.15 – 7.09 (m, 1H), 6.75 (dd, J = 6.7, 1.2 Hz, 1H), 2.14 (hept, J = 7.0 Hz, 2H), 1.25 (d, J = 7.0 Hz, 6H), 1.12 (d, J = 6.7 Hz, 6H).

^{19}F NMR (377 MHz, $CDCl_3$) δ = -63.21(s, 6F), -74.46 (s, 3F).

Cat4(TFA), yield 93%, pale yellow powder.

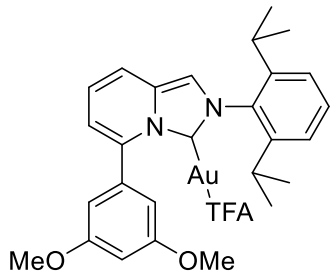

^{1}H NMR (400 MHz, $CDCl_3$) δ 7.52 – 7.44 (m, 2H), 7.35 (s, 1H), 7.26 (s, 1H), 7.24 (s, 1H), 7.08 (dd, *J* = 9.3, 6.7 Hz, 1H), 6.86 (d, *J* = 2.3 Hz, 2H), 6.68 (dd, *J* = 6.7, 1.2 Hz, 1H), 6.52 (t, *J* = 2.3 Hz, 1H), 3.80 (s, 6H), 2.22 (hept, *J* = 6.8 Hz, 2H), 1.24 (d, *J* = 6.8 Hz, 7H), 1.10 (d, *J* = 6.8 Hz, 6H).
^{19}F NMR (377 MHz, $CDCl_3$) δ = -73.67.

Gold(I)-catalysed naphthol dearomatization

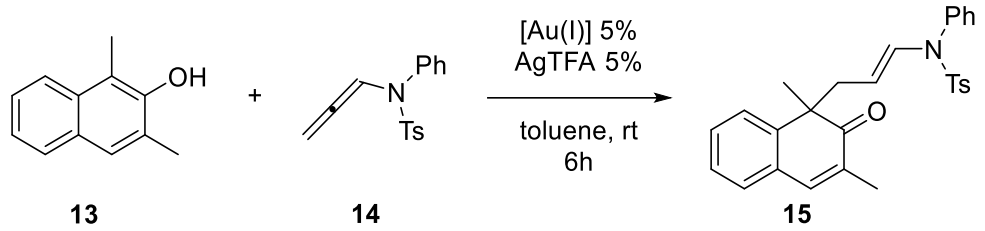

In a two-necked round bottom flask under inert atmosphere, [Au(I)] (2.5 x 10^{-3} mmol, 5 mol%) and AgTFA (0.55 mg, 2.5x10^{-3} mmol, 5 mol%) were added and dissolved in 1 mL of dry toluene and stirred. The glassware was covered in foil to provide darkness. After 15 minutes, 1,3-dimethyl naphth-2-ol (**13**, 8.6 mg, 0.05 mmol) and *N*-phenyl-*N*-tosyl allenammide (**14**, 21.3 mg, 0.075 mmol) were added. The reaction was stirred at room temperature for 6 h. After that time, the mixture was charged directly in column for purification by flash chromatography using *n*-Hex:AcOEt 9 to 1 as eluent. NMR spectra are in agreement with literature.[47c]

Kinetic experiment set up

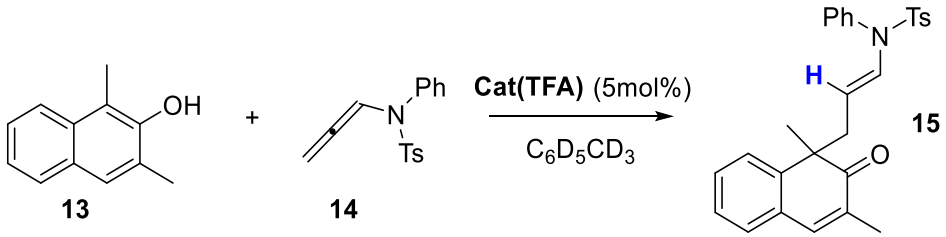

Dried NMR tubes were charged with 6 mg of 1,3-dimethylnapht-2-ol (**13**, 0.035 mmol, 15 mg allenamide (**14**, 0.053 mmol), **Cat(TFA)** (1.75 μmol, 5 mol%) and 0.035mmol of internal standard. Subsequently 0.7 mL of d^8-toluene were added (t = 0 min). NMR spectra were then collected periodically.
To evaluate the progress of the reaction we focused to the diagnostic peaks of C*H* in beta position of the enamide moiety of **15** (δ = 3.99 ppm, dt, 1H).

Olefine cyclopropanation reaction

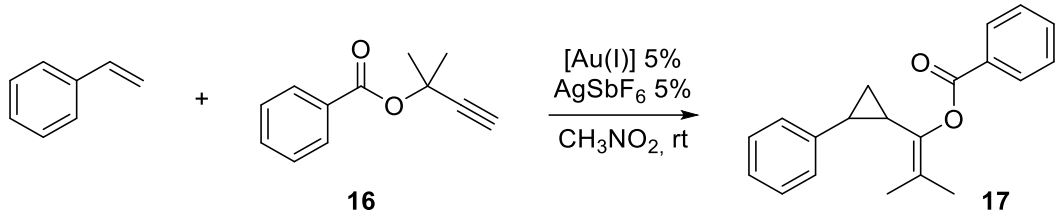

In a two neck round bottomed flask, under nitrogen atmosphere, Au catalysts (5µmol, 5%mol) was dissolved in 1mL of nitromethane (ACS reagent grade). The flask was covered with foil to provide darkness. $AgSbF_6$ (1.7mg, 5µmol) is added and the reaction was let stirring for 10minutes. Then styrene (45µL, 0.4mmol, 4eq) ad **16** (18.8mg, 0.1mmol, 1eq) were added subsequently. After 30minutes the reaction was monitored by TLC and solvent evaporated. Final product **17** was purified by flash chromatography using *n*-hexane:AcOEt 30/1 as eluent phase.

17, colourless viscous oil.

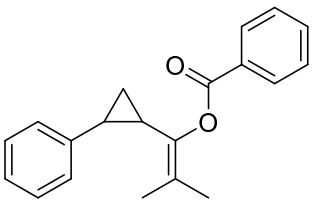

^{1}H NMR *cis*-**17** (400 MHz, $CDCl_3$) δ = 7.86 (d, *J* = 7.6 Hz, 2H), 7.55 (t, *J* = 7.6 Hz, 1H), 7.41 (t, *J* = 7.2 Hz, 2H), 7.26 – 7.20 (m, 2H), 7.20 – 7.15 (m, 1H), 7.09 (d, *J* = 7.3 Hz, 2H), 2.42 – 2.22 (m, 2H), 1.63 (s, 3H), 1.47 (s, 3H), 1.28 (dt, *J* = 13.6, 5.1 Hz, 1H), 1.09 (q, *J* = 5.9 Hz, 1H).
^{13}C NMR *cis*-**17** (100 MHz, $CDCl_3$) δ = 164.65, 139.34, 138.55, 133.03, 129.86, 129.79, 128.31, 127.63, 127.61, 125.58, 123.48, 23.76, 21.41, 18.65, 17.62, 11.70.

Alkynylbenzaldehyde cyclization

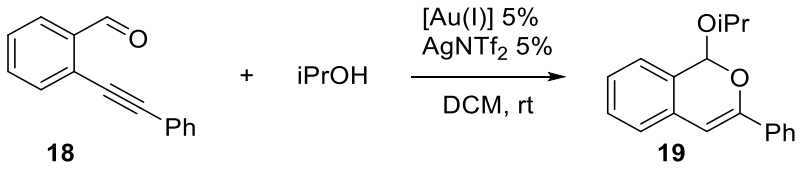

In a two neck round bottomed flask, under nitrogen atmosphere, Au catalysts (10µmol, 5%mol) was dissolved in 1mL of dichloroethane. The flask was covered with foil to provide darkness. $AgNTf_2$ (3.9mg, 10µmol) is added and the reaction was let stirring for 10minutes. Then isopropanol (15µL, 0.2mmol, 1eq) and **18** (41.2mg, 0.2mmol, 1eq) were added subsequently. After 2 hours the reaction was monitored by TLC and solvent evaporated. Final product **19** was purified by flash chromatography using *n*-hexane:AcOEt 30/1 as eluent phase.

18, pale yellow solid.

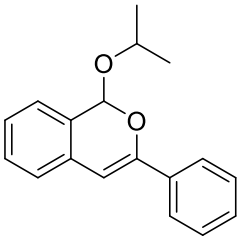

^{1}H NMR (400 MHz, $CDCl_3$) δ = 7.81 (dt, *J* = 6.5, 1.4 Hz, 4H), 7.44 – 7.38 (m, 4H), 7.35 (tt, *J* = 7.6, 1.8 Hz, 4H), 7.29 – 7.19 (m, 6H), 6.61 (s, 2H), 6.32 (s, 2H), 4.38 (hept, *J* = 6.2 Hz, 2H), 1.32 (d, *J* = 6.1 Hz, 6H), 1.19 (d, *J* = 6.3 Hz, 6H).
^{13}C NMR (100 MHz, $CDCl_3$) δ = 149.50, 134.80, 130.38, 129.15, 128.62, 128.41, 127.62, 126.64, 125.54, 124.86, 124.57, 100.38, 96.95, 69.84, 23.57, 21.97.

Synthesis of model substrate 23a

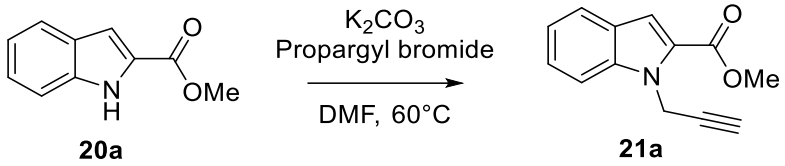

In a two necked-round-bottom flask, under inert atmosphere of nitrogen, **20a** (262 mg, 1.5 mmol) was dissolved in 10 mL of DMF and K_2CO_3 (621 mg, 4.5 mmol) was added. Then propargyl bromide (400 µL, 4.5 mmol) was added dropwise and the reaction heated to 60 °C. After 4 h the reaction was checked by TLC and quenched with saturated aqueous solution of sodium bicarbonate. The mixture was extracted with AcOEt (3 x 20 mL) and the organic phase washed with distilled water (2 x 25 mL) and brine (1 x 25 mL). The organic phase was dried over Na_2SO_4 and then evaporated. **21a** was purified by flash chromatography using *c*Hex/AcOEt 20:1 as the eluent.

21a, yield 89%, colourless solid.

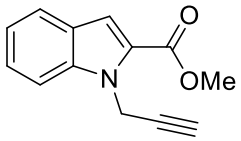

^{1}H NMR (400 MHz, $CDCl_3$) δ = 7.71 (dt, *J* = 8.0, 1.0 Hz, 1H), 7.53 – 7.46 (m, 1H), 7.41 (ddd, *J* = 8.4, 7.0, 1.2 Hz, 1H), 7.35 (d, *J* = 1.0 Hz, 1H), 7.22 (ddd, *J* = 8.0, 6.9, 1.0 Hz, 1H), 5.42 (d, *J* = 2.5 Hz, 2H), 3.93 (s, 3H), 2.29 (t, *J* = 2.5 Hz, 1H).

^{13}C NMR (100 MHz, $CDCl_3$) δ = 162.34, 138.95, 126.54, 126.24, 125.56, 122.84, 121.23, 111.56, 110.59, 78.80, 72.14, 51.79, 33.80.

GC-MS(EI): 198 (100, -Me), 213 (42%, $M^{\bullet+}$), 154 (40%, -CO_2Me).

Melting point: 92–94 °C.

Anal. El. Calc. for $C_{13}H_{11}NO_2$: C, 73.23; H, 5.20; N, 6.57; O, 15.01; found: C, 73.28; H, 5.23; N, 6.55; O, 14.95.

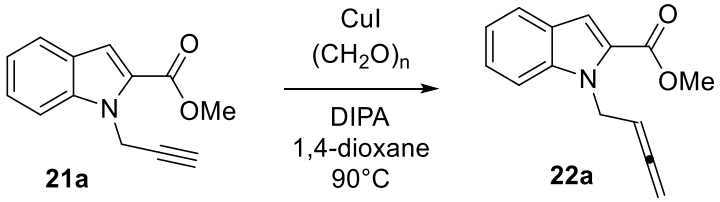

In a Schlenk tube, to a solution of pre-flamed CuI (143 mg, 0.75 mmol) in 1,4-dioxane (2.5 mL), **21a** (320 mg, 1.5 mmol) and paraformaldehyde (72 mg, 2.4 mmol) were added. Then diisopropyl amine (DIPA, 260 µL, 1.8 mmol) was added dropwise and the reaction heated at 90 °C for 16 h. The conversion was monitored by TLC and quenched with 5 mL of water ad diluted with 10 mL of AcOEt. Product was extracted with AcOEt (2 x 15 mL) and then, the organic phase, washed with diluted ammonia solution (2 x 20 mL) to remove copper traces from organic phase. Organic phase was dried over Na_2SO_4 and evaporated under reduced pressure, product **22a** was purified by flash chromatography using *c*Hex/AcOEt 10:1 as the eluent.

22a, yield 86%, colourless solid.

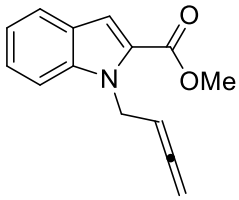

^{1}H NMR (400 MHz, $CDCl_3$) δ = 7.67 (d, *J* = 8.0 Hz, 1H), 7.42 (dd, *J* = 8.6, 1.1 Hz, 1H), 7.34 (ddd, *J* = 8.4, 6.9, 1.2 Hz, 1H), 7.29 (d, *J* = 0.9 Hz, 1H), 7.15 (ddd, *J* = 8.0, 6.9, 1.0 Hz, 1H), 5.36 (p, *J* = 6.5 Hz, 1H), 5.20 (dt, *J* = 6.4, 2.7 Hz, 2H), 4.74 (dt, *J* = 6.6, 2.7 Hz, 2H), 3.91 (s, 3H).
^{13}C NMR (100 MHz, $CDCl_3$) δ = 208.77, 162.42, 139.10, 126.88, 126.11, 125.10, 122.66, 120.73, 110.81, 110.78, 87.86, 76.84, 51.66, 43.29.
GC-MS(EI): 168 (100%, -CO_2Me), 188 (33%, -CH=C=CH_2), 227 (29%, $M^{\bullet+}$).
Melting point: 51–55 °C.
Anal. El. Calc. for $C_{14}H_{13}NO_2$: C, 73.99; H, 5.77; N, 6.16; O, 14.08; found: C, 73.96; H, 5.82; N, 6.14; O, 14.10.

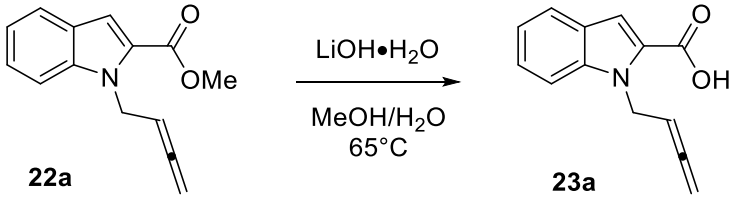

In a round bottomed flask containing 5 mL of MeOH, **22a** (227 mg, 1 mmol) was added, and the flask heated to 65 °C. Next, LiOH•H_2O (420 mg, 10 mmol) was dissolved in 5mL of water and the solution added to the methanolic one. The closed flask was maintained at the same temperature until **22a** was completely consumed. The mixture was concentred at rotavapor and then THF (10 mL) and brine (10 mL) were added. The biphasic mixture was cooled to 0 °C and HCl 2 M was added dropwise under vigorous stirring until pH ≈ 4. Water phase was extracted with THF (3 x15 mL), the organic phase dried over Na_2SO_4, evaporated and the product purified by flash chromatography using *c*Hex/THF 5:1 as the eluent.

23a, yield 93%, colourless solid.

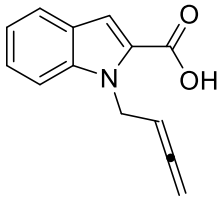

^{1}H NMR (400 MHz, $CDCl_3$) δ = 7.70 (dq, *J* = 8.1, 0.9 Hz, 1H), 7.46 (d, *J* = 0.8 Hz, 1H), 7.45 – 7.42 (m, 1H), 7.37 (tt, *J* = 7.0, 0.9 Hz, 1H), 7.16 (ddt, *J* = 7.8, 6.9, 0.8 Hz, 1H), 5.37 (p, *J* = 6.5 Hz, 1H), 5.21 (dt, *J* = 6.1, 2.7 Hz, 2H), 4.79 – 4.72 (m, 2H).
^{13}C NMR (100 MHz, Acetone-d_6) δ = 208.57, 162.37, 139.19, 127.21, 126.20, 124.89, 122.44, 120.59, 110.88, 110.62, 87.87, 76.11, 42.67.
LC-MS(ESI+): 214.4 $(M+H)^+$.
Melting point: 164–170 °C
Anal. El. Calc. for $C_{13}H_{11}NO_2$: C, 73.23; H, 5.20; N, 6.57; O, 15.01; found: C, 73.30; H, 5.23; N, 6.54; O, 14.95.

General procedure for the gold(I)-catalysed lactonization of *N*-allenyl indole-2-carboxylic acid

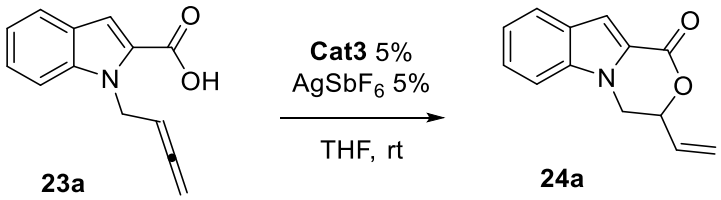

In a two neck round bottomed flask, dried and under nitrogen atmosphere, **Cat3** (3.6 mg, 5 µmol, 5 mol%) was dissolved in 1 mL of anhydrous THF. The flask was covered in foil to provide darkness and then $AgSbF_6$ (1.7 mg, 5 µmol) was added, and the reaction stirred for 10 minutes. Next, **23a** (21.3 mg, 0.1 mmol) was added. The reaction was stirred for 24 h and conversion of **23a** was monitored by TLC. To the reaction mixture was added dry silica and solvent evaporated. Final product was purified by flash chromatography using *n*Hex/AcOEt 5:1 as the eluent.

2a, yield 90%, colourless solid.

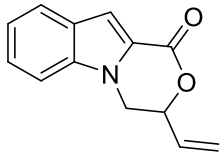

^{1}H NMR (400 MHz, $CDCl_3$) δ = 7.72 (dt, *J* = 8.1, 1.0 Hz, 1H), 7.42 (d, *J* = 0.9 Hz, 1H), 7.41 – 7.36 (m, 1H), 7.34 – 7.31 (m, 1H), 7.19 (ddd, *J* = 8.0, 6.8, 1.1 Hz, 1H), 6.01 (ddd, *J* = 17.3, 10.7, 5.8 Hz, 1H), 5.59 (ddd, *J* = 17.3, 1.5, 0.7 Hz, 1H), 5.44 (dt, *J* = 10.6, 1.1 Hz, 1H), 5.25 (dddt, *J* = 8.5, 6.1, 3.5, 1.4 Hz, 1H), 4.41 (dd, *J* = 12.8, 3.5 Hz, 1H), 4.08 (dd, *J* = 12.8, 9.3 Hz, 1H).
^{13}C NMR (100 MHz, $CDCl_3$) δ = 159.35, 136.60, 131.98, 126.98, 126.07, 123.29, 123.25, 121.48, 120.22, 110.17, 109.88, 77.79, 44.12.
GC-MS(EI): 129 (100%), 213 (45%, $M^{\bullet+}$), 168 (19%).
Melting point: 108–109 °C.
Anal. El. Calc. for $C_{13}H_{11}NO_2$: C, 73.23; H, 5.20; N, 6.57; O, 15.01; found: C, 73.31; H, 5.22; N, 6.16; O, 14.95.

For the synthesis of all the other substrates and for a complete characterization see ref. [51].

Table 16. *Crystal data and experimental details for* ***Cat1-4****.*

Compound	**Cat1**	**Cat2**	**Cat3**	**Cat4**
Formula	$C_{25}H_{26}AuClN_2$	$C_{31}H_{30}AuClN_2 \bullet C_6H_5CH_3$	$2(C_{27}H_{24}AuClF_6N_2) \bullet CH_2Cl_2$	$C_{27}H_{30}AuClN_2O_2$
Fw	586.89	755.12	1530.72	646.94
T, K	296(2)	296(2)	100(2)	296(2)
λ, Å	0.71073	0.71073	0.71073	0.71073
Crystal system	Monoclinic	Monoclinic	Triclinic	Triclinic
Space group	Cc	$P2_1/c$	P-1	P-1
***a*, Å**	14.603(5)	11.3017(7)	12.8783(5)	8.581(1)
***b*, Å**	13.510(3)	25.342(2)	15.0377(6)	10.434(2)
***c*, Å**	11.732(3)	11.6502(8)	15.6241(6)	15.176(3)
α	90	90	91.396(1)	104.303(5)
β	97.942(13)	100.307(2)	107.936(1)	91.153(7)
γ	90	90	99.023(1)	98.151(6)
Cell volume, Å^3	2292.4(1)	3282.9(4)	2834.6(2)	1301.3(4)
Z	4	4	2	2
D_c, Mg m^{-3}	1.701	1.528	1.793	1.651
μ(Mo-K$_\alpha$), mm^{-1}	6.547	4.591	5.438	5.781
F(000)	1144	1504	1484	636
Crystal size/ mm	0.34 x 0.28 x 0.20	0.34 x 0.21 x 0.17	0.22 x 0.17 x 0.14	0.21 x 0.16 x 0.07
θ limits, °	2.063 to 28.360	1.950 to 25.999	1.687 to 25.500	2.152 to 30.595
Reflections collected	20699	58242	37649	29642
Unique obs. Reflections [$F_o > 4\sigma(F_o)$]	5664 [R(int) = 0.0537]	6434 [R(int) = 0.0561]	10531 [R(int) = 0.0326]	7975 [R(int) = 0.0435]
Goodness-of-fit-on F^2	0.898	1.218	1.105	1.027
R_1 (F)[a], wR_2 (F^2) [I > 2σ(I)][b]	R1 = 0.0286, wR2 = 0.0745	R1 = 0.0259, wR2 = 0.0544	R1 = 0.0388, wR2 = 0.0883	R1 = 0.0248, wR2 = 0.0580
Largest diff. peak and hole, e. Å^{-3}	0.541 and -2.425	0.639 and -1.342	2.817 and -2.043	1.048 and -1.107

[a)] $R_1 = \Sigma||F_o|-|F_c||/\Sigma|F_o|$. [b)] $wR_2 = [\Sigma w(F_o^2-F_c^2)^2/\Sigma w(F_o^2)^2]^{1/2}$ where $w = 1/[\sigma^2(F_o^2) + (aP)^2 + bP]$ where $P = (F_o^2 + F_c^2)/3$.

Table 17. *Crystal data and experimental details for* ***Cat5-7****.*

Compound	**Cat5**	**Cat6**	**Cat7**
Formula	$C_{23}H_{24}AuClN_2S$	$C_{27}H_{26}AuClN_2S_2$	$C_{31}H_{28}AuClN_2S_3$
Fw	592.92	675.03	757.15
T, K	296(2)	296(2)	100(2)
λ, Å	0.71073	0.71073	0.71073
Crystal system	Monoclinic	Monoclinic	Triclinic
Space group	Cc	C2/c	P-1
***a*, Å**	14.5656(3)	26.832(1)	9.9008(4)
***b*, Å**	13.4438(3)	9.3547(4)	11.8021(5)
***c*, Å**	11.6052(2)	21.9411(9)	12.8588(5)
α, °	90	90	90.483(1)
β, °	97.303(1)	106.099(2)	99.696(1)
γ, °	90	90	93.561(1)
Cell volume, Å^3	2254.06(8)	5291.4(4)	1478.0(1)
Z	4	8	2
D_c, Mg m^{-3}	1.747	1.695	1.701
μ(Mo-K$_\alpha$), mm^{-1}	6.748	5.837	5.303
F(000)	1152	2640	744
Crystal size/ mm	0.28 x 0.22 x 0.20	0.20 x 0.16 x 0.10	0.11 x 0.08 x 0.06
θ limits, °	2.069 to 26.398	1.580 to 28.355	1.607 to 26.000
Reflections collected	18724	38550	19132
Unique obs. Reflections [$F_o > 4\sigma(F_o)$]	4606 [R(int) = 0.0372]	6546 [R(int) = 0.0513]	5731 [R(int) = 0.0297]
Goodness-of-fit-on F^2	1.055	0.861	1.046
R_1 (F)[a], wR_2 (F^2) [$I > 2\sigma(I)$][b]	R1 = 0.0184, wR2 = 0.0487	R1 = 0.0458, wR2 = 0.1053	R1 = 0.0196, wR2 = 0.0483
Largest diff. peak and hole, e. Å^{-3}	0.991 and -0.355	2.313 and -1.041	1.034 and -0.653

[a)] $R_1 = \Sigma||F_o|-|F_c||/\Sigma|F_o|$.[b)] $wR_2 = [\Sigma w(F_o^2-F_c^2)^2/\Sigma w(F_o^2)^2]^{1/2}$ where $w = 1/[\sigma^2(F_o^2) + (aP)^2 + bP]$ where $P = (F_o^2 + F_c^2)/3$.

Table 18. *Crystal data and structure refinement for compounds* ***Cat8-10.***

Compound	**Cat8**	**Cat9**	**Cat10**
Formula	$C_{27}H_{31}AuClN_3$	$C_{27}H_{31}AuBrN_3$	$C_{21}H_{27}AuClN_3$
Fw	629.96	674.42	553.87
T, K	296 (2)	296(2)	296 (2)
λ, Å	0.71073	0.71073	0.71073
Crystal system	Monoclinic	Monoclinic	Orthorhombic
Space group	$P2_1/n$	$P2_1/c$	$P2_12_12_1$
***a*, Å**	10.6885(8)	10.8669(7)	8.150(1)
***b*, Å**	16.120(1)	11.9595(8)	15.359(2)
***c*, Å**	15.127(1)	19.914(1)	17.032(2)
α, °	90	90	90
β, °	92.152 (2)	100.258(2)	90
γ, °	90	90	90
Cell volume, Å^3	2604.5(4)	2546.8(3)	2132.0(5)
Z	4	4	4
D_c, Mg m^{-3}	1.607	1.759	1.726
μ(Mo-K$_\alpha$), mm^{-1}	5.770	7.364	7.035
F(000)	1240	1312	1080
Crystal size/ mm	0.15 x 0.13 x 0.08	0.32 x 0.16 x 0.14	0.24 x 0.22 x 0.11
θ limits, °	1.847 to 25.496	1.904 to 26.000	1.785 to 25.496
Reflections collected	31627	32398	20519
Unique obs. Reflections [$F_o > 4\sigma(F_o)$]	4835 [R(int) = 0.0784]	5009 [R(int) = 0.0611]	3966 [R(int) = 0.0843]
Goodness-of-fit-on F^2	0.971	1.012	1.117
R_1 (F)[a], wR_2 (F^2) [I > 2σ(I)][b]	R1 = 0.0487, wR2 = 0.1150	R1 = 0.0450, wR2 = 0.1080	R1 = 0.0412, wR2 = 0.0901
Largest diff. peak and hole, e. Å^{-3}	2.299 and -1.801	1.876 and -1.714	2.100 and -0.846

[a)] $R_1 = \Sigma||F_o|-|F_c||/\Sigma|F_o|$. [b)] $wR_2 = [\Sigma w(F_o^2-F_c^2)^2/\Sigma w(F_o^2)^2]^{1/2}$ where $w = 1/[\sigma^2(F_o^2) + (aP)^2 + bP]$ where $P = (F_o^2 + F_c^2)/3$.

3. *Chiral ImPyAu(I) complexes for asymmetric catalysis*

3.1 Introduction: gold(I) in enantioselective transformations

The fascinating role of gold(I) in organometallic chemistry pushed the researcher to develop efficient stereoselective processes involving gold(I). Even if the very first gold-catalysed reaction was enantioselective (Figure 4), results demonstrating efficacy of gold(I) in enantioselective catalysis had to wait some years, until the end of the first decade of 2000s. The principal limitation that were faced are directly connected with the coordination mode of Au(I) (Figure 73). The linear geometry places the chiral ligand (L*) on the opposite site of the substrate, far from the chiral environment, secondly the anti-addition from the outer coordination sphere are even far less affected by the chiral ligand and lastly the low rigidity of the system by free rotation along L*-Au and Au-substrate decreases more the possibility of enantio induction.[67,68]

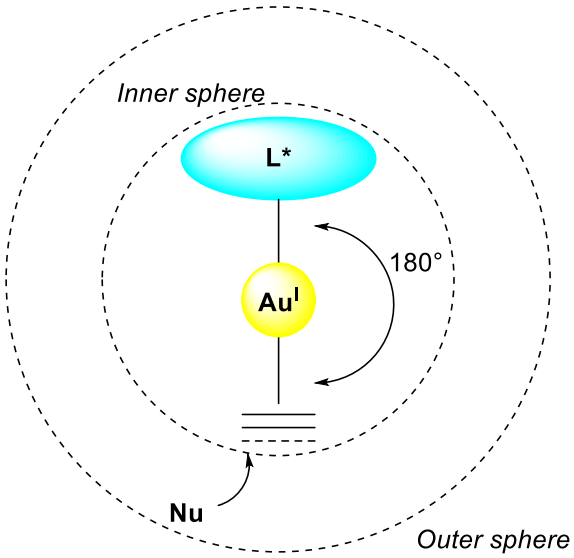

Figure 73. *Coordination and activation mode for Au(I).*

However, by time, several synthetic methodologies have been developed to overcome intrinsic barriers imposed by gold, and can be divided into three main groups:

- Asymmetric Counterion Directed Catalysis (ACDC);
- Dinuclear gold catalysts with chiral atropoisomeric bisphosphine;
- Chiral monodentate phosphoramidites.

Some significant examples of each group will be presented.

Asymmetric Counterion Directed Catalysis

In gold(I) catalysis the counter anion have a crucial role for the results of the reactions. From the counter anion might depend the activity or the selectivity or both for a catalytic transformation. This relies in the coordination and acidic/basic nature and the interaction that may occur with the substrate.[69]

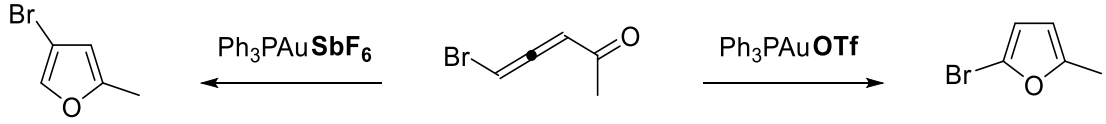

Figure 74. *Example of counterion effect in the gold(I)-catalysed bromo-furan synthesis.*[70]

In gold catalysis, H-bonding interaction between substrate/intermediate and slightly basic counter anion are commonly observed, and therefore chemists invested efforts to develop chiral anions suitable for enantioselective gold catalysis. In particular one scaffold has been investigated so far: the BINOL, and similar, monophosphate.

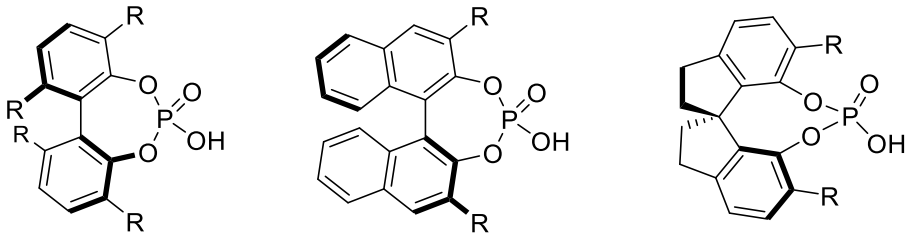

Figure 75. *Biphenol (left), BINOL (centre) and SPINOL (right) derivatives.*

These phosphoric acids possess a similar pKa (13.60 in I)[71] to trifluoro acetic acid (TFA, 12.65 in I) and therefore can assist the catalysis by H-bonding activation of nucleophile as TFA does. They are not used as acid (except when the catalyst is Lau-Me) but as silver salts to display chlorine scavenging activity.

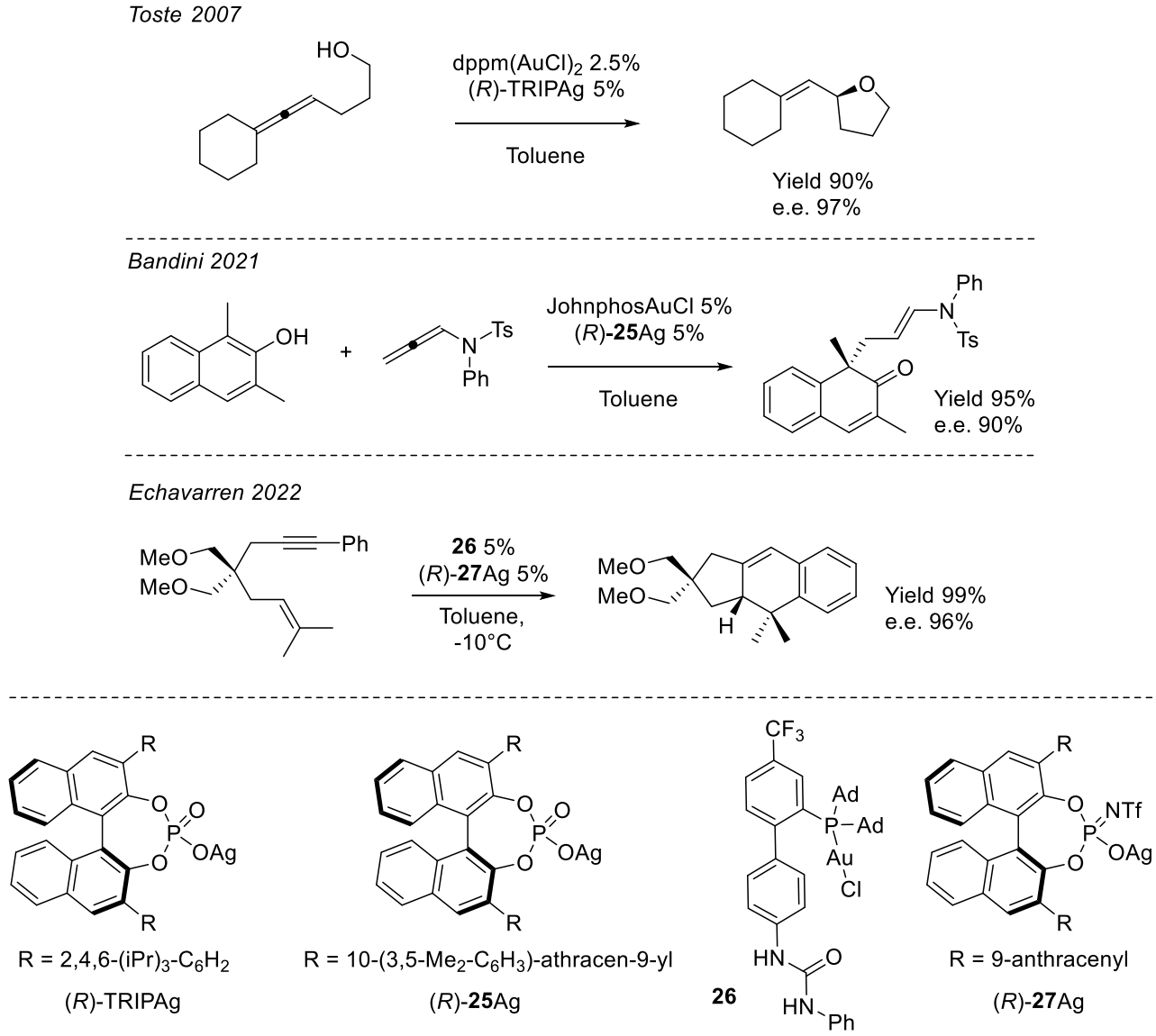

Figure 76. *Examples of application of chiral counter anion in gold(I) catalysis.*

Dinuclear gold catalysts with chiral atropoisomeric biphosphine

The use of bidentate atropoisomeric chiral biphosphines for the synthesis of dinuclear gold complexes is the most adopted strategy in asymmetric gold(I) catalysis.

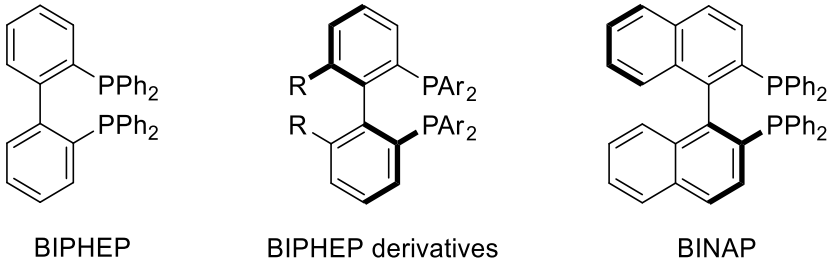

Figure 77. *Bidentate phosphines ligands.*

Typically used in this chemistry are the derivatives of BIPHEP and BINAP ligands. The generated dinuclear complexes are more rigid than monodentate chiral phosphines due to the restricted rotation of the stereogenic axis, aurophilic interactions and Ar…Au interactions and thus provides more enantio-induction. However, the role of second Au(I) metal centre is still debated by the community, and the general accepted theory is that one is responsible for the catalytic process and the other one contribute to the rigidity of the system to provide enantiomeric excess.

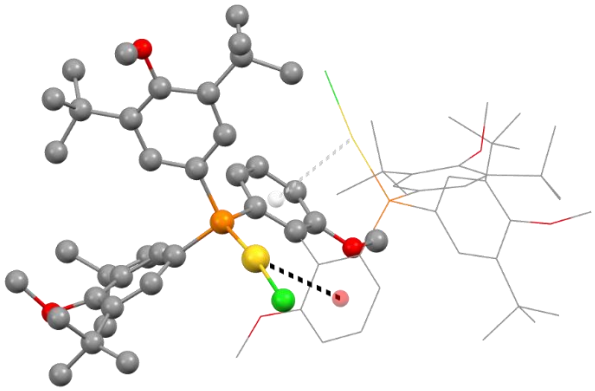

Figure 78. *Cystal structure of (S)-3,5-t-Bu-4-MeO-MeOBIPHEP. Ar(centroid)···Au interaction highlighted in black and grey dashed lines. Half molecule in wireframe style for clarity.*

In some cases, chiral biphosphine digold complexes can be coupled with chiral counter anion to provide high complex chiral catalysts, where Au-Au aurophilic interaction is observed.

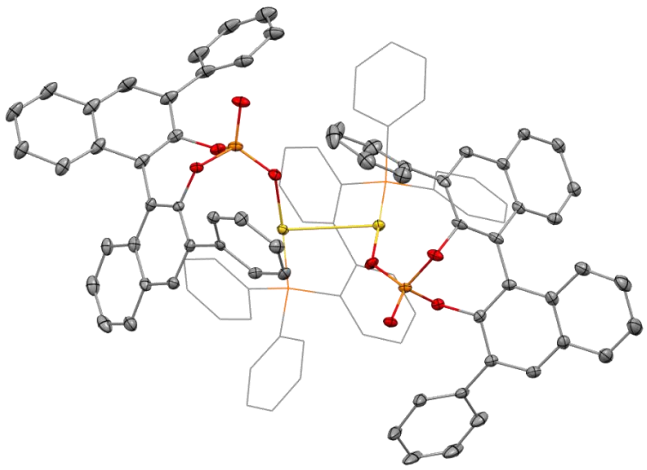

Figure 79. *Chiral biphosphine digold complex with chiral BINOL derivative of phosphoric acid. Badini 2015*

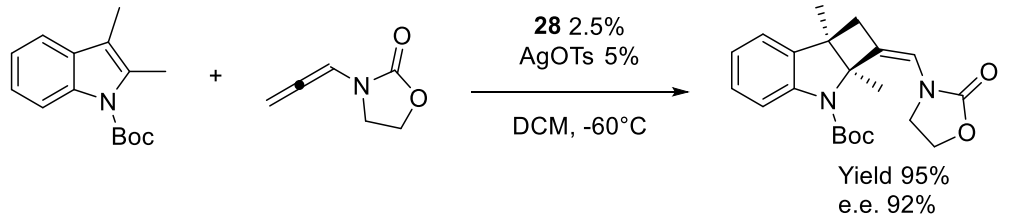

Toste 2011

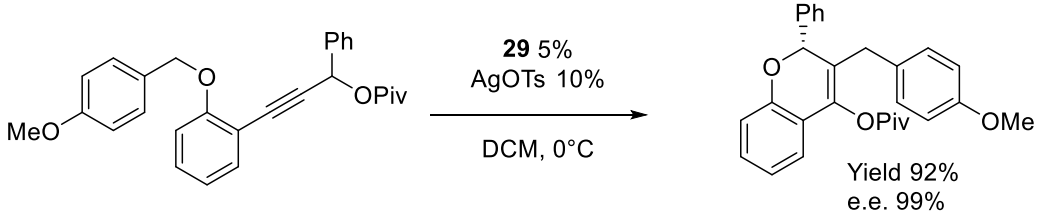

Davies 2012

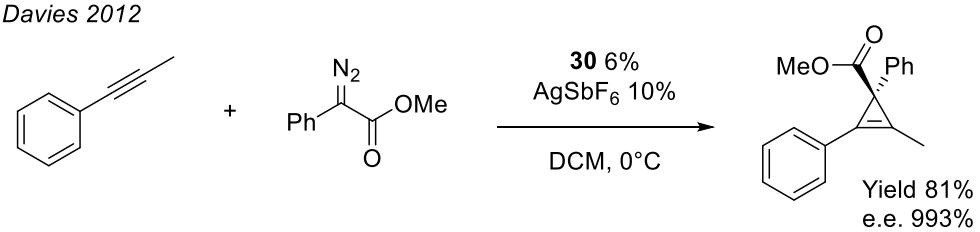

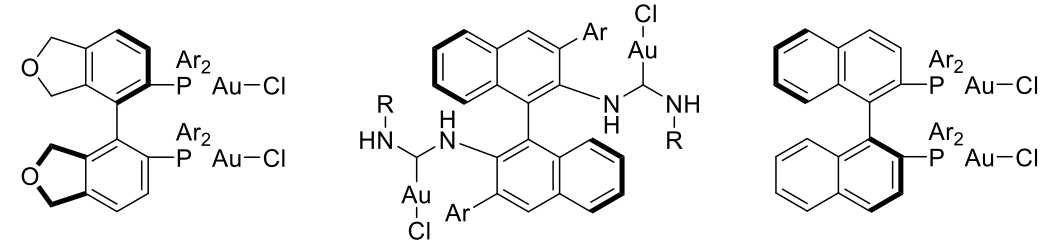

Figure 80. *Application of atropoisomeric bimetallic gold complexes.*

Bulky phosphoramidites

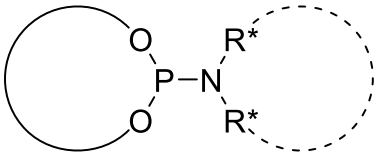

Figure 81. *General structure of phosphoramidite ligands.*

The peculiarity phosphoramidite ligands relies in the electronic properties of the phosphorus atom, which is a better π-acceptor than in phosphines and less than in phosphites, allowing an intermediate reactivity of the generated complexes. The synthesis is easy and allows the preparation of a wide library of ligands (Figure 82).[72] Commonly utilized are the BINOL and TADDOL derivatives, where amine can be cyclic or not, carrying the same substituents or different as proof of high tunability of these ligands.

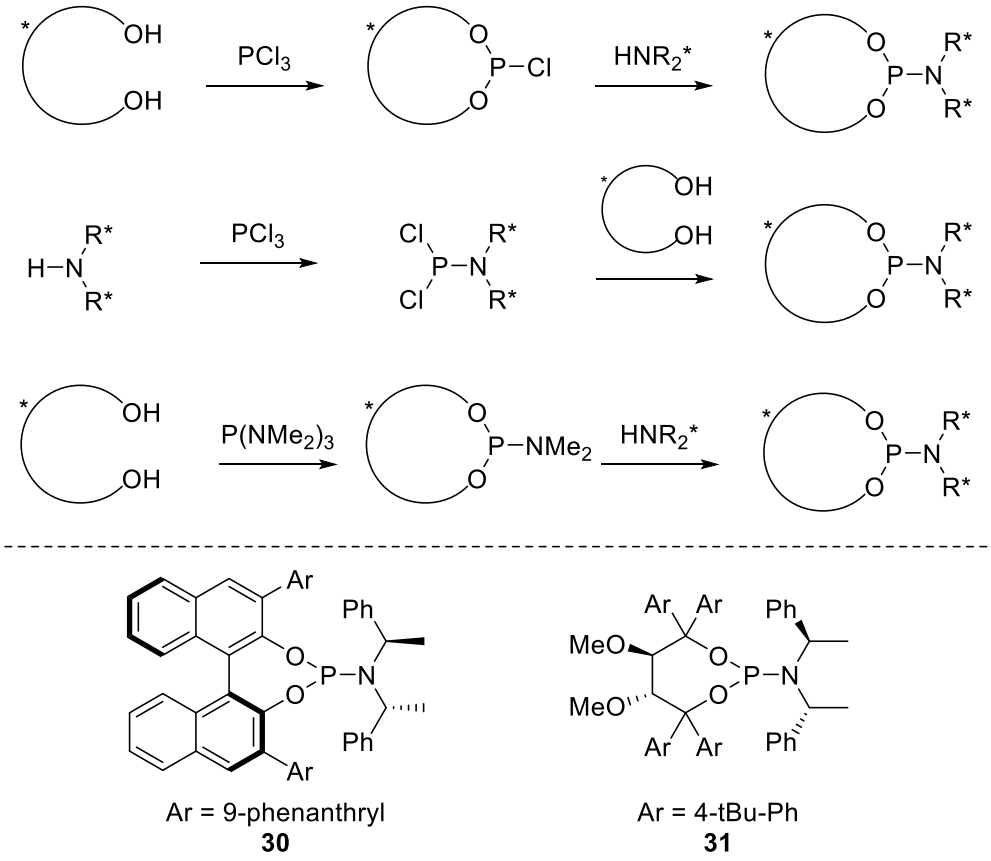

Figure 82. Synthetic strategies for the synthesis of phosphoramidite ligands (top), BINOL derivative (bottom left) and TADDOL derivative (bottom right).

These ligands provide-a highly hindered chiral pocket around the metal centre resulting in very high enantiomeric excess levels.

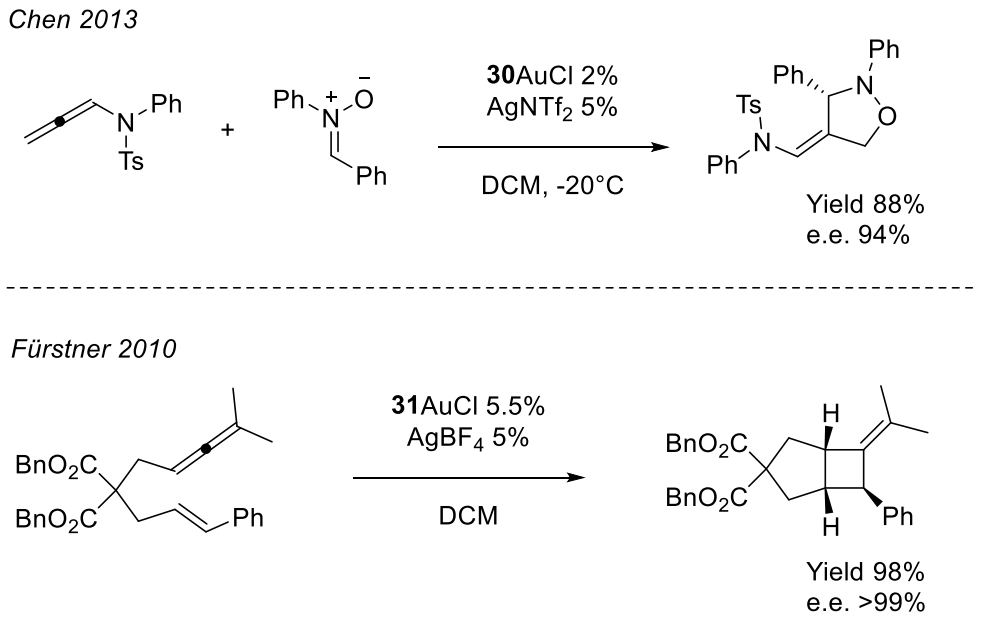

Figure 83. *Application of phosphoramidite ligands in asymmetric gold catalysis.*

3.2 Chiral NHC ligands and chiral ImPy related ligands for gold(I) asymmetric catalysis

Not only chiral phosphorus-based ligands are employed in gold catalysis but also carbenes. A large number of chiral ligands have been synthesized and adopted in gold(I) catalysis including ADC and NHC.[73,74] Some common scaffolds are presented below in Figure x.

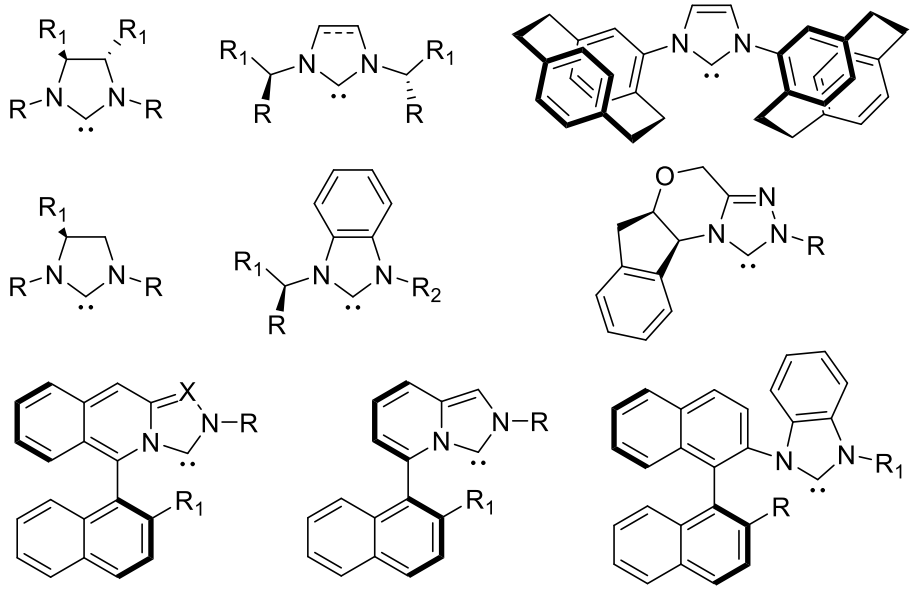

Figure 84. *Representative types of chiral NHC ligands.*

Ligands can be both C_1 or C_2 symmetric, and have the chiral element on the back-bone structure or on the nitrogen. Different scaffold are suitable for these ligands: dihydroimidazoles, imidazoles, benzimidazoles, triazoles and more complex imidazopyridines, imidazo isoquinolines allowing the obtaining of atropoisomeric monodentate NHC ligands.

An example of efficacy of chiral carbene-Au(I) catalysts has already be shown in Paragraph 2.2 and 3.1. Other great results were obtained by Mascareñas and Lassaletta after the development of chiral axial isoquinoline triazole derivatives (Figure 85).

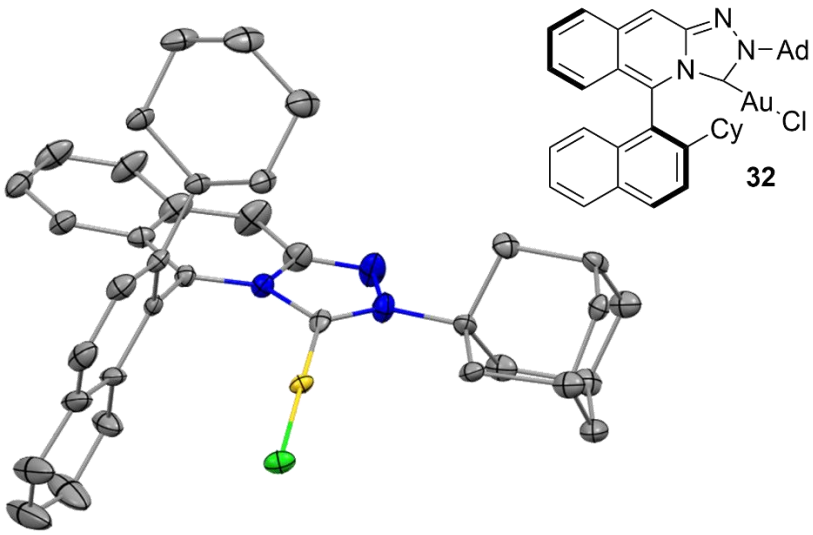

Figure 85. *Molecular drawing of* ***32****.*

The Au(I) complex shows high chiral congestion near the catalytic side, where the naphthyl is stacked to the gold by π-interaction and the cyclohexyl moiety is pointing above gold while the other side is blocked by the steric hindrance of the adamantyl. It was applied in [2+2+2][75] and [4+2][76] cycloadditions with excellent results. Other chiral NHC-Au complexes with chirality in the backbone structure or on nitrogen arms results in insufficient enantio-induction.

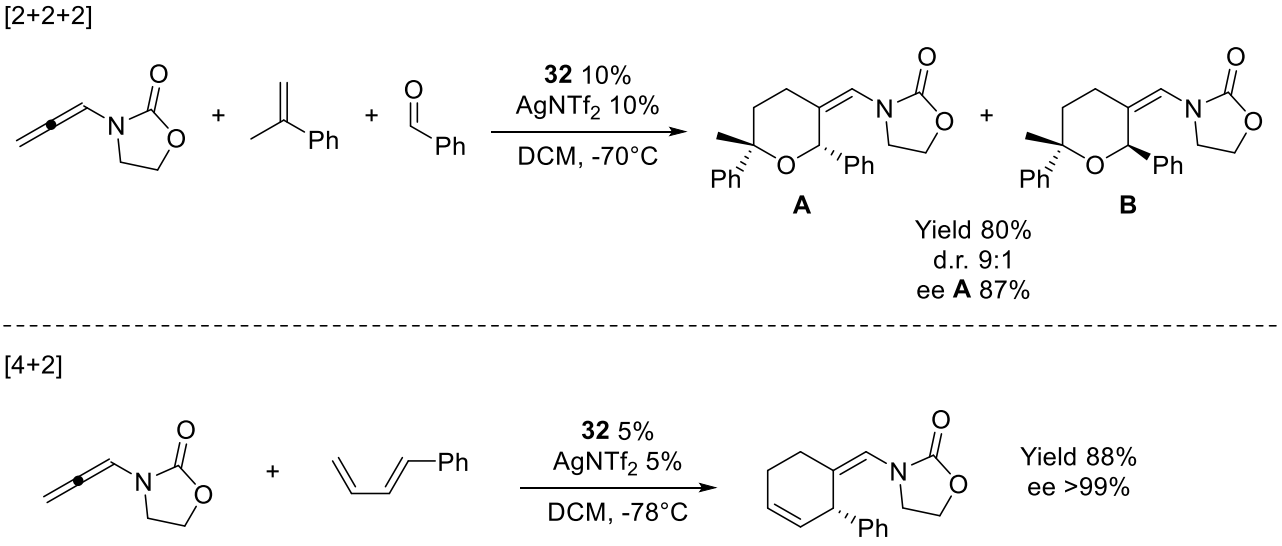

Figure 86. *Application of* ***32*** *in cycloaddition reactions.*

Despite these selected highlights, generally, other chiral NHC do not provide satisfactory e.e. and only the ones with chiral axis exhibit results worthy of mention.

3.3 Abstract

The ImPy scaffold gained an increasing interest as ligand in homogenous gold catalysis from the peculiar activity and enantioselectivity of its derivatives. This highly tunable scaffold allows steric as well as electronic manipulation to achieve desired reactivity and selectivity. A new class of chiral C_1 symmetry ImPy-Au(I) complexes with high activity and promising enantioselectivity is presented here.

3.4 Chiral ligand design and synthesis

After the great results obtained in the intramolecular cyclization of *N*-allenyl-indole-2-carboxylic acid with a broad class of ImPy-Au(I) catalysts, we explored the possibility to achieve the same transformation in an enantioselective fashion. The aim was to keep the ImPy core in order to enhance the catalytic activity of NHC-Au(I) complexes and to put the chiral information next to the gold metal centre.[51]

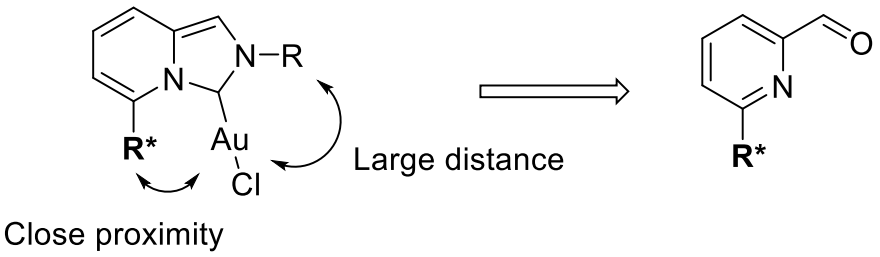

Figure 97. *Rationalization behind ligand design.*

To prepare the desired ligands some easy-to-prepare chiral pyridine-2-carboxaldehydes were needed in order to proceed with the previously discussed synthetic strategy. These scaffolds can be easily prepared by formylation of corresponding chiral 2-bromo pyridines, some of which are known to be the starting material for the synthesis of Bolm ligands.[77] Therefore, in collaboration with Prof. Thierry Ollevier from Laval University (Quebec) we planned the synthesis of chiral **Cat11-14**. Two different bulky groups (tBu and Ad) and different functionalization of the hydroxyl moiety were taken into account, to evaluate both steric and H-bonding effects.

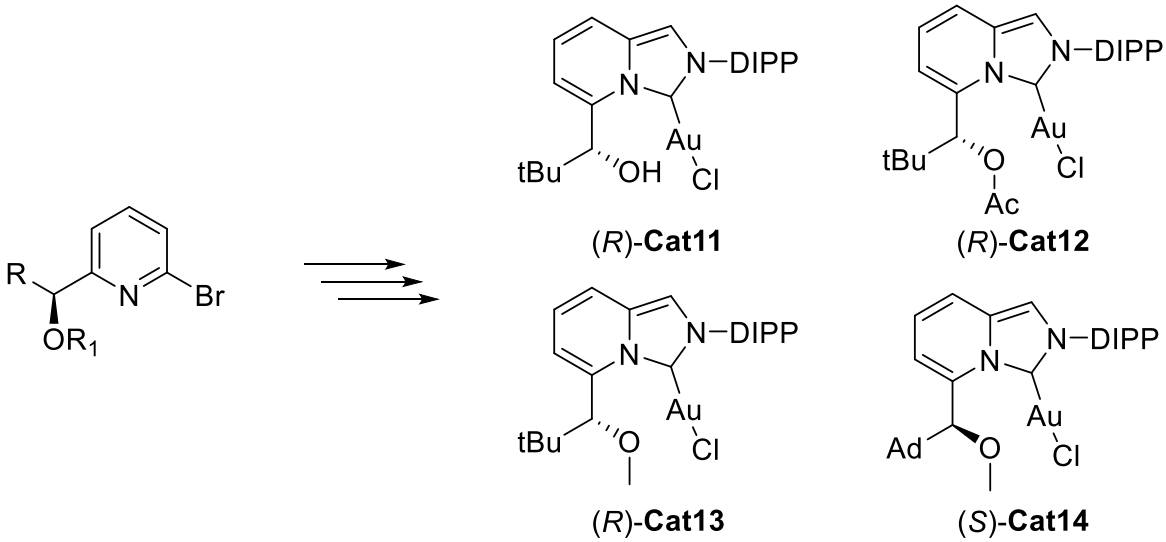

Figure 98. *Design of new ImPy chiral complexes.*

The synthesis starts from the protection of the corresponding alcohols (*R*)-**33** and (*S*)-**34** which were synthetized with very high enantiomeric excess following known literature.[78]

(*R*)-**33a** was protected as trimethyl silyl ether under common silylation condition providing (*R*)-**35a** in 93% yield. This labile protecting group provide good stability through next step and easy removal to afford (*R*)-**Cat11** and (*R*)-**Cat12**.

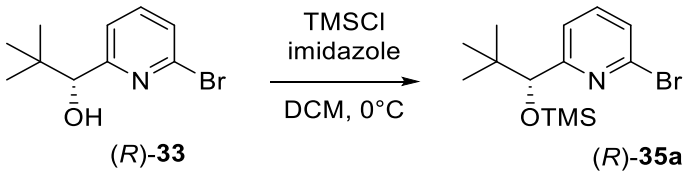

(*R*)-**33** (*R*)-**35a**

The two alcohols were also protected as methyl ether by use of methyl iodide, yielding in elevated quantity the desired products.

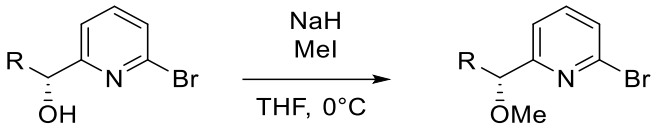

Reagent	R	Product	Yield
(*R*)-**33**	tBu	(*R*)-**35b**	85%
(*S*)-**34**	Ad	(*S*)-**36**	90%

Table 19. *Methylation results.*

The key step of the whole synthesis was the formylation reaction. We were able to obtain the corresponding aldehydes by lithiation with nBuLi in THF at -78°C and formylation with DMF as COH source. To succeed in this step it was crucial to use strictly anhydrous solvent, otherwise debrominated pyridine was obtained as major product. Yields were not excellent but were synthetically useful.

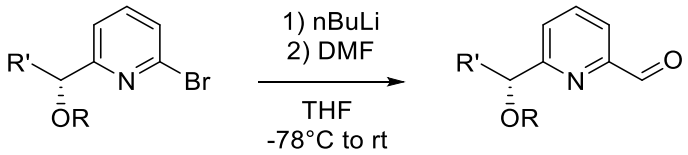

Compound	R	R’	Yield
(*R*)-**37a**	TMS	tBu	66
(*R*)-**37b**	Me	tBu	57
(*S*)-**38**	Me	Ad	48

Table 20. *Formylation reaction results.*

Before proceeding with the condensation to imine, (*R*)-**37a** was deprotected to the free hydroxyl group by a fluoride source, in our case TBAF was utilized, giving (*R*)-**39** in 83% yield.

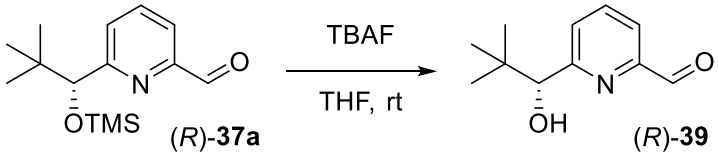

(*R*)-**37a** (*R*)-**39**

(*R*)-**38**9 was splitted in two samples, one was maintained as it was and the other was employed for the synthesis of the acetylated derivative. By simple use of acetic anhydride as acetylating agent and DMAP as activator, (*R*)-**40** was obtained in moderate 62% yield.

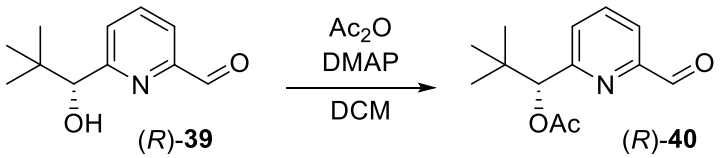

The imine condensation and the imidazole ring closure were carried out with the same procedures described in Paragraph 2.4, and also in this case the imine was employed immediately without storage.

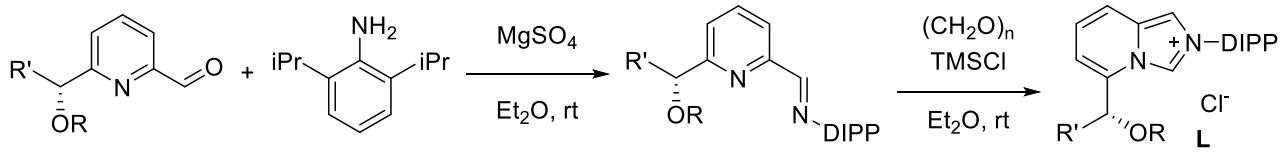

Ligand	R	R’	Yield [a]
(*R*)-**L11**	H	tBu	83%
(*R*)-**L12**	Ac	tBu	82%
(*R*)-**L13**	Me	tBu	97%
(*S*)-**L14**	Me	Ad	88%

Table 21. *Two steps synthesis of chiral ImPy ligands. a) yields over two steps.*

Finally, the corresponding Au(I) complexes were obtained by direct metalation *via* weak base route.

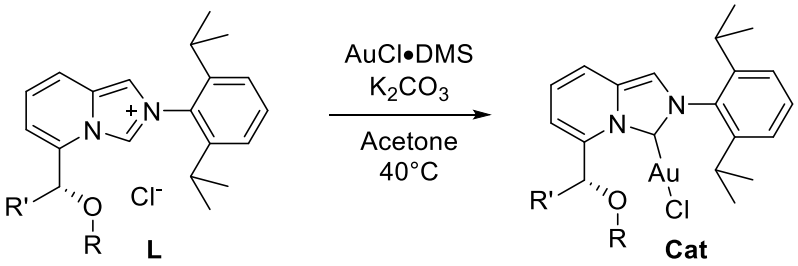

Catalyst	R	R’	Yield
(*R*)-**Cat11**	H	tBu	99%
(*R*)-**Cat12**	Ac	tBu	99%
(*R*)-**Cat13**	Me	tBu	99%
(*S*)-**Cat14**	Me	Ad	87%

Table 22. *Chiral complexes synthesis results.*

The resulting complexes were subjected to crystallization from homogenous solution of THF and *n*-hexane, by slow evaporation of THF, and the cystals were analysed by SC-XRD.

3.5 SC-XRD analysis

Figure 89. *ORTEP molecular drawing of (rac)-**Cat11** (top) and (R)-**Cat12** (bottom), thermal ellipsoids are draw at 30% of the probability level. In **Cat11** also the solvated THF molecule is represented. The dotted light-blue line shows the presence of a classical O-H…O bond.*

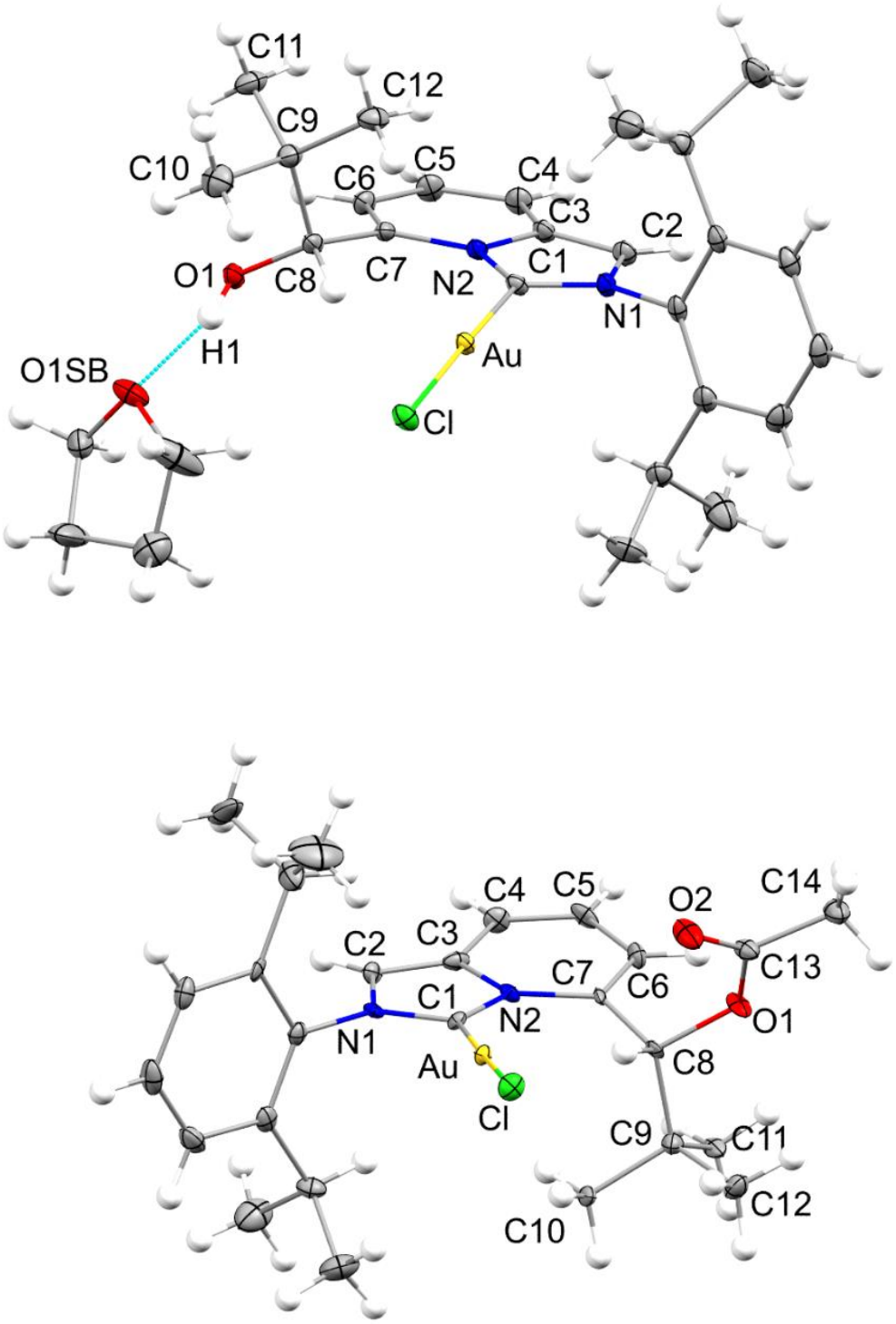

Figure 90. *ORTEP molecular drawing of (rac)-**Cat13** (top) and (S)-**Cat14** (bottom), thermal ellipsoids are drawn at 30% of the probability level.*

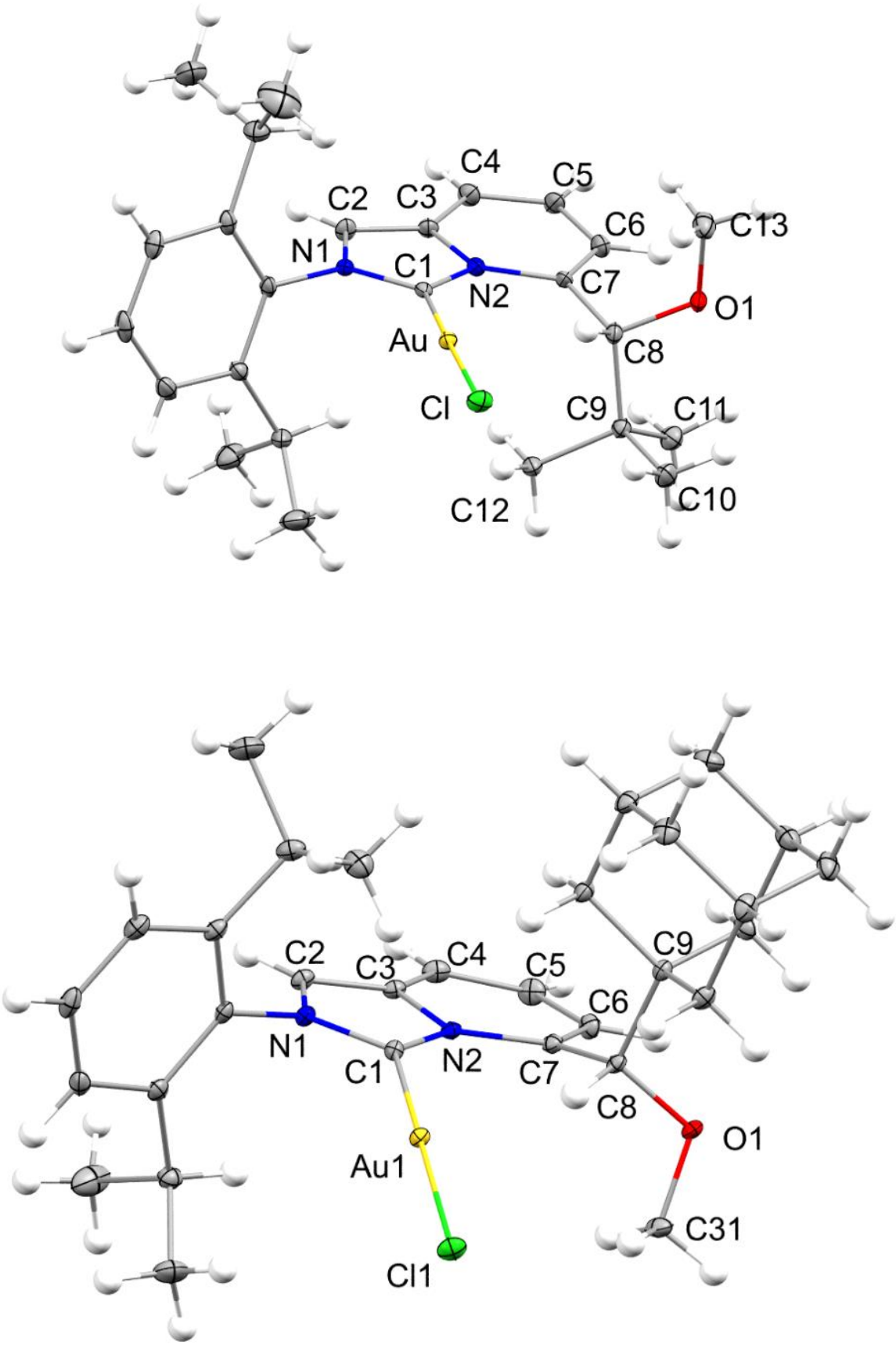

Some common features between these crystal structures were observed. The DIPP ring is perpendicular to the ImPy scaffold as observed for the achiral ones, except for **Cat13** where the observed dihedral angle is 74.96°. Also the chiral alkyl moiety assumed a perpendicular position with respect to the ImPy ring, without exception, displaying the bulkier tBu, or Ad, right above the gold metal centre. This conformation is the one that provides the less intramolecular steric repulsion and the most hindered chiral pocket. For these reasons, no O···Au interactions were possible and therefore not observed.

	N2-C7-C8-C9 torsion angle, °	**ImPy-DIPP, °**	**Au-C1, Å**	**Au-Cl, Å**
(*rac*)-**Cat11•THF**	94.1(3)	90.03	1.988(3)	2.2787(8)
(*R*)-**Cat1**2	92(1)	87.09	1.99(1)	2.267(4)
(*rac*)-**Cat1**3	92.2(7)	74.96	1.989(6)	2.276(2)
(*S*)-**Cat14**	93.4(3)	86.52	1.992(3)	2.2805(8)

Table 23. *Relevant structural parameters.*

The crystal structure of **Cat11** revealed the presence of a solvated molecule of THF engaging H-bonding interaction with the hydroxyl group, and positioned near the catalytic centre of gold. This interaction was very important during the rationalization of the enantiomeric excess obtained in the asymmetric catalysis, and will be discussed in the next paragraph.

3.6 Enantioselective lactonization of *N*-allenyl indole-2-carboxylic acid

The new chiral ImPy-Au(I) catalysts were then tested in the previously illustrated intramolecular cyclization of *N*-allenyl indole-2-carboxylic acid. The catalysts were tested on the model substrate **23a** and optimization of chiral conditions are reported in the table below.

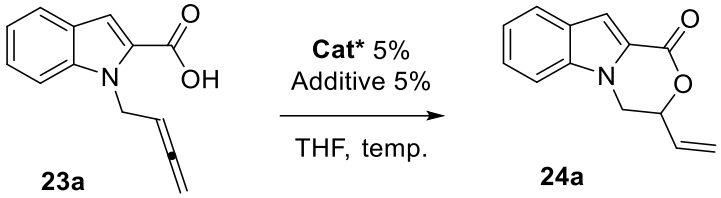

Entry	**Cat**	**Additive**	**Temperature**	**Yield [%]**	**e.r.**
1	*(R)*-Cat11	$AgSbF_6$	rt	89	66:33
2	(*R*)-Cat12	$AgSbF_6$	rt	89	72.5:27.5
3	(*R*)-Cat13	$AgSbF_6$	rt	80	75:25
4	(*S*)-Cat14	$AgSbF_6$	rt	86	19:81
5	(*S*)-Cat14	$AgSbF_6$	10 °C	81	25:75
6	(*S*)-Cat14	$AgSbF_6$	40 °C	66	26.5:73.5
7	(*S*)-Cat14	AgOTs	rt	31	53.5:46.5
8	(*S*)-Cat14	$Ag(NTf_2)$	rt	75	26:74
9 [a]	(*S*)-Cat14	AgTFA	rt	< 20	55:45

10 [a]	(*S*)-Cat14	$AgBF_4$	rt	< 20	0
11 [a]	(*S*)-Cat14	AgOTf	rt	< 20	32.5:67.5
12 [a]	(*S*)-Cat14	$AgPF_6$	rt	< 20	43:57
13	(*S*)-Cat14	NaBArF	rt	no reaction	-

Table 24. *Conditions screening for asymmetric lactonization. a) e.r. determined on crude due to the low conversion.*

All the reaction conditions were screened in THF due to the very low solubility of **23a** in other media. All the catalysts provided desired product with high yields (>80%) using $AgSbF_6$ as chlorine scavenger. The role of hydroxyl substituent appeared only to be steric, since THF saturates all H-bonding with the substrate. At the first impact, (*R*)-**Cat11** had to show the best e.r. due to the large difference of steric hindrance between tBu and OH moieties. However the interaction of -OH with THF generates an aggregate that is comparable in size with tBu and therefore a lower steric induced enantioselectivity (entry 1). In the other two complexes of tBu series, (*R*)-**Cat13**, with the smallest substituent, provided a discrete e.r. of 75:25 *vs* 72.5:27.5 of (*R*)-**Cat12** (entry 2 and 3). Finally, (*S*)-**Cat14** which displays a huge steric difference between adamantyl and methoxyl groups provided **24a** with a good yield and e.r of 19:81 (entry 4). (*S*)-**Cat14** was then utilized to test different conditions as temperature and additives but always resulted in erosion of yield and e.r. (entry 8-13).

Re-crystallization to achieve enantiopure **24a** failed, and therefore there are no hints about the absolute configuration of the stereocentre.

A possible explanation of the not exceptional e.r. results was that the chiral steric hindrance is too close to the gold metal centre rather than the catalytic site, were better results should be obtained.

3.7 Conclusion

In conclusion, four new C_1 chiral ImPy-A(I) complexes have been presented. Synthesis is efficient and the catalysts were obtained with high yields. SC-XRD analysis showed high rigidity of all the systems analysed providing essential information for the rationalization of catalytic results. Stereocontrol of this reaction is governed by the differences of steric hindrance of alkyl and alkoxy moieties, thus (*S*)-**Cat14** resulted the best catalysts for the intramolecular lactonization of *N*-allenyl indole-2-carboxylic acid. (*R*)-**Cat11** showed that H-bonding interaction are possible for such catalysts and therefore will be applied in other catalytic transformations.

3.8 Experimental section

^{1}H NMR spectra were recorded on Varian 400 (400 MHz) spectrometers. Chemical shifts are reported in ppm from TMS with the solvent resonance as the internal standard (deuterochloroform: 7.27 ppm). Data are reported as follows: chemical shift, multiplicity (s = singlet, d = doublet, t = triplet, q = quartet, sext = sextet, sept = septet, p = pseudo, b = broad, m = multiplet), coupling constants (Hz).

^{13}C NMR spectra were recorded on a Varian 400 (100 MHz) spectrometers with complete proton decoupling. Chemical shifts are reported in ppm from TMS with the solvent as the internal standard (deuterochloroform: 77.0 ppm).
GC-MS spectra were taken by EI ionization at 70 eV on a Hewlett-Packard 5971 with GC injection. They are reported as: m/z (rel. intense).

LC-electrospray ionization mass spectra were obtained with Agilent Technologies MSD1100 single-quadrupole mass spectrometer.

Elemental analyses were carried out by using a EACE 1110 CHNOS analyser.

Melting points were determined with Bibby Stuart Scientific Melting Point Apparatus SMP 3 and are not corrected.

Chromatographic purification was done with 240-400 mesh silica gel.

Anhydrous solvents were supplied by Sigma Aldrich in Sureseal® bottles and used without any further purification. Ethyl acetate was dried on activated 5Å molecular sieves.

Commercially available chemicals were purchased from Sigma Aldrich, Fluorochem and TCI and used without any further purification.

The X-ray intensity data were measured on a Bruker Apex II CCD diffractometer. Cell dimensions and the orientation matrix were initially determined from a least-squares refinement on reflections measured in three sets of 20 exposures, collected in three different ω regions, and eventually refined against all data. A full sphere of reciprocal space was scanned by 0.5° ω steps. The software SMART[3] was used for collecting frames of data, indexing reflections and determination of lattice parameters. The collected frames were then processed for integration by the SAINT program,[61] and an empirical absorption correction was applied using SADABS.[62] The structures were solved by direct methods (SIR 2014)[63] and subsequent Fourier syntheses and refined by full-matrix least-squares on F^2 (SHELXTL)[64] using anisotropic thermal parameters for all non-hydrogen atoms. The aromatic, methyl, methylene and methine hydrogen atoms were placed in calculated positions, refined with isotropic thermal parameters *U(H)* = 1.2 *Ueq*(C) and allowed to ride on their carrier carbons. Molecular drawings were generated using Mercury.[65] In **Cat11** one THF molecule was found in the asymmetric unit. Compound **Cat13** crystallizes as racemic twin in the chiral space group $P2_12_12_1$.
Crystallographic data have been deposited with the Cambridge Crystallographic Data Centre (CCDC) as supplementary publication number CCDC 2164549-2164552. Copies of the data can be obtained free of charge via www.ccdc.cam.ac.uk/getstructures .

Synthesis of aldehydes

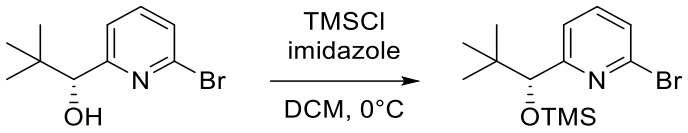

(*R*)-**33** (*R*)-**35a**

In a two-necked-round bottom flask, under inert atmosphere of nitrogen, (*R*)-**33** (244 mg, 1 mmol) was dissolved in 5 mL of DCM, then imidazole (87 mg, 1.3 mmol) was added, and the reaction cooled to 0 °C. After 5 minutes, TMSCl (140 µL, 1.1 mmol) was added dropwise. The reaction was slowly warmed-up to room temperature and let stirring until complete conversion of (*R*)-**33**. The reaction was quenched with distilled water and extracted with DCM (3 x 10 mL) and the organic phases washed with brine (1 x 15 mL), dried over Na_2SO_4 and volatile compounds evaporated. (*R*)-**35a** was purified by flash chromatography using *n*Hex/AcOEt 20:1 as the eluent.

(*R*)-**8a**, yield 93%, colourless solid.

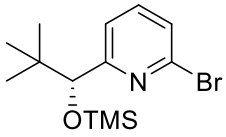

^{1}H NMR (400 MHz, $CDCl_3$) δ = 7.46 (t, *J* = 7.7 Hz, 1H), 7.37 (dd, *J* = 7.7, 1.0 Hz, 1H), 7.29 (dd, *J* = 7.7, 1.0 Hz, 1H), 4.40 (s, 1H), 0.84 (s, 9H), -0.05 (s, 9H).
^{13}C NMR (100 MHz, $CDCl_3$) δ = 165.15, 139.89, 138.01, 126.17, 121.28, 82.69, 36.32, 26.06, 0.13.

GC-MS(EI): 73 (100%), 261 (93%, -tBu (^{81}Br), 259 (93%, -tBu (^{79}Br), 302 (13%, -Me (^{81}Br)), 300 (13%, -Me (^{79}Br)).
Melting point = 81-83 °C.
$[\alpha]^{D}_{20}$ = + 55.6° (*c* 1.18, DCM).
Anal. El. Calc. for $C_{13}H_{22}BrNOSi$: C, 49.36; H, 7.01; N, 4.43; O, 5.06; found: C, 49.66; H, 7.91; N, 11.65.

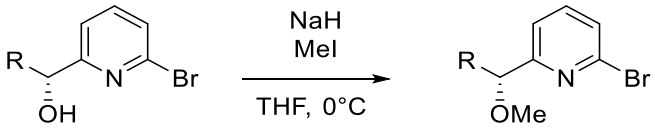

In a two necked-round-bottom flask, under inert atmosphere of nitrogen, starting alcohol (0.82 mmol, 1 eq) was dissolved in THF and cooled to 0 °C, then NaH (43 mg, 60%wt in mineral oil, 1.06 mmol, 1.3 eq) was added one portion. After H_2 stops developing, MeI (102 µL, 1.64 mmol, 2eq) was added dropwise and the reaction was stirred at 0 °C for 30 minutes. After that time, the reaction was allowed to warm to room temperature. The reaction was checked by TLC and then quenched with saturated ammonium chloride solution. The crude was extracted with diethyl ether (3 x 15 mL) and the organic phases dried over Na_2SO_4. Product was purified by flash chromatography using *n*Hex/AcOEt 15:1 as the eluent.

(*R*)-**35b**, yield 85%, crystalline colourless solid.

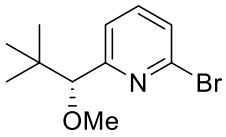

^{1}H NMR (400 MHz, $CDCl_3$) δ = 7.50 (t, *J* = 7.7 Hz, 1H), 7.33 (dd, *J* = 7.8, 0.9 Hz, 1H), 7.30 (dd, *J* = 7.7, 1.0 Hz, 1H), 3.91 (s, 1H), 3.19 (s, 3H), 0.86 (s, 10H).
^{13}C NMR (100 MHz, $CDCl_3$) δ = 162.42, 140.51, 138.08, 126.37, 120.65, 91.90, 57.87, 35.61, 26.00.

GC-MS(EI): 186 (100%, (^{79}Br)), 188 (95%, (^{81}Br)), 201 (48%, -tBu (^{79}Br)), 203 (47%, -tBu (^{81}Br)).
Melting point: 70-73 °C.

$[\alpha]^{D}_{20}$ = + 90.1° (*c* 1.24, DCM).
Anal. El. Calc. for $C_{11}H_{16}BrNO$: C, 51.18; H, 6.25; Br, 30.95; N, 5.43; O, 6.20; found: C, 51.09; H, 6.40; N, 5.48; O, 6.08.

(*S*)-**36**, yield 90%, crystalline colourless solid.

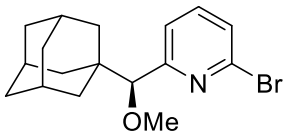

^{1}H NMR (400 MHz, $CDCl_3$) δ = 7.50 (t, *J* = 7.7 Hz, 1H), 7.33 (dd, *J* = 7.9, 1.0 Hz, 1H), 7.25 (dd, *J* = 7.7, 1.0 Hz, 1H), 3.76 (s, 1H), 3.16 (s, 3H), 1.88 (p, *J* = 3.2 Hz, 3H), 1.62 (ddt, *J* = 13.6, 11.3, 2.5 Hz, 6H), 1.56 – 1.50 (m, 3H), 1.43 – 1.35 (m, 3H).
^{13}C NMR (100 MHz, $CDCl_3$) δ = 161.66, 140.55, 137.94, 126.35, 120.93, 92.61, 57.94, 38.11, 37.41, 36.98, 28.25.
GC-MS(EI): 135 (100%, $Ad^{\bullet+}$), 305 (7%, -OMe (^{79}Br)).
Melting point: 80-82 °C.
$[\alpha]^{D}_{20}$ = – 122.4° (*c* 0.99, DCM).
Anal. El. Calc. for $C_{17}H_{22}BrNO$: C, 60.72; H, 6.59; N, 4.17; O, 4.76; found: C, 61.05; H, 6.43; N, 4.14; O, 4.84.

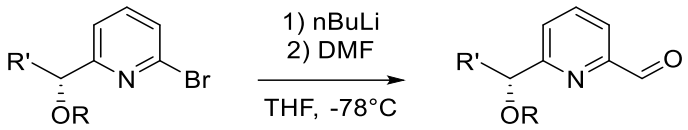

In a two necked-round-bottom flask, under inert atmosphere of nitrogen, protected alcohol (0.90 mmol) was dissolved in 5 mL of THF and cooled to –78 °C with an acetone/liquid N_2 bath. *n*BuLi (430 µL, 1.08 mmol, 2.5 M in *n*Hex) was added dropwise and the solution turned light orange. After 15 minutes at the same temperature, DMF (140 µL, 1.8 mmol) was added one-shot. The reaction was let stirring at –78 °C for 30 minutes and then raised to room temperature. After complete consumption of bromopyridine, monitored by TLC, the reaction was quenched with saturated aqueous ammonium chloride solution and extracted with diethyl ether (3 x 15 mL). The organic phases were dried over Na_2SO_4, evaporated and the product purified by flash chromatography using *n*Hex/AcOEt 15:1 as the eluent.

(*R*)-**37a**, yield 66%. colourless oil.

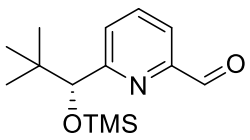

^{1}H NMR (400 MHz, $CDCl_3$) δ = 10.02 (s, 1H), 7.83 – 7.77 (m, 2H), 7.66 (dd, *J* = 5.9, 3.2 Hz, 1H), 4.53 (s, 1H), 0.87 (s, 10H), -0.03 (s, 9H).
^{13}C NMR (100 MHz, $CDCl_3$) δ = 193.89, 164.10, 150.94, 136.31, 126.61, 119.92, 82.93, 36.04, 25.88, -0.12.
GC-MS(EI): 209 (100%, -tBu), 73 (91%), 178 (22%, -$SiMe_3$), 250 (10%, -Me). $[\alpha]^{D}_{20}$ = + 64.7° (*c* 1.12, DCM).
Anal. El. Calc. for $C_{14}H_{23}NO_2Si$: C, 63.35; H, 8.73; N, 5.28; O, 12.06; found: C, 63.51; H, 8.77; N, 5.23; O, 12.20.

(*R*)-**37b**, yield 57%, colourless oil.

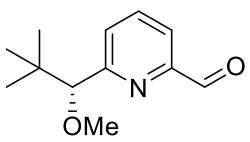

^{1}H NMR (400 MHz, $CDCl_3$) δ = 10.03 (s, 1H), 7.85 – 7.78 (m, 2H), 7.57 (dd, *J* = 5.5, 3.5 Hz, 1H), 4.03 (s, 1H), 3.22 (d, *J* = 0.6 Hz, 3H), 0.89 (d, *J* = 0.7 Hz, 9H).

^{13}C NMR (100 MHz, $CDCl_3$) δ = 193.78, 161.57, 151.69, 136.64, 126.18, 120.23, 92.33, 57.92, 35.62, 26.06.
GC-MS(EI): 136 (100%), 151 (43%, -*t*Bu).
$[\alpha]^{D}_{20}$ = + 90.3° (*c* 0.9, DCM).
Anal. El. Calc. for $C_{12}H_{17}NO_2$: C, 69.54; H, 8.27; N, 6.76; O, 15.44; found: C, 69.61; H, 8.34; N, 6.68; O, 15.38.

(*S*)-**38**, yield 48%, colourless solid.

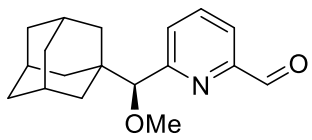

^{1}H NMR (400 MHz, $CDCl_3$) δ = 9.98 (s, 1H), 7.83 – 7.74 (m, 2H), 7.48 (dd, *J* = 5.3, 3.7 Hz, 1H), 3.83 (s, 1H), 3.14 (s, 3H), 1.83 (p, *J* = 3.3 Hz, 3H), 1.58 (ddt, *J* = 23.5, 14.5, 2.6 Hz, 6H), 1.51 – 1.42 (m, 3H), 1.37 (dq, *J* = 12.2, 2.6 Hz, 3H).
^{13}C NMR (100 MHz, $CDCl_3$) δ = 193.73, 160.72, 151.65, 136.44, 126.38, 120.21, 92.95, 57.90, 38.19, 37.34, 36.92, 28.19.
GC-MS(EI): 135 (100%, $Ad^{\bullet+}$), 285 (9%, $M^{\bullet+}$), 270 (5%, -Me).
Melting point: 75-77 °C.
$[\alpha]^{D}_{20}$ = – 85.9° (*c* 0.86, DCM).
Anal. El. Calc. for $C_{18}H_{23}NO_2$: C, 75.76; H, 8.12; N, 4.91; O, 11.21; found C, 75.86; H, 8.08; N, 4.84; O, 11.21.

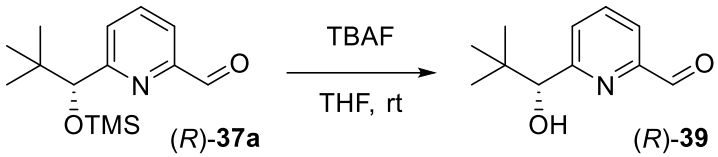

In a two necked-round-bottom flask, under inert atmosphere, (*R*)-**37a** (157 mg, 0.59 mmol) was dissolved in 3 mL of THF, then tetrabutylammonium fluoride monohydrate (TBAF•H_2O, 182 mg, 0.65 mmol) was added one portion. The reaction was stirred at room temperature until full conversion of starting material monitored by TLC. The reaction was quenched with 5 mL of water and the mixture extracted 3 x 15 mL of diethyl ether. The organic phase was dried over Na_2SO_4, evaporated and the product purified by flash chromatography using *n*Hex/AcOEt 10:1 as the eluent.

(*R*)-**39**, yield 83%, colourless oil.

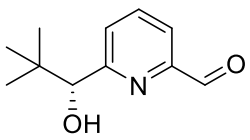

^{1}H NMR (400 MHz, $CDCl_3$) δ = 10.01 (d, *J* = 0.8 Hz, 1H), 7.85 – 7.73 (m, 2H), 7.42 (dd, *J* = 7.3, 1.6 Hz, 1H), 4.42 (d, *J* = 7.2 Hz, 1H), 4.06 (d, *J* = 7.3 Hz, 1H), 0.88 (s, 9H).
^{13}C NMR (100 MHz, $CDCl_3$) δ = 193.19, 161.09, 151.05, 136.61, 126.99, 120.24, 80.39, 36.30, 25.79.
GC-MS(EI): 137 (100%, -tBu), 178 (3%, -Me).
$[\alpha]^{D}_{20}$ = – 0.9° (*c* 1.18, DCM).
Anal. El. Calc. for $C_{11}H_{15}NO_2$: C, 68.37; H, 7.82; N, 7.25; O, 16.56; found: C, 68.42; H, 7.72; N, 7.20; O, 16.63.

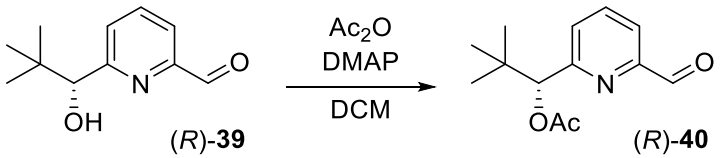

In a two necked-round-bottom flask, under inert atmosphere, (*R*)-**39** (150 mg, 0.77 mmol) was dissolved in 3 mL of DCM, then some crystals of DMAP are added to the solution. Acetic anhydride (150 µL, 1.55 mmol) was added dropwise. The reaction was stirred at room temperature and the progress was monitored by TLC. Water (10 mL) was added to quench the reaction and the mixture extracted with DCM (3 x 10 mL). The organic phase was dried over Na_2SO_4 and evaporated under reduced pressure. (*R*)-**40** was purified by flash chromatography using *n*-Hex/AcOEt 5:1 as the eluent.

(*R*)-**40**, yield 62%, colourless oil.

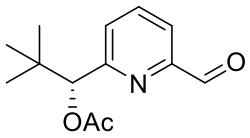

^{1}H NMR (401 MHz, $CDCl_3$) δ = 10.01 (d, *J* = 0.8 Hz, 1H), 7.85 – 7.74 (m, 2H), 7.45 (dd, *J* = 6.8, 2.1 Hz, 1H), 5.57 (s, 1H), 2.10 (s, 3H), 0.94 (s, 9H).
^{13}C NMR (100 MHz, $CDCl_3$) δ = 193.74, 170.26, 159.32, 151.64, 136.85, 125.96, 120.13, 83.14, 34.94, 26.02, 20.98.

GC-MS(EI): 137 (100%), 179 (16%, -tBu), 160 (15%).
$[\alpha]^{D}_{20}$ = – 33.9° (*c* 1.28, DCM).
Anal. El. Calc. for $C_{13}H_{17}NO_3$: C, 66.36; H, 7.28; N, 5.95; O, 20.40; found: C, 66.51; H, 7.31; N, 5.86; O, 20.32.

Condensation to imine

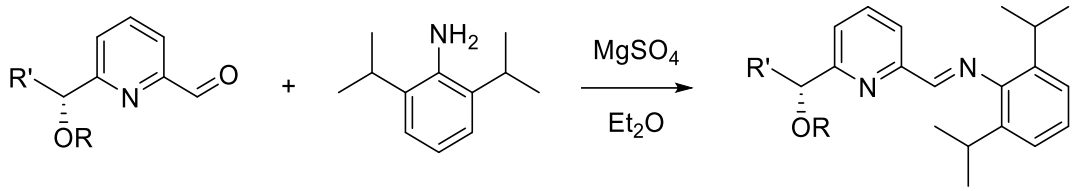

A 2 necked-round bottom flask, under inert atmosphere, was charged with aldehyde (1 eq), 0.5g of anhydrous $MgSO_4$, 10 mL diethyl ether and 2,6-diisopropylaniline (1.2 eq). The reaction was stirred at room temperature overnight. The complete consumption of starting aldehyde was evaluated by GC-MS. Then $MgSO_4$ was filtered off and washed with diethyl ether. The organic phase was evaporated and the excess of aniline was distilled at 140 °C 0.2 mbar. Resulting imine was used immediately in the next steps without further purification.

Imidazole ring closure

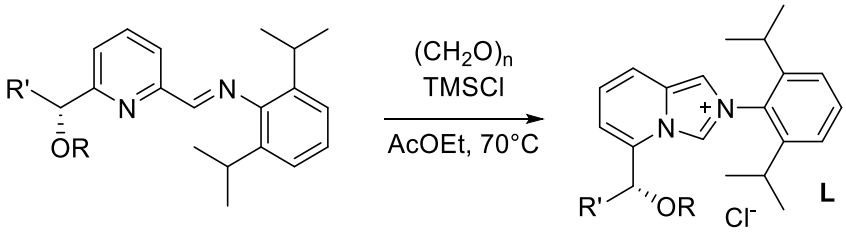

In a 2 necked-round bottom flask, under inert atmosphere, imine (1 eq) was dissolved in 5mL of dried AcOEt and then paraformaldehyde (1.1 eq) was added and heated at 70 °C. After 15 minutes at the same temperature TMSCl (1.1 eq.) was added dropwise. The reaction was stirred at the same temperature until starting material was consumed. TLC *c*Hex/AcOEt 5:1. The reaction was cooled to

0 °C and filtered with a Gooch funnel. The solid was washed once with cold ethyl acetate and twice with diethyl ether. The solid was dried in vacuum and used without further purification.

(*R*)-**L11**, yield 83%, pale yellow solid.

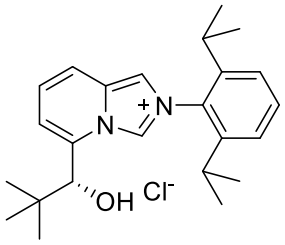

^{1}H NMR (400 MHz, $CDCl_3$) δ = 10.07 (d, *J* = 1.8 Hz, 1H), 7.75 (d, *J* = 9.3 Hz, 1H), 7.73 – 7.68 (m, 1H), 7.56 (t, *J* = 7.8 Hz, 1H), 7.36 – 7.25 (m, 3H), 6.98 (d, *J* = 6.9 Hz, 1H), 5.04 (s, 1H), 2.28 (hept, *J* = 6.7 Hz, 1H), 2.06 – 1.92 (m, 1H), 1.19 (d, *J* = 6.7 Hz, 3H), 1.16 – 1.08 (m, 9H), 1.00 (s, 9H).
^{13}C NMR (100 MHz, $CDCl_3$) δ = 145.72, 144.91, 132.08, 131.98, 130.48, 128.47, 125.89, 124.86, 124.34, 118.22, 116.41, 113.38, 79.00, 37.41, 28.62, 28.56, 26.78, 24.52, 24.50, 24.33, 24.22.
LC-MS(ESI+): 365.9 (-Cl^-).
Melting point: decomposition.
$[\alpha]^{D}_{20}$ = – 23.8° (*c* 1.02, DCM).
Anal. El. Calc. for $C_{24}H_{33}ClN_2O$: C, 71.89; H, 8.30; Cl, 8.84; N, 6.99; O, 3.99; found: C, 71.78; H, 8.35; N, 7.02; O, 4.02.

(*R*)-**12**, yield 97%, colourless solid.

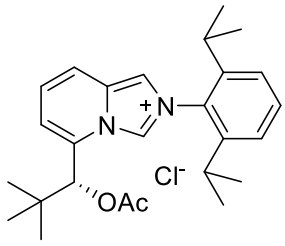

^{1}H NMR (400 MHz, $CDCl_3$) δ = 11.65 (bs, 1H), 8.16 (bs, 2H), 7.47 (t, *J* = 7.8 Hz, 1H), 7.24 (ddd, *J* = 10.8, 8.7, 5.4 Hz, 3H), 6.99 (d, *J* = 7.0 Hz, 1H), 6.18 (s, 1H), 2.10 – 1.86 (m, 5H), 1.20 – 1.06 (m, 12H), 1.04 (s, 9H). Diagnostic ^{13}C NMR (100 MHz, $CDCl_3$) δ 170.04, 145.10, 144.75, 131.80, 131.26, 130.73, 127.80, 124.92, 124.38, 124.17, 118.93, 116.22, 36.28, 28.76, 28.73, 25.22, 24.59, 23.65, 20.59.
LC-MS(ESI+): 407.2 (-Cl^-).
Melting point: 147–150 °C.
$[\alpha]^{D}_{20}$ = – 54.8° (*c* 0.99, DCM).
Anal. El. Calc. for $C_{26}H_{35}ClN_2O_2$: C, 70.49; H, 7.96; N, 6.32; O, 7.22; found: C, 70.61; H, 7.86; N, 6.40; O, 7.19.

(*R*)-**13**, yield 82%, colourless solid.

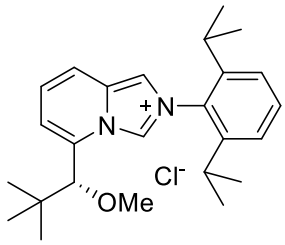

^{1}H NMR (400 MHz, $CDCl_3$) δ = 9.91 (bs, 1H), 8.69 (bs, 1H), 8.54 (bs, 1H), 7.53 (t, *J* = 7.8 Hz, 1H), 7.39 – 7.32 (m, 1H), 7.31 – 7.28 (m, 2H), 7.15 (d, *J* = 6.9 Hz, 1H), 4.67 (s, 1H), 3.34 (s, 3H), 2.14 – 2.06 (m, 1H), 2.01 – 1.90 (m, 1H), 1.15 (dd, *J* = 6.7, 2.8 Hz, 6H), 1.11 (d, *J* = 6.5 Hz, 6H), 0.96 (s, 9H).
^{13}C NMR (100 MHz, $CDCl_3$, diagnostic signals) δ = 145.03, 144.87, 132.38, 132.07, 130.51, 124.94, 124.65, 124.48, 58.44, 37.87, 28.72, 26.51, 24.76, 24.37, 24.14, 23.76.
LC-MS(ESI+): 379.6 (-Cl^-).
Melting point: decomposition.
$[\alpha]^{D}_{20}$ = – 12.99° (*c* 0.84, DCM).
Anal. El. Calc. for C, 72.35; H, 8.50; N, 6.75; O, 3.86; found: C, 72.33; H, 8.58; N, 6.77; O, 3.78.

(*S*)-**L14**, yield 88%, pale yellow solid.

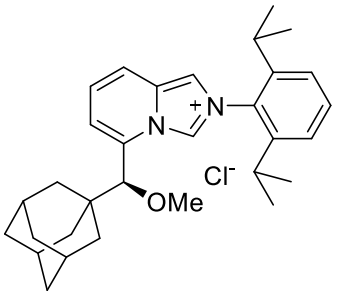

^{1}H NMR (400 MHz, $CDCl_3$) δ = 9.04 (bs, 1H), 8.72 (bs, 1H), 8.44 (bs, 1H), 7.35 (t, *J* = 7.9 Hz, 1H), 7.15 (dd, *J* = 9.3, 7.0 Hz, 1H), 7.10 (d, *J* = 7.9 Hz, 2H), 7.01 – 6.93 (m, 1H), 3.11 (s, 3H), 1.95 – 1.64 (m, 5H), 1.35 (dt, *J* = 23.8, 12.6 Hz, 12H), 0.92 (dt, *J* = 32.1, 8.8 Hz, 12H).
Diagnostic ^{13}C NMR (100 MHz, $CDCl_3$) δ = 144.84, 144.66, 131.92, 130.34, 124.80, 124.46, 124.32, 121.61, 120.41, 117.12, 58.27, 39.42, 39.04, 36.28, 28.56, 28.52, 27.90, 24.55, 24.08, 23.88, 23.53.
LC-MS(ESI+): 457.4 (-Cl^-).

Melting point: 132–135 °C.
$[\alpha]^{D}_{20}$ = + 72.6° (*c* 1.07, DCM).
Anal. El. Calc. for $C_{31}H_{41}ClN_2O$: C, 75.51; H, 8.38; N, 5.68; O, 3.24; found: C, 75.58; H, 8.44; N, 5.62; O, 3.19.

Synthesis of chiral Au(I) metal complexes

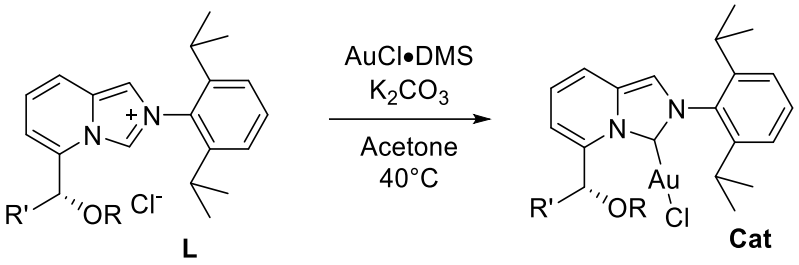

Ligand precursor **L** (0.05 mmol), K_2CO_3 (20.7 mg, 0.15 mmol) and AuCl•DMS (14.7 mg, 0.05 mmol) are added into a vial. Then, 1 mL of acetone (reagent grade) was added, and the closed vial stirred at 40 °C for 2 h. After complete consumption of starting salts, acetone was evaporated under reduced pressure and the crude dissolved in DCM and filtered on Celite® pad. DCM was evaporated yielding [Au(I)] complexes that were triturated in *n*Hex before use.

(*R*)-**Cat11**, yield 99%, pale yellow powder.

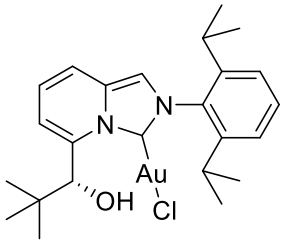

^{1}H NMR (400 MHz, $CDCl_3$) δ = 7.61 (s, 1H), 7.48 (t, *J* = 7.8 Hz, 1H), 7.39 (dd, *J* = 8.5, 1.9 Hz, 1H), 7.31 (s, 1H), 7.28 – 7.20 (m, 2H), 7.08 – 6.99 (m, 2H), 2.18 (hept, *J* = 6.7 Hz, 1H), 2.01 (hept, *J* = 6.5 Hz, 1H), 1.27 (d, *J* = 6.8 Hz, 3H), 1.24 (s, 3H), 1.09 (s, 9H), 1.08 (d, *J* = 2.4 Hz, 3H), 1.07 (d, *J* = 2.4 Hz, 3H).
^{13}C NMR (100 MHz, $CDCl_3$) δ 163.42, 145.29, 145.00, 142.31, 135.53, 131.93, 130.75, 124.23, 124.06, 123.01, 116.64, 114.72, 113.26, 73.34, 38.38, 28.44, 28.41, 25.83, 24.64, 24.34, 24.22, 24.05.
Melting point: decomposition.
$[\alpha]^{D}_{20}$ = + 92.2° (*c* 0.55, DCM).
Exact mass: calc. for $C_{24}H_{32}AuClN_2O$: 596.1869; found: 596.1863.

(*R*)-**Cat12**, yield 99%, colourless powder.

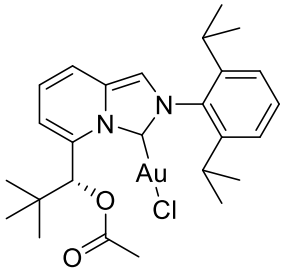

^{1}H NMR (400 MHz, $CDCl_3$) δ = 8.26 (s, 1H), 7.49 (t, *J* = 7.8 Hz, 1H), 7.38 (dd, *J* = 9.2, 1.3 Hz, 1H), 7.32 (s, 1H), 7.25 (ddd, *J* = 10.9, 7.8, 1.4 Hz, 2H), 6.96 (dd, *J* = 9.2, 6.9 Hz, 1H), 6.71 (dd, *J* = 7.0, 1.3 Hz, 1H), 2.25 (p, *J* = 6.8 Hz, 1H), 2.08 (s, 3H), 2.02 (p, *J* = 6.9 Hz, 1H), 1.32 (d, *J* = 6.8 Hz, 3H), 1.26 (d, *J* = 6.8 Hz, 3H), 1.18 (s, 9H), 1.08 (d, *J* = 6.9 Hz, 3H), 1.08 (d, *J* = 6.8 Hz, 3H).

^{13}C NMR (100 MHz, $CDCl_3$) δ = 169.96, 164.22, 145.27, 145.18, 139.93, 135.61, 131.68, 130.74, 124.29, 124.00, 122.47, 117.09, 113.47, 113.44, 75.39, 36.81, 28.48, 28.44, 26.03, 24.52, 24.31, 24.25, 24.12.

Melting point: decomposition.

$[\alpha]^{D}_{20}$ = – 30,3° (*c* 1.02, DCM).

Exact mass: calc. for $C_{26}H_{34}AuClN_2O_2$: 638.1974; found: 638.1978.

(*R*)-**Cat13**, yield 99%, colourless powder.

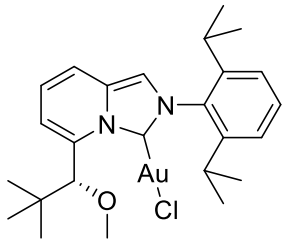

^{1}H NMR (400 MHz, $CDCl_3$) δ = 7.50 (t, *J* = 7.8 Hz, 1H), 7.40 (dd, *J* = 9.1, 1.3 Hz, 1H), 7.32 (s, 1H), 7.29 – 7.23 (m, 2H), 7.21 (s, 1H), 7.06 (dd, *J* = 9.1, 6.9 Hz, 1H), 6.91 (dd, *J* = 6.9, 1.4 Hz, 1H), 3.42 (s, 3H), 2.25 (hept, *J* = 6.8 Hz, 1H), 1.97 (hept, *J* = 7.1 Hz, 1H), 1.29 (d, *J* = 6.9 Hz, 3H), 1.24 (d, *J* = 6.8 Hz, 3H), 1.11 (d, *J* = 6.9 Hz, 3H), 1.09 – 1.04 (m, 12H).

^{13}C NMR (100 MHz, $CDCl_3$) δ = 168.19, 145.41, 144.88, 140.52, 135.50, 132.04, 130.78, 124.25, 124.10, 123.00, 116.57, 114.18, 113.21, 83.43, 58.13, 38.30, 28.46, 28.42, 25.87, 24.67, 24.33, 24.31, 24.07.

Melting point: decomposition.

$[\alpha]^{D}_{20}$ = + 88.1° (*c* 0.54, DCM).

Exact mass: calc. for $C_{25}H_{34}AuClN_2O$: 610.2025; found: 610.2030.

(*S*)-**Cat14**, yield 87%, colourless powder.

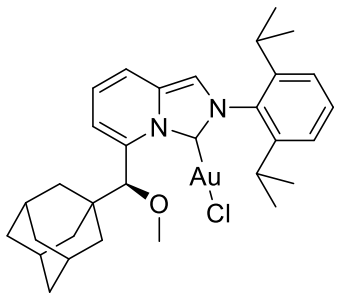

^{1}H NMR (400 MHz, $CDCl_3$) δ = 7.49 (t, *J* = 7.8 Hz, 1H), 7.40 (dd, *J* = 9.1, 1.3 Hz, 1H), 7.32 (s, 1H), 7.25 (ddd, *J* = 11.3, 7.8, 1.4 Hz, 2H), 7.12 (s, 1H), 7.05 (dd, *J* = 9.2, 6.9 Hz, 1H), 6.84 (dd, *J* = 6.9, 1.3 Hz, 1H), 3.41 (s, 3H), 2.35 – 2.22 (m, 1H), 2.12 – 2.02 (m, 3H), 2.00 – 1.86 (m, 4H), 1.62 – 1.55 (m, 6H), 1.49 (d, *J* = 11.9 Hz, 3H), 1.29 (d, *J* = 6.9 Hz, 3H), 1.25 (d, *J* = 6.9 Hz, 3H), 1.12 (d, *J* = 6.9 Hz, 3H), 1.07 (d, *J* = 6.9 Hz, 3H).

^{13}C NMR (100 MHz, $CDCl_3$) δ = 163.91, 145.48, 144.82, 139.33, 135.53, 132.04, 130.73, 124.25, 124.09, 122.95, 116.45, 114.18, 113.01, 83.85, 58.22, 40.26, 37.69, 36.89, 28.47, 28.42, 28.41, 24.67, 24.33, 24.18, 24.05.

Melting point: decomposition.

$[\alpha]^{D}_{20}$ = – 153.6° (*c* 0.62, DCM).

Exact mass: calc. for $C_{31}H_{41}AuClN_2O$: 689.2573; found: 689.2571.

Table 25. *Crystal data and structure refinement for compounds* ***Cat11-12.***

Compound	**(*rac*)-Cat11•THF**	**(*R*)-Cat12**
Formula	$C_{24}H_{32}AuClN_2O•C_4H_8O$	$C_{26}H_{34}AuClN_2O_2$
Fw	669.03	638.97
T, K	100 (2)	100 (2)
λ, Å	0.71073	0.71073
Crystal system	Triclinic	Orthorhombic
Space group	*P-1*	$P2_12_12_1$
***a*, Å**	8.9407 (5)	9.8777(7)
***b*, Å**	9.6395 (6)	13.289(1)
***c*, Å**	17.239 (1)	19.872(1)
α	98.233 (2)	90
β	94.272 (2)	90
γ	106.185 (2)	90
Cell volume, Å^3	1401.9 (1)	2608.4(3)
Z	2	4
D_C, Mg m^{-3}	1.585	1.627
μ(Mo-Kα), mm^{-1}	5.368	5.766
F(000)	668	1264
Crystal size/ mm	0.14 x 0.13 x 0.04	0.41 x 0.08 x 0.07
θ limits, °	2.348 to 25.500	1.844 to 25.248
Reflections collected	16780	30416
Unique obs. Reflections [$F_o > 4\sigma(F_o)$]	5216 [R(int) = 0.0290]	4669 [R(int) = 0.0626]
Goodness-of-fit-on F^2	1.180	0.766
R_1 (F)[a], wR_2 (F^2)[b] [$I > 2\sigma(I)$]	R1 = 0.0217, wR2 = 0.0492	R1 = 0.0388, wR2 = 0.0997
Largest diff. peak and hole, e. Å^{-3}	1.146 and -1.421	2.630 and -2.891

[a] $R_1 = \Sigma||F_o|-|F_c||/\Sigma|F_o|$. [b] $wR_2 = [\Sigma w(F_o^2-F_c^2)^2/\Sigma w(F_o^2)^2]^{1/2}$ where $w = 1/[\sigma^2(F_o^2) + (aP)^2 + bP]$ where $P = (F_o^2 + F_c^2)/3$.

Table 26. *Crystal data and structure refinement for compounds* ***Cat13-14.***

Compound	(*rac*)-**Cat1**3	(*S*)-**Cat14**
Formula	$C_{25}H_{34}AuClN_2O$	$C_{31}H_{40}AuClN_2O$
Fw	610.96	689.06
T, K	100 (2)	100(2)
λ, Å	0.71073	0.71079
Crystal system	Orthorhombic	Orthorhombic
Space group	$P2_12_12_1$	$P2_12_12_1$
***a*, Å**	10.118 (1)	12.7402(8)
***b*, Å**	12.940 (2)	13.7979(8)
***c*, Å**	19.485 (3)	16.0681(9)
α	90	90
β	90	90
γ	90	90
Cell volume, Å^3	2551.1 (6)	2824.6(3)
Z	4	4
D_C, Mg m^{-3}	1.591	1.620
μ(Mo-Kα), mm^{-1}	5.889	5.329
F(000)	1208	1376
Crystal size/ mm	0.36 x 0.21 x 0.14	0.24 x 0.13 x 0.10
θ limits, °	1.889 to 25.993	1.945 to 30.572
Reflections collected	33295	63032
Unique obs. Reflections [$F_o > 4\sigma(F_o)$]	4997 [R(int) = 0.0371]	8646 [R(int) = 0.0600]
Goodness-of-fit-on F^2	1.028	1.024
R_1 (F)[a], wR_2 (F^2)[b] [$I > 2\sigma(I)$]	R1 = 0.0200, wR2 = 0535	R1 = 0.0169, wR2 = 0.0384
Largest diff. peak and hole, e. Å^{-3}	2.423 and -1.083	1.638 and -0.748

[a] $R_1 = \Sigma||F_o|-|F_c||/\Sigma|F_o|$. [b] $wR_2 = [\Sigma w(F_o^2-F_c^2)^2/\Sigma w(F_o^2)^2]^{1/2}$ where $w = 1/[\sigma^2(F_o^2) + (aP)^2 + bP]$ where $P = (F_o^2 + F_c^2)/3$.

4. *New o-biaryl phosphine ligands: Au(I) case study*

4.1 (Biaryl)phosphine in Au(I) catalysis

As already illustrated, phosphorus-based and phosphine in particular are without doubt the most employed ligands in homogenous gold(I) catalysis.[79] Ortho-biaryl phosphines are a particular family of phosphine that was initially designed for palladium chemistry by Buchwald,[80] but rapidly became very effective also in gold chemistry.[81]

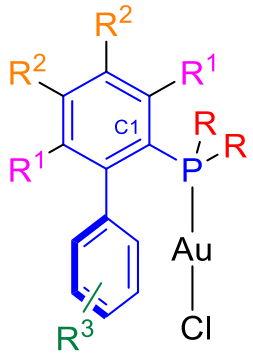

Figure 91. *General structure of o-biaryl phophine gold chloride complexes.*

The fundamental skeleton (blue) is the *o*-biaryl moiety, this allows gold to be displayed parallel to the pendant phenyl and engaging π-interaction, which promote catalytic activity and prevent catalyst decomposition to gold nanoparticles. All the other substituents are responsible for fine tuning of the catalytic properties. R groups can be both aliphatic (most common) and aromatic (phenyl) and to them are attributed other relevant effects because they provide steric hinderance, electronic influences on P and rigidity to C1-P rotation. R_1 (both position or only one) functionalities as well act as rigidifying groups (mostly methyl) and also partially electronic (methoxy). R_2 generally explored for electronic influences of P by resonance effects. R_3 groups in Pd catalysis are placed in 2,6 positions to prevent the formation of cyclometallated species, however this hypothesis is not plausible for gold(I) and therefore the substitution in those positions are only steric and electronic that is reflected on gold by π-interactions. Common substituent on the lower phenyl ring are 2,6-diisopropyl, 2,4,6-triisopropyl 2,6-diisopropoxy, 2,6-dimethoxy. More modern ligands, designed *ad hoc* for gold catalysis, have remote basic amide and amine group to participate in bifunctional catalysis.[26]

A broad and complete benchmark comparison of reactivity of all the biaryl phosphine, but also other phosphine, is not present in literature since different complexes were tested for the same reactions but small variation (e.g. temperature, concentration etc.) impeded a clear comparison. However, two main researches by Xu[82] and Toste[83] attempted to fill this gap.

Xu focused his attention to the main step involved in gold(I) catalysis such electrophile activation, protodeauration and also side pathway as gold decomposition. Through kinetic experiments the following conclusions were drawn:

- Electron poor ligands are the best for electrophile activation step;
- Electron rich ligands are the best for protodeauration step;
- Biaryl ligands prevent gold decomposition.

Biaryl ligands founds elevated importance in those processes where protodeauration and activation of electrophile are the rate determining steps. The first case is the case of hydroamination of C-C multiple bonds where the nucleophile is a base which is in large amount and sequester the H^+

necessary to the protodeauration, this lead to a deactivated gold catalysts. In these transformation briaryl bulky electron rich ligands provided the desired product, while triaryl or trialkyl phosphines failed. The second case is when scarcely active C-C multiple bonds or nucleophile are adopted, and also in this case a deactivated gold intermediate is generated. Electron poor biaryl phosphines resulted the optimal ligands for such reactions. In both cases the biaryl unit is crucial to prevent the decomposition of the deactivated intermediates.

Toste also performed some structure activity relationship on phosphines ligands. In particular the studies were focused con correlation of solid state parameters and catalytic results.

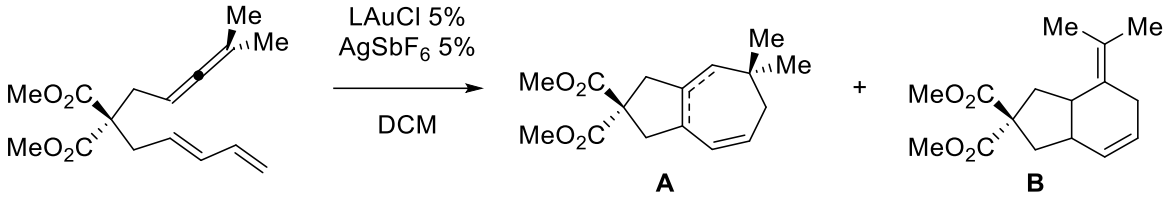

Figure 92. *[4+3] vs. [4+2] cycloaddition reaction.*

For Buchwald-type phosphines with many substituents is difficult to rationalize and separate electronic and steric effects, however and overall sum of effect is represented by Au-Cl distance which is affected by trans effect of phosphorus atom. For the illustrated reactions (Figure 92), the divergent step is influenced by 1,2-hydride shift or 1,2-alkyl shift and the selectivity is attributed to the ligand influence to the common intermediate. A fine correlation of selectivity was found with Au-Cl distance, where complexes that shown short Au-Cl bonds were **A** selective and the ones with high Au-Cl distances were **B** selective. In other transformations Au-Cl distances were not correlating at all, but other parameter as sterimol was found satisfying. Furthermore, through this analysis was possible to design and predict reactivity of new catalyst, which after application in catalysis demonstrated the solidity of the hypothesis.

4.2 Abstract

Buchwald-type phosphines are superior ligands in gold(I) catalysis for those processes where one of the steps is particularly unfavoured by preventing gold decomposition. Moreover, fine tuning of both electronic and steric properties allows selectivity in divergent reactions. Here we investigate the role of electron poor phenyl ring in biaryl phosphine ligands in benchmark reaction. Different substrates ad ligands were employed to carefully draw the results.

4.3 Ligands design and synthesis

In biaryl phosphine ligands family, EWG group are scarcely used and only placed as substituents on phosphorus and top phenyl ring (Figure 92).

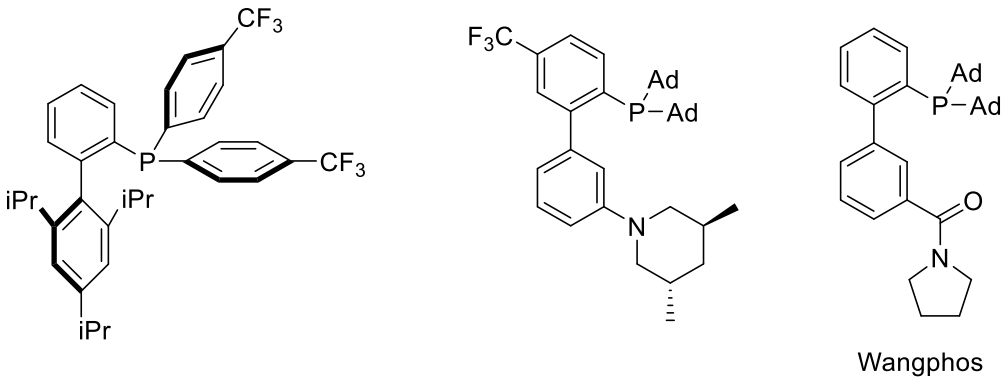

Figure 92. *examples of EWG groups in biaryl phosphine ligands.*

Surprisingly, no ligands with EWG on the pendent phenyl are present in literature, only Wangphos and its derivatives but their activity is exclusively related to bifunctional catalysis.

After our discovery in the field of NHC ligands and the effects of secondary interactions, we envisioned the possibility to synthetize particular phosphines with electron deficient ancillary penyl. We also synthetized a ligand with electron donating group in 3,5 positions instead of common 2,6 (Figure 93).

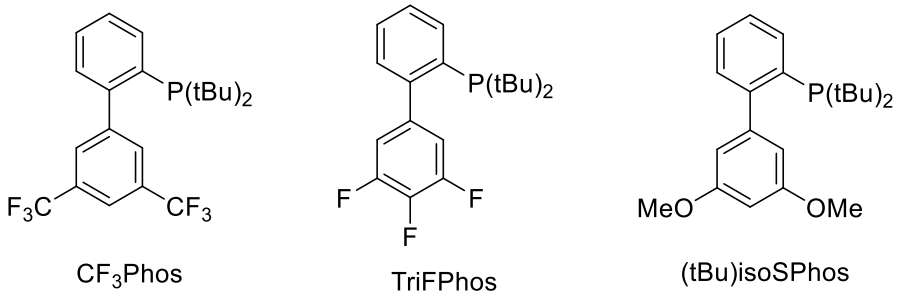

Figure 93. *Ligands target of this project.*

The synthesis of these ligands is a 2 step process, where the first is the coupling reaction to provide the desired ortho-bromo biaryl and then subjected to phosphorylation.

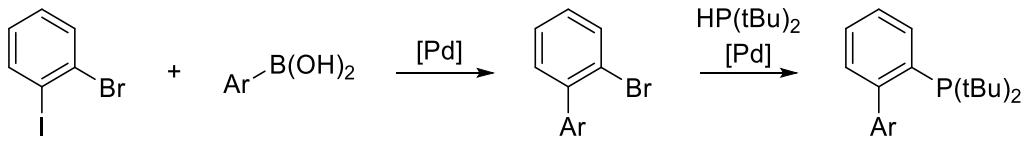

Figure 94. *Synthetic step for phosphine ligands synthesis.*

All the biaryl bromides **41** were obtained by palladium catalysed cross coupling from 1-bromo-2-iodobenzee with the corresponding aryl boronic acid. Only 0.1eq of boronic acid were added in excess to avoid yield erosion by double cross coupling.

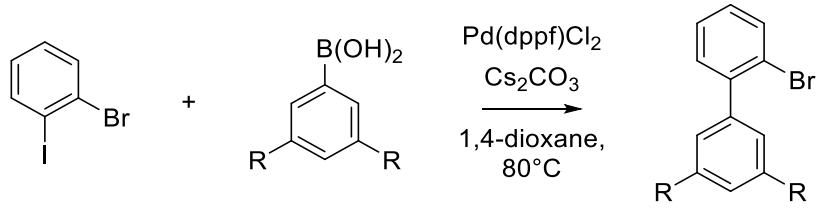

Compound	R	Yield

41a	CF_3	84%
41c	OMe	89%

Table 26. *bromo biaryl synthesis.*

The same conditions were not suitable for **41b**, due to the low rate of transmetallation of the boronic acid bearing three fluorine atoms. Desired product was obtained with 84% yield by addition of CsF as additive, that produce fluoroborate intermediate that undergo easily to transmetallation.

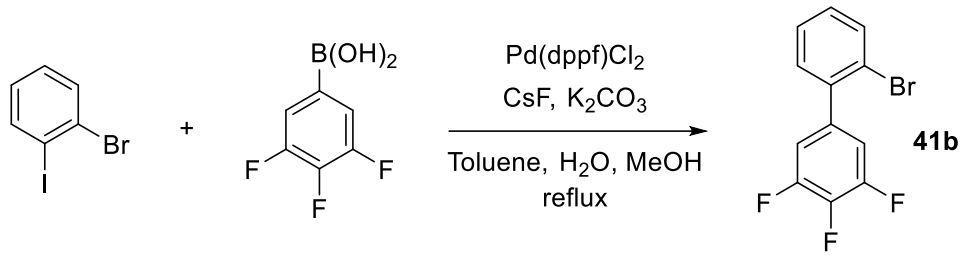

To achieve the phosphine, several procedure are present in literature, using dialkyl chlorophosphines or dialkyl phosphines. In the present thesis, both precursors were tested.

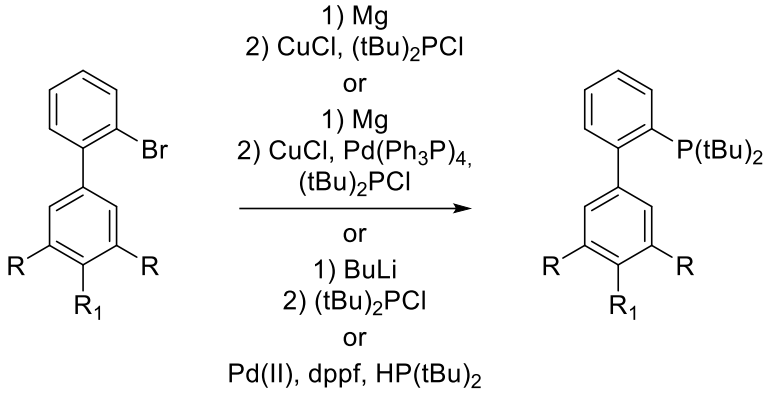

Figure 95. *Possible synthetic strategies for the synthesis of target phosphines.*

Dialkyl chloro phosphine

The use of BuLi as lithiating agent did not provided the desired phosphine but a complex mixture. The Grignard reagent and use of catalytic amount of Pd lead to a complex mixture too, with the Wutrz coupling as major product. Working in stoichiometric conditions with generation of Grignard intermediate and CuCl leaded as well to Wurtz coupling as major product but traces of desired phosphine were observed. This was a consequence of traces of O_2 in the reaction atmosphere, so after application of same conditions but several vacuum/N_2 cycles before addition of CuCl, Wurtz coupling was suppressed and desired phosphine was the major product observed. Reactions were quenched with concentred ammonia aqueous solution to complex copper(I) salts and to hydrolyse remaining chlorophosphine. Traces of biaryl homocoupling (Wurtz product) were isolated by precipitation from hexane/ether. Usually, Buchwald phosphines are purified by precipitation, but in these cases CF_3 and F functionalities provided high lipophilicity and therefore no precipitation was observed. Good levels of purity were obtained by precipitation of phosphines as hydrochloride salts with HCl in dioxane from hexane/ether 1 to 1.

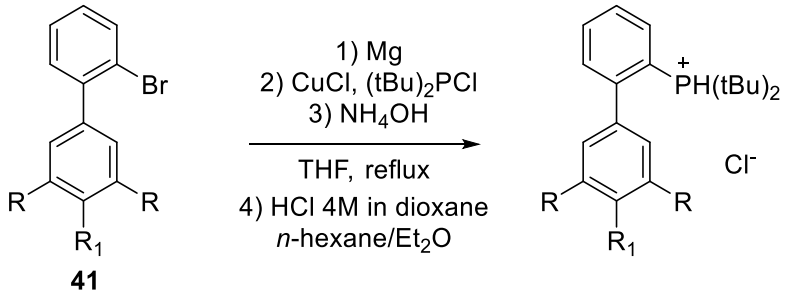

Substrate	R	R_1	Yield
41a	CF_3	H	53%
41b	F	F	44%
41c	OMe	H	41%

Table 27. *Phosphines hydrochloride synthesis.*

Yields are not so good but are in line with common results obtained in this kind of reaction (50 to 60%). These compounds gave only broad peaks at NMR so we proceeded with gold complexation. By use of a mild base as Na_2CO_3 or K_2CO_3 in DCM and in presence of AuCl(DMS), the desired gold complexes were obtained with good yields.

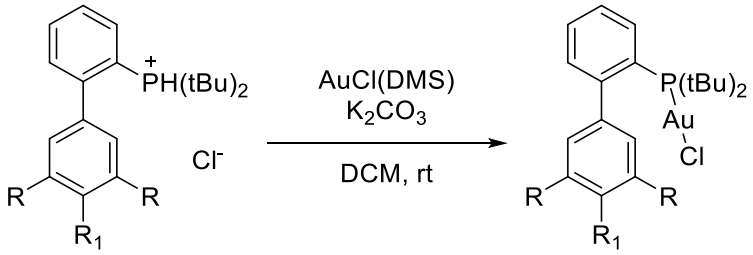

Compound	R	R_1	Yield
CF_3PhosAuCl	CF_3	H	78%
TriFPhosAuCl	F	F	87%
(tBu)isoSPhosAuCl	OMe	H	71%

Table 28. *Gold complexes synthesis.*

A bit of erosion in the yield is observed, this is attributed to the presences of tBu_2POH in the phosphine hydrochlorides. Comparing the abundancies at NMR of phosphine and tBu_2POH and the yield of the complexation, >99% of phosphine is converted into the gold complex, and the eroded yield is attributed to the tBu_2POH. Crude reaction mixtures were filtered through Celite® and thin layer of silica and the obtained complexes are pure, without traces of other products (by ^1H NMR and ^{31}P NMR).

Dialkyl phosphine

Free phosphine can be achieved by direct cross coupling of the bromo biaryl with the corresponding dialkyl phisphine. The dialkyl phosphines are easily oxidable, and therefore strictly inert atmosphere and degassed solvent are recommended. The synthesis of the targeted ligands proceed *via* palladium

catalysis and dppf ligand in toluene at reflux. With this procedure both ditertbutyl and, more sterically demanding, diadamantly biaryl phosphines.

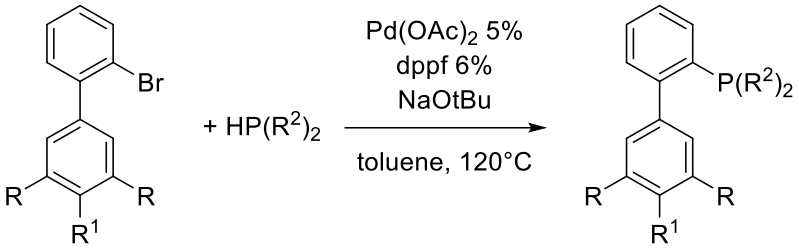

Compound	R	R^1	R^2	Yield
CF_3Phos	CF_3	H	tBu	77%
TriFPhos	F	F	tBu	69%
(tBu)isoSPhos	OMe	H	tBu	73%
AdCF_3Phos	CF_3	H	Ad	48%
AdTriFPhos	F	F	Ad	55%

Table 29. *Phosphine synthesis results through cross coupling procedure.*

These ligands were more stable and therefore were purified by flash chromatography with moderate to good yield (Table 29). The synthesis of the corresponding gold(I) chloride complexes was done with the common procedure for phosphine Au(I) catalysts with almost quantitative results (Table 30).

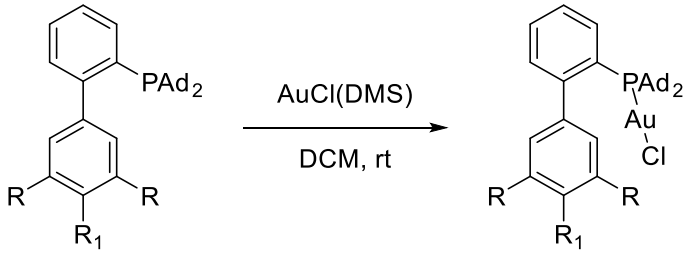

Compound	R	R_1		Yield
CF_3PhosAuCl	CF_3	H	tBu	93%
TriFPhosAuCl	F	F	tBu	95%
(tBu)isoSPhosAuCl	OMe	H	tBu	96%
AdCF_3PhosAuCl	CF_3	H	Ad	99%
AdTriFPhosAuCl	F	F	Ad	99%

Table 30. *Phosphine gold(I) complexes synthesis from free ligands.*

4.4 SC-XRD analysis

The desired new catalysts were crystallized from DCM/*n*-hexane by slow evaporation and subjected to SC-XRD.

Figure 96. *ORTEP molecular drawing of* ***CF_3PhosAuCl*** *(top) and* ***TriFPhosAuCl*** *(bottom), thermal ellipsoids are draw at 30% of the probability level.*

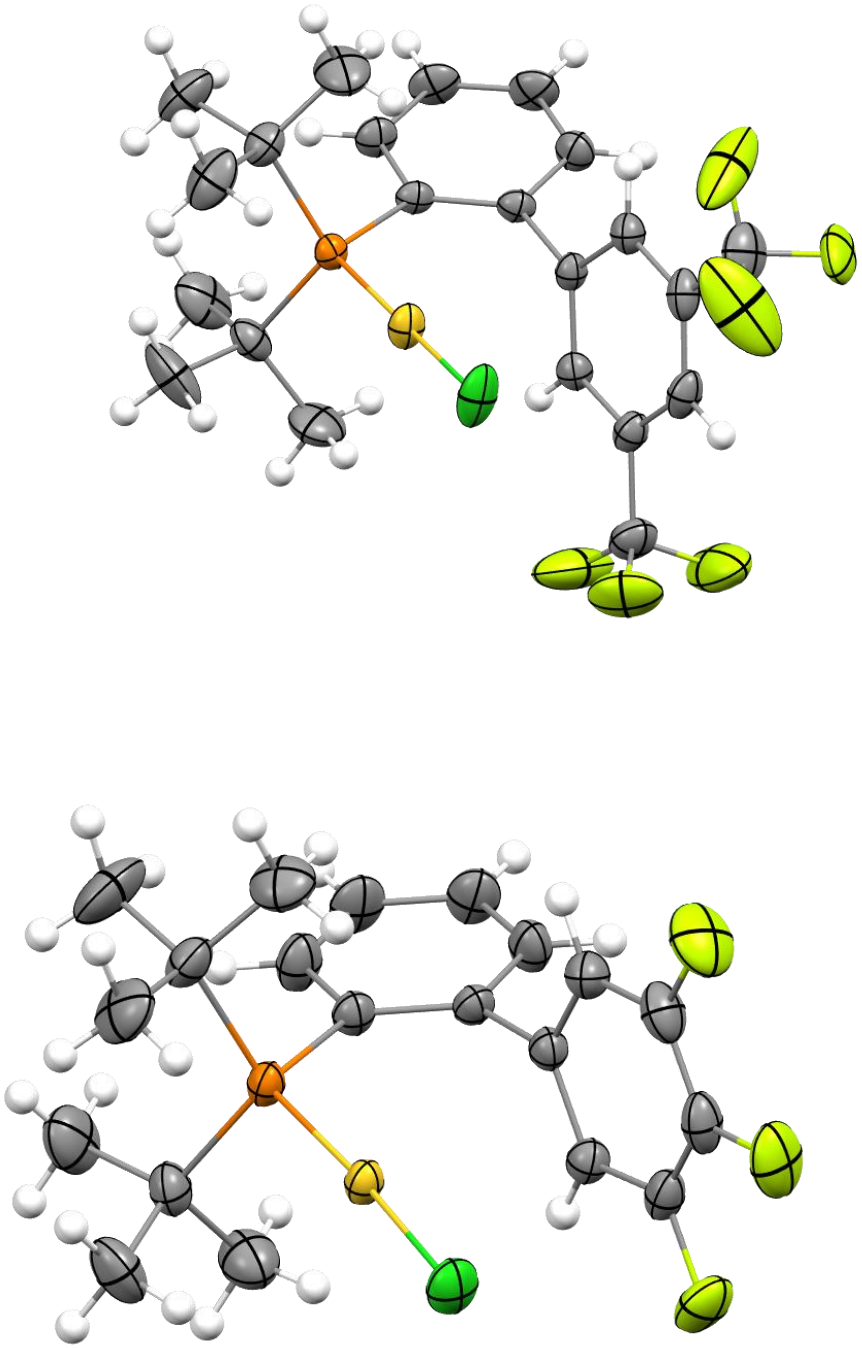

Figure 97. *ORTEP molecular drawing of* ***(tBu)isoSPhosAuCl*** *(top) and* ***AdCF$_3$PhosAuCl*** *(bottom), thermal ellipsoids are draw at 30% of the probability level.*

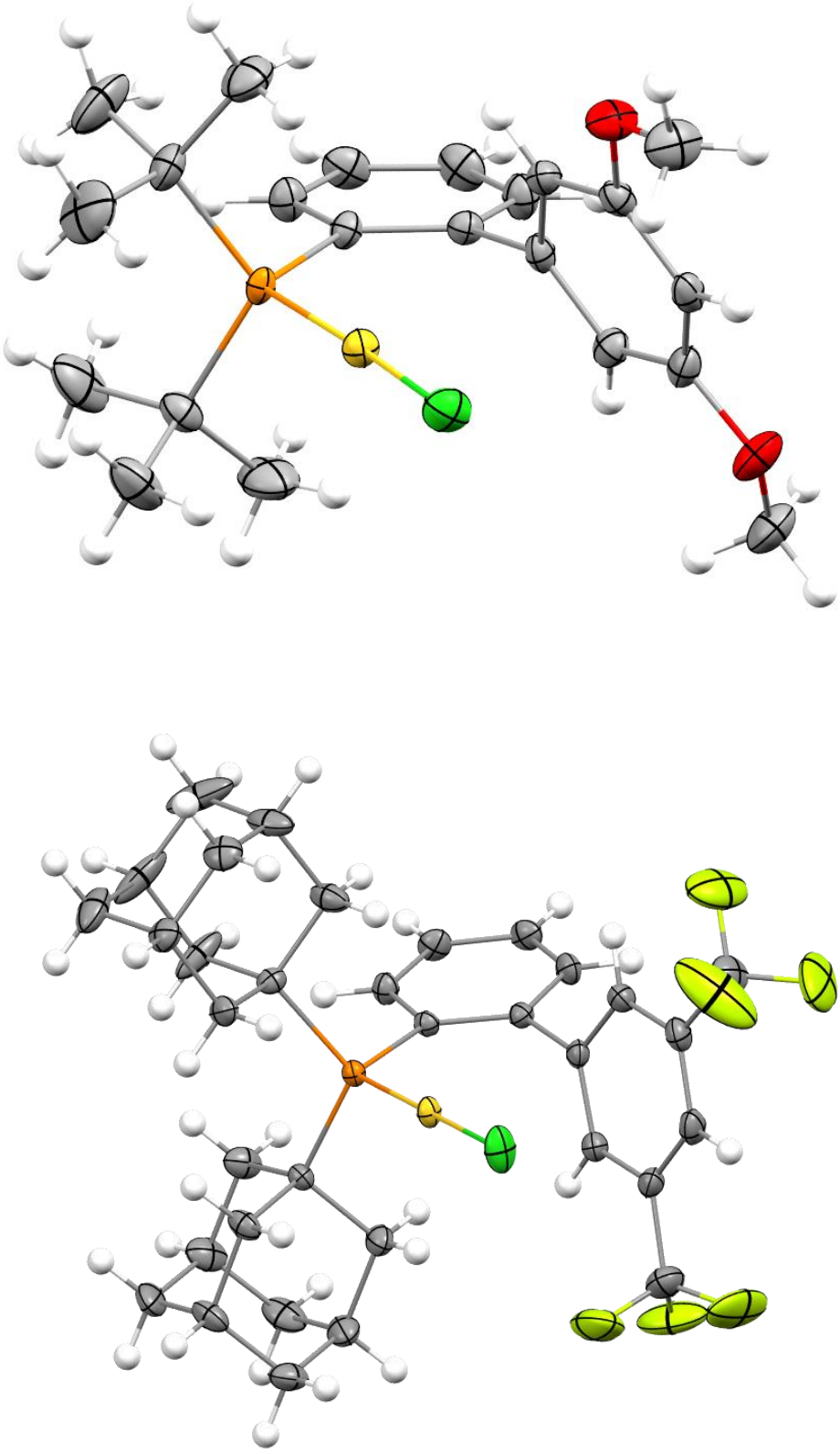

Figure 98. *ORTEP molecular drawing of* ***AdTriFPhosAuCl****, thermal ellipsoids are draw at 30% of the probability level.*

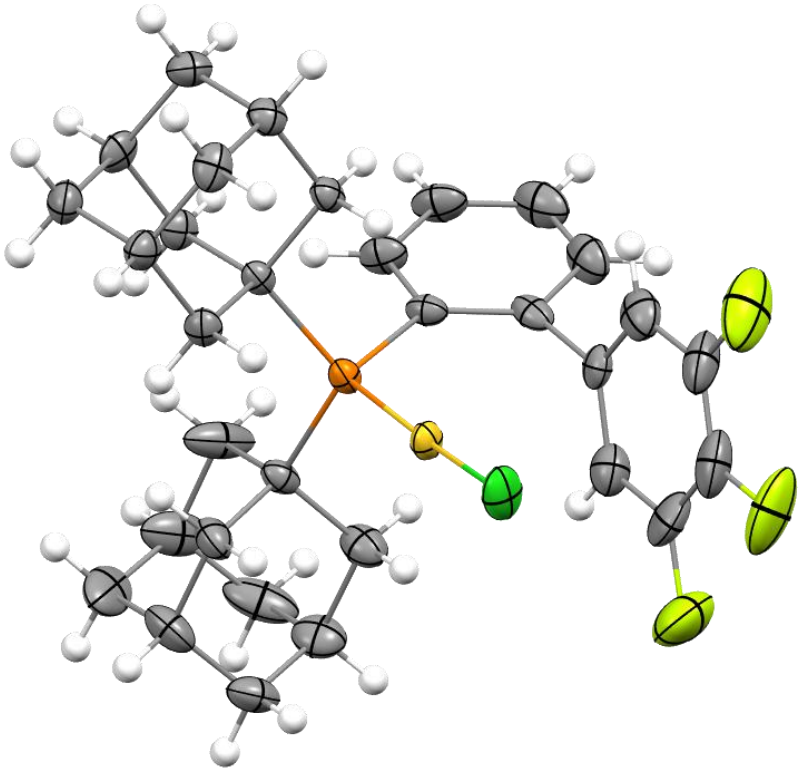

The structural parameters of these new catalysts were compared to already known JohnphosAuCl and AdJohnphosAuCl.

Catalyst	Au-P, Å	Au-Cl, Å	Ar···Au, Å [a]	Biaryl torsion, ° [a]
JohnphosAuCl	2.254(3)	2.303(4)	3.350	92.71
CF_3PhosAuCl	2.235(1)	2.286(1)	3.250	74.82
TriFPhosAuCl	2.238(1)	2.281(1)	3.292[b]	83.94[b]
(tBu)isoSPhosAuCl	2.262(2)	2.304(2)	3.267	69.66
AdJohnphosAuCl	2.2543(6)	2.3009(6)	3.337	65.56
AdCF_3PhosAuCl	2.2536(7)	2.2856(8)	3.241	73.46
AdTriFPhosAuCl	2.257(2)	2.293(2)	3.213	77.21

Table 31. *Comparison of structural parameters. a) calculated by Mercury, b) average of the two independent molecules in the asymmetric unit.*

All the catalysts showed a slightly contraction of Au-Cl bond, and P-Au bond only in the tBu series, suggesting that the gold metal centre has a greater partially positive charge inducted by π-interaction with electron poor aromatic systems. On the contrary, **(tBu)isoSPhosAuCl**, which is the only catalysts with an electron rich arene, presents no variation on Au-Cl bond (with respect to **JohnphosAuCl**) and a small increase in P-Au bons. In this case the π-interaction has the opposite trend of EWG substituent and the positive charge of the metal is decreased causing a weakening in P-Au bond. In all cases, electronic modifications (both EWG and EDG) of aryl pendant generate a

stronger Ar…Au(I) interaction which may affect the catalytic behaviour and therefore we moved on and tested them in homogeneous catalysis.

4.4 Catalytic applications

To evaluate the catalytic activity of the new catalysts, we searched in literature for benchmark reactions where JohnphosAuCl was the catalyst of choice. Several transformations adopt this complex as precatalyst, and finally we chose the 1,6-enyne cycloisomerization in presence of carbon nucleophile. As already shown in the introduction, these scaffold might undergo to a very large number of pathways leading to different products and this is strongly dependent on the substrate and catalyst nature. Therefore, this kind of reaction is perfect to evaluate the reactivity and selectivity of new catalysts.
In detail, we chose the specific reaction in the Figure 99 below.[84]

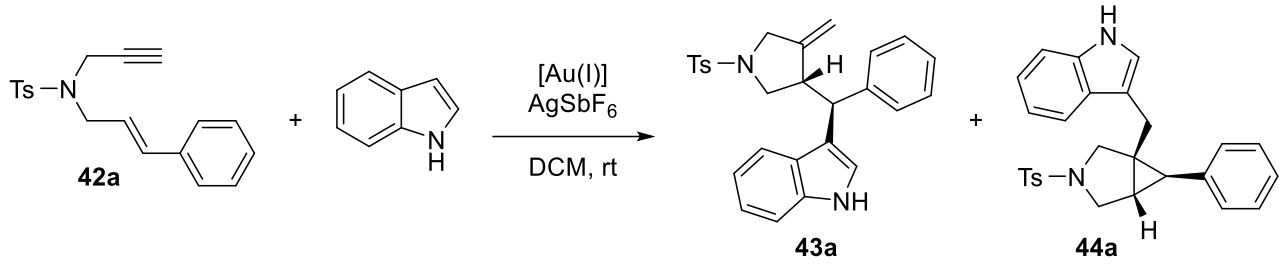

Figure 99. *Model reaction for testing new catalysts.*

We started by testing **CF_3PhosAuCl** and **JohnphosAuCl** at different catalysts loading and results are reported in Table 32.

Catalyst	% catalyst	% $AgSbF_6$	Conversion	43a/44a
JPAu(ACN)SbF_6[b]	5	-	100%	82/18
CF_3PhosAuCl	5	5	100%	97/3
JPAu(ACN)SbF_6[b]	2	-	42%[a]	88/12
CF_3PhosAuCl	2	2	95%[a]	100/0

Table 32. *Initial screening of catalytic activity. a) determined by NMR with internal standard. b) cationic [JohnphosAu(ACN)]SbF_6 catalyst was used.*

Applying same conditions from reference (5% of catalyst), full conversion was observed within 10 minutes with both catalysts. Since no differences were observed in catalytic reactivity of the catalysts, only selectivity was analysed and **CF_3PhosAuCl** showed a significantly higher selectivity through **43a** product. From our previous consideration of the activation role of electron poor phenyl pendant, we then decreased the catalyst loading to 2mol%, and with these conditions we started to observe differences in reactivity of the catalysts. The decrease of catalyst loading yielded, with both complexes, a better selectivity where **CF_3PhosAuCl** was completely selective to **43a**. Moreover, **CF_3PhosAuCl** resulted more catalytically active, leading to an almost complete conversion in 10 minutes. With these very promising results we decreased further the catalyst loading to 1mol% and we also tested the other synthetized catalysts (Table 33).

Catalyst	Yield[a]	43a/44a[b]
JPAu(ACN)SbF$_6$	70%	78/22
CF$_3$PhosAuCl	95%	100/0
TriFPhosAuCl	93%	96/4
(tBu)isoSPhosAuCl	48%	100/0
AdCF$_3$PhosAuCl	40%	>99/1

Table 33. *Catalytic results at 1mol% catalyst loading. a) isolated yield, b) determined by NMR.*

At 1mol% of catalysts loading the full conversion for the catalysis with **CF$_3$PhosAuCl** was achieved after 1 hour, thus to accurately compare the results with other catalysts every reaction was stopped after 1 hour. All the new catalysts provided exclusively, or almost exclusively, **43a** with very excellent yield, with exception for **(tBu)isoSPhosAuCl**. The more sterically hindered **AdCF$_3$PhosAuCl** was not comparable in terms of yield with the other catalyst but preserved an high selectivity. Johnphos ligand was still efficient at this loading but less than the newly reported ligands and with a remarkably less selectivity. These results are in line with our hypothesis of high electrophilic activation by secondary L-M interactions (or quenching in case of **(tBu)isoSPhosAuCl**).

However, this reaction is not that simple as nucleophilic addition to a C-C multiple bond. This transformation is thought to be a four step mechanism (Figure 100), where coordination of alkyne and protodeauration are very low barrier step because alkyne is not scarcely activated and there are no bases that sequester H^+ (as explained in paragraph 4.1). The key transition states are the cyclopropanation reaction and the nucleophilic addition (**II** and **IIIa/b** respectively).

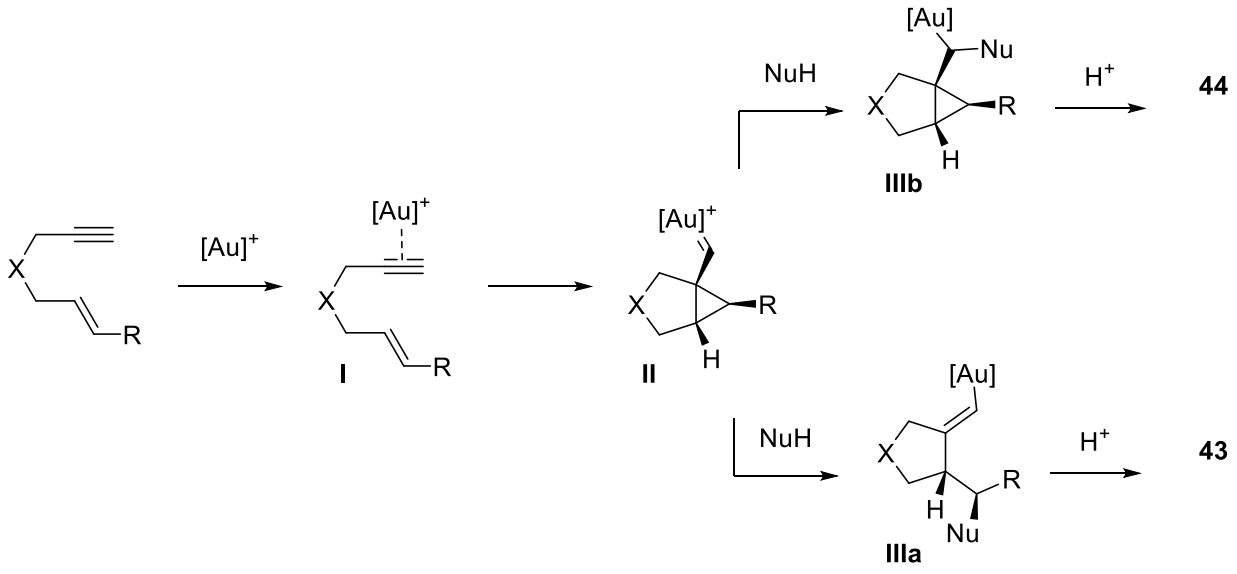

Figure 100. *Mechanistic steps of 1,6-enyneg Au(I) catalysed cycloisomerization.*

After the resulted obtained in Table 33 is not clear which is the rate determining step, however is clear that the electronic properties of Au(I) complex influences the selectivity in the reactivity of intermediate **II**.

Another parameter that can influence both reactivity and selectivity is the electronic nature of R, because it may make the alkene more, or less, nucleophilic and influence the charge distribution in

intermediate **II** and direct the selectivity to **43** or **44**. For this reason we synthetized four further substrates **42b-e** and subjected them to the same reaction conditions using 1mol% of all catalysts yielding products **43b-e**.

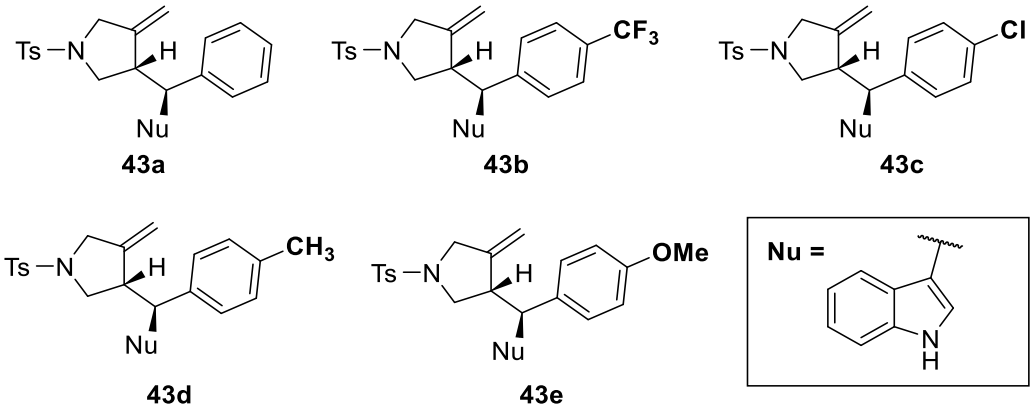

Figure 101. *Electronically modified products.*

Cat. / Sub.	43b[c]	43c[c]	43a	43d	43e
CF_3PhosAuCl	14% (85%)[a]	49% (85%)[b]	95%	93%	99%
TriFPhosAuCl	10% (27%)[a]	30% (67%)[b]	93%	73%	96%
JPAu(ACN)SbF_6	4% (13%)[a]	23% (54%)[b]	70%	59%	80%
(tBu)isoSPhosAuCl	6% (29%)[a]	21% (54%)[b]	48%	48%	72%

Table 34. *Substrates scope catalytic results. All the yields are reported after 1h of reaction and are isolated yields if not differently noted. a) Isolated yield after 22h; b) Isolated yield afters 5h; c) NMR yield after 1h with internal standard*

Cat. / Sub.	43b/44b	43c/44c	43a/44a	43d/44d	43e/44e
CF_3PhosAuCl	100/0	98/2	100/0	98/2	99/1
TriFPhosAuCl	ND[a]	94/6	94/6	96.5/3.5	97.5/2.5
JPAu(CAN)SbF_6	ND[a]	90/10	78/22	94/6	97/3
(tBu)isoSPhosAuCl	ND[a]	91.5/8.5	100/0	93.5/6.5	97.5/2.5

Table 35. *Selectivity results by NMR before purification. a) signals with too low intensity to be determined.*

Some interesting information can be obtained by these results. With all the substrates tested, the general trend of yield provided by catalysts is maintained (CF_3Phos > TriFPhos > JohnPhos > (tBu)isoSPhos) and it also correlate wonderfully with the electronic nature of the biarly unit (EWG best, EDG worst). In only one case this is was not observed and it's the case of **42b**, where probably due to the low reactivity of the substrate, catalyst stability plays a key role. Also the reactivity of substrates has a trend, as supposed, and the more electron rich (**42a,d-e**) performed better than electron poor (**42b-c**).

In terms of selectivity, all the catalysts provided **43** as major product. With highly reactive substates **42d** and **42e** small deviation was observed, while with neutral **42a** and electron deficient **42b** and **42c** selectivity was eroded by the decreasing activity of the catalyst even if a linear trend is not clear. However, **CF_3PhosAuCl** provided with all the substates almost exclusively product **43**, proving it is the best catalysts in both yield and selectivity among all the others.

4.5 Conclusions

In this ongoing project new *ortho*-biaryl phosphine Au(I) complexe having unprecedent electron poor phenyl ring were synthetized, characterized in solid state and compared with already known structures. Application of the catalysts in benchmark reaction allowed comparison of reactivity and selectivity. These new catalysts turned out to be superior to the largely employed JohnphosAuCl catalyst allowing lower catalyst loading without loss of reactivity and increasing the selectivity. The elevated capability of electrophile activation permitted to achieve reactivity even with very low nucleophilic alkenes, which was a challenging task in gold chemistry.

Other organic transformation and DFT calculation are now under investigation to provide a complete view of the role of the EWG Ar···Au(I) interaction in biaryl phosphine Au(I) complexes.

4.6 Experimental section

NOTE: This experimental section may be incomplete in several parts and full data will be provided as soon as possible.

^{1}H NMR spectra were recorded on Varian 400 (400 MHz) spectrometers. Chemical shifts are reported in ppm from TMS with the solvent resonance as the internal standard (deuterochloroform: 7.27 ppm). Data are reported as follows: chemical shift, multiplicity (s = singlet, d = doublet, t = triplet, q = quartet, sext = sextet, sept = septet, p = pseudo, b = broad, m = multiplet), coupling constants (Hz).

^{13}C NMR spectra were recorded on a Varian 400 (100 MHz) spectrometers with complete proton decoupling. Chemical shifts are reported in ppm from TMS with the solvent as the internal standard (deuterochloroform: 77.0 ppm).

^{19}F NMR spectra were recorded on a Varian 400 (377 MHz). Chemical shifts are reported in ppm from CFCl3.

^{31}P NMR spectra were recorded on a Varian 400 (162 MHz). Chemical shifts are reported in ppm and not corrected

GC-MS spectra were taken by EI ionization at 70 eV on a Hewlett-Packard 5971 with GC injection. They are reported as: m/z (rel. intense).

LC-electrospray ionization mass spectra were obtained with Agilent Technologies MSD1100 single-quadrupole mass spectrometer.

Elemental analyses were carried out by using a EACE 1110 CHNOS analyser.

Melting points were determined with Bibby Stuart Scientific Melting Point Apparatus SMP 3 and are not corrected.

Chromatographic purification was done with 240-400 mesh silica gel.

Anhydrous solvents were supplied by Sigma Aldrich in Sureseal® bottles and used without any further purification. Ethyl acetate was dried on activated 5Å molecular sieves.

Commercially available chemicals were purchased from Sigma Aldrich, Fluorochem and TCI and used without any further purification.

The X-ray intensity data were measured on a Bruker Apex II CCD diffractometer. Cell dimensions and the orientation matrix were initially determined from a least-squares refinement on reflections measured in three sets of 20 exposures, collected in three different ω regions, and eventually refined against all data. A full sphere of reciprocal space was scanned by 0.5° ω steps. The software SMART[3] was used for collecting frames of data, indexing reflections and determination of lattice parameters. The collected frames were then processed for integration by the SAINT program,[61] and an empirical absorption correction was applied using SADABS.[62] The structures were solved by direct methods (SIR 2014)[63] and subsequent Fourier syntheses and refined by full-matrix least-squares on F^2 (SHELXTL)[64] using anisotropic thermal parameters for all non-hydrogen atoms. The aromatic, methyl, methylene and methine hydrogen atoms were placed in calculated positions, refined with isotropic thermal parameters *U(H)* = 1.2 *Ueq*(C) and allowed to ride on their carrier carbons. Molecular drawings were generated using Mercury.[65] Crystal structure are not depositated yet.

Synthesis of *o*-biaryl bromides

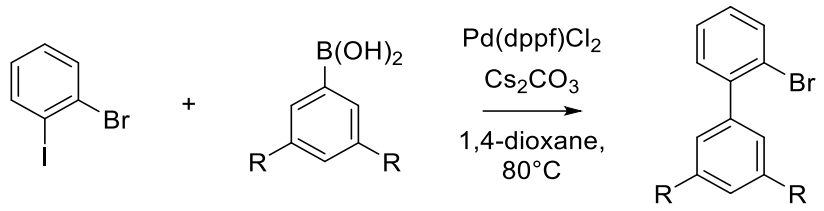

To a Schlenk tube under nitrogen atmosphere are added aryl boronic acid (1.05mmol, 1.05eq), cesium carbonate (975mg, 3mmol, 3eq) and Pd(dppf)Cl_2•DCM (40mg, 0.05mmol, 5%), then 5mL of dioxane are added and mixture purged with nitrogen flux for 2 minutes. 1-bromo-2-iodobenzene (130µL, 1mmol, 1eq) is added via syringe and the reaction heated at 80°C overnight. Reaction is diluted with 15mL of ethyl acetate and 15mL of distilled water and transferred to a separatory funnel. Crude is extracted 3x15mL with ethyl acetate and organic phase washed with water (30mL), brine (30mL), dried over Na_2SO_4 and volatile compounds removed at rotavapor. Desired product is purified by flash chromatography using 100% *n*-hexane as eluent.

41a, yield 84%, colourless oil.

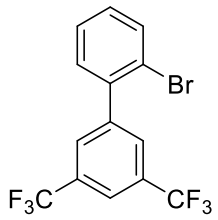

^{1}H NMR (400 MHz, $CDCl_3$) δ = 7.92 – 7.89 (m, 1H), 7.88 (s, 2H), 7.71 (dd, J = 8.0, 1.2 Hz, 1H), 7.42 (td, J = 7.5, 1.2 Hz, 1H), 7.33 (dd, J = 7.7, 1.8 Hz, 1H), 7.29 (td, J = 7.8, 1.8 Hz, 1H).

^{13}C NMR (100 MHz, $CDCl_3$) δ = 142.77, 139.50, 133.50, 131.39 (q, *J* = 33.5 Hz), 131.00, 130.10, 129.88 – 129.50 (m), 127.84, 124.61, 122.19, 121.66 – 121.27 (m).

^{19}F NMR (377 MHz, $CDCl_3$) δ = -62.86 (s, 6F).

41c, yield 89%, colourless oil.

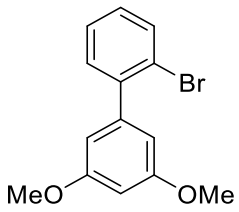

^{1}H NMR (400 MHz, $CDCl_3$) δ = 7.66 (dt, *J* = 8.0, 0.9 Hz, 1H), 7.37 – 7.31 (m, 2H), 7.20 (dt, *J* = 8.0, 4.6 Hz, 1H), 6.57 (d, *J* = 2.3 Hz, 2H), 6.52 (t, *J* = 2.3 Hz, 1H), 3.83 (s, 6H).

^{13}C NMR (100 MHz, $CDCl_3$) δ = 160.30, 142.99, 142.52, 133.13, 131.11, 128.84, 127.31, 122.44, 107.62, 99.76, 55.41.

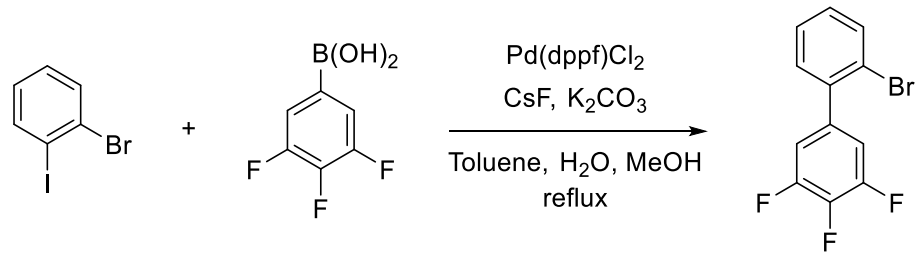

To a Schlenk tube under nitrogen atmosphere are added 3,4,5-trifluorobenzene boronic acid (97mg, 0.55mmol, 1.1eq), cesium fluoride (91mg, 0.6mmol, 1.2eq), potassium carbonate (151mg, 1.1mmol, 2.2eq) and Pd(dppf)Cl_2•DCM (20mg, 0.025mmol, 5%), then 2mL of toluene, 0.5mL of methanol and 0.5mL of water are added and mixture purged with nitrogen flux for 2 minutes. 1-bromo-2-iodobenzene (65µL, 0.5mmol, 1eq) is added via syringe and the reaction heated to reflux overnight. Reaction is diluted with 15mL of ethyl acetate and 15mL of distilled water and transferred to a separatory funnel. Crude is extracted 3x15mL with ethyl acetate and organic phase washed with water

(30mL), brine (30mL), dried over Na_2SO_4 and volatile compounds removed at rotavapor. Desired product is purified by flash chromatography using 100% *n*-hexane as eluent.

41b, yield 84%, colourless oil.

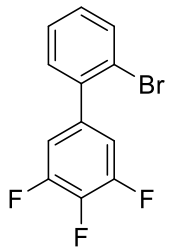

^{1}H NMR (400 MHz, $CDCl_3$) δ = 7.66 (dd, *J* = 8.0, 1.2 Hz, 1H), 7.37 (td, *J* = 7.5, 1.3 Hz, 1H), 7.29 – 7.20 (m, 2H), 7.07 – 6.96 (m, 2H).
^{13}C NMR (100 MHz, $CDCl_3$) δ = 150.71 (ddd, *J* = 250.0, 10.0, 4.2 Hz), 139.62, 139.40 (dt, *J* = 252.4, 15.2 Hz), 136.79 (td, *J* = 8.3, 5.1 Hz), 133.38, 130.89, 129.70, 127.63, 122.19, 114.23 – 113.34 (m).
^{19}F NMR (377 MHz, $CDCl_3$) δ = -134.57 – -134.74 (m, 2F), -161.76 (tt, *J* = 20.5, 6.6 Hz, 1F).

Phosphorylation reaction

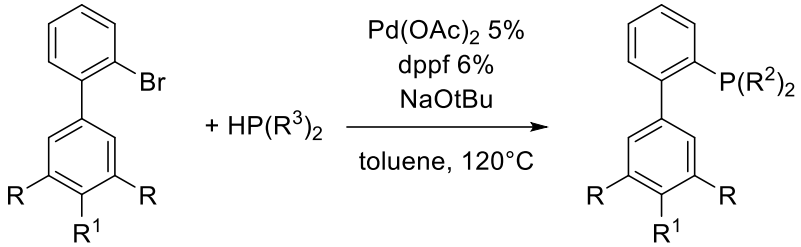

In a Schlenk tube under nitrogen atmosphere, bromo biraryl (0.24mmol, 1eq) is dissolved in 1.2mL of toluene. Subsequently, $Pd(OAc)_2$ (2.7mg, 0.012mmol, 5%), bis diphenylphosphino ferrocene (7.7mg, 0.014mmol, 6%) and NaOtBu (27mg, 0.28mmol, 1.2eq) are added and the reaction stirred at room temperature for 15 minutes. Finally, di alkyl phosphine (0.26mmol, 1.1eq) is added and the reaction heated at 120°C overnight. The reaction is cooled to room temperature and diluted with water and extracted 3x ethyl aetate. The organic phase was dried over Na_2SO_4 and volatile compounds removed with rotavapor. Final product was purified by flash chromatography from 100% *n*-hexane (until elution of unreacted SM) and then 30/1 *n*-hexane/ethyl acetate.

CF_3Phos, yield 77%, deliquescent colourless crystals.

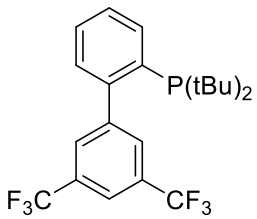

^{1}H NMR (400 MHz, $CDCl_3$) δ = 8.00 – 7.94 (m, 1H), 7.86 – 7.82 (m, 1H), 7.74 (d, *J* = 1.7 Hz, 2H), 7.48 – 7.41 (m, 2H), 7.33 – 7.27 (m, 1H), 1.14 (d, *J* = 11.8 Hz, 18H).
^{13}C NMR (100 MHz, $CDCl_3$) δ = 148.26 (d, *J* = 32.8 Hz), 145.64 (d, *J* = 7.5 Hz), 135.97 (d, *J* = 29.5 Hz), 135.68 (d, *J* = 3.0 Hz), 130.87 (dq, *J* = 4.9, 1.4 Hz), 130.23 (q, *J* = 33.1 Hz), 129.95 (d, *J* = 6.0 Hz), 128.91 (d, *J* = 1.2 Hz), 127.13, 123.58 (q, *J* = 272.5 Hz), 120.17 (p, *J* = 3.8 Hz), 32.94 (d, *J* = 24.8 Hz), 30.50 (d, *J* = 15.2 Hz).
^{19}F NMR (377 MHz, $CDCl_3$) δ = -62.88 (s, 6F).
^{31}P NMR (162 MHz, $CDCl_3$) δ = 17.52.

TriFPhos, yield 69%, colourless cystals.

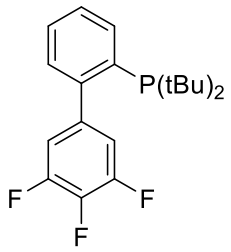

^{1}H NMR (400 MHz, $CDCl_3$) δ = 7.92 (ddd, *J* = 6.4, 3.0, 1.7 Hz, 1H), 7.44 – 7.35 (m, 2H), 7.20 (dt, *J* = 5.8, 3.8 Hz, 1H), 6.86 (dd, *J* = 8.4, 6.6 Hz, 2H), 1.16 (d, *J* = 11.8 Hz, 20H).
^{13}C NMR (100 MHz, $CDCl_3$) δ = 150.13 (ddd, *J* = 249.0, 9.9, 4.2 Hz), 148.26 (dt, *J* = 31.8, 2.1 Hz), 139.76 (qd, *J* = 7.9, 5.0 Hz), 137.47 (dt, *J* = 250.2, 15.3 Hz), 135.78, 135.48 (d, *J* = 3.1 Hz), 130.09 (dd, *J* = 5.9, 0.9 Hz), 128.74 (d, *J* = 1.4 Hz), 126.78, 114.68 (ddd, *J* = 15.6, 5.6, 3.9 Hz), 32.85 (d, *J* = 24.2 Hz), 30.63 (d, *J* = 15.2 Hz).
^{19}F NMR (377 MHz, $CDCl_3$) δ = -135.47 – -136.73 (m, 2F), -163.85 (tt, *J* = 20.5, 6.5 Hz, 1F).
^{31}P NMR (162 MHz, $CDCl_3$) δ = 18.07.

(tBu)isoSPhos, yield 73%, pale yellow powder.

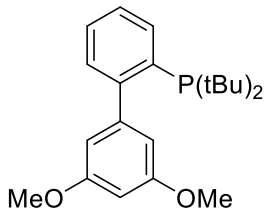

^{1}H NMR (400 MHz, $CDCl_3$) δ = 7.90 (dt, *J* = 7.9, 1.8 Hz, 1H), 7.42 – 7.31 (m, 2H), 7.26 (ddd, *J* = 8.8, 4.4, 2.1 Hz, 1H), 6.44 (t, *J* = 2.3 Hz, 1H), 6.41 (d, *J* = 2.3 Hz, 2H), 3.79 (s, 6H), 1.17 (d, *J* = 11.6 Hz, 18H).
^{13}C NMR (100 MHz, $CDCl_3$) δ = 159.51, 151.22 (d, *J* = 33.5 Hz), 145.94 (d, *J* = 7.3 Hz), 135.48 (d, *J* = 27.8 Hz), 135.22 (d, *J* = 3.4 Hz), 130.18 (d, *J* = 6.2 Hz), 128.33 (d, *J* = 1.2 Hz), 125.85, 108.83 (d, *J* = 3.5 Hz), 98.76, 55.23, 32.68 (d, *J* = 25.2 Hz), 30.82 (d, *J* = 15.6 Hz).
^{31}P NMR (162 MHz, $CDCl_3$) δ 18.66.

AdCF$_3$Phos, yield 48%, white powder.

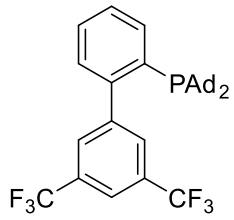

^{1}H NMR (400 MHz, $CDCl_3$) δ = 7.95 – 7.88 (m, 1H), 7.79 (s, 1H), 7.68 (s, 2H), 7.47 – 7.37 (m, 2H), 7.27 (dd, *J* = 5.9, 2.9 Hz, 1H), 1.89 – 1.73 (m, 18H), 1.63 (d, *J* = 3.4 Hz, 12H).
^{13}C NMR (100 MHz, $CDCl_3$) δ = 148.69 (d, *J* = 32.4 Hz), 145.70 (d, *J* = 7.3 Hz), 136.94 (d, *J* = 2.7 Hz), 133.50 (d, *J* = 29.1 Hz), 130.99, 129.96 (d, *J* = 6.0 Hz), 128.67, 126.68, 124.94, 122.23, 120.06 (t, *J* = 4.0 Hz), 41.86 (d, *J* = 12.6 Hz), 37.52 (d, *J* = 25.2 Hz), 36.83, 28.74 (d, *J* = 8.7 Hz).
^{19}F NMR (377 MHz, $CDCl_3$) δ = -62.79 (6F).
^{31}P NMR (162 MHz, $CDCl_3$) δ = 20.05.

AdTriFPhos, yield 55%, white powder.

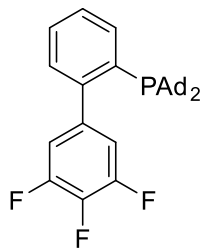

^{1}H NMR (401 MHz, $CDCl_3$) δ = 7.93 – 7.82 (m, 1H), 7.41 – 7.33 (m, 2H), 7.21 – 7.14 (m, 1H), 6.81 (dd, *J* = 8.4, 6.6 Hz, 2H), 1.89 (m, 18H), 1.68 (m, 12H).
^{19}F NMR (377 MHz, $CDCl_3$) δ = -133.30 – -137.70 (m, 2F), -164.03 (tt, *J* = 20.7, 6.6 Hz, 1F).

Gold complex synthesis

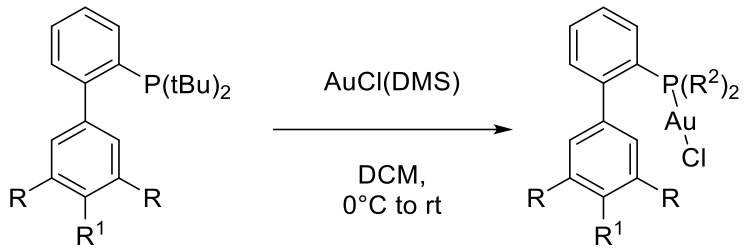

To a three-neck flask under inert atmosphere and equipped with dropping funnel, AuCl(DMS) (15.2mg, 0.051mmol, 1eq) is dissolved in 2mL of DCM and phosphine (0.051mmol, 1eq) is dissolved in 3mL of DCM transferred in the dropping funnel. The flask is covered with foil to provide darkness and put at 0°C. The phosphine is added dropwise over a period of 15 minutes and then the reaction is slowly warmed to room temperature. When reaction is completed (check by TLC 2:1 *n*Hex:AcOEt) DCM is removed by vacuum affording the gold complex.

CF_3PhosAuCl, yield 93%, colourless powder.

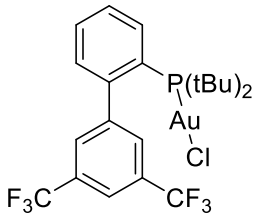

^{1}H NMR (400 MHz, $CDCl_3$) δ = 8.07 (s, 1H), 7.95 – 7.88 (m, 1H), 7.58 (ddd, *J* = 5.4, 2.8, 1.5 Hz, 2H), 7.53 (s, 2H), 7.34 – 7.27 (m, 1H), 1.40 (d, *J* = 15.8 Hz, 18H).
^{19}F NMR (377 MHz, $CDCl_3$) δ = -62.89 (6F).
^{31}P NMR (162 MHz, $CDCl_3$) δ = 60.42.

TriFPhosAuCl, yield 87%, colourless powder.

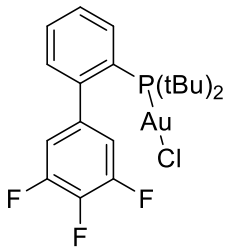

^{1}H NMR (400 MHz, $CDCl_3$) δ = 7.86 (td, *J* = 7.4, 4.0 Hz, 1H), 7.58 – 7.48 (m, 2H), 7.28 (dd, *J* = 5.7, 3.0 Hz, 1H), 6.72 (t, *J* = 6.7 Hz, 2H), 1.40 (d, *J* = 15.7 Hz, 18H).
^{19}F NMR (377 MHz, $CDCl_3$) δ = -132.94 (dd, *J* = 21.0, 7.1 Hz, 2F), -160.85 (tt, *J* = 20.9, 6.4 Hz, 1F).

Table 35. *Crystal data and structure refinement for compounds* ***CF₃PhosAuCl***, ***TriFPhosAuCl*** *and* ***(tBu)isoSPhosAuCl****.*

Compound	**CF_3PhosAuCl**	**TriFPhosAuCl**	**(tBu)isoSPhosAuCl**
Formula	$C_{22}H_{25}AuClF_6P$	$C_{20}H_{24}AuClF_3P$	$C_{22}H_{31}AuClO_2P$
Fw	666.80	584.78	590.85
T, K	296 (2)	293(2)	296(2)
λ, Å	0.71073	0.71079	0.71073
Crystal symmetry	Monoclinic	Triclinic	Monoclinic
Space group	*C2/c*	*P-1*	$P2_1/n$
***a*, Å**	28.889(2)	10.3440(9)	8.530(2)
***b*, Å**	8.6259(6)	14.739(1)	10.205(3)
***c*, Å**	20.032(1)	15.695(1)	26.581(8)
α	90	80.768(2)	90
β	101.026(2)	86.013(2)	97.56(1)
γ	90	74.571(2)	90
Cell volume, $Å^3$	4899.6(6)	2275.9(3)	2293.9(1)
Z	8	4	4
D_C, Mg m^{-3}	1.808	1.707	1.711
μ(Mo-$K_α$), mm^{-1}	6.232	6.677	6.613
F(000)	2576	1128	1160
Crystal size/ mm	0.36 x 0.24 x 0.20	0.31 x 0.21 x 0.18	0.28 x 0.12 x 0.08
θ limits, °	2.623 to 25.249	1.945 to 30.572	1.546 to 25.495
Reflections collected	29141	28269	25188
Unique obs. Reflections [$F_o > 4σ(F_o)$]	4366 [R(int) = 0.0267]	8251 [R(int) = 0.0382]	4253 [R(int) = 0.0432]
Goodness-of-fit-on F^2	1.056	1.060	1.215
R_1 (F)[a], wR_2 (F^2)[b] [I > 2σ(I)]	R1 = 0.0333, wR2 = 0.0874	R1 = 0.0324, wR2 = 0.0664	R1 = 0.0409, wR2 = 0.0885
Largest diff. peak and hole, e. $Å^{-3}$	0.995 and -1.167	0.895 and -1.052	2.215 and -3.625

[a] $R_1 = \Sigma||F_o|-|F_c||/\Sigma|F_o|$. [b] $wR_2 = [\Sigma w(F_o^2-F_c^2)^2/\Sigma w(F_o^2)^2]^{1/2}$ where $w = 1/[\sigma^2(F_o^2) + (aP)^2 + bP]$ where $P = (F_o^2 + F_c^2)/3$.

Table 36. *Crystal data and structure refinement for compounds* ***AdCF$_3$PhosAuCl*** *and* ***AdTriFPhosAuCl.***

Compound	**AdCF$_3$PhosAuCl**	**AdTriFPhosAuCl**
Formula	$C_{34}H_{37}AuClF_6P$	$C_{32}H_{36}AuClF3P$
Fw	823.02	740.99
T, K	296 (2)	293(2)
λ, Å	0.71073	0.71079
Crystal symmetry	Monoclinic	Monoclinic
Space group	*C2/c*	*P2$_1$/c*
***a*, Å**	24.4231(9)	10.1009(6)
***b*, Å**	10.6355(4)	27.464(2)
***c*, Å**	24.3200(9)	11.0036(7)
α	90	90
β	103.117(1)	100.449(2)
γ	90	90
Cell volume, Å^3	6152.3(4)	3001.9(3)
Z	8	4
D_C, Mg m^{-3}	1.777	1.640
μ(Mo-Kα), mm^{-1}	4.982	5.081
F(000)	3248	1464
Crystal size/ mm	0.27 x 0.18 x 0.14	0.22 x 0.17 x 0.11
θ limits, °	1.712 to 25.499	2.396 to 25.998
Reflections collected	50603	37886
Unique obs. Reflections [$F_o > 4\sigma(F_o)$]	5727 [R(int) = 0.0568]	5896 [R(int) = 0.0374]
Goodness-of-fit-on F^2	1.191	1.315
R_1 (F)[a], wR_2 (F^2)[b] [I > 2σ(I)]	R1 = 0.0226, wR2 = 0.0497	R1 = 0.0508, wR2 = 0.1027
Largest diff. peak and hole, e. Å^{-3}	0.687 and -0.753	1.310 and -2.451

[a] $R_1 = \Sigma||F_o|-|F_c||/\Sigma|F_o|$. [b] $wR_2 = [\Sigma w(F_o^2-F_c^2)^2/\Sigma w(F_o^2)^2]^{1/2}$ where $w = 1/[\sigma^2(F_o^2) + (aP)^2 + bP]$ where $P = (F_o^2 + F_c^2)/3$.

5 References

[1] M.-C. Daniel, D. Astruc, *Chem. Rev.*, **2004**, 104, 1, 293–346.
[2] K. Saha, S. S. Agasti, C. Kim, X. Li, V. M. Rotello, *Chem. Rev.*, **2012**, 112, 5, 2739–2779.
[3] C. C. C. J. Seechurn, M. O. Kitching, T. J. Colacot, V. Snieckus, *Angew. Chem. Int. Ed*., **2012**, 51, 5062 – 5085.
[4] P. Font, X. Ribas, *Eur. J. Inorg. Chem*., **2021**, 2556-2569.
[5] S. G. Bratsch, *J. Phys. Chem. Ref. Data*, **1989**, 18, 1–21.
[6] Y. Ito, M. Sawamura, T. Hayashi, *J. Am. Chem. Soc*., **1986**, 108, 6406-6407.
[7] Y. Fukuda, K. Utimoto, *J. Org. Chem.*, **1991**, 56, 11, 3729–3731.
[8] S. Brode, M. Chabanas, J. H. Teles, *Angew. Chem. Int. Ed.*, **1998**, 37, 1415-1418.
[9] E. Mizushima, K. Sato, T. Hayashi, M. Tanaka, *Angew. Chem. Int. Ed*., **2002**, 41, 4563-4565.
[10] P. Pyykkö, J. P. Desclaux, *Acc. Chem. Res*., **1979**, 12, 8, 276–281.
[11] P. Pyykkö, *Angew. Chem. Int. Ed*., **2002**, 41, 3573-3578.
[12] P. Pyykkö, *Angew. Chem. Int. Ed*,. **2004**, 43, 4412 –4456.
[13] D. Gorin, F. D. Toste, *Nature*, **2007**, 446, 395–403.
[14] M. S. Nechaev, V. M. Rayón, G. Frenking, *J. Phys. Chem. A*, **2004**, 108, 15, 3134–3142.
[15] Y. Wang, M. E. Muratore, A. M. Echavarren, *Chem. Eur. J.*, **2015**, 21, 7332-7339.
[16] For a 360° view on gold catalysis see: "Gold chemistry", *Chem. Rev.*, **2021**, 121, 14, 8309-9164.
[17] J. J. Kennedy-Smith, S. T. Staben, F. D. Toste, *J. Am. Chem. Soc.*, **2004**, 126, 14, 4526–4527.
[18] A. S. K. Hashmi, J. P. Weyrauch, W. Frey, J. W. Bats, *Org. Lett.*, **2004**, 6, 23, 4391–4394.
[19] A. S. K. Hashmi, L. Schwarz, J.-H. Choi, T. M. Frost, *Angew. Chem. Int. Ed.*, **2000**, 39, 13, 2285-2288.
[20] S. Kobayashi, K. Kakumoto, M. Sugiura, *Org. Lett.*, **2002**, 4, 8, 1319-1322.
[21] M. Bandini, A. Eichholzer, *Angew. Chem. Int. Ed*., **2009**, 48, 9533 –9537.
[22] N. W. Sun, C.-G. Yang, Z. Shi, C. He, *Synlett.*, **2006**, 8, 1278-1280.
[23] J. Zhang, C.-G. Yang, C. He, *J. Am. Chem. Soc*., **2006**, 128, 6, 1798–1799.
[24] X.Yao, C.-J. Li, *J. Am. Chem. Soc*., **2004**, 126, 22, 6884–6885.
[25] A. S. K. Hashmi, *Chem. Rev*. **2007**, 107, 3180−3211.
[26] D. Campeau, D. F. León Rayo, A. Mansour, K. Muratov, F. Gagosz, *Chem. Rev*,. **2021**, 121, 8756−8867.
[27] V. Michelet, P. Y. Toullec, J.-P. Genêt, *Angew. Chem. Int. Ed*., **2008**, 47, 4268 – 4315.
[28] E. Jiménez-Núñez, A. M. Echavarren, *Chem. Rev.*, **2008**, 108, 3326–3350.
[29] Y.-C. Lee, K. Kumar, *Isr. J. Chem.*, **2018**, *58*, 531-556.
[30] A. J. Arduengo, R. L. Harlow, M. Kline, *J. Am. Chem. Soc.*, **1991**, 113, 1, 361–363.
[31] M. N. Hopkins, C. Richter, M. Schedler, F. Glorius, *Nature*, **2014**, 510, 485-496.
[32] D. Benitez, N. D. Shapiro, E. Tkatchouk, Y. Wang, W. A. Goddard, F. D. Toste, *Nature Chem*., **2009**, 1, 482–486.
[33] K. Luo, L. Zhang, H. Jiang, L. Chen, S. Zhu, *Chem. Commun.* **2018**, 54, 1893-1896.
[34] C. A. Tolman, *Chem. Rev*., **1977**, 77, 313–348.
[35] A. C. Hiller, W. J. Sommer, B. S. Yong, J. L. Petersen, L. Cavallo, S. P. Nolan, *Organometallics*, **2003**, 22, 21, 4322–4326.
[36] J. J. Dunsford, K. J. Cavell, B. M. Kariuki, *Organometallics*, **2012**, 31, 4118−4121.
[37] A. Cervantes-Reyes, F. Rominger, M. Rudolph, A. S. K. Hashmi, *Adv. Synth. Catal*., **2020**, 362, 2523− 2533.
[38] V. Vethake, V. Claus, M. C. Dietl, D. Ehjeij, A. Meister, J. F. Huber, L. K. Paschai Darian, M. Rudolph, F. Rominger, A. S. K. Hashmi, *Adv. Synth.Catal*., **2022**, 364, 536–554.
[39] M. Alcarazo, S. J. Roseblade, A. R. Cowley, R. Fernánez, J. M. Brown, J. M. Lassaletta, *J. Am. Chem. Soc*., **2005**, 127, 3290-3291.
[40] C. Burstein, C. W. Lehman, F. Glorius, *Tetrahedron*, **2005**, 61, 6207-6217.
[41] M. Alcarazo, T. Stork, A. Anoop, W. Thiel, A. Fürstner, *Angew. Chem. Int. Ed*., **2010**, 49, 2542–2546.
[42] Y. Kim, Y. Kim, M. Y. Hur, E. Lee, *J. Organomet. Chem.*, **2016**, 820, 1-7.
[43] E. Herrero-Gómez, C. Nieto-Oberhuber, S. López, J. Benet-Buchholz, A. M. Echavarren, *Angew. Chem. Int. Ed*., **2006**, 45, 5455 –5459.
[44] M. Espina, I. Rivilla, A. Conde, M. M. Díaz-Requejo, P. J. Pérez, E. Álvarez, R. Fernández, J. M. Lassaletta, *Organometallics*, **2015**, 34, 1328−1338.
[45] Y. Tang, I. Benaissa, M. Huynh, L. Vendier, N. Lugan, S. Bastin, P. Belmont, V. César, V. Michelet, *Angew. Chem. Int. Ed.*, **2019**, *58*, 7977-7981.
[46] Y. Wang, Z. Wang, Y. Li, G. Wu, Z. Cao, L. Zhang, *Nat. Commun.*, **2014**, 5, 3470.
[47] X. Cheng, Z. Wang, C. D. Quintanilla, L. Zhang, *J. Am. Chem. Soc*., **2019**, 141, 9, 3787–3791.
[48] J.-Q. Zhang, Y. Liu, X.-W. Wag, L. Zhang, *Organometallics*, **2019**, 38, 3931−3938.
[49] Selection of works: a) R. Pedrazzani, J. An, M. Monari, M. Bandini, *Eur. J. Org. Chem*., **2021**, 1732–1736; b) J. An, R. Pedrazzani, M. Moari, M. Marin-Luna, C. S. Lopez, M. Bandini, *Chem. Commun.*, **2020**, 56, 7734-7737; c) J. An, L.

Lombardi, S. Grilli, M. Bandini, *Org. Lett*. **2018**, 20, 23, 7380–7383; d) J. An, A. Parodi, M. Monari, M. C. Reis, C. S. Lopez, M. Bandini, *Chem. Eur. J*., **2017**, 23, 17473-17477; e) E. Manoni, M. Daka, M. M. Mastandrea, A. De Nisi, M. Monari, M. Bandini, *Adv. Synth. Catal.*, **2016**, 358: 1404-1409; f) M. Jia, M. Monari, Q.-Q. Yang, M. Bandini, *Chem. Commun*., **2015**, 51, 2320-2323.

[50] R. Pedrazzani, A. Pius, R. De Ventura, M. Marchini, P. Ceroni, C. S. Lopez, M. Monari, M. Bandini, *ACS Org. Inorg. Au*, **2022**, 2, 3, 229–235.

[51] R. Pedrazzani, E. Pinosa, G. Bertuzzi, M. Monari, S. Lauzon, T. Ollevier, M. Bandini, *Chem. Commun*., **2022**, 58, 8698-8701.

[52] G. J. Domski, E. B. Lobokovsky, G. W. Coates, *Macromolecules*, **2007**, 40, 9, 3510–3513.

[53] N. Rizeq, S. N. Georgiades, *Eur. J. Org. Chem*., **2016**, 1, 122-131.

[54] H. M. J. Wag, I. J. B. Lin, *Organometallics*, **1998**, 17, 972-975.

[55] R. Visbal, A. Laguna, M. C. Ginemo, *Chem. Commu.*, **2013**, 49, 5642-5644.

[56] A. Collado, A. Gómez-Suárez, A. R. Marin, A. M. Z. Slawin, S. P. Nolan, *Chem. Commun*., **2013**, 49, 5541-5543.

[57] H. F. Jónsson, A, Fiksdahl, A. J. Harvie, *Dalton Trans.*, **2021**, 50, 7969-7975.

[58] I. Caracelli, J. Zukerman-Schpector, E. R. T. Tiekink, *Gold Bull.*, **2013**, 46, 81-89.

[59] M. J. Johansson, D. J. Gorin, S. T. Staben, F. D. Toste, *J. Am. Chem. Soc*., **2005**, 127, 51, 18002–18003.

[60] S. Handa, L. M. Slaughter, *Angew. Chem. Int. Ed*. **2012**, 51, 2912 –2915.

[61] *SMART & SAINT Software Reference Manuals*, version 5.051 (Windows NT Version), Bruker Analytical X-ray Instruments Inc.: Madison, Wi, **1998.**

[62] Sheldrick, G. M.; *SADABS-2008/1 - Bruker AXS Area Detector Scaling and Absorption Correction*, Bruker AXS: Madison, Wisconsin, USA, **2008**.

[63] Burla, M.C.; Caliandro, R.; Carrozzini, B.; Cascarano, G.L.; Cuocci, C.; Giacovazzo, C.; Mallamo, M.; Mazzone, A.; Polidori, G.; "Crystal structure determination and refinement via SIR2014" *J. Appl. Cryst.* **2015**, *48*, 306-309

[64] Sheldrick, G. M.; *Acta Cryst C71***, 2015**, 3-8.

[65] C. F. Macrae, I. Sovago, S. J. Cottrell, P. T. A. Galek, P. McCabe, E. Pidcock, M. Platings, G. P. Shields, J. S. Stevens, M. Towler and P. A. Wood, *J. Appl. Cryst*., **2020**, ***53***, 226-235.

[66] Y. Alvarez-Casao, B. Estepa, D. Monge, A. Ros, J. Iglesias-Siguenza, E. Alvarez, R Fernandez, J.M. Lassaletta, *Tetrahedron*, **2016**, 72, 5184-5190.

[67] W. Zi, F. D. Toste, *Chem. Soc. Rev*., **2016**, 45, 4567-4589.

[68] A. S. K. Hashmi, *Nature*, **2007**, 449, 292-293.

[69] M. Jia, M. Bandini, *ACS Catal*., **2015**, 5, 1638−1652.

[70] Y. Xia, A. S. Dudnik, V. Gevorgyan, Y. Li, *J. Am. Chem. Soc*., **2008**, 130, 22, 6940–6941.

[71] K. Kaupmess, N. Tolstoluzhsky, S. Raja, M. Rueping, I. Leito, *Angew. Chem. Int. Ed.*, **2013**, 52, 44, 11569-11572.

[72] J. F. Teichert, B. L. Feringa, *Angew. Chem. Int. Ed.*, **2010**, 49, 14, 2486-2528.

[73] D. Jassen-Müller, C. Schlepphorst, F. Glorius, *Chem. Soc. Rev*., **2017**, 46, 4845-4854.

[74] S. Budagumpi, R. S. Keri, G. Achar, K. N. Brida, *Adv. Synth. Catal*., **2020**, 362, 970-997.

[75] I. Varela, H. Faustino, E. Díez, J. Iglesias-Sigüenza, F. Grande-Carmona, R. Fernández, J. M. Lassaletta, J. L. Mascareñas, F. López, *ACS Catal*., **2017**, 7, 2397−2402. J. Iglesias-Sigüenza,

[76] J. Francos, F. Grande-Carmona, H. Faustino, J. Iglesias-Sigüenza, E. Díez, I. Alonso, R. Fernández, J. M. Lassaletta, F. López, J. L. Mascareñas, *J. Am. Chem. Soc*., **2012**, 134, 14322−14325.

[77] C. Bolm, M. Ewald, M. Felder, G. Schlingloff, *Chem. Ber*., **1992**, 125: 1169-1190.

[78] S. Lauzon, L. Schouwey, T. Ollevier, *Org. Lett*., **2022**, 24, 4, 1116–1120.

[79] A. Collado, D. J. Nelson, S. P. Nolan, *Chem. Rev.*, **2021**, 121, 8559-8612.

[80] D. W. Old, J. P. Wolfe, S. L. Buchwald, *J. Am. Chem. Soc*., **1998**, 120, 9722-9723.

[81] A. S. K. Hashmi, B. Bechem, A, Loos, M. Hamzic, F. Rominger, H. Rabaa, *Aust. J. Chem.*, **2014**, 67, 481-499.

[82] W. Wang, G. B. Hammond, B. Xu, *J. Am. Chem. Soc*., **2012**, 134, 5697−5705.

[83] A. H. Christian, Z. L. Niemeyer, M. S. Sigma, F. D. Toste, *ACS Catal*., **2017**, 7, 3973−3978.

[84] C. H. M. Amijs, C. Ferrer, A. M. Echavarren, *Chem. Commun*., **2007**, 7, 698-700